THE FORMATION OF CHEMICAL PRECIPITATES IN THE HAL PROCESS AND ITS IMPACT ON ELECTROSTATIC SEPARATION OF ZIRCON AND RUTILE MINERALS

by

André Prinsloo

Thesis submitted in partial fulfilment
of the requirements for the Degree

of

MASTER OF SCIENCE IN ENGINEERING
(MINERAL PROCESSING)

in the Department of Process Engineering
at the University of Stellenbosch

Supervised by
Dr. J.F. Görgens
Dr. R. Els

STELLENBOSCH

December 2005

DECLARATION

I, the undersigned, hereby declare that the work contained in this thesis is my own original work and that I have not previously, in its entirety or in part, submitted it at any university for a degree.

André Prinsloo 16 November 2005

ACKNOWLEDGEMENTS

This study taught me the real meaning of discipline, dedication and endurance. I acknowledge God, who reveals His knowledge to men, my wife for her support during the many hours of hard work and sacrifice in terms of time, the people of Namakwa Sands who invested their trust and resources in me, and Johann for his excellent guidance and patience. The outcome of this study was a tremendous benefit to Namakwa Sands in terms of the Mineral Wash Plant and to me in terms of knowledge, academic skills and life experience.

SYNOPSIS

This study provided scientific proof of the precipitation of iron and other metal species in the HAL circuit at the Mineral Separation Plant of Namakwa Sands. Iron and aluminium hydroxides were the most abundant precipitate complexes that formed in the HAL circuit. Sulphates formed bridges with the iron complexes. It was found that precipitation of iron in the HAL circuit was a function of the pH, ferric ion concentration and temperature of the process water. Experimental work provided abundant evidence that the precipitated iron hydroxide and other species adsorb to the surfaces of zircon and rutile mineral particles due to opposite zeta potentials of the mineral particles and iron hydroxide. These adsorbed species altered the electrostatic potential of the mineral surfaces, which reduced the electrostatic separation efficiency of these minerals. It was determined that an improvement of 7% could be expected if the precipitation and attachment of iron could be minimised. Based on the experimental results, conceptual processes were developed and iterative simulations were set up to determine the optimum solution that would maximise the removal of dissolved iron. This solution would ensure clean mineral surfaces free of any adsorbed precipitates. This process circuit was constructed in May to August 2004 at a total capital cost of R4.8m and removed 99.97% of the total dissolved iron prior to caustic addition. Prime zircon recoveries were increased by 3-7%.

OPSOMMING

Hierdie studie het wetenskaplike bewyse gelewer dat yster en ander spesies neerslae vorm in die HAL proses van die Mineraal Skeidings Aanleg van Namakwa Sands. Yster- en aluminium hidroksiede was die vernaamste neerslag komplekse wat gevorm het in die HAL proses. Sulfaat spesies het verbindings gevorm met die yster komplekse. Die neerslag van yster was ‘n funksie van pH, ferric ioon konsentrasie en temperatuur van die proses water. Eksperimentele werk het genoegsame bewyse gelewer dat die yster hidroksied neerslag en ander spesies adsorbeer op die oppervlaktes van sirkoon en rutiel minerale weens teenoorgestelde zeta potensiale van die mineraal partikels en yster hidroksiede. Hierdie geadsorbeerde spesies het die elektrostatiese potentiaal van die mineraal oppervlaktes verander wat sodoende die elektrostatiese skeidingsvermoë van hierdie minerale verminder het. ‘n Verbetering van 7% in elektrostatiese skeiding van sirkoon en rutiel minerale kan verwag word indien die neerslag en adsorbsie van yster minimiseer word. Konseptuele prosesse, gebasseer op die eksperimentele resultate, is ontwikkel. Itteratiewe simulasies is opgestel om die optimum proses te bepaal wat sodoende die maksimum verwydering van die opgeloste yster sou verseker. Hierdie oplossing sou skoon mineraal oppervlaktes, vry van enige geadsorbeerde neerslae, verseker. Hierdie prosesaanleg was opgerig in Mei tot Augustus 2004 teen ‘n kapitaalkoste van R4.8m en dit het 99.97% van die totale opgeloste yster verwyder voordat natrium hidroksied bygevoeg is. Primêre sirkoon opbrengste het sodoende toegeneem met 3-7%.

TABLE OF CONTENTS

CHAPTER 1

INTRODUCTION

Objectives of Chapter 1:

- Provide a geological background of the mineral ore-body of Namakwa Sands.
- Provide a brief process overview of Namakwa Sands.
- Provide a detailed process description of the HAL process.
- Define the problem statement and outline the objectives of the study.

The thesis mainly focuses on one of the sub-circuits, namely the hot acid leach (HAL) process, of the mineral separation plant (MSP) of the Namakwa Sands operations. The study will show that this circuit has the same function as a human heart and malfunctioning will result in poor performances of the downstream dry mill circuit.

1.1 GEOLOGICAL BACKGROUND

The Namakwa Sands ore-body is located on the West Coast of South Africa, approximately 100km north of Vredendal. The economic suite of minerals includes ilmenite, rutile, zircon and leucoxene. Hornblende, garnet, magnetite, feldspar, monazite and other species occur as gangue minerals. Namakwa Sands forms part of Anglo Base operations.

The heavy mineral assemblages originate from pre-Cambrian age metamorphic rocks of the Namaqualand Metamorphic Complex and Van Rhynsdorp Group. Continental uplift occurred during the late Cretaceous period and was followed by erosive events, which liberated the mineral assemblages. During Miocene times (6 million years ago), east-west draining fluvial systems eroded the hinterland and transported these sediments into a J-shaped, paleo-bay coastal environment. Sea level still-stands, trans and regression events during the Tertiary and Quaternary periods (6 to 2 million years ago) produced enriched heavy mineral deposits (strandlines) at the 20, 35 and 50m elevations above sea level.

The interaction of the northerly Benguela current and incoming south-westerly waves around a headland in the south produced concentrated wave action within the paleo-bay. This allowed the preferential deposition of heavy minerals and the removal of lighter and fine-grained fractions.

Westward progradation of the dune field was followed by massive redistribution of the mineral-bearing sediments by the prevailing south-southwest winds.

1.2 OPERATIONS OVERVIEW

Namakwa Sands operations consisted of three sites at three different locations. Mining, primary and secondary concentration took place at Brand-se-Baai (approximately 70 km north of Koekenaap). Concentrate from the mine was transported by rail trucks to the mineral separation plant (MSP) at Koekenaap where it was separated into technical complex circuits to produce ilmenite, zircon and rutile products. These products were transported by rail trucks to the smelter plant at Saldanha where ilmenite was processed further. Zircon and rutile were transported to the overseas markets. A simplified process flow diagram of the Namakwa Sands operations is shown in Figure 1.1.

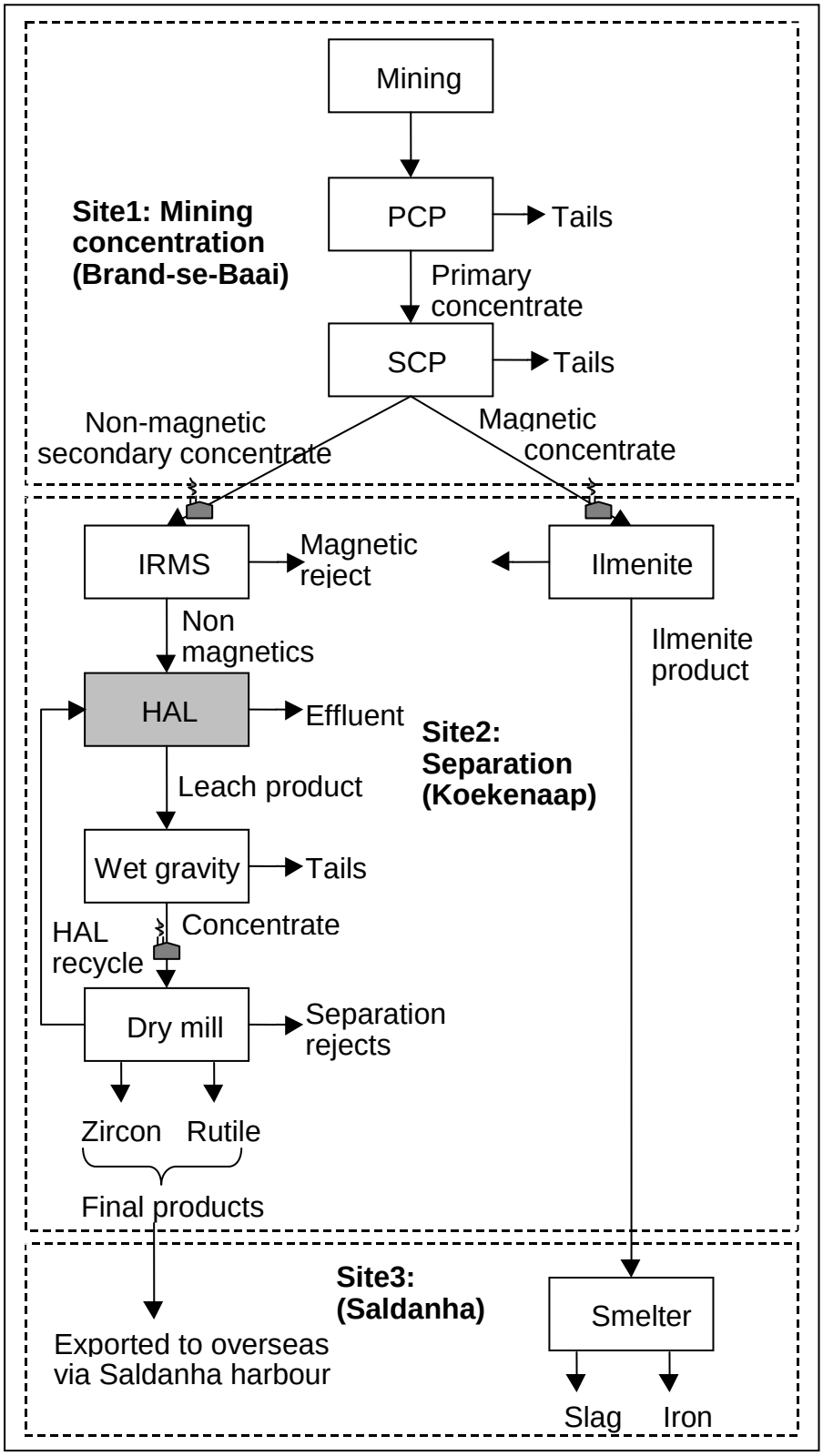

Figure 1.1: A simplified block diagram of the process flow of the Namakwa Sands operations. The thesis focuses on the HAL circuit and its impact on the proceeding circuits.

1.2.1 MINING

Mining operations consisted of loading the mineral enriched sand with front-end loaders and excavators, and discharging it onto a conveyor system after oversize material (>300 μm) had been removed. The ore was then transported to the primary concentration plant (PCP). The tailings from the PCP were transported back to the mining area where they were used to rehabilitate the mined out area.

1.2.2 PRIMARY CONCENTRATION PLANT (PCP)

Felspathic and Aeolian sand received from the mine contained 6 to 8 mass% heavy minerals, which were upgraded by gravity separation (using mainly spirals) to a concentrate containing 90% heavy minerals.

1.2.3 SECONDARY CONCENTRATION PLANT (SCP)

Concentrate from the PCP was pumped to the SCP where it was separated into magnetic and non-magnetic fractions by means of WHIMS (Wet High Intensity Magnetic Separators). These streams were further upgraded by spirals to produce non-magnetic (55% zircon, 15% rutile, 12% leucoxene and 18% gangue minerals) and magnetic concentrates (90% ilmenite and 10% garnets). The magnetic and non-magnetic concentrates were attritioned to reduce siliceous and iron oxide surface coatings, respectively.

1.2.4 MINERAL SEPARATION PLANT (MSP)

1.2.4.1 Mineralogy

The magnetic feed to the MSP comprised approximately 90% ilmenite together with 10% predominantly garnets and trace amounts of other minerals.

In contrast, the mineral suite of the non-magnetic feed was much more diverse and in addition to the valuable zircon, rutile and high grade leucoxene hosted a range of gangue minerals including garnet, ilmenite, pyroboles, staurolite, monazite, kyanite, cassiterite, titanite, low grade leucoxene, and quartz. Typically, a non-magnetic feedstock contained about 52% zircon, 14% rutile and 10% leucoxene with the remainder being a mixture of the gangue minerals above, commonly specified as ‘others’. However, deviations of up to 5% occurred and generally related to varying feedstock grades from the SCP.

Research has shown that the rutile minerals mined at Namakwa Sands show very little variation in chemical composition and consist of nearly 98% pure TiO_2. Zircon, leucoxene and ilmenite, however, displayed a broad range in their respective compositions. Zircon was generally distinguished by two types, namely pure (clear) and impure (metamic) varieties, and although both types contain approximately 65% ZrO_2, the metamic type hosted an undesirable amount of relatively high concentrations of Fe, U and Th. Silica-rich intergrowths commonly lowered the titanium content of leucoxene to as low as 85% TiO_2. Similarly, Ti-poor ilmenite particles that are rich in Fe and Si degrade the titanium content of the final ilmenite product to approximately 46% TiO_2. Fe-Al silicate coatings were present on all mineral grains as surface deposits and did not only affect the quality of the products, but also impaired electrostatic and magnetic separation. Apart from these diverse chemical compositions, the various minerals also exhibited different physical properties and mineral separation was accomplished by exploiting these. The MSP processed the magnetic and non-magnetic concentrates in two separate circuits, namely the magnetic ilmenite and non-magnetic circuits.

1.2.4.2 Magnetic circuit

Magnetic concentrate from the SCP was dried in a fluidised bed dryer prior to magnetic and electrostatic separation. This circuit consisted of four mini circuits known as the rougher, cleaner, middlings and scavenger circuits. The design objective of the ilmenite circuit was to lower the silica content of the final ilmenite product by removing silica rich garnet particles. The ilmenite product produced is transported by rail to the smelter for further processing.

1.2.4.3 Non-magnetic circuit

The non-magnetic circuit consisted of four main circuits, which were all divided into mini circuits with different levels of complexity. The main circuits were induced roll magnetic separation (IRMS), hot acid leach (HAL), wet gravity separation and dry Mill separation.

(a) IRMS circuit

The non-magnetic concentrate from the SCP was dried in a fluidised bed dryer prior to processing in a three-stage IRMS circuit. Moderate to strong magnetic misplaced material was removed, which contained mainly garnets, ilmenite and monazite. The removal of the monazite ahead of the leaching process was important to prevent the dissolution of this radioactive mineral in sulphuric acid, thereby reducing the radioactive content of the effluent of the HAL circuit.

(b) HAL circuit

The upgraded non-magnetic product of the IRMS circuit was further processed in the chemical leaching HAL circuit. This circuit design was based on the Hepworth process, which consisted of two reactors in parallel where the main reaction took place and a simplistic counter-current circuit to remove dissolved species.

Al-Fe-Si rich mineral surface coating, which affected electrostatic and magnetic dry mill separation, and contributed to iron contamination of zircon products, was removed in this circuit. Feed to the HAL circuit was heated to 150^{o}C and fed into two parallel insulated rotary reactors where a 40% hot sulphuric acid solution was added to the sand. The heat of the sand baked and concentrated the acid onto the mineral surface ensuring a chemical reaction between Fe_2O_3 (and Al_2O_3) and sulphuric acid to form iron (and aluminium) sulphate. The residence times were 45 and 90 minutes for the two individual reactors, respectively. The almost dry reactor products were quenched by repulping with cold process water in two parallel sumps, reducing the temperature to approximately 40^{o}C. The majority of the excess sulphuric acid, iron and other dissolved species were removed to effluent by means of a hydrocyclone (cyclone 1) followed by an upflow classifier. The upflow classifiers removed dissolved species based on the principle of hindered settling. Solid particles fell through a column of upward flowing water. Dissolved species were removed as overflow water by the upward flowing water current. This overflow water of the classifier was used as reticulation water (sump make-up and agitation water) for the quench sumps.

The densified and relatively clean underflow discharged into three parallel banks of attritioners, consisting of four cells each. The remaining mineral coatings, which were not removed by the leaching process, were physically removed by abrasion. Diluted caustic was added in the third cell of each attritioner to neutralise the slurry by increasing the pH from approximately 2 to 5.5. The residence time per cell was approximately 3 to 5 minutes. The discharge streams of the attritioners were repulped in the wash sumps with neutral process water from the HAL water supply tank.

Excess water was removed by means of hydrocyclones (wash cyclone 2), known as wash cyclones, to densify the slurry. Cyclone overflow water was used as teeter water for the upflow classifiers after solid removal using a solid trap. The underflow of the cyclone was gravity fed to the primary hydrosizer, which formed the first separation stage of the wet gravity circuit. Overflow water from the primary hydrosizer was fed to the HAL water supply tank after solids were removed by means of a hydrocyclone (fine cyclone 3). Wet gravity process water was used to supplement the HAL water supply tank by maintaining a constant level. The process flow of the two parallel streams discussed

was identical and the process flow diagram of one of these streams is shown in Figure 1.2. The purpose of the HAL counter current wash circuit was to remove as much of the soluble iron and other species as possible prior to processing in the wet gravity circuit.

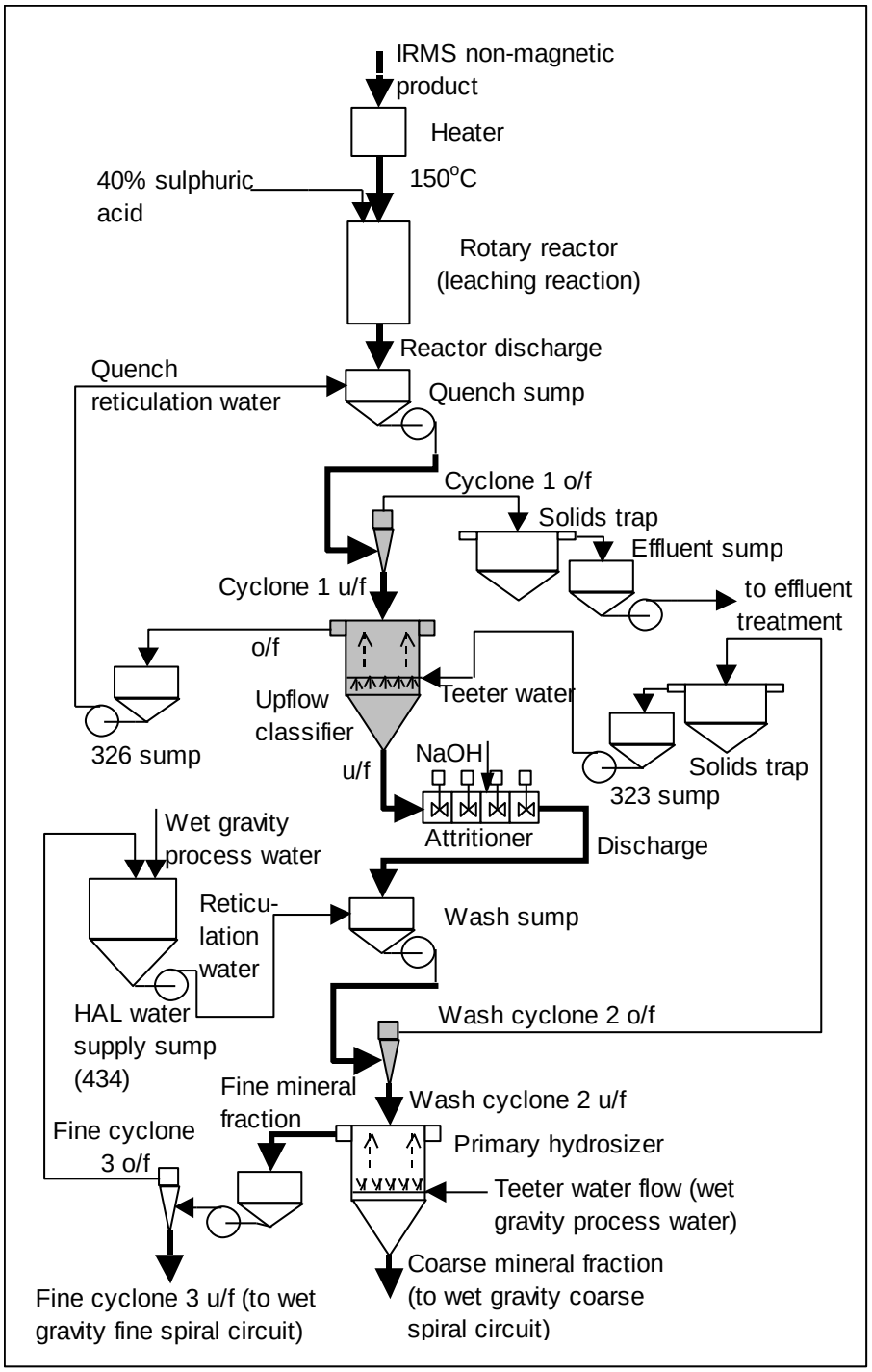

Figure 1.2: Process flow diagram of one of the parallel streams of the existing HAL circuit at Namakwa Sands. Thick lines indicate solid/slurry streams and normal lines indicate water streams. Mineral washing and dewatering equipment of the HAL circuit is indicated in bold.

A temperature and pH profile of the HAL circuit is shown in Table 1.1. At this stage, it is also worth mentioning that the residence time of minerals in the HAL wash circuit, which include cyclones 1 and 2 and the upflow classifier, is approximately 20 to 30 minutes. This information is important and would allow us to identify the formation of complex iron species as discussed in Chapter 2 – *Literature review and Theoretical considerations*.

Table 1.1: Temperature and pH profile of the HAL A circuit (measured with an infrared temperature meter). The ambient air temperature was 35^{o}C when the temperatures of the solutions were taken.

Stream	A process stream	
	pH	Temperature (^{o}C)
Reactor discharge		88
Quench sump	1.67	40
Quench water sump (326)	1.88	33
Cyclone 1 underflow	1.51	36
Cyclone 1 overflow	1.61	37
Upflow classifier overflow	1.88	33
Upflow classifier underflow	2.83	34
Upflow classifier teeter water sump (323)	5.26	31
Attritioner discharge	~5	43
Wash sump	~5	30
Wash cyclone 2 underflow	4.03	33
Wash cyclone 2 overflow	5.26	33
Fine cyclone 1 underflow	~4	29
Fine cyclone 1 overflow	~4	30
HAL effluent	1.74	37
Primary hydrosizer overflow	~4	31
HAL water supply tank (434)	4.08	29

(c) Wet gravity circuit

The purpose of this circuit was to remove the less dense gangue minerals, namely quartz, siliceous leucoxene, kyanite, garnets, pyroboles and other non-valuable minerals from the underflow and overflow streams of the primary hydrosizer.

The coarser mineral fraction (80 mass%), reporting to the underflow of the hydrosizer, was processed in the coarse spiral circuit to produce the bulk of the primary concentrate being fed to the dry mill circuit. The finer mineral fraction (20 mass%), reporting to the overflow of the hydrosizer, was processed in the fine spiral circuit, which recycles valuable minerals to the coarse spiral circuit.

To ensure separation stability in the dry mill circuit, the wet gravity concentrate should ideally contain 75% zircon, rutile to leucoxene ratio of 2:1, and gangue mineral content of less than 1.5%. The wet

gravity concentrate was either fed to a horizontal vacuum belt filter or diverted to drying bays from where it was conveyed to a fluidised dryer to be dried and heated for dry mill separation.

(d) Dry mill circuit

This circuit was a complex combination of multiple dry stages of mainly electrostatic separators complemented by magnetic, density and size separators. The circuit was divided into six interrelated sub-circuits, namely rougher, middlings, zircon, rutile, secondary rutile (Tiokwa), and secondary zircon (Zirkwa) circuits.

Electrostatic separators included High Tension Roll Separators (HTR), Electrostatic Plate Separators (EPS), Electrostatic Screen Plate Separators (ESPS), Coronastats and Ultrastats. The last two separators were improved models of the HTR and EPS, respectively. Magnetic separators included IRMS and High Force Magnets (HFM). Air Tables, Rotex and Sweco Screens were the main density and size separators.

Primary and secondary products of zircon and rutile were produced in the dry mill circuit. Magnetic and conductive mineral particles, rejected by the zircon cleaner circuit, were recycled to the HAL circuit. This stream was referred to as the HAL recycle.

1.2.5 SMELTER

The ilmenite was sourced from the MSP. The smelter process comprised the carbonaceous reduction of ilmenite to produce titania slag with a TiO_2 content of 86% and iron with a carbon content of 2.5%. Carbon was injected to increase the carbon content to 4.1% and calcium carbide was injected to reduce the sulphur content to below 0.012%. Ferrosilicon was also added to increase the silicon content.

The tapped slag was milled and classified in fine and coarse size fractions. Chloride slag was the coarser product and sulphate slag the finer.

1.3 PROBLEM STATEMENT AND OBJECTIVES OF THE STUDY

Very little information was available on the chemistry of the HAL circuit and its effect on mineral separation performances on the dry mill circuit proceeding the HAL circuit.

Namakwa Sands reported that poor dry mill production was often linked to pH control in the HAL circuit. Elevated pH levels (pH > 8) resulted in ineffective electrostatic separation and consequently lower output zircon and rutile output tons. Zircon product iron levels increased during these periods and yellow-brown precipitates were visible in the HAL, and sometimes in the wet gravity circuit.

Another unexplained phenomenon was that the mineral separation efficiency in the dry mill circuit seemed to be a function of the colour of the wet gravity process water. Purging of the process water resolved this problem. It was also noticed that the correlation error between the AMDEL and the XRF analysers, which monitored final zircon and rutile product grades, increased during these periods. The AMDEL picked up a lot of 'noise' during these periods. It was believed that some changes or unexplained chemical reactions took place in the HAL circuit and these reactions changed the mineral electrostatic and/or magnetic separation behaviour in the dry mill circuit. Early observations suggested that iron, which was removed from the mineral surfaces, might re-attach to the original minerals and could be the reason for some of these process deviations. However, no concrete facts, nor explanations, could be found to explain any of these phenomenon.

The objective of this study was to provide scientific explanations for all the phenomena mentioned, determine if iron re-attached to the mineral surfaces, and also to provide a process solution to overcome these problems. The objectives can be outlined as follows:

(1) Outline the chemistry of the HAL circuit

(2) Determine if species were precipitated in the HAL circuit and what the major precipitate complexes were; and to determine what the physical conditions required for precipitation to take place were.

(3) Provide the most probable form of iron complexes formed in the HAL circuit.

(4) Determine whether these species attached to the surfaces of mineral particles.

(5) Determine the effect of these complexes on electrostatic separation and consequent recovery of zircon and rutile mineral particles.

(6) Determine the effect of these complexes on the grade of zircon and rutile products.

(7) Provide explanations for:

- The downstream effect of poor pH control in the HAL circuit.
- The impact of the ‘colour’ of the wet gravity process on dry mill separation performance.
- Poor AMDEL and XRF correlation.

(8) Determine a process solution to resolve the problems.

CHAPTER 2

LITERATURE REVIEW AND THEORETICAL CONSIDERATIONS

Objectives of Chapter 2:

- Provide the theoretical basis for this study.
- Provide an understanding of the precipitation of iron.
- Determine the relevant adsorption theory.
- Provide the direction for the experimental work.

It was identified early in the study that dissolved iron present in the HAL process water could form complexes that affected the surface properties of the minerals that were being processed in the HAL circuit. These changed surface properties could contribute to a loss in the production of zircon and rutile at Namakwa Sands. It was important, therefore, to gain a thorough understanding in the relevant complex formation associated with iron. This chapter mainly deals with the formation and stability of iron hydr(oxide) complexes, adsorption and desorption of these complexes to mineral particles. It also provides an overview of the electrostatic mineral separation processes.

The conditions of formation of iron complexes in hydrometallurgical processes are discussed with the objective of identifying which of these complexes would probably form in the HAL process of Namakwa Sands. Once the iron complexes have been identified, the conditions for adsorption of these complexes to mineral particle surfaces are summarised.

2.1 THE CHARACTERISTICS OF NATURAL AND IRON HYDR(OXIDE) COMPLEXES

2.1.1. CHEMICAL LEACHING OF HEAVY MINERAL SANDS

According to Collins and Farmer (2003) heavy mineral sand particles are often coated or stained by oxides of iron or fine clays. These iron coatings are chemically removed in acid leaching circuits, commonly referred to as hot acid leaching (HAL) due to the elevated temperatures at which the reactions occur.

2.1.2. IRON HYDR(OXIDE)

In hydrometallurgical processes, iron is commonly removed by its precipitation as hematite (α-Fe_2O_3), as 'goethite' (mostly α-FeOOH, less β-FeOOH), or as various jarosite compounds, $MFe_3(SO_4)_2(OH)_6$, where M is H_3O^+, Na, Rb, Ag, Tl, K, NH_4, ½Pb, or ½Hg. Two forms of Fe_2O_3 (hematite and maghemite), four forms of FeOOH (goethite, akaganeite, lepidocrocite and feroxyhyte) and six jarosite compounds (jarosite, hydroniumjarosite, ammoniojarosite, argentojarosite, natrojarosite and plumbojarosite) are known to occur in natural environments. The stability of the minerals found in nature can serve as a guide to the stability of hydrometallurgical precipitated compounds in storage ponds exposed to weathering (Dutrizac and Monhemius, 1986).

Hematite and maghemite minerals, Fe_2O_3

The core of the earth is believed to consist mainly of iron and nickel. According to Dutrizac and Monhemius (1986) iron typically occurs in ilmenite, magnetite (Fe_3O_4) and hematite (Fe_2O_3). Two polymorphs of Fe_2O_3 are found in nature: α-Fe_2O_3 (hematite) and γ-Fe_2O_3 (maghemite). The main differences between these polymorphs, according to Dutrizac and Monhemius (1986), are summarised in Table 2.1.

Table 2.1: Mineralogical data for the Fe_2O_3 minerals (Dutrizac and Monhemius, 1986)

	Maghemite	Hematite
1	Magnetic	Mostly non-magnetic, some are highly magnetic.
2	Syntheses generally involve water, e.g. through oxidation of magnetite or dehydration of lepidocrocite (γ-FeOOH), under hydrous conditions.	In hematite-ilmenite solution assemblage, hematite usually contains high amounts of Ti.
3	Maghemite is common in highly weathered soil of tropical and subtropical climates.	During weathering, hematite is formed by oxidation of ferrous minerals (including goethite and magnetite), through reactions of ferric sulphates, or ferric chloride solutions with other sulphide and silicate minerals and through precipitation from these solutions. Synthesized by precipitation from ferrihydrite at relatively high temperatures.

According to Cigan et al. (1980) the hematite industrial process has been in operation since 1972 at the Iijima Electrolytic Zinc Plant. During this process, the neutral leach residue is subject to attack by

return electrolyte and SO_2 at 95-100^oC; this results in the reduction of ferric ion to ferrous ion as follows:

$$2Fe^{3+} + SO_2 + 2H_2O \rightarrow 2Fe^{2+} + SO_4^{2-} + 4H^+ \qquad \textbf{Equation 2.1}$$

After copper removal, the solution is neutralised in two stages to pH 4.5 with limestone. Since the iron is present as $FeSO_4$, it remains in solution during neutralisation. Finally the iron is precipitated as α-Fe_2O_3 (hematite) by heating it to 180-200^oC for 3 hours at 18 atm O_2 pressure. Hematite exhibits excellent filtration properties. Magnetite formation will be avoided provided that the pH remains below 7-8.

Although Fe_2O_3 appears to be slightly more stable than goethite, formation of the latter would occur under these conditions at temperatures below 100^oC. Above 130^oC, Fe_2O_3 is kinetically and thermodynamically favoured.

Magnetite, Fe_3O_4

The magnetite industrial process is used for the removal of metallic impurities from process waste streams (Cigan et al., 1980). Magnetite is stable under weakly reducing and neutral to alkaline conditions. Under reducing conditions imposed by hydrogen, the magnetite is slightly more stable with respect to $Fe(OH)_2$. Moderate variations in temperature, pressure and ionic strength do not appear to alter the magnetite stability significantly. Complete oxidation of the solution followed by neutralisation is likely to give rise to the formation of iron hydroxide, hematite or goethite. Cigan et al. (1980) identified three methods for removing iron from metallurgical streams as magnetite. These methods are:

(1) Partial oxidation of iron to the ferric state with subsequent neutralisation with ammonia.
(2) Simultaneous oxidation and neutralisation of ferrous sulphate solution with ammonia.
(3) Separate precipitation of $Fe(OH)_2$ and $Fe(OH)_3$ followed by their mixing and reaction in alkaline media.

The second method is the preferred technique. The process solution is completely reduced to Fe^{2+} followed by heating to a temperature of 50-100^oC. A slightly elevated oxygen pressure (0.05Mpa) is maintained and the solution is neutralised by injecting ammonia. Reaction rates are fast with complete iron removal achieved in 5-15 minutes at 100^oC, NH_3/S ratio of 2 and a final pH >8. Hematite precipitate has good settling and filtration rates and is environmentally stable.

FeOOH minerals

Dutrizac and Monhemius (1986) divided FeOOH in four polymorphs according to mineralogical differences as summarised in Table 2.2.

Table 2.2: Mineralogical data for the FeOOH minerals (Dutrizac and Monhemius, 1986)

FeOOH-minerals	
	Goethite, α-FeOOH
1.	Orthorhombic symmetry.
2.	Natural goethite contains trace amounts of Al, Ni, Co, Cr, Ca, Mn, etc. due to co-precipitation from solution.
3.	Can be easily synthesised from ferrihydrite.
4.	Found frequently intergrown with hematite and commonly occurs as a weathering product of iron-bearing sulphides, oxides, carbonates, silicates, etc.
5.	Goethite is the most frequently occurring form of iron oxide in soils.
	Akaganeite, β-FeOOH
1.	Tetragonal symmetry
2.	Frequently has a small Cl content (2-6 wt. %); thus the formula $FeOOH.Cl_n$ has been suggested.
3.	Synthetic compound is usually formed by hydrolysis of $FeCl_3$ solution.
4.	Natural akaganeite is rare. Found as an alteration product of acidic volcanic fumaroles, in association with goethite, lepidocrocite, hematite, jarosite, residual pyrrhotite and iron sulphate minerals.
5.	Upon heating to 220^{o}C, akaganeite dehydrates to hematite.
	Lepidocrocite, γ-FeOOH
1.	Orthorcombic symmetry
2.	Usually contains small amounts of Mn, Co and Al.
3.	Usually formed from the alteration of pyrite and arsenopyrite; occurs as platy crystals associated with goethite, or as botryoidally masses, as thin stringers filling the shrinkage cracks of collorform goethite; in gossans, clays and sediments. It occurs in hydromorphic soils by oxidation of precipitated ferrous hydroxy compounds.
4.	Lepidocrocite dehydrates to maghemite on heating.
5.	Can be synthesized by reacting oxygen with $FeCl_2$ solution at a pH of 7. And can be converted to goethite with a high concentration of KOH.
	Feroxyhyte, δ-FeOOH
1.	Hexagonal
2.	Non-magnetic
3.	Very rare; originally found in Fe-Mn concentrations in the Pacific Ocean and in the Baltic and White Seas. Subsequently found in Fe-oxide precipitates from groundwater in glaciofluvial sands and gravels, in association with goethite and lepidocrocite.
4.	Can be synthesized by oxidation of $FeCl_2$ solution with H_2O_2 at a pH between 5 and 8, or by oxidation of $Fe(OH)_2$.
5.	The mineral and the synthetic compound convert to hematite or maghemite at high temperatures depending on the amount of air supply during heating and the amount of organic matter present.

Goethite, FeOOH

Naturally goethite is usually formed as a weathering product of iron-bearing sulphides, oxides, carbonates and silicates. The mineral is very stable, after hematite, particularly under hydrous conditions as in soils. Most goethite contains small quantities of other elements in solid solution.

The relative stability of hematite and goethite has been the subject of several publications. Literature has not been clear on the exact physical properties at which the different iron hydr(oxide) species have formed. However, approximate ranges of stability conditions are similar.

Dutrizac and Monhemius (1986) used the relative abundance of these minerals in nature as indicative of their relative stabilities under weathering conditions. Goethite is the most common, feroxyhyte is very rare; akaganeite, although rare, is relatively common in soils. Lepidocrocite will dehydrate to maghemite and the other three compounds usually dehydrate to hematite.

Under natural surficial weathering, the relative stabilities of hematite and goethite are very similar to each other, but vary with the condition of the environment. Under humid conditions (tropical weathering) goethite may be more stable than hematite. Under hot, dry desert weathering, hematite is more stable. Higher temperatures (70-90^{o}C) favour the formation of hematite at the expense of goethite. The maximum stability temperature for goethite at 1 atm is 40^{o}C. Weathering of hematite in a humid environment usually produces goethite, whereas hematite is the more common mineral in a dry, hot environment. In general, higher temperature favours hematite over goethite, whereas high pH and high water activity favour goethite stability. Minor variations in the system, such as elemental substitutions, associated minerals and the solution composition can affect the hematite-goethite relative stability relationship (Dutrizac and Monhemius, 1986).

Dutrizac and Monhemius (1986) also stated that aluminium in the goethite structure increases its stability with respect to hematite under natural weathering conditions (25^{o}C, 1 atm) and that Al-bearing goethite in soils is probably thermodynamically more stable than hematite. This was also supported by experimental results, which indicate increasing AlO(OH) substitution in goethite with increasing pH. They concluded the following from literature:

(1) Goethite and hematite have similar stabilities under natural surficial conditions, but minor variations in conditions such as pH or associated minerals and solutions can easily change their relative stabilities.
(2) Higher temperatures (70-90^{o}C) favour the stability of hematite over goethite.

(3) High pH values favour goethite stability.
(4) The stability of goethite is enhanced by Al substitution at low temperatures.
(5) Low pH and relatively high Eh (acidic environment) favour the stability of jarosite, whereas higher pH and relatively low Eh (normal weathering environment) favour goethite stability.

The synthetic preparation of goethite is more important since it could provide the necessary understanding of precipitation of iron in hydrometallurgical processes. Kosmulski et al. (2003) had prepared goethite by mixing 2.5 M KOH with a 0.15 M $Fe(NO_3)_3$ solution. This solution was stirred vigorously and allowed to age for 48 hours at 80^{o}C. The precipitate was then centrifuged to remove the excess solution and washed with a HNO_3 solution. The drying and washing were repeated a few times. One portion of the yellow-brownish precipitate was freeze-dried. The resulting material was referred to as goethite 25. The other portion of goethite was dried in an oven at 140^{o}C overnight. The resulting material was referred to as goethite 140 (although in fact it is a goethite-hematite composite). X-ray diffraction results obtained for goethite 25 were typical for pure goethite. The results obtained for goethite 140 revealed two phases, namely goethite and hematite. It is interesting to note that Dutrizac and Monhemius (1986) are under the impression that hematite will form at temperatures between 70-90^{o}C, but Kosmulski et al. showed that pure goethite formed at 80^{o}C. However, Dutrizac and Monhemius do not mention the time frame of formation, which is a very important parameter in iron complex formation. This could explain the temperature differences.

According to Cigan et al. (1980) Fe^{3+} concentration of less than 1 g/L, moderately high pH values and relatively high temperatures (75-95^{o}C) are required to precipitate goethite. It is precipitated by the oxolation of iron polymers in solution (see Equation 2.22, Paragraph 2.1.3.2 – *Precipitation pathways*). Goethite precipitation requires sufficient pH control since a relatively high pH is required to neutralise the protons that are generated. If the pH is too high, the polymerisation reactions will be driven to the iron gel stage. Commercial precipitations are conducted in the pH range 2-3.5 although it seems that part of the reason for the relatively high pH is the need to oxidise Fe^{2+} that is facilitated by high pH. All hydrolysis reactions are favoured by increases in temperature. The higher temperatures favour the formation of hematite at the expense of goethite according to the following reaction:

$$2FeOOH \rightarrow Fe_2O_3 + H_2O \qquad \textbf{Equation 2.2}$$

The iron polymer, which is the precursor of goethite, is certainly an anion-hydroxyl polymer, and the anion plays a significant role in determining the actual compound precipitated. It appears that anions such as ClO_4, NO_3 and Br, with weak complexion tendencies for iron produce α- or γ-FeOOH;

anions such as F or Cl which are stronger seem to form β-FeOOH. Temperature also plays a role and Fe_2O_3 eventually forms as the temperature is increased (Cigan et al., 1980).

The precipitate has a high surface area and both anions and cations can adsorb to the FeOOH particles. Transition metal cations such as Zn Cu, Co and Ni are also readily incorporated into the precipitate, presumably by substitution for Fe in the FeOOH structure.

The main qualities of goethite and the precipitation process according to Cigan et al. (1980) are:

(1) Excellent filterability of goethite.
(2) Goethite is relatively stable.
(3) No additional alkalis are required for the precipitation process (compared with the jarosite process).
(4) Relatively high pH values are required.
(5) Goethite precipitates from relatively dilute Fe^{3+} media.
(6) Goethite residues include some cations and anions (e.g. SO_4^{2-} and Cl^-).
(7) Goethite is relatively stable above pH 2 (Welham et al, 2000).
(8) Removing iron (III) by means of goethite precipitation will not remove Fe^{2+} since the latter precipitates at a relatively high pH.

Jarosites, $MFe_3(SO_4)_2(OH)_6$

Abundant information on jarosite is available in literature mainly due to its importance to industry. Dutrizac and Monhemius (1986) have conducted a substantial amount of work on jarosite. The jarosites are the iron containing members of a large family, the alunites $AB_3(SO4)_2(OH)_6$ in which A = H_3O^+, Na, Rb, Ag, Tl, K, NH_4, ½Pb, ½Hg and B = Al, Cu or Fe^{3+}. The elements from A and B can be easily incorporated in the jarosite structure during iron removal in hydrometallurgical processing.

Only six jarosite-type minerals are known, but nine have been formed synthetically. The six are hydronium jarosite, $(H_3O)Fe_3(SO4)_2(OH)_6$; ammoniojarosite, $(NH_4)Fe_3(SO4)_2(OH)_6$; argentojarosite, $AgFe_3(SO4)_2(OH)_6$; jarosite, $KFe_3(SO4)_2(OH)_6$, natrojarosite, $NaFe_3(SO4)_2(OH)_6$; and plumbojarosite, $PbFe_3(SO4)_2(OH)_6$. Jarosite is the most common. According to Dutrizac (1983) the hydronium ion, H_3O^+, substitutes for the various alkalis. The relative order of increasing hydronium substitution in the alkali jarosites is Na > NH_4 > K.

The minerals can be synthesized by precipitation from a ferric sulphate and appropriate salt solution at low pH. Jarosite minerals are stable in highly acidic and oxidizing conditions and are typically found in gossans, siliceous limonitic veins in limestones, acidic soils and sulphide-rich mine dumps. Natural jarosites usually form by oxidation of pyrite and are commonly intergrown with 'limonite' (i.e. goethite and other hydrated iron oxides) or less commonly with hematite. During weathering, the jarosites break down into goethite, hematite or 'limonite' (Dutrizac and Monhemius, 1986).

Dutrizac (1983) and Dutrizac and Monhemius (1986) report the relative stabilities of the jarosites to be in the sequence of $K>NH_4>Na$. Dutrizac and Monhemius (1986) express the relative stability of jarosite and goethite under natural weathering conditions in terms of the Eh-pH diagram, which is commonly used by most authors. The reader is referred to the Eh-pH diagram provided by Dutrizac and Monhemius (1986). The Eh-pH diagram indicates that goethite is stable in the normal weathering environment (higher pH) and that jarosite is stable in an acidic environment (pH<3) with Eh>0.6V and Fe^{3+} $>10^{-3}$M. Extensive percolation of fresh water will convert jarosite to goethite particularly in storage ponds in regions of high rainfall. The equation is as follows:

$$KFe_3(SO4)_2(OH)_6 \Leftrightarrow 3FeO.OH + K^+ + 2SO_4^{2-} + 3H^+ \qquad \textbf{Equation 2.3}$$

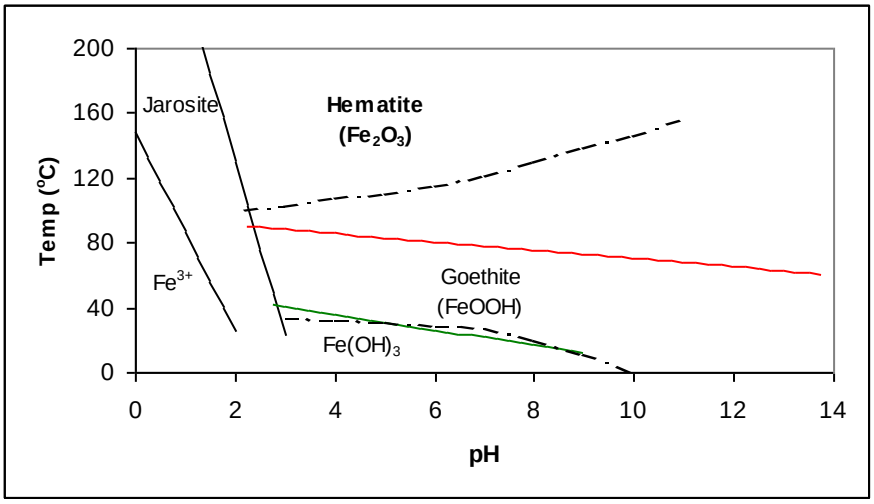

Figure 2.1: Fe(III) stability diagram as a function of pH and temperature. Formation from 0.5M $Fe_2(SO_4)_3$ solution at 20-200°C (Dutrizac and Monhemius, 1986). Dotted lines illustrate the stability of goethite and hematite as reported by Dutrizac (1983).

The relative stabilities of jarosite, goethite and hematite in terms of pH and temperature can be visualised from Figure 2.1. Jarosite is stable in the region of low pH (<3). Temperatures between 70

and 90^{o}C and pH higher than 3 favours the formation of goethite. The figure also shows that high temperatures favour the formation of hematite at the expense of goethite, and that higher pH values favour the stability of goethite with respect to hematite. It is important to note that literature does not agree on the exact temperature range required for the formation of goethite versus hematite. According to Dutrizac (1983), hematite forms at temperatures above 100^{o}C and goethite at lower temperatures.

Despite the clearly defined stability fields of jarosite, goethite and hematite (as derived from experiments in pure systems), in nature jarosite is commonly associated with goethite, goethite with hematite, and all three can occur together. This is attributable to the slow reaction rates of jarosite $\Leftrightarrow$ goethite and of goethite $\Leftrightarrow$ hematite, as well as the presence of several chemical contaminants (Dutrizac and Monhemius, 1986). Cigan et al. (1980) contradicts this last statement of Dutrizac and Monhemius (1986) by observing that hematite frequently forms from goethite, but not vice versa. Goethite forms at low iron and acid concentrations; jarosite forms at moderate iron and high acid concentrations (Cigan et al., 1980).

Cigan et. al. (1980) studied jarosite precipitation in the lead, zinc and tin industry. They found that it was possible to neutralise excess acid to a concentration of 5 g/l without premature precipitation of jarosite. This arises from the increased solubility of jarosite at lower temperatures. The solution was heated to 95^{o}C, the pH regulated to 1.1-1.5, and jarosite forming cations, such as NH_4^+, Na^+ and K^+, were added to form jarosite precipitate. It was also found that recycling jarosite assists in the precipitation of the iron due to the seeding effect. As jarosite forms acid is generated, and eventually the reaction virtually ceases. The amount of iron precipitated depends on the initial concentrations of ferric ion and free acid. Jarosite settles rapidly and can be thickened and filtered.

According to Welham et al. (2000) the solubility of jarosite is a function of both pH and local sulphate (VI) activity. The pH stability range of jarosite is relatively small and is bound by conversion to goethite (schwertmannite probably forms as an intermediate phase).

According to Cigan et al. (1980) the main properties of the jarosite process are as follows:

(1) Relatively small amounts of alkali are needed and the theoretical amount is further reduced by the substitution of alkali by H_3O^+. The effect of alkali concentrations above the stochiometric requirements is almost negligible.

(2) Jarosite precipitation operates at pH ~ 1.5, therefore it requires relatively small quantities of alkali. Commercially useful rates only occur at temperatures > 90^{o}C; ideal conditions for precipitation are pH 1.5-1.6 at 100^{o}C (Dutrizac, 1983).
(3) Jarosite precipitation occurs at ambient pressure.
(4) The oxidation of Fe^{2+} to Fe^{3+} is a slow process in an acidic medium. Therefore, removing iron (III) by means of jarosite precipitation will not remove Fe^{2+}.
(5) Elevated temperature favours the stability and precipitation of jarosite.
(6) Close process control, especially in terms of temperature and pH, is required for the successful precipitation of jarosite.

Laboratory experiments were performed by Cigan et al. (1980) where ferric sulphate-alkali solutions were rapidly heated to 90-100^{o}C. It was found that jarosite did not form immediately. There was an induction period of approximately an hour before appreciable jarosite formation occurred. Once jarosite precipitation commenced, complete reactions were recorded in relatively rapid reaction rates of 4-6 hours at 95^{o}C. Heating the solution to 140^{o}C resulted in an increase in reaction rates, which reduced the complete reaction time to less than 1 hour. The rate of iron precipitation increased as the iron concentrations increased, providing that above-stoichiometric amounts were present.

Dutrizac (1983) states that the formation rate of sodium, potassium and ammonium jarosite at 25^{o}C is very slow. For example, potassium jarosite was experimentally precipitated at 25^{o}C from a K_2SO_4-$Fe_2(SO_4)_3$ solution over the pH range 0.82 to 1.72 and for periods of 4 to 6 months. Jarosite precipitation becomes relatively rapid above 80^{o}C and is nearly complete in several hours at 100^{o}C. Commercially useful rates are realised only above 90^{o}C. The precipitation rate increases rapidly above 100^{o}C, but an upper limit for jarosite stability exists. Although this limit will most likely vary with the composition of the solution, it seems to be about 180-200^{o}C. The extent of jarosite precipitation increases with increasing M^{+}/Fe^{3+} ratios to slightly above stoichiometric and is thereafter nearly independent of the amount of alkali. Jarosite is also readily precipitated from solutions containing 0.025-3.0 M Fe^{3+}; the lower limit for jarosite production is approximately 10^{-3} M Fe^{3+}. Once jarosite has formed, a higher acid concentration is required to dissolve the product in a reasonably short period.

Iron sulphate minerals

Dutrizac and Monhemius (1986) provide a comprehensive discussion on sulphate, iron arsenate and iron phosphate minerals. Iron sulphates, as well as arsenate and phosphate compounds, are precipitated to control impurities in hydrometallurgical processing. Scorodite ($FeSO_4.2H_2O$) is

frequently precipitated to control iron. There are 78 iron sulphate mineral species in nature of which only three are anhydrous. The remainder are hydrous, hydroxyl or both. Most of the sulphate minerals dissolve in cold water. The ones that are insoluble in water dissolve in dilute acids. According to Cigan et al. (1980), $Fe(SO_4)(OH)$ species form at very high concentrations of iron sulphate.

Iron arsenate minerals

Forty-three arsenate/arsenite compounds are known as minerals. Most of these hydrated arsenate minerals are insoluble in water, but are soluble in dilute acids. Scorodite ($FeAsO_4.2H_2O$) has been reported as a potential compound for arsenic control in hydrometallurgy. It can be precipitated in hydrometallurgical systems at the temperature range 25-200^oC at a low pH (e.g. pH 2). At higher pH values it decomposes to FeOOH and at higher temperatures it co-precipitates as jarosite. Basic ferric arsenate compounds with Fe/As $\geq$ 4 have very low solubility in the pH range of 3 to 7, and thus will be relatively stable under surficial weathering (Dutrizac and Monhemius, 1986).

Iron phosphate minerals

According to Dutrizac and Monhemius (1986) it is commonly recognised that iron controls the migration of phosphorus in aqueous systems. Of the 107 known phosphate minerals, 14 are anhydrous. Among the remaining hydrated or hydroxyl minerals, 24 are of the ferrous species, 44 are of the ferric species and 25 are of the ferrous-ferric species. All phosphorus-bearing minerals have pentavalent P. Most are insoluble in water but will dissolve in dilute acids. The authors provide a summary in a table format of the iron phosphate minerals, which may occur in gossans, soils and sub-aqueous environments (such as lake sediments). They have divided these phosphates in five classes namely ferric phosphate hydrates, ferrous phosphate hydrates, basic ferric phosphate-beudanite/crandalite, basic ferric phosphates and basic ferro-ferric phosphates.

Phosphorus has been reported to precipitate as ferrous and ferric phosphates (hydrated) during impurity control in waste water treatment. These iron phosphates are most likely strengite/phosphosiderite, amorphous ferric phosphate, and vivianite. Based on thermodynamic data, strengite ($FePO_4.2H_2O$) is stable under high Eh ($\geq$0), has a low to moderate pH (4-7.5), and has a high PO_4^{3-} concentration. In the presence of HS^-, its stability field is very restricted. Vivianite, $Fe_3(PO_4)_2.8H_2O$; ludlamite, $Fe_3(PO_4)_2.4H_2O$; and phosphoferrite, $Fe_3(PO_4)_2.3H_2O$, are the three most common ferrous phosphate minerals. They are also the most stable Fe (II) phosphate in a reducing aqueous or sub-aqueous environment (pH 6.5-9, Eh<0) with a moderately high PO_4^{3-} concentration at

high ferrous ion activity. In a high HS^- environment ($a_{HS^-} \geq 10^{-1.5}$), vivianite is unstable except at extremely high PO_4^{3-} concentrations.

Dutrizac and Monhemius (1986) also found that basic iron phosphate minerals are stable in an aerobic environment and commonly occur in association with 'limonite'. If manganese is present in the environment, mangano-ferric hydroxyphosphates and the substitution of iron by manganese in the basic iron phosphates may occur. Basic ferro-ferric phosphate species are more stable than the basic phosphate species in natural aqueous or sub-aqueous environments such as lake sediments or soils. Consequently, these minerals may be potentially useful compounds for use in iron and phosphorous removal.

2.1.3. RAISING THE PH OF SOLUTIONS CONTAINING DISSOLVED IRON

In sulphate rich solutions, experimental results show that the first precipitate to form on raising the pH is jarosite. Jarosites are usually regarded as forming at temperatures greater than 60^{o}C. As the pH increases schwertmannite becomes predominant and goethite only forms at near neutral pH (Bhatti et al.,1993; Tuovinen et al.,1994; Scwertmann et al., 1995 and Bigham et al., 1996). Although not mentioned by the authors, these species do not form immediately. For example, jarosite will take a couple of hours to form, depending on the temperature.

This section provides important insight into iron complex formation in hydrometallurgical processes where it deals mainly with the formation of iron complexes over a short period of time when the pH is rapidly increased.

Cigan et al. (1980) provides a very valuable discussion on the physical chemistry of iron species and its precipitation in the zinc industry. The physical-chemical properties of typical solutions are outlined and it is shown how these ultimately influence the iron compounds formed. Conditions leading to the precipitation of jarosite, goethite, hematite and magnetite are enumerated.

2.1.3.1. Iron species in solution

(a) Ferrous iron hydr(oxide)

Ferrous ion will be thermodynamically oxidised to the ferric state in the presence of air, although the rate of oxidation is relatively slow in acidic media. Ferrous ion shows only a slight tendency to hydrolyse before precipitation as $Fe(OH)_2$ or Fe_3O_4 at a pH above 7.

(b) Ferric iron hydr(oxide)

Ferric sulphate

Ferric sulphate is extensively soluble. Crystallization of $Fe_2(SO_4)_3.9H_2O$ is most unlikely at relatively low concentrations of iron.

Hydrated ferric ion

The simple hydrated Fe^{3+} ion is stable at low iron concentrations, acidic conditions and in the absence of strong complexion anions such as sulphates. Small concentrations of $Fe(H_2O)_6^{3+}$ probably exist in most ferric solutions although the more strongly absorbing hydroxyl and sulphate complexes generally mask the light purple colour of these species.

Formation of hydroxyl complexes for ferric ion concentrations < 10^{-3} M

As hydroxyl ions are introduced as the pH is raised, a series of Fe^{3+} - hydroxyl complexes are formed. Simple complexes exist for ferric concentrations less than 10^{-3}M. These complexes are formed as follows:

$Fe^{3+} + H_2O \rightarrow Fe(OH)^{2+} + H^+$ $\log K_{11} = -3.05$ **Equation 2.4**

$Fe^{3+} + 2H_2O \rightarrow Fe(OH)_2^{+} + 2H^+$ $\log K_{12} = -6.31$ **Equation 2.5**

$Fe(OH)^{2+} + H2O \rightarrow Fe(OH)_2^{+} + H^+$ **Equation 2.6**

Formation of hydroxyl complexes for ferric ion concentrations > 10^{-3} M

A dimerized species predominates in a more concentrated iron media:

$2Fe^{3+} + 2H_2O \rightarrow Fe_2(OH)_2^{4+} + 2H^+$ $\log K_{22} = -2.91$ **Equation 2.7**

The dimer is assumed to be linked via hydroxyl bridges:

$Fe_2(OH)_2^{4+}$ ≡ 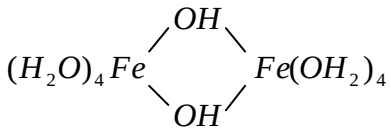

There is a general agreement concerning the above species, although other polynuclear complexes such as $Fe_3(OH)_4^{5+}$ and $Fe_2(OH)^{5+}$ have also been advanced as minor species. Regardless of the complex, the extent of hydrolysis increases with increasing temperature. Table 2.3 shows the formation constant, K_{22}, for the above dimer as a function of temperature.

Table 2.3: The formation constant of a dimerized species at a high iron concentration as a function of temperature.

Temp (^oC)	10^3 x K_{22}
15	4.9
25	7.3
35	10.2
45	16.3
51	25.1

Stability regions of ferric hydroxyl complexes

Figure 2.2 illustrates the approximate stability regions of the various ferric hydroxyl complexes as a function of the ferric ion concentration and the pH of a pure water system. Fe^{3+} is the predominant species at iron concentrations lower than 10^{-3} M and pH values less than 3.

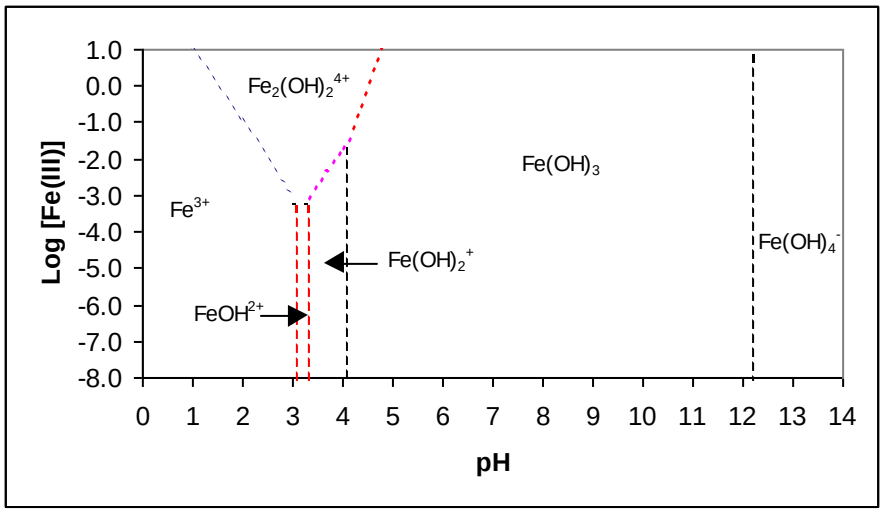

Figure 2.2: Solution species present in the Fe^{3+}-H_2O system at 25°C as a function of iron concentration and pH (Cigan et al., 1980).

Sulphate – iron (III) complexes

In strongly acidic sulphate solutions (in the absence of hydroxyl, OH), simple sulphate-iron (III) complexes are formed. The reactions are:

$Fe^{3+} + SO_4^{2-} \rightarrow FeSO_4^{+}$ $\log K_{13} = 2.03$ **Equation 2.8**

$FeSO_4^{+} + SO_4^{2-} \rightarrow Fe(SO_4)_2^{-}$ $\log K = 0.97$ **Equation 2.9**

Only the Fe^{3+} and $FeSO_4^{+}$ species exist in moderately diluted solutions of iron (III) perchlorate in Na_2SO_4-$HClO_4$ media. According to Cigan et al. (1980), $Fe(SO_4)_2^{-}$ forms at SO_4 concentrations greater than 0.3M. The stability constant for reaction 2.8 increases with increasing temperature, which can be expressed by the following equation:

$\text{Ln } K_f^0 = 21.713 - 8895.59/T + 115509/T^2$ **Equation 2.10**

This equation simply implies that iron-sulphate complexes become more stable as the temperature is increased.

According to Cigan et al. (1980) the effect of the bisulphate ion (HSO_4^{-}) in the precipitation of iron is not clear. It is prevalent at low pH values whereas SO_4^{2-} is the major species at pH > 2. Bisulphate stability increases with increasing temperature by virtue of the following reaction:

$SO_4^{2-} + H^{+} \rightarrow HSO_4^{-}$ **Equation 2.11**

Bisulphate might be expected to play a major role during the hydrolytic precipitation of iron. High concentrations of HSO_4^{-} in acidic solutions result in the formation of SO_4^{2-}, HSO_4^{-} and $HSO_4.SO_4^{3-}$ complexes of Fe(III). Welham et al. (2000) established that the effect of sulphur is greater at low pH. At higher pH's, the effect of the sulphur anions on iron precipitation is little (refer to Paragraph 2.1.4.1 – *Iron (III)/goethite equilibriums*).

When a solution containing predominantly iron (III)-sulphate species is heated or neutralised, the sulphato complexes themselves undergo hydrolysis to form a mixed sulphato-hydroxyl iron (III) species.

The reaction is as follows:

$2FeSO_4^+ + 2H_2O \rightarrow Fe_2(OH)_2SO_4^{2+} + H_2SO_4$ **Equation 2.12**

Direct experimental evidence for a mixed species is not extensive. The hydrolysis behaviour of Fe(III) sulphate solutions is approximately the same as uncomplexed Fe(III) solutions and the sulphate-hydroxyl dimer, $Fe_2(OH)_2(SO4)_2$, is the prevalent species.

Hydrolysis of sulphate - Fe^{3+} solutions is expressed by the following equations:

$Fe_2(SO_4)_3 + 3H_2O \rightarrow Fe_2(OH)_3(SO_4)_{\frac{3}{2}} + \frac{3}{2} H_2SO_4$ **Equation 2.13**

$\frac{3}{2} Fe_2(SO_4)_3 + 2H_2O \rightarrow Fe_3(OH)_2(SO_4)_{\frac{7}{2}} + H_2SO_4$ **Equation 2.14**

These complexes differ substantially from those where complex anions are not present.

2.1.3.2. Precipitation pathways

(a) Thermodynamic data

According to Hayes (1993), the most widely used method of removing impurities, such as iron, is by controlled changes in the pH. Figure 2.3 summarises the thermodynamic data for the precipitation of ferric and ferrous ion as a function of pH and concentration. The diagrams may also be used to estimate the theoretical solubility of the ions in equilibrium with the metal hydroxide at a given pH. For example, at pH 2 the solubility of Fe^{3+} in the solution is 10^{-3}M. Thus, at pH 2, Fe(III) precipitates as an hydroxide and 10^{-3} M Fe^{3+} ions remain in solution. Although not mentioned by the author, the opposite will also be true; at pH 2 and 25^{o}C iron(III) hydroxide will only precipitate if the theoretical ferric ion concentration equals or exceeds 10^{-3}M. It is important to note that Fe(II) starts to precipitate at approximately pH 5.5. However, Cigan et al. (1980) is of the opinion that Fe(II) precipitation is only considered at pH 7-8.

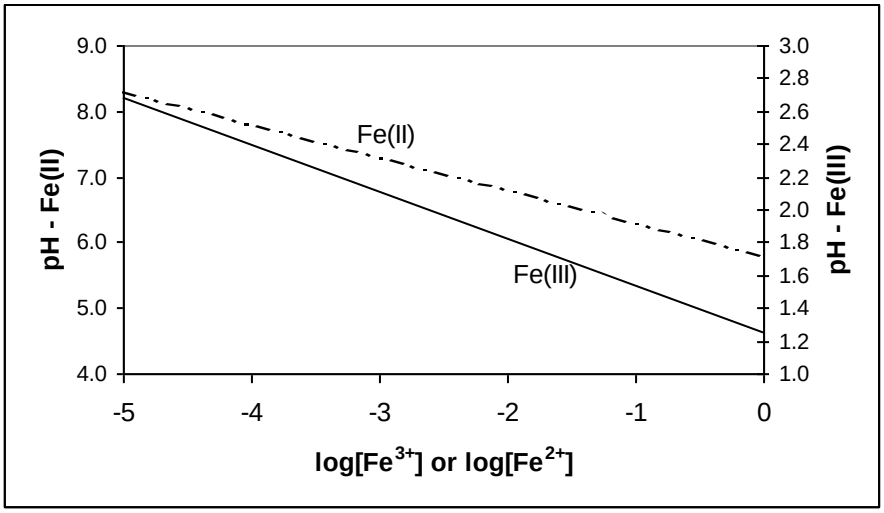

Figure 2.3: The theoretical iron hydroxide diagram at 25°C (Hayes, 1993).

(b) Formation of ferric ion hydroxyl complexes

The iron complexes described by Cigan et al. (1980) in Paragraph 2.1.3.1 – *Iron species in solution*, are true solution species, which attain equilibrium in their surroundings in a matter of seconds. Such species do not themselves appear to precipitate although they form polymers, which eventually lead to iron precipitation. The mechanism by which a soluble entity is transformed into a solid precipitate is very complex and not all the steps are well understood. As mentioned before, the addition of ferric ion to an aqueous sulphate system can result in the rapid formation of hydroxyl complexes:

$$Fe^{3+} + H_2O \rightarrow Fe(OH)^{2+} + H^+ \qquad \textbf{Equation 2.4}$$

$$2Fe^{3+} + 2H_2O \rightarrow Fe_2(OH)_2{}^{4+} + 2H^+ \qquad \textbf{Equation 2.5}$$

(c) Formation of ion polymers in an aqueous sulphate medium

These hydroxyl species can also contain sulphate, bisulphate or sulphate-bisulphate ligands as mentioned in Paragraph 2.1.3.1 – *Iron species in solution*. Such iron solutions undergo slow reactions with the aqueous environment that can continue for several days. During this period the pH of the solution falls gradually and the colour changes from yellow to intense reddish brown; the solution begins to scatter light, indicating the presence of small colloidal particles. The rate at which such changes occur depends on temperature, Fe^{3+}/OH^- ratio, pH, iron concentration, ionic strength as well as the specific anions and cations present. Reactions that take days at 25°C can occur in a few hours at

elevated temperatures and suitable pH. The above changes seem to be associated with the formation of small polymers:

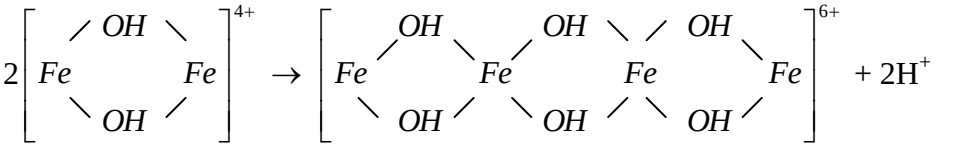

A **B** **Equation 2.15**

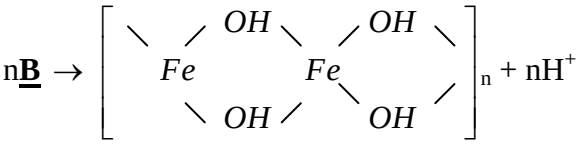

C **Equation 2.16**

The reactions are reversible although the rates of acid dissolution of polymers are very slow. Larger polymers are progressively more inert. Although the polymers are shown as Fe-OH species, they include significant amounts of the anions present in the solution. The critical step in the precipitation of crystalline iron compounds seems to be the growth of the small polymers into larger polymer units, which become the immediate precursors of precipitation.

Cigan et al. (1980) also provides valuable information on the precipitation of iron (III) in iron sulphate media, although the specific role of the SO_4^{2-} ion is not well defined by them. The polymer growth process can occur in a sulphate media by at least three pathways, which are polymer formation, hematite and goethite particle formation, and jarosite formation.

(d) Formation of iron polymers in aqueous sulphate media when the pH is rapidly increased

If the pH of the solution is rapidly increased, thereby raising the OH/Fe^{3+} ratio, continued growth of the Fe-OH chains occurs because the hydroxyl ions neutralise the acid produced during polymerisation. The reaction is as follows:

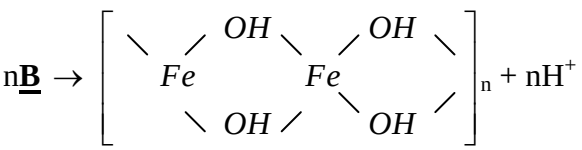

Equation 2.17

$$H^+ + OH^- \rightarrow H_2O$$ **Equation 2.18**

The lengthy polymer chains become cross linked via hydroxyl bridges and large iron hydroxide gel colloids are formed that still contain some coordinated sulphate and appreciable bound water.

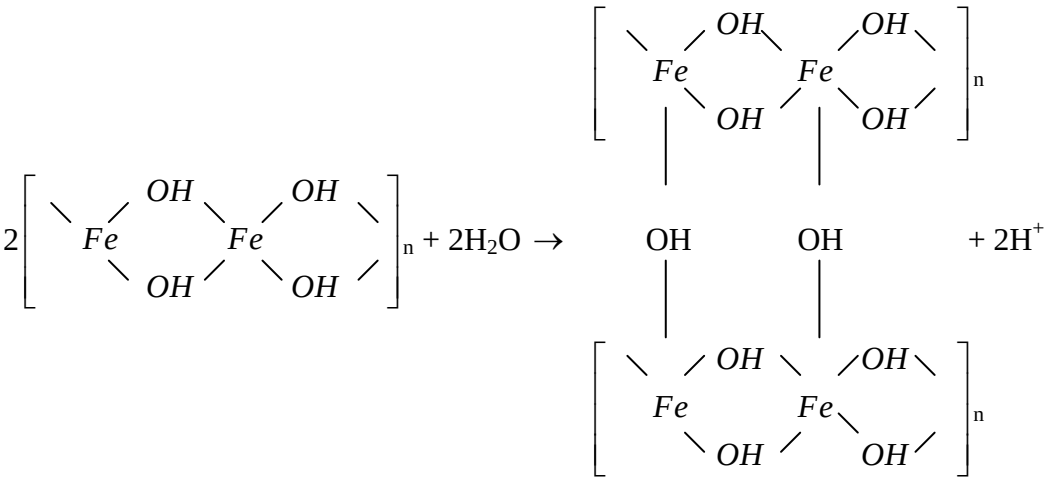

Equation 2.19

Coagulation of the large gel colloids by OH^- or other anions leads to massive gel precipitation. Such a process is nearly temperature independent in contrast with the other precipitation processes, which are strongly temperature dependent. This gel precipitation occurs when a ferric sulphate solution is simply neutralised with excess base and is clearly undesirable due to the poor filtering and settling properties of these iron gels. Gel formation is promoted by the presence of excess base, the rapid addition of a base, poor agitation and low temperatures that prevent the formation of oxygen (as opposed to hydroxyl) bridges (Cigan et al., 1980). According to Hayes (1993) high temperatures, controlled additions of a base and good agitation can result in the formation of discrete goethite, magnetite or hematite crystals.

If the quantity of base is insufficient to cause immediate gel formation, but is still moderately high, oxolation (formation of –O- bridges) can occur.

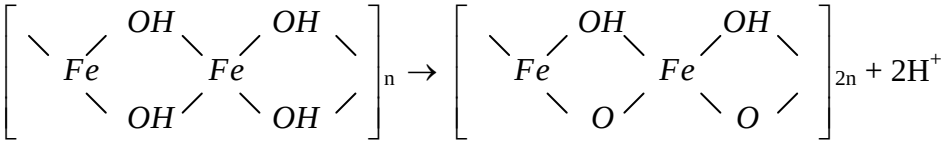

Equation 2.20

The presence of moderate base concentrations is required to neutralise the acid produced in Equation 2.20 and to encourage further polymer growth. The tolerance of the oxolation reaction to acid

increases with increasing temperature, and Fe_2O_3 can be precipitated at 200^oC in the presence of large amounts of acid.

(e) Formation of goethite, hematite and jarosite

The oxolated structure is the precursor of goethite and hematite precipitation, with growth likely to occur with the addition of low molecular weight species such as $Fe(OH)_2^+$ or $Fe_2(OH)_2^{4+}$ to the polymer unit. The large polymers formed by the oxolation process are of colloidal size and appear to be fully or partly crystalline. These polymers form quickly, but dissolve slowly in acids once formed.

The large polymers grow into crystallites and eventually agglomerate into coarse precipitate particles, which settle rapidly as FeOOH (e.g. goethite). Hematite is precipitated by a different mechanism since it tends to form distinct crystals as opposed to agglomerated particles. The precipitation of crystalline jarosite or other basic iron sulphates, such as $FeSO_4$.OH, occurs by yet another reaction pathway, which according to Cigan et al. (1980) is not well defined. Since jarosite tends to be an acidic species, it is assumed that protons play an important role in the opening of polymer chains. Refer to Paragraph 2.1.2 – *Iron hydr(oxide)* for a detailed discussion on the formation of goethite, hematite and jarosite.

(f) The formation of iron(IIII) hydroxide by the rapid addition of ammonia

The book of Weiser (1939) provides a very important discussion on the precipitate formed by rapid neutralisation. He describes the precipitate that forms when ammonia or other basic solutions are added rapidly to an iron (III) solution at room temperature – amorphous ferric hydroxide forms.

Weiser and Milligan (1939) mention that the terms hydroxide and hydrous oxide are often used more or less synonymously in literature. To be more theoretically correct, a metal hydroxide has a definite composition corresponding to the chemical formula, such as $Fe(OH)_3$ and $Al(OH)_3$. Precipitates of quadrivalent, trivalent and many divalent metal hydroxides are never obtained as such, but present themselves in the form of highly-voluminous hydrous oxides. Thus, the precipitate ferric hydroxide does not actually exist and the precipitate should rather be referred to as hydrous ferric oxide. These precipitates have no definite stoichiometric composition, but consist of metal oxide or hydroxide with variable amounts of water. The latter may be bound partially chemically and partially physically (adsorption). The total amount of water held by the precipitate depends upon the manner of precipitation and on ageing before filtration.

The ferric hydroxide, or rather hydrous ferric oxide, that forms after rapid addition of ammonia (see Equation 2.17), becomes more or less crystalline (submicroscopically) when ageing occurs.

Depending on conditions, α-FeOOH (goethite) and α-Fe_2O_3 (hematite) are preferentially formed. Under special ageing conditions, β- FeOOH and γ-FeOOH (lepidocrocite) are formed. Precipitation from a hot solution produces a precipitate showing an X-ray diffraction pattern of α-Fe_2O_3, hematite (Weiser and Milligan, 1939). Weiser (1939) also reported solubility in terms of the solubility constant, K_{sp}. A freshly formed hydrous ferric oxide precipitate may have a K_{sp} value as large as 10^{-38} at room temperature. On ageing, the solubility of the precipitate decreases with an increase in particle size so that the K_{sp} may decrease to 10^{-39}. The K_{sp} of α-Fe_2O_3 is $10^{-42.7}$. The intrinsic solubility of hydrous ferric oxide precipitate is extremely small (< $2x10^{-9}$M). Errors owing to incomplete precipitation and soluble loss of iron in washing will be evidently negligible.

Due to the very low solubility of the hydrous oxide precipitate, the relative super saturation during precipitation will be very great and the precipitate will have a tremendous surface development. Even on ageing, the size of the particles increase slowly. Hydrous ferric oxide is a typical example of a flocculated colloid. The primary particles agglomerate to large aggregates that retain much absorbed water (see Equation 2.19). The coagulation of a colloidal precipitate, and especially the agglomeration of the primary particles, is aided enormously by raising the temperature of the solution.

According to Weiser (1939) hydrous ferric oxide is converted into ferric oxide when it is intensely heated (800-1000^{0}C). Although not mentioned by the author, hematite is probably formed. Formation of ferric oxide can be explained by the following reaction:

$$Fe_2O_3.xH_2O \rightarrow Fe_2O_3 + xH_2O$$ **Equation 2.21**

The igniting of the precipitate should be made under good oxidizing conditions, especially during the burning of the paper filter as ferric oxide may otherwise be partially reduced by carbon or reducing gases to magnetic oxide, Fe_3O_4, or even to metal. These reduction products can be converted back to ferric oxide by the continued heating of the residue with free access of air, although the reoxidation may be slow if much magnetic oxide has been formed. When heated intensely, ferric oxide decomposes into magnetic oxide and oxygen:

$$6Fe_2O_3 \rightarrow 4Fe_3O_4 + O_2$$ **Equation 2.22**

Fortunately a very high temperature must be attained before this decomposition becomes analytically significant. Baxter and Hoover (1912) found that a sample of pure ferric oxide heated at approximately 1100^{o}C formed only about 0.12% Fe_3O_4. The resulting magnetic oxide forms a solid

solution with the ferric oxide. Ferric oxide is rendered water-free by ignition at 1000^0C. Ferric oxide can be converted to analytically significant masses of magnetic iron oxide at temperatures above 1200^0C.

2.1.4. THERMODYNAMIC MODELLING OF THE PRECIPITATION OF IRON HYDR(OXIDE) COMPLEXES AS A FUNCTION OF PH

This section explains the construction of thermodynamic equilibriums graphs of soluble iron (III) and iron (II) systems in equilibrium with FeOOH and $Fe(OH)_2$, respectively.

2.1.4.1. Iron (III)/goethite equilibrium

$Fe(OH)_3$ is not stable and therefore it does not exist in nature (Welham et al., 2000). Raising the pH of acidic iron (III) solutions results in the precipitation of either goethite or akaganèite (Schwertmann and Cornell, 1991; Cornell and Schwertmann, 1994).

(a) Phase equilibriums equations

Goethite was chosen by Welham et al. (2000) as the solid iron (III) species to formulate the phase equilibriums as follows:

$Fe^{3+} + 2H_2O = FeOOH + 3H^+$ **Equation 2.23**

$FeOH^{2+} + H_2O = FeOOH + 2H^+$ **Equation 2.24**

$Fe(OH)_2^+ = FeOOH + H^+$ **Equation 2.25**

$Fe(OH)_3 = FeOOH + H_2O$ **Equation 2.26**

$Fe(OH)_4^- + H^+ = FeOOH + 2H_2O$ **Equation 2.27**

(b) Equilibrium constant

The equilibrium constant, K_n, can be calculated using the free energies of reaction:

$$\Delta G = -2.303Rt\log(K_n) \quad \textbf{Equation 2.28}$$

At equilibrium:

$$K_1 = [FeOOH][H^+]^3/[Fe^{3+}] \quad \textbf{Equation 2.29}$$

$$K_2 = [FeOOH][H^+]^2/[FeOH^{2+}] \quad \textbf{Equation 2.30}$$

$$K_3 = [FeOOH][H^+]/[Fe(OH)_2^+] \quad \textbf{Equation 2.31}$$

$$K_4 = [FeOOH]/[Fe(OH)_3] \quad \textbf{Equation 2.32}$$

$$K_5 = [FeOOH]/\{[Fe(OH)_4^-][H^+]\} \quad \textbf{Equation 2.33}$$

Taking logarithms and rearranging:

$$\text{Log}[Fe^{3+}] = -\log K_1 + \log[FeOOH] - 3pH \quad \textbf{Equation 2.34}$$

$$\text{Log}[FeOH^{2+}] = -\log K_2 + \log[FeOOH] - 2pH \quad \textbf{Equation 2.35}$$

$$\text{Log}[Fe(OH)_2^+] = -\log K_3 + \log[FeOOH] - pH \quad \textbf{Equation 2.36}$$

$$\text{Log}[Fe(OH)_3] = -\log K_4 + \log[FeOOH] \quad \textbf{Equation 2.37}$$

$$\text{Log}[Fe(OH)_4^-] = -\log K_5 + \log[FeOOH] + pH \quad \textbf{Equation 2.38}$$

The activity of the solid phase is considered to be unity and the log[FeOOH] terms therefore become zero.

The total soluble iron (III) in solution is simply the sum of the concentrations of the individual iron species:

$$[Fe^{III}] = [Fe^{3+}] + [FeOH^{2+}] + [Fe(OH)_2^{+}] + [Fe(OH)_3] + [Fe(OH)_4^{-}]$$

Equation 2.39

(c) Total soluble iron

Equations 2.34 to 2.38 can be used to calculate the total soluble iron (Fe^{III}) as a function of pH.

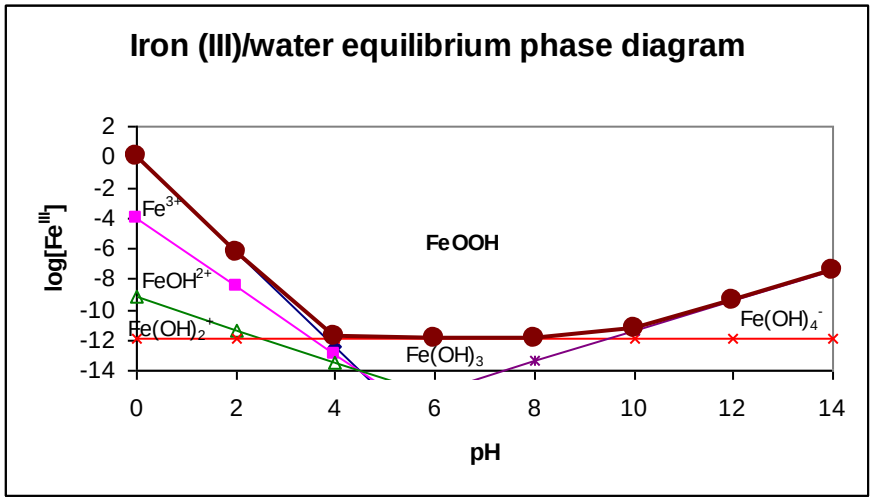

Figure 2.4: Activity – pH diagram for the soluble iron (III)/water system in equilibrium with FeOOH, goethite. The thick line is the sum of the activities of all the iron species and represents the total predicted activity for iron (III) in equilibrium with goethite. Data points were obtained directly from graphs provided by Welham et al., 2000.

Three major equilibriums control the solubility of goethite (refer to Figure 2.4). They are:

(1) Fe^{3+} at low pH;
(2) $Fe(OH)_3$ where disposal of acid ferric solutions by neutralisation is typically carried out, and
(3) $Fe(OH)_4^{-}$ at high pH.

The minimum predicted activity of iron (III) in solution is approximately constant between 5 and 9, which indicates that goethite is stable between these pH ranges. The iron (III)/water equilibrium system forms the basis of equilibrium systems. In systems where a complexion ligand is present, the formation of solution species (e.g. $FeSO_4^{+}$, $FeCl_2^{+}$) and changes in speciation with pH of the ligands themselves (i.e. H_2SO_4, HSO_4^{-} and SO_4^{2-}) also need to be accounted for in the equilibrium calculations. These additional equilibriums lead to solubility, which are functions of both pH and total ligand activity (Welham et al., 2000).

(d) Effect of chloride or sulphate ions

Welham et al. (2000) established that the addition of chloride or sulphate ions to the system only have a slight impact on the solubility of goethite. Neither have a significant effect until near unity activity of chloride or sulphate ions is attained. The effect of chloride is smaller than sulphur (VI) at low pH (pH < 3), but with increasing pH the effect of sulphur diminishes. This effect is due to the change in speciation of sulphur. Below pH 1.99, HSO_4^- is predominant and above pH 1.99, SO_4^{2-} predominates. Clearly the effect of HSO_4^- on the solubility of goethite is greater than SO_4^{2-}.

Despite there being an increase in solution activity due to the formation of complexes, the magnitude of the increase is very small compared to the change due to pH. The presence of these ligands does not greatly affect the pH range or magnitude of the minimum solubility, which is controlled by aqueous $Fe(OH)_3$. Typically, precipitation is carried out until the remaining solution is of neutral pH (5-9). Consequently, there is little practical effect of either chloride or sulphur (VI) anions on the precipitation of iron (III) from solution (Welham et al., 2000).

2.1.4.2. Iron (II)/$Fe(OH)_2$ equilibrium

The total soluble ferrous ion (II) in solution can also be determined as a function of pH by making use of equilibriums between $Fe(OH)_2$ precipitate and the soluble iron (II) species (see Figure 2.5).

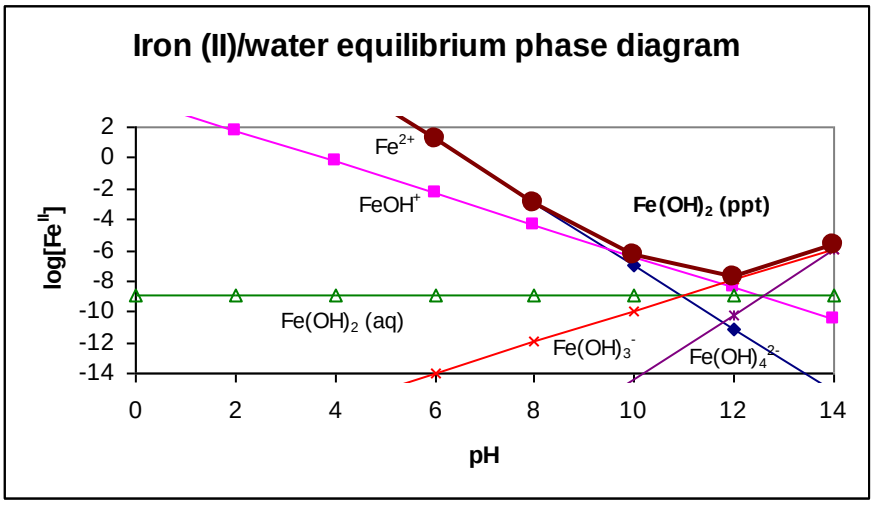

Figure 2.5: Activity – pH diagram for the soluble iron (II)/water system in equilibrium with $Fe(OH)_2$. The thick line is the sum of the activities of all the iron species and represents the total predicted activity for iron (II) in equilibrium with $Fe(OH)_2$ (Welham et al., 2000).

It is clear from Figure 2.5 that the minimum activity of Fe (II) is approximately 10^{-8} at pH 11.7. This activity is controlled over the whole pH range by three main species, which are:

(1) Fe^{2+}
(2) $FeOH^{+}$ and
(3) $Fe(OH)_3^{-}$

Figure 2.5 indicates that Fe(II) starts precipitating at a relatively low pH, but with a very high solubility, which implies that $Fe(OH)_2$ precipitate is not stable at near neutral pH. The solubility of $Fe(OH)_2$ precipitate decreases to a minimum at pH 11.7 and increases thereafter. The relatively narrow pH range (pH ~ 11.7) of minimum solubility indicates that $Fe(OH)_2$ is not very stable and fluctuations in the local pH would increase the solubility significantly.

2.2. ADSORPTION AND DESORPTION OF IRON COMPLEXES TO MINERAL SURFACES

2.2.1. ADSORPTION THEORY

(a) Adsorption of anions and cations to the surface of hydrous oxide

Weiser (1939) provides an interesting insight into the adsorption theory. According to the author, hydrous ferric oxide (and other hydrous oxides) exhibits pronounced adsorptive properties due to its large surface development as discussed in Paragraph 2.1.3.2 – *Precipitation pathways*.

There will primarily be anion adsorption from solutions that are acidic. The surface of the hydrous oxide attracts the protons (hydrogen ions) and consequently an equivalent amount of anion (A^-) is adsorbed, as expressed by the following equation:

$$\begin{array}{l} OH^- \\ Fe^{3+}OH^- \\ OH^- \end{array} + H^+ + A^- \rightarrow \begin{array}{l} OH^- \\ Fe^{3+}OH^- \\ OH_2 \end{array} \Big| A^- \qquad \textbf{Equation 2.40}$$

(surface) (acid in solution) (surface)

The absorbability of the anions increases with increasing charge. For example, sulphate, chromate, and oxalate adsorb much more strongly than chloride and nitrate. In addition, the adsorption increases with increasing hydrogen-ion concentration. Therefore a co-precipitation of anions can be expected if

the precipitate is formed in an acid medium. When adding ammonion hydroxide slowly to a solution of ferric salt, a co-precipitation of anions occurs because the solution remains acidic as a result of the strong hydrolysis of the ferric ions – as long as some of these remain in solution. The co-precipitated anions are more or less rapidly given off again in the presence of an excess of ammonia.

Hydrous ferric oxide tends to adsorb hydroxyl ions in alkaline media (e.g. excess ammonia), with the result that an equivalent amount of cation (B^+) is carried down as shown by the following equation:

$$\begin{array}{c} OH^- \\ Fe^{3+}OH^- \\ OH^- \end{array} + OH^- + B^+ \rightarrow \begin{array}{c} OH^- \\ Fe^{3+}OH^- \\ OH^- \\ OH^- \end{array} \Big| B^+ \qquad \textbf{Equation 2.41}$$

(surface) (basis in solution) (surface)

Therefore, in precipitation from alkaline media, there may be a pronounced co-precipitation of cations. The absorbability of the cations increases with decreasing solubility of their hydroxides and with their charge. Thus cations such as calcium, magnesium, copper ($Cu(NH_3)_4^{2+}$), zinc ($Zn(NH_3)_4^{2+}$) are much more strongly adsorbed and co-precipitated than sodium, potassium and ammonium. A large excess of ammonium ion decreases the adsorption and co-precipitation of other cations. There is a competition between the ammonium and other cations to be adsorbed; increase of the ammonium concentration therefore favours the adsorption of the ammonium ions at the cost of the other cations (Weiser, 1939).

It is clear from the discussion of Weiser (1939) that hydrous ferric oxide adsorbs anions and cations depending on the acidity of the water. Therefore, the surface charge of the iron precipitates is controlled by the acidity, and thus pH, of the solution.

(b) Adsorption of hematite to quartz and galena particles

Bandini et al. (2001) investigated the adsorption of colloidal iron oxide (hematite) on 25-38 μm quartz and galena (PbS) particles. His study is of high importance since it could provide an explanation for the adsorpsion of precipitated iron on heavy mineral sand particles. Previous investigations (Learmont and Iwasaki, 1984; Gaudini et al., 1960; Fuerstenau et al., 1958; and Parsonage, 1985) have suggested an electrostatic mechanism for iron oxide slime-particle interaction. Surface and solution studies on iron (III) treated galena particles (Prestidge et al., 1995) have shown

that the nature and concentration of absorbed iron (III) species are pH dependent and the mechanism of interaction is controlled by the surface chemistry of galena as well as by the iron (III) speciation.

Bandini et al. (2001) studied complementary iron oxide particle adsorption and desorption on quartz particles to further elucidate the mechanisms of iron oxide slime coating, and to characterise the strength of their attachment and ease of removal. Both physical and chemical methods for removing adsorbed slimes were investigated. Colloidal iron oxide particles (hematite) were prepared by thermal hydrolysis (at 100^{o}C for 7 days) of an acidified (10^{-3}M HCl) solution at $3.15x10^{-2}$M iron (III) chloride. Electrophoretic mobility of colloidal hematite particles was determined using laser Doppler electrophoresis (Malvern zetasizer). Electrophoretic mobility of quartz particles in the presence and absence of adsorbed iron oxide slimes were determined using micro electrophoresis (Rank Brothers). Electrophoretic mobility was determined whilst incrementally reducing the pH by 20-minute equilibration time between measurements; these were converted to zeta potentials using the Smoluchoski equation (Hunter, 1981). The concentration of colloidal Fe_2O_3 (hematite) particles in solution was determined from absorbance measurements, which were recorded in a 1cm pathlength quartz cell. A linear relationship between the absorbance at 600nm and the concentration of hematite particles was observed.

Particle adsorption measurements were undertaken by combining an accurate known mass of quartz particles to a known volume of Fe_2O_3 dispersion, under conditions of controlled pH and electrolyte concentration. The slurry was agitated with a mechanical stirrer. After various time intervals the stirring was halted for a period of 2 minutes, during which time the quartz particles settled and 5ml of the Fe_2O_3 dispersion was extracted, as well as the absorbance at 600nm monitored. A reduction in the absorbance is related to a decrease in concentration of iron oxide particles, hence the amount may be determined. Particle desorption studies were performed under the influence of shear, sonication and chemical agents (ethyl xanthate, CMC, PEO and Calgon). In the particle desorption investigations, Fe_2O_3 was pre-adsorbed at pH 4 prior to the introduction of chemical and/or physical treatments.

Experimental methodology developed within this investigation has enabled the absorbed amount of iron oxide slimes on quartz particles to be quantitively determined with good precision and reproducibility. The kinetics of the slime coating has been shown to depend on the slime particle concentration, the solution conditions, and the intensity of mixing. It was also found that the iron oxide/galena and iron oxide/quartz adsorption systems have similar thermodynamic driving forces.

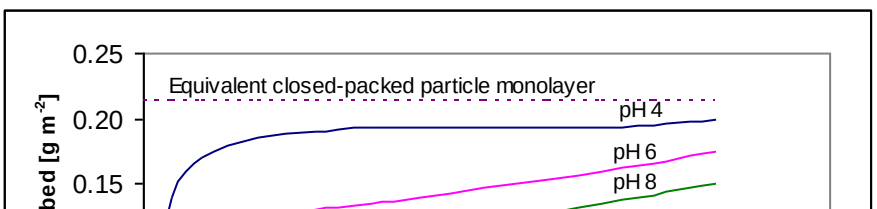

Figure 2.6: Adsorption isotherms form iron oxide (hematite) slimes on galena (PbS) particles (25 to 38 μ m) at pH 4, pH 6, pH 8 and pH 10 in the presence of 10^{-3} M KNO_3 as an inert electrolyte (Bandini et al., 2001).

Adsorption isotherms for Fe_2O_3 slimes on galena (PbS) are given in Figure 2.6. In the pH range 3 to 7, high affinity Fe_2O_3 adsorption is observed and the surface coverage approached for an equivalent closely-packed particle monolayer, calculated to be 0.214 $g.m^{-3}$. In contrast, in mildly alkaline solutions, the Fe_2O_3 particle adsorption isotherms are of lower affinity, with plateau surface coverage significantly less than an equivalent closely-packed particle monolayer.

To reconcile the thermodynamics of iron oxide slime coating it is important to compare the surface-electrical properties of iron oxide and galena. The common intersection point on experimental potentiometric acid-base titration curves, corresponding to different concentrations of basic electrolyte, is defined as the pH of the point-of-zero net proton charge. In the case of any other interacting ions, the common intersection point is defined as the point-of-zero-charge (PZC) if this point corresponds to the zero surface charge (Gaboriaud and Ehrhardt, 2002). Zeta potential versus pH plots for hematite and galena particles are given in Figure 2.7.

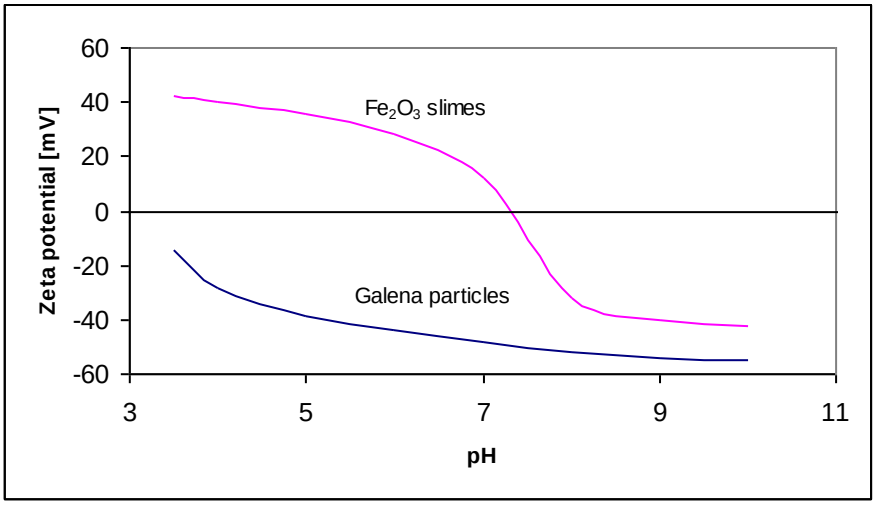

Figure 2.7: Zeta potential versus pH for iron oxide (hematite) slimes and 25 to 38 μm galena (PbS) particles in the presence of 10^{-3}M KNO_3 as an inert electrolyte (Bandini et al., 2001).

The isoelectric points (IEP) of iron oxide and galena are at approximately pH 7 and 2, respectively. For galena, the IEP value and zeta potential versus pH curve is characteristic of unoxidised galena particle surfaces and is similar to quartz. In general, zeta potentials of quartz are approximately 30% greater than those for galena under equivalent condition.

In mildly acidic solutions, iron oxide slimes are positively charged and the galena surfaces negatively charged, hence the extensive slime coating observed may be considered to occur as a result of attractive electrostatic forces. For galena, iron oxide slimes coating is also considered to be due to the heterogeneous and time-dependent surface chemistry of galena and iron oxide. This phenomenon can be explained as follows:

- Galena particle surfaces undergo a series of oxidation reactions in aqueous solution, resulting in surface groups with different surface electrical properties to unoxidised galena (Fornsiero et al., 1994). Localised areas on the galena surface may form which are positively charged in a mildly alkaline pH range and electrostaticly attract iron oxide slimes.
- Hematite has a finite solubility; ionic ion species may therefore enter the solution and interact with galena particle surfaces (Prestidge et al., 1995), altering their surface electrical properties.
- The hematite surface is chemically heterogeneous, e.g. at pH 8, even though the zeta potential is negative, positively charged surface groups are present which may interact with galena. It should be recognised that zeta potentials are representative of the average electrical properties of a particle (Prestidge et al., 1995).

(c) Electrokinetic potential of goethite, goethite-hematite mixture and other iron hydr(oxides)

Kosmulski et al. (2003) determined the electrokinetic potential of synthetically prepared pure goethite (goethite 25) and a goethite-hematite mixture (goethite 140). Potentiometric titration was carried out under a nitrogen atmosphere using NaOH as titrant. Titrations were always started at acidic pH to facilitate removal of CO_2 from the system. The electrokinetic potential was determined with Acustosizer (Matec) and DT-1200 (Dispersion Technology) instruments at 10% mass fraction of precipitate. The results obtained at high ionic strengths were corrected for the electrolyte background. The dispersions were not insulated from atmospheric CO_2 during the electrokinetic measurements. The electrokinetic and potentiometric titrations were carried out at 25^{o}C. $NaNO_3$ and NaI were used to establish a constant ionic strength (See Figure 2.8 - 2.11).

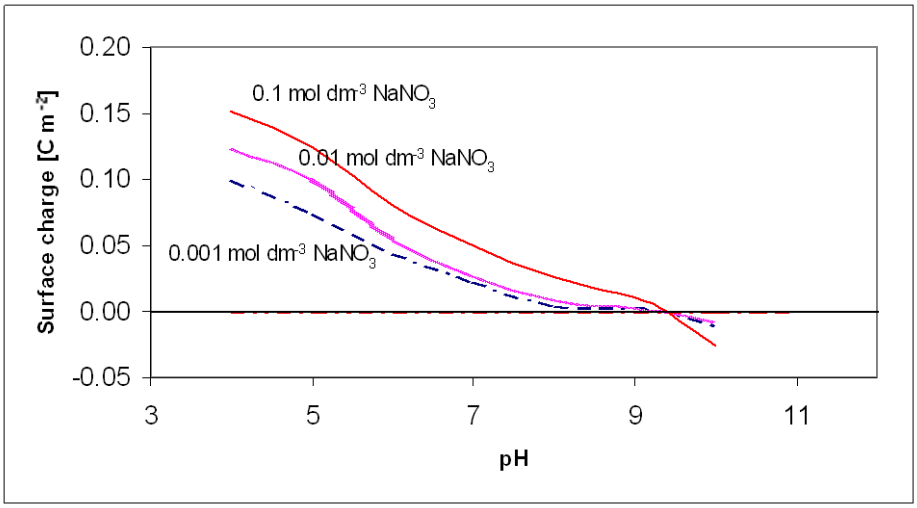

Figure 2.8: Surface charge density versus pH for pure goethite (goethite 25). $NaNO_3$ was used as a basic electrolyte solution (Kosmulski et al., 2003).

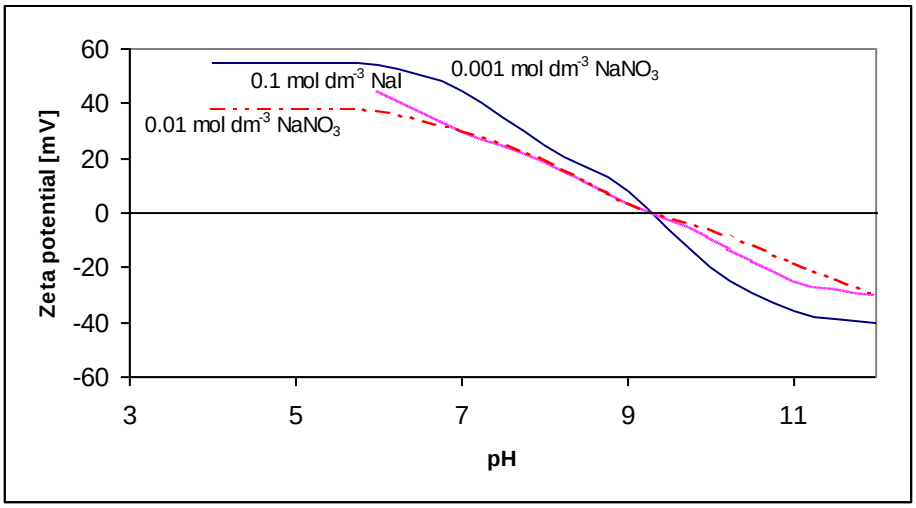

Figure 2.9: Zeta potential versus pH for pure goethite (goethite 25). $NaNO_3$ and NaI were used as basic electrolyte solutions. The electrokinetic potential, except for the 0.01 mol dm^{-3} $NaNO_3$ solution, was measured with an Acustosizer instrument. The DT-1200 instrument was used for the 0.01 mol dm^{-3} solution (Kosmulski et al., 2003).

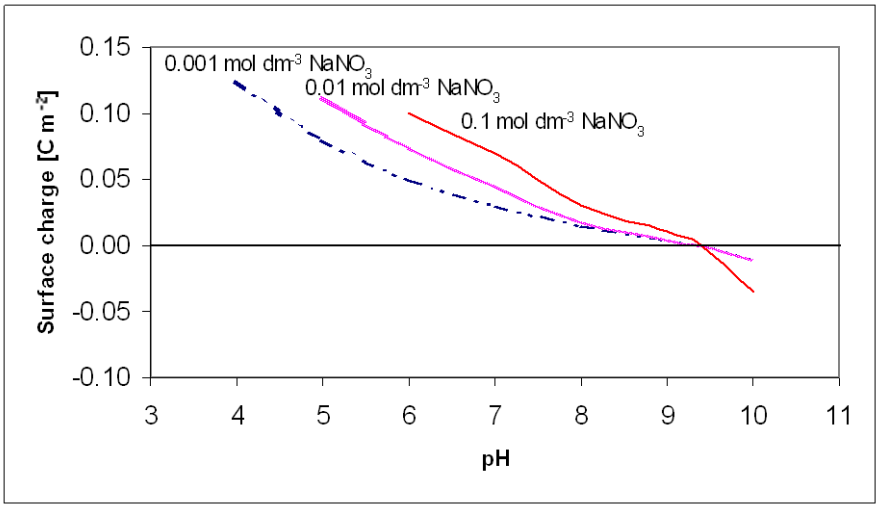

Figure 2.10: Surface charge density versus pH for the synthetic goethite-hematite composition (goethite 140). $NaNO_3$ was used as the basic electrolyte solution (Kosmulski et al., 2003).

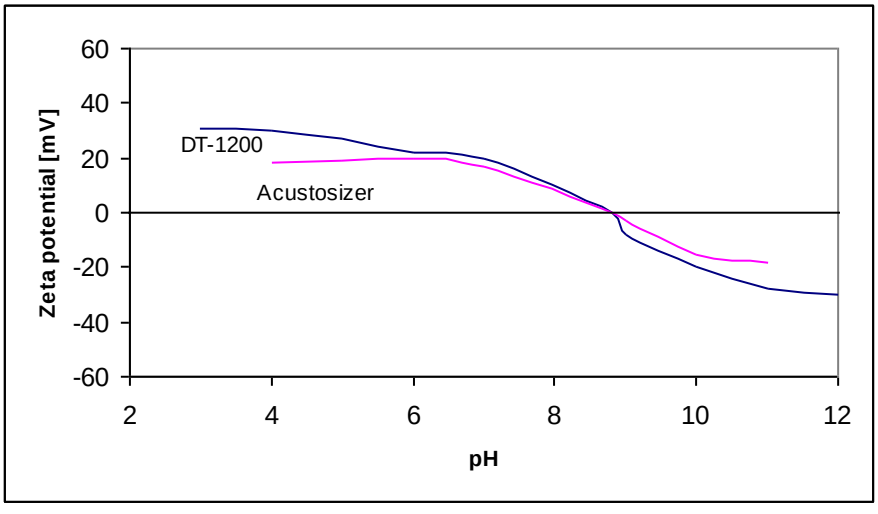

Figure 2.11: Zeta potential versus pH for the goethite-hematite mixture (goethite 140) 0.01 mol dm^{-3} $NaNO_3$ was used as basic electrolyte solution. The electrokinetic potential was measured with a DT-1200 and Acustosizer instrument (Kosmulski et al., 2003).

Kosmulski et al. (2003) confirmed that iron hydr(oxides) substantially contribute to the adsorption of toxic elements in natural mineral assemblies, even when the mass fraction of iron hydr(oxides) in these assemblies is relatively low. The affinity of iron hydr(oxides) to anions and cations is pH-dependent, and this can be explained in terms of the pH-dependent surface charging. The surface carries a positive charge at pH below the point of zero charge (PZC) and a negative proton charge at pH above the PZC. This results in electrostatic attraction or repulsion of all ions other than protons, and a change in pH by one or two units can enhance or depress the adsorption of ions by an order of magnitude. Thus, knowledge of the PZC point is of the utmost importance in order to understand the adsorption of ions.

From Figure 2.8 and 2.9 it is clear that the PZC of synthetic pure goethite (goethite 25) is at pH 9.4 as the common intersection point of potentiometric titration curves at different ionic strengths and the isoelectric point (IEP). Petrucci and Harwood (1997) state that at a pH above the IEP, the precipitate has a negative charge, and below the IEP it has a positive charge. For the goethite-hematite composite (goethite 140), the common intersection point (pH 9.4), and the IEP (pH 8.8) do not match (see Figure 2.10 and 2.11). The authors did not provide an explanation for this difference. Average PZC/IEP values do not depend on the degree of hydration (oxide or hydroxide). The PZC and IEP results of Kosmulski et al. are higher than most published results, which according to the authors confirm the allegation that electro acoustic measurements produce a higher IEP than the average IEP obtained by means of classical electrokinetic methods (compare PZC values with Table 2.4).

Table 2.4: A literature survey on the PZC values of iron hydr(oxides) as a function of hydration and the crystalline structure (Kosmulski et al., 2003).

	Entries	Median	Average	Standard deviation
Hematite, synthetic	62	8.1	7.82	1.17
Hematite, natural	7	5.4	5.64	1.56
Fe_2O_3 other than hematite, mixtures of different forms or structure unknown	22	7.2	6.89	1.51
Goethite	66	8.4	8.32	0.89
FeOOH other than goethite, mixtures of different forms or structure unknown	14	7.25	7.27	0.77
Fe(III) hydroxides and hydrous oxides	22	8	7.99	0.69
Total	193	8	7.8	1.23

The results of the literature survey sorted by composition are summarised in Table 2.4. Apparently the effect of the degree of hydration of the sample on the PZC is rather insignificant, namely the average and median PZC for synthetic hematite and iron hydrous oxide and hydroxide are close to the average and median PZC in the entire data set. The average and median PZC for goethite are only slightly higher. The PZC of natural hematite is significantly lower than that of the other species, but this is due to a substantial amount of silica that is found in natural hematite. Although Kosmulski et al. (2003) do not mention the adsorption of iron hydr(oxides) to mineral surfaces, the same opposite charge mechanism is applicable and would result in attraction and adsorption to mineral surfaces as discussed by Bandini et al. (2001). Therefore, the PZC values of Table 2.4 can be used to predict the adsorption of iron hydr(oxides), such as hydrous ferric oxide, to mineral surfaces of opposite charge. For example, hydrous oxides will adsorb to negatively charged surfaces at pH values less than 7.8.

2.2.2. PHYSICAL AND CHEMICAL REMOVAL OF ADSORBED IRON HYDR(OXIDE)

Bandini et al. (2001) has investigated different methods for the removal of adsorbed hematite slimes coatings from the surfaces of both galena and quartz particles. The methods used for hematite slime particle removal include pH control, high shear mixing, sonication, additions of chemical reagents, and combinations of these. Physical and chemical treatment of coated galena particles displaced colloid material (presumably oxidation products) from the galena surfaces. This displaced material entered the solution and increased the absorbance of the solution, which affected the accuracy of the results negatively. Quartz was rather used as a model for deslimed galena, since it showed similar surface electrical properties and slime particle adsorption characteristics as for galena. Fe_2O_3 slime removal studies on quartz were considered to be more quantitive than using galena.

The use of pH control alone was ineffective in removing iron oxide slime coatings from galena or quartz (compare graphs (b) of Figure 2.12 and 2.13). However, on coupling pH control with high shear mixing or sonication, iron oxide slime removal is relatively rapid and complete. It is also worth mentioning that the effect of acidic solutions (pH << 4) was not investigated.

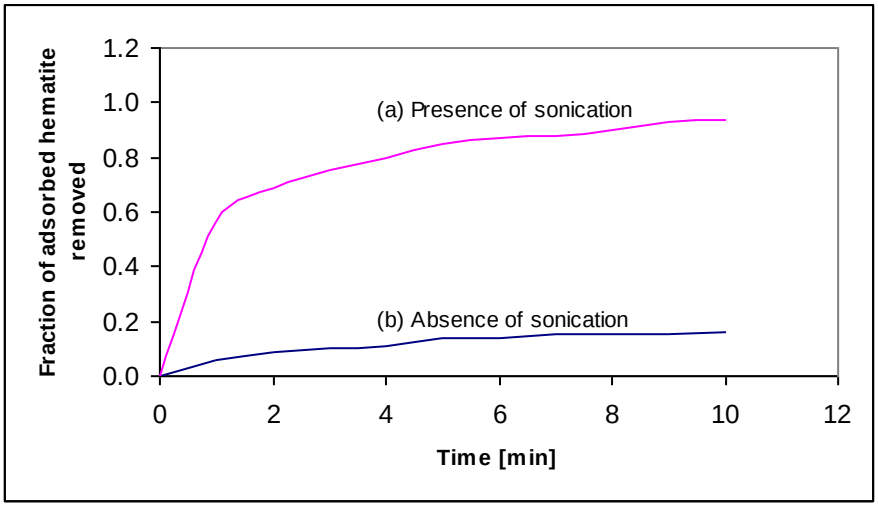

Figure 2.12: The fraction of hematite particles removed from 25 to 38 μm quartz particles surfaces by pH control (pH 10), in the absence and presence of sonication using a 150 watt sonic bath (Bandini et al., 2001).

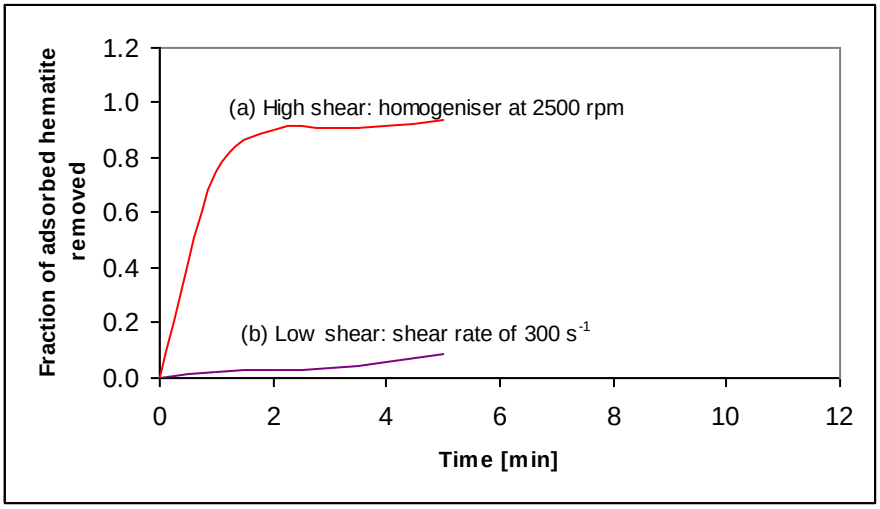

Figure 2.13: The fraction of hematite particles removed from 25 to 38 μm quartz particles surfaces at pH 4 under low and high shear conditions: shear shell operating at 300 s^{-1} and in the presence of a homogeniser operating at 2500 rpm (Bandini et al., 2001).

By increasing the pH, both iron oxide slime and galena/quartz particles become negatively charged (see Figure 2.7). However, there is still an energy barrier to overcome for physically slime detachment; this is provided by sonication in the case shown in Figure 2.12. In Figure 2.13 the influence of shear on the removal of iron oxide slimes is further exemplified. A shear shell operating in laminar flow at a shear rate of 300 s^{-1} proved relatively ineffective at slime particle removal, whereas a high-speed blender at 2500 rpm removed more than 90% of the adsorbed slime in 2 minutes.

The performance of both a non-ionic and ionic chemical reagent in the removal of iron oxide (hematite) slimes is shown in Figure 2.14. The reagents are: Calgon (a polyphosphate, supplied by Albright and Wilson Group, Australia), CMC (carboxymethyl cellulose, supplied by the Tall-Bennett Group, Australia) and PEO-PPO-PEO (polyethylene oxide-polypropylene oxide-polyethylene oxide, a non-ionic copolymer; F108, supplied by Orica Pty. Ltd., Australia).

The non-ionic PEO-PPO-PEO copolymer showed no surface cleaning properties in the sense that it did not detach adsorbed iron oxide slimes. In contrast, the polyphosphate reagents CMC and Calgon removed iron oxide slime coatings from quartz. The polyphosphate reagent Calgon is more highly charged with a lower molecular weight than CMC and is more effective at removing iron oxide slime coatings. These findings give further evidence that electrical interaction forces control slime adsorption of hematite slimes to quartz (and galena) surfaces. Small and highly charged reagents can adsorb to the surface of the iron oxide slimes and effectively reverse their surface charge and zeta potential from positive to negative, hence introducing a repulsive force to overcome the original attraction between the slime and the host surface.

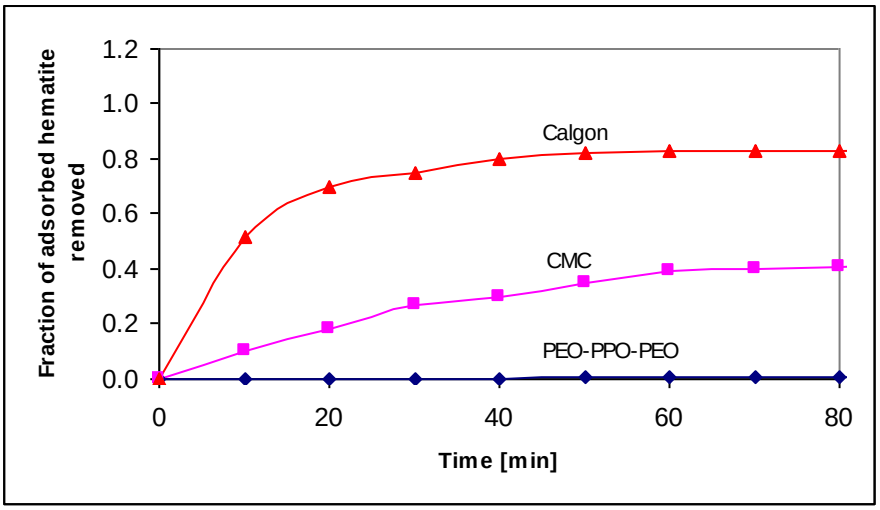

Figure 2.14: The fraction of iron oxide (hematite) slimes particles detached from 25 to 38 μm quartz particles at pH 4, by the addition of chemical dispersants (200 ppm): Calgon, CMC and PEO-PPO-PEO (Bandini et. al, 2001).

Figure 2.15 shows the slime desorption kinetics in the presence of both a chemical reagent and sonication. There is clearly a synergistic effect when adding these surface-cleaning agents in the presence of high-level agitation. For example, the rate of adsorbed iron oxide removal in the presence of Calgon is increased by approximately 5 times in the presence of sonication. It is apparent that the optimum performance of chemical dispersants and pH control for slime coating control requires simultaneous control of the shear conditions and reagent addition.

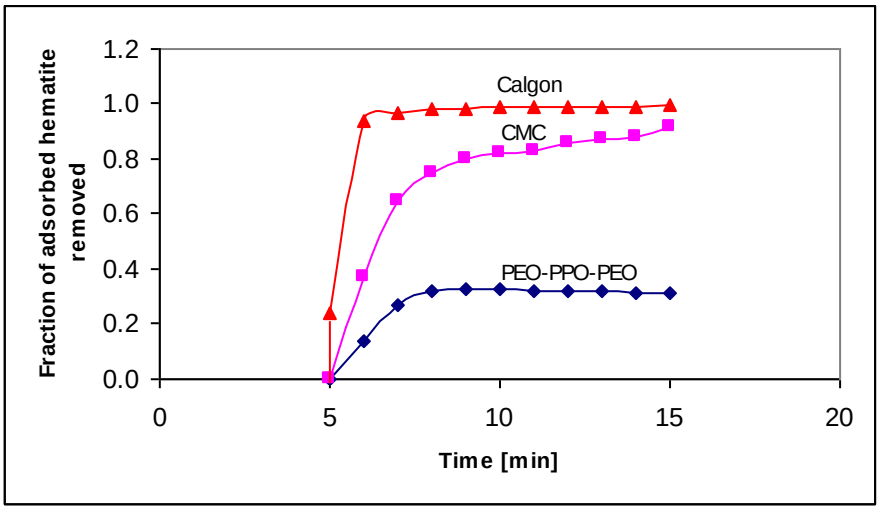

Figure 2.15: The fraction of iron oxide (hematite) slimes particles detached from 25 to 38 μm quartz particles at pH 4, by the addition of 200 ppm Calgon, 200 ppm CMC and 200 ppm PEO-PPO-PEO in the presence of sonication – 150 watt sonic bath (Bandini et. al, 2001).

2.2.3. PROCESS CONSIDERATION FOR THE PREVENTION OR REMOVAL OF IRON ATTACHMENTS

It is clear from the literature studied that coating of mineral particles by iron oxide slimes, such as hydrous ferric oxide and hematite, can either be prevented by pH and temperature control, or removed by chemical and/or physical desorption.

2.2.3.1. Prevention of iron oxide adsorption onto mineral particles

It is clear from literature that iron precipitation (both Fe(II) and Fe(III)) can be prevented by controlling the pH and temperature of the solution in order that these species remain in solution. Keeping the solution at a low pH (< 2) and at ambient temperatures will ensure that the majority of the total iron remains in solution. Effective separation of the solution (rich in dissolved iron) from the mineral particles prior to neutralisation will prevent precipitation of iron hydr(oxides) and adsorption to mineral surfaces.

Veglió et al. (1998) investigated the use of oxalic and sulphuric acid for the leaching of naturally formed Fe_2O_3 coating from the surfaces of quartz minerals. The leaching process was carried out at 90^{o}C for a period of 3-5 hours. A process diagram was developed that involved a solid-liquid separation step directly preceding the leaching vessel. The purpose of this step is to remove the dissolved iron from the quartz particles. The solid-liquid separation step is preceded by a mineral-washing step (reblunge) to dilute the retained leach liquor of the first solid-liquid separation step. Fresh water is used for the washing step. The wash water being generated in the washing step will contain small amounts of iron and needs to be removed from the quartz in a second solid-liquid separation step. The removed water (low iron concentrations) can be recycled back into the process to minimise the overall water consumption.

2.2.3.2. Solid-liquid separation

According to Woollacott and Eric (1994), solid-liquid separation is the most widely used separation technique in hydrometallurgy. In leaching, the separation of the leach liquor from the solids completes the process of extracting a metal from a solid feed material. The solid and solution phases must be separated for re-processing, re-cycling, or discarded.

In many hydrometallurgical processes, incomplete separation of the liquid from the solids is problematic due to the presence of valuables or contaminants in the liquid. To overcome this problem,

the liquid that remains entrained with the solids after a dewatering operation must be replaced by a second liquid that is free of either valuables or contaminants. In filtration, this is done simply by washing the filter cake with a second liquid. In thickening operations, it can be done by a process known as counter-current decantation.

(a) Filtration

In filtration, liquid is removed from a slurry by being drawn through a porous filter medium, i.e. the filter cloth, which prevents the passage of the solid particles. The solids build up on the medium and form a cake. As the cake builds up, it acts as a filtration medium in itself, allowing passage only to the liquid phase. The liquid that passes through the cake and cloth is termed the filtrate. Once a cake has been built up, a significant quantity of liquid remains associated with the solids. This moisture content is reduced significantly if air under pressure is drawn through the cake, producing a relatively dry cake.

The most widely used type of filtration in minerals engineering is vacuum filtration. The principle of this type of filter is to create an effective differential pressure across the filter cloth and cake by the application of a vacuum on the filtrate side of the cloth. There are three stages in filtration, which are the formation of the cake, drying and washing of the cake if washing is required, and discharging of the cake. The way in which these three stages are engineered distinguishes the three major types of vacuum filters. Three different types of equipment are commonly used, namely drum, disk and horizontal-belt filters. On a belt filter, the control of cake formation, drying and cake washing is superior to that in any other vacuum filter.

Figure 2.16 is a schematic diagram of a horizontal belt filter. According to Svarovsky (1985) the top strand of the belt is used for filtration, cake washing and drying, while the bottom return is used for tracking and washing of the cloth. There is appreciable flexibility in the relative areas allocated to filtration, washing and drying. Horizontal belt filters are well suited to either fast or slowly draining solids, especially where washing requirements are critical. Multi-stage counter-current washing can be effectively carried out due to the sharp separation of filtrates. Horizontal belt vacuum filters are classified according to the method employed to support the filter cloth. One common design is typified by a rubber belt mounted in tension. The belt is grooved to provide drainage towards the centre. Covered with the filter cloth, the belt has raised edges to contain the feed slurry, and is dragged over stationary vacuum boxes located at the belt centre. Wear caused by friction between the belt and the vacuum chamber is reduced by using replaceable belts made of suitable material such as Terylene. The main disadvantages of rubber belt filters are the high replacement costs of the belts, the relatively

low vacuum levels, and limitations on the type of rubber that can be used in the presence of certain solvents.

The belt filter shown in Figure 2.16 uses reciprocating vacuum trays mounted under a continuously travelling filter cloth. The trays move forward with the cloth as long as the vacuum is applied and return quickly to their original position after the vacuum is released. This overcomes the problem of friction between the belt and the trays.

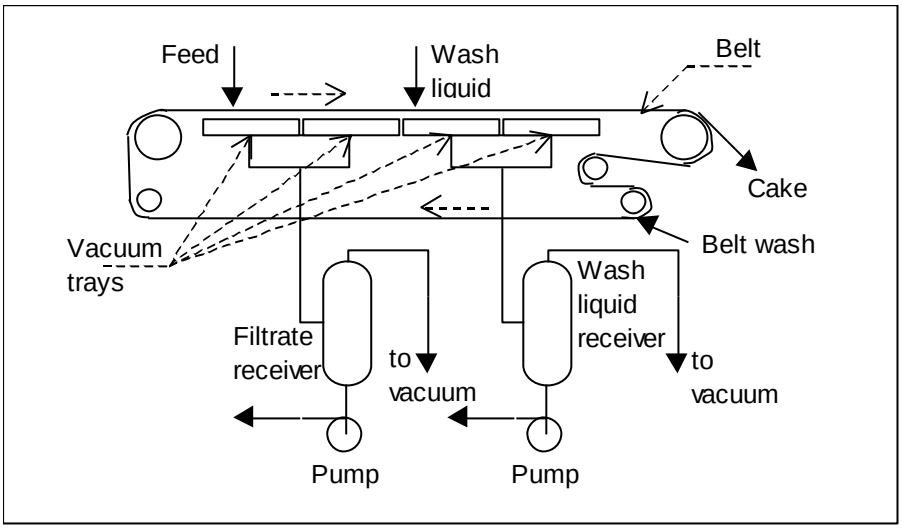

Figure 2.16: Schematic diagram of a horizontal belt vacuum filter (Svarovsky, 1985).

Hydrocyclones are used to improve the performance of filtration by separating the feed into coarse and fine particles as illustrated by Figure 2.17. The coarse material is fed onto the belt filter first as a pre-coat, with the fines to follow. This will result in good clarity of the filtrate, but in some cases at the expense of the final moisture content due to the poorer dewatering characteristics of non-homogeneous cakes (Svarovsky, 1985).

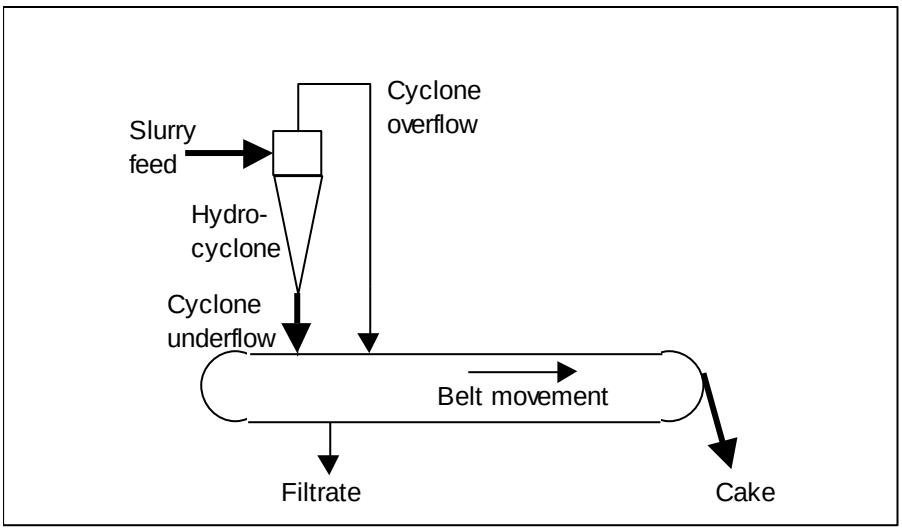

Figure 2.17: Schematic presentation of a horizontal belt filter utilising a hydrocyclone (Svarovsky, 1985).

(b) Counter-current decantation

As discussed previously, it is not practical to obtain a liquid-free solid. Significant proportions of liquid always remain entrained with the solids, which contaminate the solids. In filtration, this problem can be overcome if the filter cake is washed. In counter-current decantation, the problem is handled in a different way.

Counter-current decantation is a solid-liquid separation process utilising sedimentation and decantation. The solids are allowed to settle in the solution to form sludge at the bottom of a decantation vessel. This leaves a layer of solution above the sludge that is essentially free of solids. It is possible to obtain a solution that is essentially free of solids; some of the solution will always remain entrained with the sludge. To overcome this problem, the sludge is 'washed' by being mixed with water that contains little or no concentrations of contaminants or valuables. The decantation process is then repeated. This achieves a dilution of the solids entrained with the solution. Thus, while the second decantation operation still does not succeed in recovering all the values, it reduces the amount of contaminants that remain entrained with the solids. The degree of dilution that is used, the concentration of contaminants in the 'wash water', and the pulp density of the sludge determine the amount that remains with the solid phase. If the process is repeated many times, a very high removal efficiency of contaminants (or valuable species) can be achieved.

The process of repeated washing and decantation is sound in principle, but in practice gives rise to several solution streams, each with decreasing concentrations of contaminants (or valuable species). In addition, the use of fresh water at each stage significantly increases the total volume of solution that

needs to be treated. Both problems can be overcome to a large extent by the use of a counter-current approach as shown in Figure 2.18. The supernatant liquid from one stage is used as the wash water in the previous stage. Addition of fresh water is required at only one stage and this water removes in counter current to the flow of solids (Woollacott and Eric, 1994).

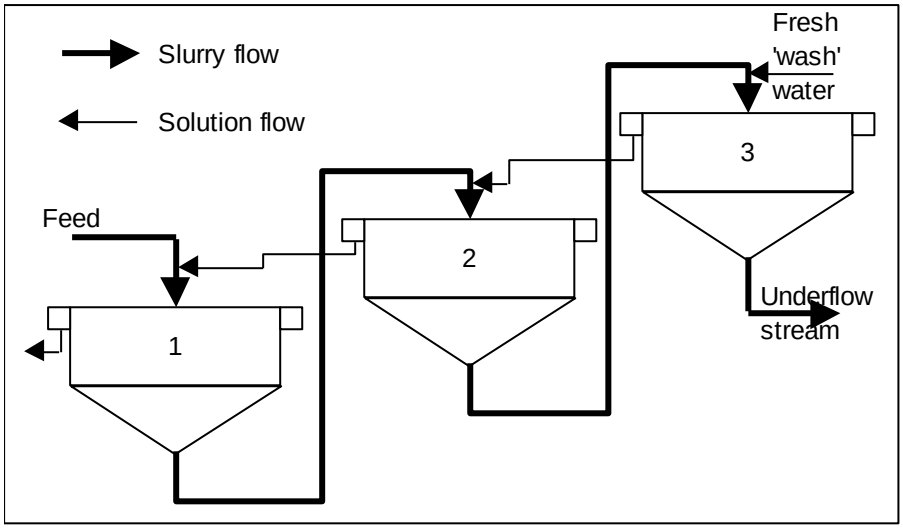

Figure 2.18: Counter current decantation with three clarifier wash stages. Clarifier 3 overflow stream dilutes the slurry feeding clarifier 2. The proportion of dissolved species in the slurry decreases from clarifiers 1 to 3 and the concentration of dissolved species in the clarifier overflows increases from 3 to 1 (Woollacott and Eric, 1994).

The degree of recovery (E) of the contaminants (or valuable species) in a counter-current decantation process will depend on the number of stages employed (n) and the flow rates of solution in the overflow stream (L) and underflow streams (H) in each stage. The ratio of these two flow rates is defined as the wash ratio, R (R = L/H). If the concentration of contaminants in the wash water is zero, the recovery of contaminants, E, depends on the wash ratio and on the number of decantation stages as shown by the following equation (Svarovsky, 1985):

$$E = \frac{R^{n+1} - R}{R^{n+1} - 1}$$ **Equation 2.42**

Hydrocyclones can also be used for washing of solids by arranging several stages in a counter-current arrangement similar to that used with gravity thickeners (clarifiers). The removal of soluble from the feed is achieved by counter-current decantation. Two or more cyclones are used in series through which the solids and liquid move in opposite directions as shown schematically in Figure 2.19 (Svarovsky, 1985).

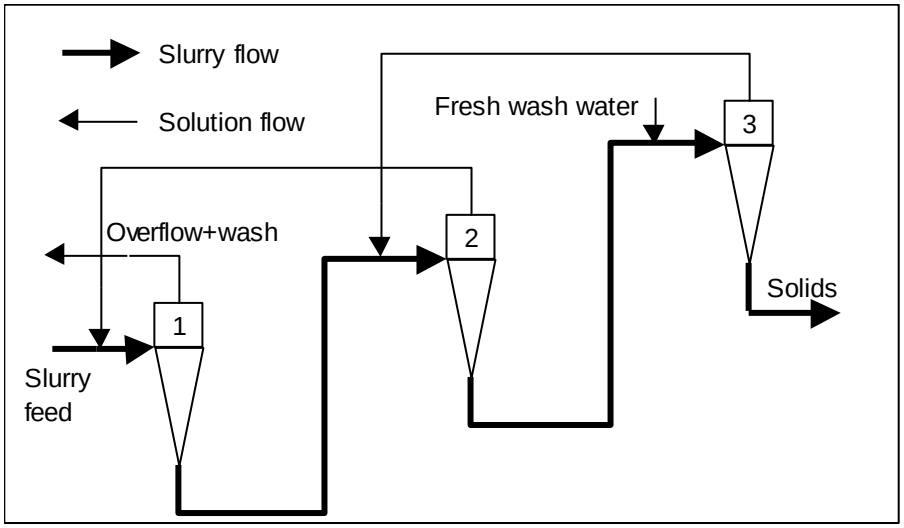

Figure 2.19: Counter current washing with cyclones (Svarovsky, 1985)

2.2.3.3. Removal of adsorbed iron oxides

Desorption of adsorbed species was thoroughly discussed in Paragraph 2.2.2 – *Physical and chemical removal of adsorbed iron hydr(oxide).* Bandini et al. (2001) showed that adsorbed hematite (Fe_2O_3) could be effectively removed (>90% removal) in a relatively short period (< 10minutes) by:

(i) pH control (increasing the pH) and high shear forces.
(ii) pH control, addition of chemical dispersants and applying shear forces.

Bandini et al. (2001) provides insight into the desorption of the other iron hyr(oxide) species, such as hydrous ferric oxide. It is expected that the desorption methods would still be applicable, but that different solutions would require slightly different pH control strategies and possibly other chemical dispersants or using different concentrations of chemical dispersants.

Ernstsson and Larson (1999) investigated the desorption of iron oxide and/or oxohydroxide (refer to Equation 2.20 for the chemical structure of oxohydroxide) on quartz mineral particles. It is important to highlight their method of desorption. Several 5 g batches of quartz samples were mixed with 140 ml aliquots of 4 M hydrochloric acid in ultra-pure water for 30 minutes. In the next step the sand was extensively rinsed with 1 M HCl, followed by rinsing in ultra-pure water in a filter funnel. The washed quartz samples were then left to dry at room temperature. In essence, their method consisted of a high acidity treatment to dissolve the iron, followed by a dilute acid rinse. The iron ‘rich’ water is

then separated from the minerals by means of a solid-liquid separation step (filtration) followed by cake washing with fresh water. ESCA (Electron Spectroscopy for Chemical Analysis) mineral surface analysis revealed a reduction of more than 90% in adsorbed surface iron. It is important to note that, regardless of which desorption method is followed, the desorbed iron is effectively removed in a sequence of solid-liquid separation steps to prevent potential re-adsorption.

2.3. IMPACT OF RE-ATTACHED IRON COMPLEXES ON THE ELECTRICAL CONDUCTIVITY AND ELECTROSTATIC BEHAVIOUR OF MINERAL PARTICLES

Dance and Morrison (1991) provide a valuable general explanation on the basic principles of electrostatic separation, which is based mainly on differences in mineral conductivity. A schematic profile of the high-tension roll separator is shown in Figure 2.20. Material is fed onto a grounded, rotating roll, which carries the particles into the corona-charging zone. Within this region, the particles are highly charged by the flow of ions from the corona wire electrode. As each particle exits the corona field, its surface charge begins to decay to the grounded rotor at a rate proportional to its surface conductivity. The static electrode generates a non-uniform static field, which concentrates the corona field strength and enhances the discharge rate of particles by conductive induction.

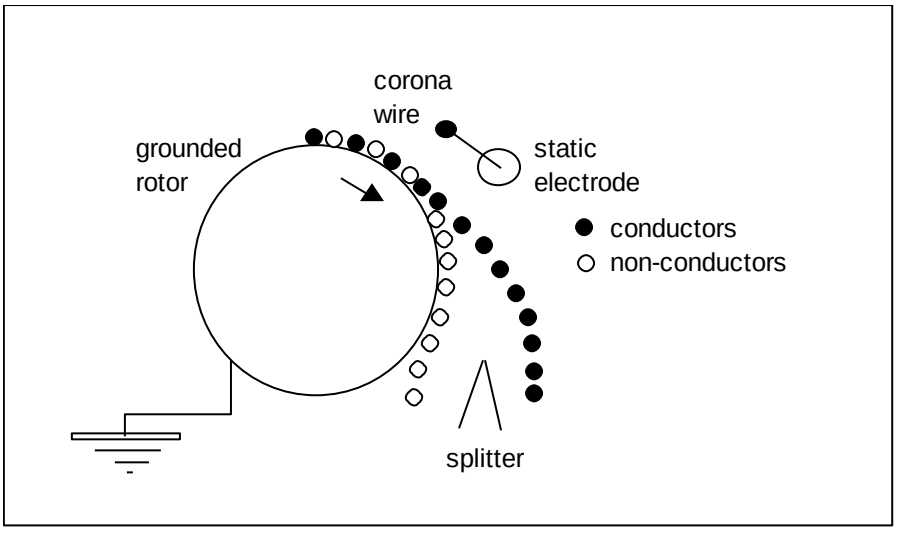

Figure 2.20: Schematic diagram of a high tension roll machine (Dance and Morrison, 1991)

The surface charge on each particle attracts a charge of opposite sign on the rotor. This induces an attractive force, which ‘pins’ the particles to the rotor surface. This force opposes the centrifugal action resulting from the rotation of the roll. Conductive particles lose their charge relatively quickly

(thereby lowering the pinning force) and leave the rotor surface earlier than non-conductive particles. The difference in departure points between conductive and non-conductive minerals is the basis of the separation. The range of conductivities present in the feed material generates a fan of particle trajectories, which are divided into separate products by one or two movable splitters.

The profile of the electrostatic plate separator (ESP) is shown in Figure 2.21. Various designs are currently in operation in the various mineral sand operations. Material is fed down an inclined, grounded plate into the static field-charging zone. The curved profile of the plate combined with the elliptical electrode generates an intense, non-uniform static field. Within this field, particles are charged by conductive induction and develop a surface charge of opposite polarity to the electrode. This surface charge results in an attraction to the electrode as well as the pinning force towards the grounded plate surface, similar to the HTR machine. Particles will lift off the plate once the attraction to the electrode overcomes both gravity and the pinning force. Another design of ESP separator has all particles being thrown from the plate where they are deflected by the static field in proportion to their surface charge. After leaving the plate, the charged particle trajectories are divided into products by movable splitters. An industrial machine typically consists of two starts feeding five treatment stages. Machine variables include: electrode geometry, electrode voltage, plate curvature and splitter positions. The effect of particle size in the plate separator is opposite to the roll machine with coarse material preferentially reporting to the non-conductor product.

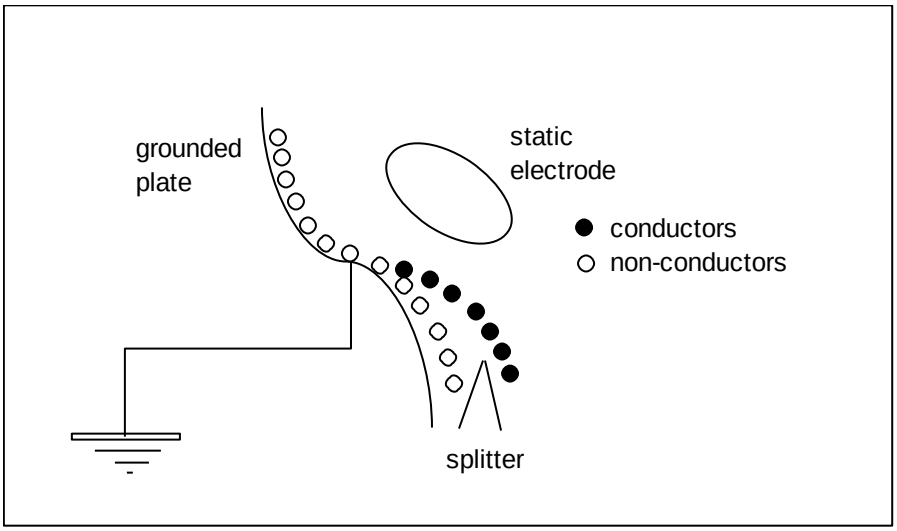

Figure 2.21: Schematic diagram of an electrostatic plate machine (Dance and Morrison, 1991)

The Australian mineral sands industry has been using electrostatic separators in the dry plant processing of mineral ore for more than 45 years (Morley, 1981). Dance and Morrison (1991) have developed mathematical models of high-tension roll (HTR) and electrostatic plate separators (ESP).

All machine, mineral and atmospheric variables have been incorporated into model structures, which predict the performance of a single stage of separation. Multiple stage machines and dry plant circuits are simulated as a series of single stages. These models accurately predict full-scale separator performance under a wide range of operating conditions.

As most electrical conduction occurs through the outermost layers of atoms, surface conditions can produce highly variable mineral conductivity. Changes in the surface properties due to adsorbed physical or chemical coatings, particle shape or orientation will cause a mineral to exhibit a different response to the same separating conditions. The same particle may exhibit a broad range of properties due to surface effects. This is a very important observation, which provides some evidence on the effect of adsorbed coatings. Howe and Pope (1970) discuss the effect of humidity adsorption from the atmosphere to the particle surfaces. They have found that adsorbed humidity results in a conductive layer, which has a significantly negative impact on electrostatic separation. Although not mentioned, the effect of adsorbed iron hydr(oxide) precipitates could be similar.

Collins and Farmer (2003) discuss the effect of cleaned surfaces on the processing of heavy mineral sands. The use of power ultrasound to clean the mineral surfaces of oxidation products and fine coatings is investigated. Ultrasound produces large localised forces by means of cavitation. Cavitation is the process by which large energy amounts are released locally when vapour bubbles collapse. These expanding and almost instantaneously collapsing vapour bubbles form when sound waves are passed through a liquid. The result is cleaned mineral surfaces, which improve the sharpness of their high-tension separation, and to a lesser extent reduced iron levels of zircon mineral grains.

According to Collins and Farmer (2003) heavy mineral sands are often coated or stained to a greater or lesser extent by oxides of iron or fine clays (natural coatings). The effect of these coatings, if not removed prior to electrostatic separation, is to mask the inherent conductive or non-conductive behaviour of the constituents of the sand grains. This masking effect results in reduced sharpness of separation, which results in increasing complexity of the electrostatic section of the dry mill plant. Increased circuit complexity increases the capital and operational costs. Removing the mineral coatings results in the conductor particles being more conductive and non-conductive particles being less conductive (and thus more non-conductive). The actual lowering of iron in the zircon product is less significant, unless the zircon is heavily coated. It was found that when treating a very clean ‘premium zircon’ of the east coast of Australia, there was little change in terms of iron reduction (XRF analysis). On the other hand, a West Coast zircon was reduced from 0.193% to 0.139% Fe_2O_3 by sonication with dilute sodium carbonate solution (0.1%) for one minute. The iron level was further reduced to 0.111% Fe_2O_3 when sonicating sequentially for half a minute with 0.1% sulphuric acid and

another half minute with sodium carbonate. There was, however, a significant change in surface properties of all the heavy mineral sand constituents, as determined by changes in resistivity using a system developed by Lawver and Wright (1969) and further refined at the Julius Kruttschnitt Mineral Research Centre (JKMRC) at the University of Queensland.

Table 2.5: Effect of sonication on the resistivity of heavy mineral products from Western Australia (Collins and Farmer, 2003).

Process	Zircon	Leucoxene	Altered ilmenite
Resistivity ohm-metres	ρ	ρ	ρ
Untreated (A)	$1.41x10^{11}$	$1.09x10^{11}$	$8.133x10^{10}$
Water sonication	$3.30x10^{11}$	$3.70x10^{10}$	$2.977x10^{10}$
Na_2CO_3 sonication (B)	$1.40x10^{11}$	$1.32x10^{10}$	$9.170x10^{9}$
Reduction in resistivity (A-B)	$1.00x10^{9}$	$9.58x10^{10}$	$7.216x10^{10}$

Table 2.5 shows that sonication with sodium carbonate (Na_2CO_3) slightly lowers the resistivity of zircon (non-conductors) as compared with sonication in pure water. However, the effect on lowering the resistivity of leucoxene and altered ilmenite (conductors) is nearly two orders of magnitude greater and makes up for the slight decrease in zircon resistivity. The reversal in the resistivity of zircon after sonication in sodium carbonate solutions was shown to be due to the reaction of the sodium ions with the mineral to produce a surface change (X-ray Photoelectron Spectroscopy).

Larger samples (approximately 1 kg each) of heavy mineral concentrates of Western Australia were sonicated in water, 1g/L HCl and 1 g/L Na_2CO_3 for subsequent testing on a laboratory high-tension roll separator to determine the effect on electrostatic separation. The best results were obtained using sodium carbonate sonication and the percentage improvement over unsonicated material is shown in Table 2.6.

Table 2.6: Comparison of grade and recovery improvement in high-tension separation between untreated mineral and sodium carbonate sonicated from Western Australia (Collins and Farmer, 2003).

	Grade % Untreated	Grade % Treated	% Grade Improve-ment	Recovery % Untreated	Recovery % Treated	% Recovery Improve-ment
Sample A						
Non-conductors (ZrO2)	35.58	39.22	10.2	86.5	87.2	0.8
Conductors (TiO2)	63.19	64.54	2.10	61.3	71.0	15.8
Sample B						
Non-conductors (ZrO2)	38.94	41.86	7.5	73.9	83.4	12.9
Conductors (TiO2)	35.0	42.14	20.4	35.7	40.0	12.1

It is important to note that Collins and Farmer (2003) mainly removed natural Fe_2O_3 and clay coatings. Unfortunately, their work does not provide information on the processes from where these samples were obtained. In other words, were these samples chemically or physically treated prior to laboratory sonification experiments? Unfortunately, the effect on electrostatic mineral separation by removing adsorbed iron hydr(oxide) species is not covered in their investigations. However, it was successfully shown that cleaner mineral surfaces of heavy mineral sands improved the performance of high-tension separation by 10-20%. According to Collins and Farmer (2003) this relatively small improvement will accumulate over the individual electrostatic stages of an industrial process circuit, which would result in significant overall improvements in separation.

Ernstsson and Larsson (1999) provide more evidence that iron precipitates would mask or alter the surface properties of mineral particles. They analysed quartz mineral surfaces by ESCA (Electron Spectroscopy for Chemical Analysis). ESCA is a straightforward surface analysis, which easily detects if any contaminating elements are present on the mineral surfaces. These contaminating elements are commonly found on mineral surfaces originating from industrial processes and normally originate from leaching/precipitation processes occurring from other iron contaminating minerals present in the quarry. Even if the amount of these elements is small, their presence can drastically change the surface properties of minerals. The authors referred to the surface properties as the number of adsorption sites associated with adsorbed iron oxide and/or oxohydroxide (see Equation 2.20 of Paragraph 2.1.3.2 – *Precipitation pathways*). Reducing the surface iron content from 1.4% to 0.1% (>90% reduction) reduced the number of adsorption sites on quartz particles. Unfortunately, their

investigation does not provide quantitive data on the effect of adsorbed iron species on mineral electrostatic behaviour.

Sousa Neto et al. (2001) provide important insight into the effect which iron oxide adsorbed to mineral surfaces will have on the surface conductivity of these coated minerals. Although their investigations of the electrical conductivity and piezoelectric properties of iron doped collagen films are applied in the medical field, they can also be used to understand mineral electrical separation behaviour in the mineral sands industry.

Collagen is the most abundant structural protein of animal connective tissue. The piezoelectric properties of collagen have been investigated in complex biological systems such as bone and tendon. The piezoelectric properties of bone are of interest in view of their role in bone modelling. The objective of their study was to understand the function of iron in the collagen structure. Sousa Neto et al.(2001) prepared moulded films from a collagen solution. The samples were doped by immersion in solutions of different concentrations of $FeCl_2$ (0.1 mol L^{-1} and 0.2 mol L^{-1}) and Fe_2O_3 (5% and 15%), followed by extensive water wash and drying in a laminar flow of air. Unfortunately, the discussion was not clear on the form of Fe_2O_3 (it was suspected to be hematite). Samples used for electrical measurements were plates with a circular surface area of 1 cm in diameter and a thickness of approximately 30 μm. Silver electrodes were applied in both the vertical and horizontal planes. The DC conductivity was measured by heating the sample slowly (6 K min^{-1}) with an applied constant DC voltage (50V) using a conventional electrometer.

For the samples under study, the highest conductivity was obtained for the sample coated with 15% Fe_2O_3. At room temperature, the conductivity measured was approximately 10 times higher than pure collagen (not coated). The conductivity of collagen samples coated with 5% Fe_2O_3 was lower by a factor of 10^{-4}, which was lower than pure collagen. The conversion of Fe^{2+} to Fe^{3+} is a fundamental factor affecting the conductivity, which could provide an explanation for the reduced conductivity of the pure collagen. For the samples prepared by immersion in $FeCl_2$, a decrease in conductivity with an increase in iron (II) concentration was observed. Therefore, the Fe(II)/Fe(total) is a critical factor for electrical conductivity. Sousa Neto et al. (2001) concluded that coating collagen with Fe_2O_3 would result in higher DC conductivity. Of particular interest is the effect of adsorbed iron on the DC electrical conductivity. It clarifies the effect that adsorbed iron has on electrostatic mineral separation. Unfortunately, literature does not provide sufficient information on the DC conductivity of the other iron hydr(oxide) species.

2.4. SUMMARY

Iron precipitates with an increase in pH and the exact pH where precipitation starts to form is dependant on the concentration of iron, temperature of the solution, amount of ferric and ferrous ion present and the presence of other species. The oxidation of ferrous to ferric ion is slow in acidic mediums. Iron (II) hydroxide precipitate is not very stable at near neutral pH and is only stable if the pH remains relatively constant at approximately 11.7. Iron (III) precipitates as complexes and the most common ones are jarosite, iron (III) hydroxide, goethite and hematite. Ideal conditions for jarosite formation are pH 1.5 – 1.6 and 100 ^{0}C (Dutrizac, 1983). Goethite complexes are stable at pH > 2 and 40 ^{0}C. Higher temperatures of 70 – 90 ^{0}C favour the formation of hematite at the expense of goethite. The thermal stability of goethite is increased with respect to hematite if aluminium is present in the goethite structure or the pH is increased. Iron hydroxide starts to form at pH 2-3 (depending on the ferric ion concentration) and is stable over a wide pH range and at temperatures < 40 ^{0}C (Figure 2.1). This iron complex has a tremendous surface development and retains much absorbed water. It forms large gel colloids and coagulation by OH^- or other anions leads to massive gel precipitation. It also attracts anions in acidic mediums and cations in alkali mediums.

Iron hydr(oxides) have positive zeta potentials above the PZC. The average PZC value is pH 7.8 (Kosmulski et al. 2003). It was shown that hematite adsorbed to the surfaces of quartz and galena particles due to opposite zeta potentials. The adsorbed hematite particles were ineffectively removed by increasing the pH to 10 to ensure equal zeta potentials of both quartz and hematite particles. Combining pH control with high shear mixing (sonification) removed these attachments effectively. It was also found that using other reagents could also reverse the surface charge of iron oxide slimes causing a repulsive force and consequently desorption. The use of low pH to dissolve the precipitates was not investigated.

Collins and Farmer (2003) showed that ineffective removal of natural surface coatings present on the minerals as they occur in the ore body hinder electrostatic separation. No information could be found, which proved that iron hydroxide adsorbs to the surfaces of zircon and rutile mineral particles and that the attached precipitates affected electrostatic separation in such a way that it could have significant economic implications.

The literature study provided a solid foundation for the remainder of this study, but it still left many questions without answers. It was clear from the literature study that iron (III) would precipitate in the neutralisation step of the HAL circuit. However, the exact pH of precipitation, and other species that

would precipitate, was not known. It was also important to determine if these precipitates would adsorb to the surfaces of zircon and rutile mineral particles and if they would remain adsorbed through the many high shear mixing of the proceeding process stages (attritioning, cycloning, pumping and spiral stages). Probably one of the most difficult tasks would be to quantify the impact of these attachments on electrostatic separation and to determine an economical solution to resolve this problem.

CHAPTER 3

MATERIALS AND METHODS

Objectives of Chapter 3:

- Discuss the purpose of the experiments and analytical methods.
- Describe the experimental set-up and procedures.
- Describe the analytical methods.

The objective of the experimental and analytical methods used was to provide accurate and repeatable experimental information that would prove the significant impact of the HAL circuit on the production of zircon and rutile products. The experiments were set-up in such a way that they would lead to a robust process solution that could be implemented. The experimental results would provide the necessary understanding of the precipitation reactions taking place in the HAL circuit, and would determine if these precipitates adsorbed to the mineral surfaces. A large number of laboratory electrostatic separation tests were conducted to quantify the impact of the attached precipitates at separation. Simplified cyclone and filtration process circuits were developed in the laboratory. These circuits, together with balances obtained by plant trials, were used to estimate the potential impact on mineral product recoveries if these circuits were to be implemented at Namakwa Sands. Plant trials were conducted by performing iron and mineral balances under normal and stable plant operating conditions and during periods when caustic addition in the HAL circuit was temporarily stopped. Results from these plant trials were used for plant scale evaluation of the problem.

This chapter describes the experimental set-up and procedures used in the study. The experimental methods were a combination of in-house development and methods used in the mineral sand industry. A nomenclature of the symbols used in the equations is provided at the end of the chapter.

3.1. EXPERIMENTAL SET-UP AND PROCEDURES

3.1.1. QUANTIFICATION OF IRON PRECIPITATION AS A FUNCTION OF pH

Experiments were conducted in order to determine at which pH would iron (III) start to precipitate. Information obtained from the literature survey was used as a guideline and provided a starting point for these experiments. Quantitive information of iron precipitation as a function of pH laid the foundation for the other experimental investigations. Water samples of 2 litres each were obtained

from two streams in the HAL circuit. These streams were the overflow water of the upflow classifier A and a combined underflow slurry sample of both upflow classifier A and B (refer to Figure 1.2). The underflow samples were combined by adding one part of A to two parts of B equalling the plant ratio. Mineral particles, especially in the underflow samples, were allowed to settle and the water was decanted. Table 3.1 shows the pH and total iron in the water. The ferric ion concentration was typically 50-100% of the total iron concentration. Using the graph of Figure 2.3 (Cigan et al., 1980) it could be concluded that iron (III) would start to precipitate at pH 1.8 and 2 in the quench sump and underflow of the upflow classifier, respectively. These pH values were used as guidelines and would be determined experimentally.

Table 3.1: Total iron (ferric and ferrous ion) and pH of the water in the overflow and underflow streams of upflow classifier A at a temperature of approximately 30-35^{o}C.

Stream	PH	Total Fe (Mol/dm^{-3})
Water in overflow	1.88	$1.6x10^{-3}$
Water in underflow	2.83	$5.4x10^{-4}$

The pH of the underflow water was reduced to well below 2 to approximately 1.5 with a few drops of concentrated sulphuric acid (98.08% H_2SO_4) to ensure that all the iron was dissolved. The volumes of sulphuric acid added were accurately monitored and used to reconcile the concentration calculations. The pH of the overflow water was about 1.5 and was consequently not adjusted.

The water samples were gravity filtered using a Millipore 0.45 μm membrane filter to remove fine suspended slime particles. The filtrate of the classifier overflow and underflow samples was divided in 10 samples each (100ml per sample). Concentrated caustic was used to adjust the pH of the individual samples using Table 3.2 as guideline. Mixing (slow rate) was applied during caustic addition. The temperature of the solution after caustic addition was recorded.

Solid-liquid separation of the individual samples directly after caustic addition was carried out by gravitational filtration using Millipore 0.45 μm membrane filters and funnels. Relatively high quantities of water remained with the precipitate due to hydrophilic characteristic of iron hydroxide. Figure 3.1 is a schematic presentation of the experimental set-up to quantify iron precipitation at a

specific pH. The amount of total iron that precipitated due to the increase in pH was determined by means of titration and Equations 3.1 to 3.8.

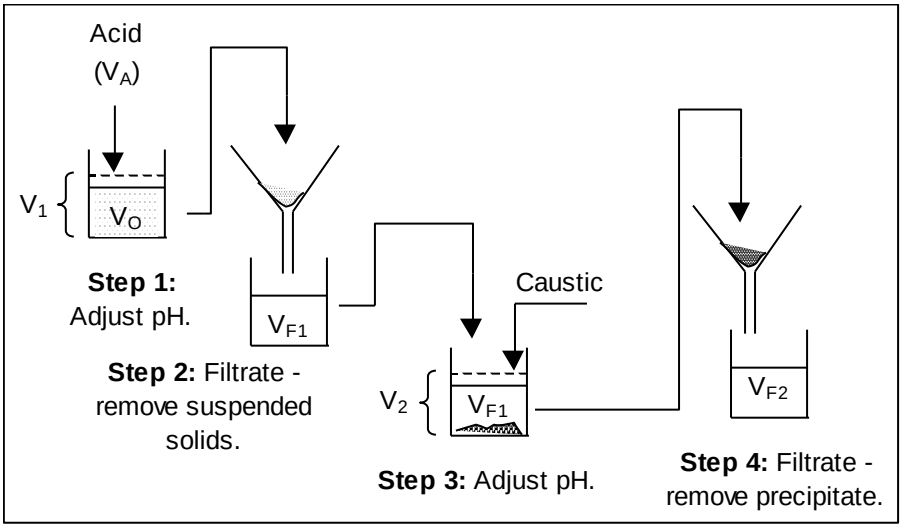

Figure 3.1: Schematic diagram showing the four steps required determining the amount of iron precipitated at a specific pH.

Table 3.2: Guideline for pH adjustments of different samples.

Solution number	PH
1 (Original sample)	1.5
2	1.7
3	2.0
4	2.5
5	3.0
6	3.5
7	4.5
8	6.0
9	9.0
10	10.0

The concentration of dissolved iron in step 2 (C_{F1}) after pH adjustment was determined by titration and could be expressed as follows:

$C_{F1} = M_{F1}/V_{F1}$ **Equation 3.1**

The dissolved iron concentration after filtration (step 2) is equal to the dissolved iron concentration after pH adjustment and before filtration assuming that the volume of suspended solids removed is negligible.

$C_{F1} = C_1$ **Equation 3.2**

The mass of dissolved and precipitated iron in the original solution (M_O) is equal to the mass of dissolved iron (M_1) expressed by Equation 3.3:

$M_1 \approx M_O$ **Equation 3.3**

$M_O = C_1 x V_1$ **Equation 3.4**

The concentration obtained by Equation 3.2 (C_1) must be reconciled to account for the volume of acid added to obtain the original concentration (C_O) of dissolved and precipitated iron. The volume of suspended solids and volume of solution retained by the filter paper, together with the potential change in volume due to the reaction(s) of sulphuric acid, can be assumed to be negligible. The original concentration can be calculated by Equation 3.5.

$$C_O = \frac{M_1}{V_1 - V_A}$$ **Equation 3.5**

The concentration of dissolved iron after caustic addition and filtration (C_{F2}) as conducted in step 4 was determined by titration. The amount of iron (M_{F2}) that remained in solution after the addition of caustic can be determined by Equation 3.6 by assuming that the volume of solution (and soluble iron) retained by the filter paper and cake is negligible.

$M_{F2} = C_{F2} x V_{F2}$ **Equation 3.6**

It is known that iron hydr(oxides) are hydrophilic and would adsorb relatively large quantities of water (Weiser, 1939). Therefore, the volume of water in the filter cake (V_{Cake}) should be incorporated in Equation 3.6 as shown by Equation 3.7.

$(M_{F2})_{corrected} = C_{F2}x(V_{F2}+V_{Cake})$ **Equation 3.7**

The filter cake was allowed to drain and the volume of water retained by the cake was assumed to be negligible relative to the volume of filtrate. Therefore, Equation 3.6 was used.

The amount of iron that precipitated was quantified by Equations 3.8 and 3.9.

$M_P = M_1 - M_{F2}$ **Equation 3.8**

$$\%M_P = \frac{M_1 - M_{F2}}{M_1} \times 100$$ **Equation 3.9**

Equation 3.9 was used to conduct the iron precipitation curves.

3.1.2. IRON CONCENTRATIONS AND ELECTROKINETIC PROPERTIES OF MINERAL SURFACES

Mineral surfaces were analysed for iron precipitates and the surface charge was determined by measuring the zeta potential of zircon and rutile mineral particles. These were very important experiments since it would provide evidence that iron adsorption to mineral surfaces did take place and it would also confirm the adsorption theory of the adsorption of iron hydr(oxides) to mineral surfaces.

3.1.2.1. Determining concentration of iron precipitates present on mineral surfaces and in liquid

Adsorbed iron precipitates concentrations were determined by washing mineral samples with acidic water at room temperature for a short period of time and analysing this wash water. It is important to note that the chemical reaction with any remaining unleached Fe_2O_3 (part of natural surface coating as received from the mine) was prevented due to the low temperature and short reaction time. The leaching reaction takes place at a rapid rate only if the temperature is increased to more than 90^oC. The procedures for determining the concentrations of iron precipitates present in process water, slurry streams and adsorbed to mineral particles are summarised in Table 3.3. Most analyses were carried out by titration to determine the amount of total soluble iron. More detailed analyses conducted by J.A. Santer from the Water Division of SABS, Cape Town, provided important quantitive information of the entire chemical species remove by the diluted acid.

Analyses of the surface chemistry of samples 1 and 2 (dry and concentrate samples) were used to provide quantitive information to confirm the adsorption theory. These grab samples were targeted, because they were actual plant samples collected after the iron precipitation and expected adsorption processes had occurred, and analyses thereof would therefore provide quantitive confirmation of the iron adsorption theory. Instantaneous grab and composite 24-hour samples were used for the analysis, with the latter more representative of the process than the former.

Acidic wash water (pH 1.5) was used to dissolve soluble species, such as iron and aluminium hydr(oxide) prior to filtration in order to remove suspended solids. The wash water was prepared by adding very small quantities of concentrated sulphuric acid (98%) to the water to obtain a pH of 1.3. This wash water was analysed by SABS and used as ‘background’ to obtain the actual assays by subtracting the background from the wash water analyses (after rinsing of the samples). This procedure is best described by Figure 3.2 and Equations 3.10-3.15.

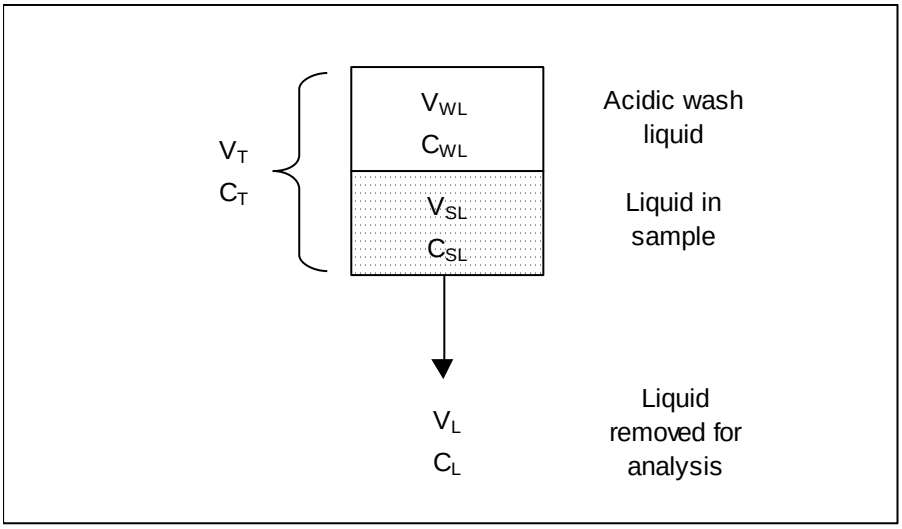

Figure 3.2: Schematic diagram showing a mass balance around a wet or dry sample to quantify the concentrations of species present on the surfaces of mineral particles or entrained in the liquid surrounding these particles.

Assuming that the system has reached equilibrium and all the species soluble in the acidic solution have desorbed from the mineral surfaces and are present in the wash liquid, the mass balance given by Equation 3.10 is applicable.

$$m_T = m_{WL} + m_{SL} + m_S \qquad \textbf{Equation 3.10}$$

Equation 3.10 can also be expressed in terms of concentrations of dissolved species present in the individual solution fractions with specific volumes (except for species adsorbed to mineral surfaces with specific masses, m_S). The equation is as follows:

$$C_T x V_T = C_{WL} x V_{WL} + C_{SL} x V_{SL} + m_S \qquad \textbf{Equation 3.11}$$

Re-arranging Equation 3.11:

$$C_{SL} x V_{SL} + m_S = C_T x V_T - C_{WL} x V_{WL} \qquad \textbf{Equation 3.12}$$

At equilibrium:

$C_T=C_L$ **Equation 3.13**

Mass% of soluble specie, X, contained in mineral sample (dry, wet or slurry):

$$X\% = \frac{C_{SL}xV_{SL} + m_S}{M} x100 \quad \textbf{Equation 3.14}$$

Combining Equation 3.12 and 3.13, the mass of soluble specie, X, can be expressed as follows:

$$X\% = \frac{C_L xV_T - C_{WL}xV_{WL}}{M} x100 \quad \textbf{Equation 3.15}$$

Equation 3.15 was used to determine the mass fraction of soluble (and dissolved) species, such as iron hydr(oxide) precipitate, in mineral streams. Table 3.3 provides the methodology and parameters used for removing precipitates from the individual samples. It was important to keep a close record of the liquid-solid ratios, which were required to calculate the amount of precipitate per dry mass of mineral sample.

Table 3.3: Methodology for removing precipitated iron hydr(oxides) and other species adsorbed to mineral surfaces (samples 1 and 2) and/or present in process water as precipitates or as dissolved species (sample 3 and 4).

No	Sample	Streams	Water content (%)	Mass sample (g)	Acidic water/98% sulphuric acid added	'Mixing' time (min)
1	Dry	Zircon product, rutile product and HAL recycle.	0%	500g	500ml (pH 1.3)	10
2	Concentrate	Primary concentrate	3-5%	200g	200ml (pH 1.3)	10
3	Slurry	Feed to primary and fine spirals, attritioner feed and cyclone underflow.	30-70%	350g	Adjust pH to 1.3 with drops of concentrated acid	10
4	Water	Process water in HAL and wet gravity circuits.	~ 100%	100g or 100ml	Adjust pH to 1.3 with drops of concentrated acid	10

3.1.2.2. Quantification of the total iron concentration present in the natural surface coating of mineral particles

Mineral samples received from the mine are coated with Fe-Al-Si formed and deposited onto the mineral surfaces during natural geochemical processes. The method for determining the total iron concentration involves chemical leaching at an elevated temperature (140-150 ^{o}C), attritioning and washing of the mineral sample, and analyses of the wash liquid after filtration (with Millipore 0.45 μ m membrane filters). The method is as follows:

(a) Add 40% sulphuric acid to a dry mineral sample of 1000 g. Mix the acid thoroughly with the sand. Approximately 120 ml of 40% is required to ensure good contact between the sand particles and acid.

(b) Bake at 140-150 ^{0}C until the sample is dry or almost dry.

(c) Add 1 litre of water to the sample and attrition for 15 minutes to liberate the softened mineral surface coating. A laboratory Wemco flotation cell (supplied by Envirotech) was used.

(d) Allow settling and decant approximately 100ml of liquid.

(e) Filter sample and determine total iron concentration by means of titration.

(f) Use Equation 3.15 to calculate mass% iron of sample.

3.1.2.3. Determining surface charge of mineral particles

The surface charge (zeta potential) of the zircon and rutile mineral particles was determined to provide an understanding of the adsorption process of iron hydr(oxides) to mineral surfaces. H. Divey of the Chemical Engineering Department, University of Cape Town, determined the zeta potential of zircon and rutile product samples. Individual mineral samples (0.1g each) were added to a 10^{-3}M Na_2SO_4 buffer. Sulphuric acid and NaOH were used to adjust the pH of the individual samples. Zeta readings were taken over the entire pH range from 2.5 to 9. The average of five readings per sample at a specific pH was taken to ensure high repeatability of results.

3.1.3. DETERMINING OF ELECTROSTATIC SEPARATION PERFORMANCES OF MINERAL PARTICLES

The objectives of the electrostatic separation experiments were:

- Determine if the precipitates formed in the HAL neutralisation stage affected electrostatic separation.
- Quantify how these precipitates affected the electrostatic behaviour of zircon and rutile minerals.
- Quantify by what amount was plant recoveries affected by the precipitates attached to the mineral surfaces.

3.1.3.1. Artificial coating of mineral samples with iron hydr(oxide) rich solutions

Mineral sand particles were artificially coated by hand mixing 1.5 kg dry mill feed samples with 1.5 litre solutions high in iron hydr(oxide) precipitates. The samples were allowed to stand for 15 minutes, after which the solution was decanted and the wet mineral samples were dried in an oven at 140^{o}C for approximately 3 to 4 hours. The dried samples were allowed to cool down after which separation tests were performed to determine the separation efficiencies of the individually coated and normal (as obtained from the plant without artificial coating) samples.

Solutions from the overflow water of the upflow classifier A, and precipitate from the concentrate of the secondary belt filter were used to coat the minerals. It is important to mention that the solutions were prepared from actual samples collected at specific locations in the plant in order to qualitively predict the impact of the HAL neutralisation stage on mineral electrostatic separation in the dry mill circuit.

(a) Overflow water of the upflow classifier A

Approximately 2 litres of overflow water from the upflow classifier A was filtered with a Millipore 0.45 μm membrane filter. The filtrate was rich in dissolved iron and other dissolved species, such as aluminium and sulphates. The pH of 1.5 litres of filtrate was adjusted from approximately 1.5 to 6 by adding concentrated caustic, mixing the solution (hand mixing), and measuring the pH after every addition. The temperature of the filtrate before pH adjustment was approximately 19^{o}C, which increased by about 2^{o}C after caustic addition. Figure 3.3 shows pictures of the solution before and after pH adjustment, respectively.

Figure 3.3: Photo's showing three flasks. The first flask contains high concentrations of dissolved iron (II) and (III) and other dissolved electrolytes after clay and other particles had been removed by filtration. A few drops of caustic were added to the second flask and small amounts of precipitate formed. The last flask contains high amounts of iron hydr(oxide) and other precipitates such as $Al(OH)_3$ after the pH had been raised to approximately 7.

(b) Concentrate from the secondary belt filter

On 09 May 2002 large quantities of yellow-brown precipitates, which were visible on the concentrate of the secondary belt filter, were reported by the production personnel (see photo of Figure 3.4). This concentrate was a side stream of the wet gravity circuit, which was rich in mainly rutile and secondly zircon minerals. These minerals were further separated in the secondary rutile and zircon circuits. These circuits were sub-circuits in the dry mill. It was interesting to note that the dry mill separation on that particular date was very unstable.

Similar precipitates were also found on the floor of the wet gravity circuit and underneath the primary concentrate belt filter. Samples were collected and the pH was reduced to approximately 1 to dissolve the precipitates. Slimes and mineral particles were removed by filtration. The filtrate contained iron (determined by titration). Precipitates were collected by scraping off approximately 1 kg of sample from the top layer of the concentrate of the secondary belt filter and mixing it with about 2 litres of water. Mineral sand particles were allowed to settle and the precipitate rich solution was decanted and used to coat 1.5 kg of mineral sample.

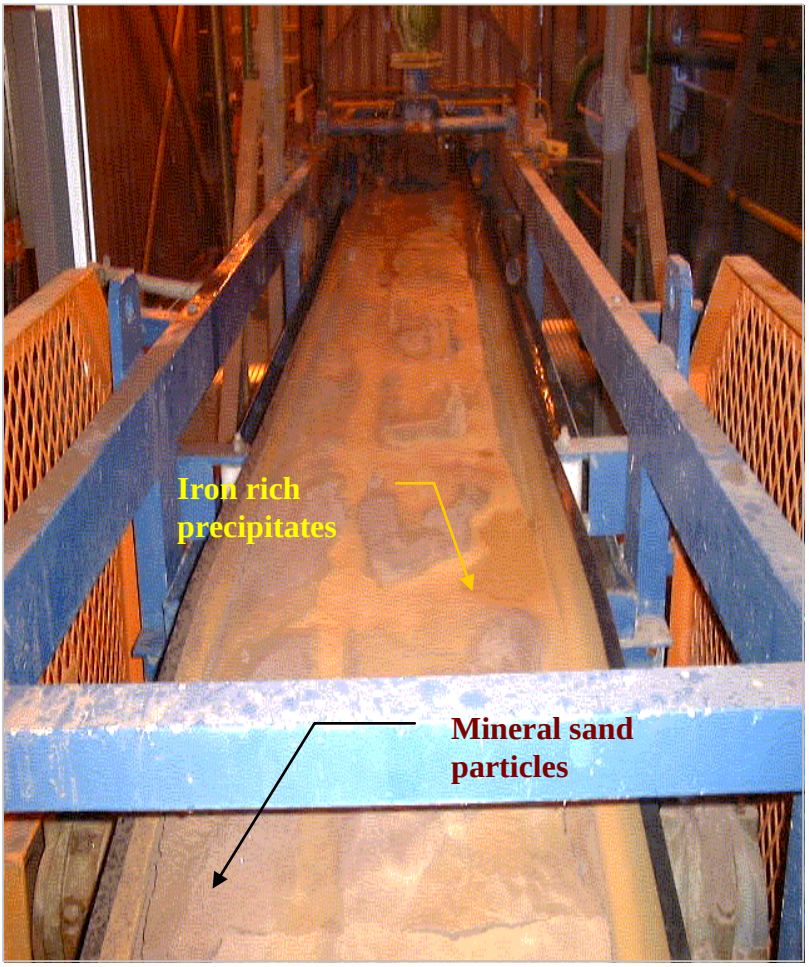

Figure 3.4: Photo's showing build-up of precipitates and slimes rich in iron on the secondary concentrate belt filter of the wet gravity circuit.

3.1.3.2. The effect of caustic on mineral electrostatic separation

The objective of this experiment was to test the effect of caustic soda itself. In other words it would verify the electrostatic behaviour of mineral particles that were relatively clean (free of iron and other precipitates) and coated with a 'layer' of caustic soda by thoroughly mixing mineral samples with a caustic solution. Therefore, it would determine if an improvement in electrostatic separation caused by switching off the caustic was due to the reduced sodium ions associated with the caustic, or reduced formation of precipitates.

Approximately 4.4 kg of primary concentrate (3-4.5% moisture) sample from the primary belt filter (main feed stream to dry mill circuit) was collected 7 hours after caustic was temporarily stopped in

the HAL circuit. The sample was divided in two representative samples (2.2 kg each) by means of a riffle splitter. The one split was dried in an oven at 140^{o}C for about 1 hour. Water (350ml) was added to the wet sample and it was thoroughly mixed (hand mixing). The pH after mixing was 3.5. Drops (~ 1 ml each) of concentrated caustic were incrementally added with a pipette and the pH was measured after thorough mixing by hand. The procedure is summarised in Table 3.4.

Table 3.4: Procedure for 'coating' a mineral sample with caustic in order to test the effect of caustic on electrostatic separation.

Step	Action	Caustic added (drops)	PH after mixing
1	Add 350 ml water and apply hand mixing.	0	3.5
2	Add caustic and mix sample.	5	7.3
3	Mix sample.	0	6.6
4	Add caustic and mix sample.	1	7.0
5	Mix sample.	0	6.9
6	Mix sample.	0	6.9
7	Decant water (moisture in cake 10-15%).	0	N.A.
8	Dry sample in oven (140^{o}C) for 3 hours.	0	N.A.

3.1.3.3. Washing of mineral samples

Dry and wet (3-4.5% moisture) mineral samples obtained from the feed to the dry mill circuit were washed with acidic water (pH ~0.7 and ~1.3) to remove potential iron hydr(oxide) and other precipitates adsorbed to the mineral surfaces. The dissolved precipitates and wash solution were partially removed by experimentally simulating water removal 'circuits' (refer to Paragraph 3.1.4 - *Experimental process simulations* for detail discussions). These tests were important and would provide more quantitive information on the occurrence and effect of adsorbed surface contaminants on electrostatic separation. It would also form the basis for the experimental circuit simulations in order to reduce the adsorption of iron hydr(oxide) and other contaminants.

3.1.3.4. *Experimental set-up of the laboratory Coronastat separator*

A laboratory Coronastat (manufactured by Ore Kinetics, Australia) was used to determine the electrostatic separation behaviour of mineral particles (see Figure 3.5). A Coronastat works on the same principle as a High Tension Roll (HTR) separator, but it is far more superior in performance mainly due to the additional plate electrode and the enlarged roll diameter. The plate electrode improves the decay efficiency of conducting particles (resulting in a lifting effect on these particles) and pinning of non-conducting particles. Coarse non-conductive particles are forced back to the roll by finger pinning electrodes. These two additional electrodes ensure separation that is less sensitive to mineral sizes and separation efficiencies were much higher than the conventional HTR.

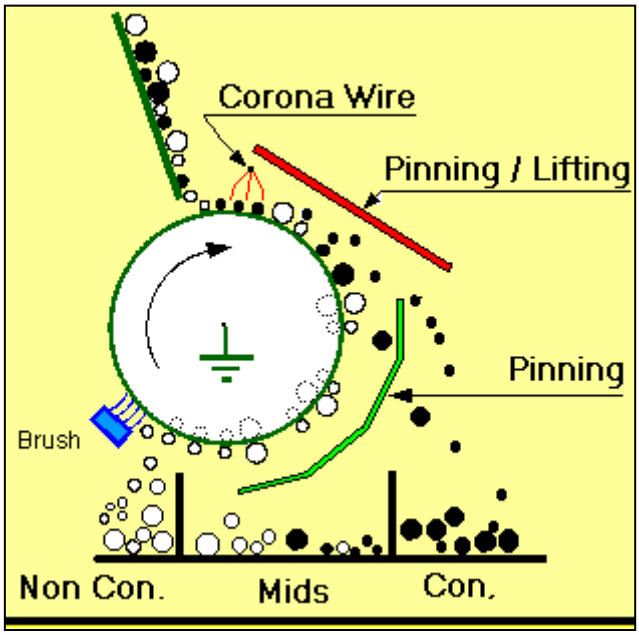

Figure 3.5: Schematic diagram of the laboratory Coronastat. Note that the laboratory Coronastat consisted of only one roll stage. Plant units installed at Namakwa Sands consisted of three roll stages.

Samples were separated by adopting the same parameters as the first stage in the dry mill circuit of Namakwa Sands, which consisted of a bank of Coronastats. Historically, this bank consisted of HTR's, but was replaced with Coronastats in 2002 due to its superior performance. Accurately and closely controlled parameters adopted in the experiments are summarised by Table 3.5. The mineral

samples were heated to above 100^{o}C on a stove with intermediate mixing ensuring uniform heating and evaporation of adsorbed surface moisture. The samples were allowed to cool down while thoroughly and continuously mixing the samples with a span. This ensured uniform mineral temperatures. A hand held electrical heat blower was used to heat the roll while rotating to approximately 55^{o}C. Uniform temperatures were ensured by allowing the roll to cool down to 50^{o}C, thereby ensuring uniform heat distribution across the surface of the roll. The roll speed and kilovolt setting of the electrodes were measured with a kV-probe (DC) and digital tachometer, respectively.

Table 3.5: Parameters used in the laboratory Coronastat. These parameters are similar to that of the production units installed in the first stage of the dry mill zircon/rutile circuit.

Variable	Setting
Feed rate (hole diameter, mm)	4.5
Mineral temperature (^{o}C)	70
Kilovolt setting of electrode (kV)	26
Electrode position	Fixed
Roll speed (rpm)	190
Roll temperature (^{o}C)	50

3.1.3.5. Spatial distribution performance curves

Spatial distribution performance curves are commonly used in the mineral sands industry to determine the electrostatic separation performances of heavy minerals by means of the various electrostatic separators. Separation characteristics of different samples can be predicted and the effect of surface contaminants can be quantified. Performance data was obtained by passing the individual mineral samples (approximately 1.5 kg each) over the laboratory Coronastat (shown in Figure 3.5) at the parameters of Table 3.5. The impact of atmospheric conditions, such as humidity, was minimised by keeping the small metallurgical laboratory closed at all times, conducting all the experiments in a relatively short time frame and by avoiding weather changes during the early mornings and late afternoons. Table 3.6 is an example of a set of performance data obtained for one sample. The stream compositions were determined by grain counting. Cumulative distribution data to the non-conductors and conductors were determined by Equation 3.16 and 3.17, respectively.

$$MD(NC)_{Fi} = \sum_{NC}^{Fi} MD_i \qquad \textbf{Equation 3.16}$$

$$MD(C)_{Fi} = \sum_{C}^{Fi} MD_i \qquad \textbf{Equation 3.17}$$

Table 3.6: Mineral spatial distribution performance data obtained by separating a mineral sample into different fractions. One pass separation was conducted with a laboratory Coronastat. Other minerals, such as leucoxene and ilmenite, were omitted in order to simplify the table.

Fraction	Mass		Stream composition		Mineral distribution		Cumulative mineral distribution to NC	
	(g)	(%)	Zirc (%)	Rut (%)	Zirc (%)	Rut (%)	Zirc (%)	Rut (%)
NC	969.4	60.3	88.8	3.3	75.2	13.7	75.2	13.7
M3	143.4	8.9	75.6	10.3	9.5	6.3	84.7	20.0
M2	149.2	9.3	59.9	20.2	7.8	12.9	92.5	32.9
M1	143.0	8.9	48.3	28.0	6.0	17.2	98.5	50.1
C	202.8	12.6	8.4	57.4	1.5	49.9	100.0	100.0
Total	1607.8	100.0	71.2	14.5	100	100	-	-

A mineral spatial distribution curve can be plotted by using the last two columns of Table 3.6 as shown in Figure 3.6.

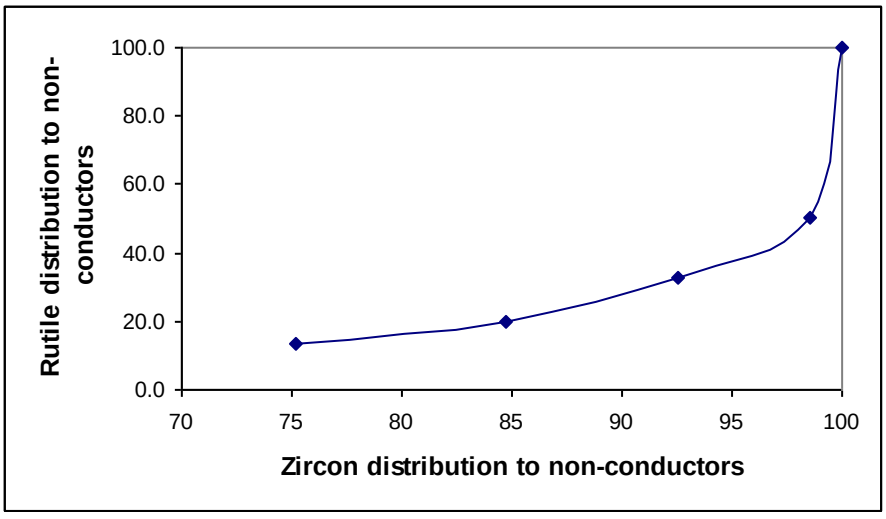

Figure 3.6: A spatial distribution curve showing electrostatic separation of zircon and rutile mineral particles obtained by passing the samples over a laboratory Coronastat.

The separation efficiency of a mineral sample can be deducted from the graph of Figure 3.6 as follows (the example of the results is shown in Table 3.7):

$$\%E = \frac{ZD_{NC} + RD_{C}}{2} x100 \qquad \textbf{Equation 3.18}$$

$$\%E = \frac{ZD_{NC} + (100 - RD_{NC})}{2} x100 \qquad \textbf{Equation 3.19}$$

Table 3.7: Electrostatic separation efficiency of a mineral sand sample as obtained by a laboratory Coronastat. Efficiency numbers are calculated by using Equation 3.19.

Fraction	Cumulative mineral distribution to non-conductors		Separation efficiency (E)
	(% Zircon)	(% Rutile)	(%)
NC	75.2	13.7	80.8
M3	84.7	20.0	82.4
M2	92.5	32.9	79.8
M1	98.5	50.1	74.3
C	100.0	100	50

3.1.4. EXPERIMENTAL PROCESS SIMULATIONS

A few process options were experimentally simulated. The objective was to experimentally set-up simplified counter-current-decantation circuits, which would maximise the removal of dissolved iron from the solutions to consequently prevent iron complex formation and produce a slurry stream containing mineral particles with clean surfaces. The effectiveness of the individual circuits was further quantified in terms of the improvement in electrostatic separation. The experimental circuits were set-up to conservatively simulate mineral wash circuits utilising dewatering cyclones and horizontal belt filters.

3.1.4.1. CCD cyclone circuit

The procedure used to simulate the counter-current-decantation (CCD) circuit of Figure 3.7 is as follows:

(a) Adjust the pH of 4000 ml water to pH 0.7 by adding small amounts of concentrated sulphuric acid to the water, while stirring.

(b) Split 3 kg of dry primary concentrate sample after the dryer (this sample is referred to as *SDO* or *secondary dryer outlet*) into two representative samples.

(c) Soak the one 1.5 g sample with 1000 ml acidic water (pH 0.7) for 15 minutes. Rinse after 15 minutes and decant the water completely. The water content after decantation is normally 85%-90%.

(d) Wash three times with 1500 ml acidic water and decant after every cycle. Allow 5 minutes washing time per cycle.

(e) Add 1000 ml acidic water to obtain a slurry content of approximately 56% solids and 44% water. Attrition for 10 minutes with a laboratory flotation cell. It is important to note that optimum plant scale attritioning is obtained by attritioning slurry with a solid content of 80%. The slurry of the laboratory scale unit had to be diluted to reduce dead zones from forming in the attritioner vessel due to the small volume of the slurry mixture at a higher solid content.

(f) Add concentrated caustic and attrition for 25 minutes and measure the pH after every 5 minutes until pH 5.5-7 is obtained.

(g) Decant 50% (590 ml) of the water and replace with fresh water (590 ml); measure the pH.

(h) Add 500 ml fresh water and decant 500 ml water after mixing for 4 times.

(i) Add caustic to adjust pH to 10.

(j) Add 500 ml fresh water and decant 500 ml water after mixing twice.

(k) Measure pH (target > 3.5).

(l) Dry sample in an oven.

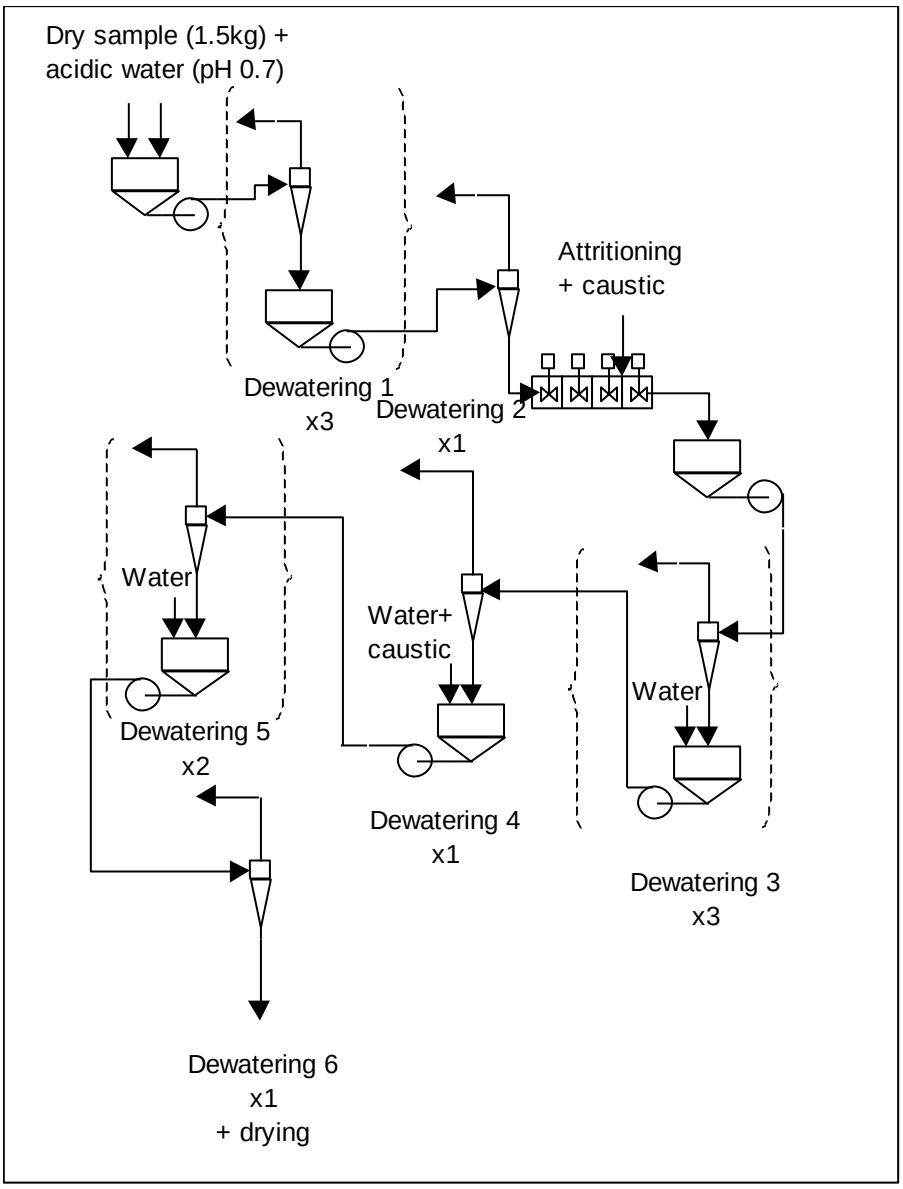

Figure 3.7: CCD circuit for the removal of precipitated iron and other mineral surface contaminants, which was simulated in the laboratory. The cyclones utilised in this circuit were simulated by manual decantation of the water. The sump-pump stages, which are in effect mixing stages due to the mixing action of the centrifugal pumps and also due to some mixing that occurs in a sump, were replaced by hand mixing in the laboratory.

3.1.4.2. Filtration circuits

The procedure used to simulate the washing circuit utilising a horizontal belt filter as shown in Figure 3.8 is as follows:

(a) Adjust the pH of 1000 ml water to pH 0.7 and 150 ml of water (required for cake washing) by adding small amounts of concentrated sulphuric acid to the water, while stirring.

(b) Split 1.53 kg of wet primary concentrate sample (3.5-4.5% moisture) collected from the primary belt filter with a riffle splitter into two 765 g samples.

(c) Repulp the concentrate sample with acidic water (pH 0.7) to obtain a solid content of approximately 70% (add 330 ml water). Mix for 5 minutes.

(d) Filter the sample with the vacuum filter funnel (see Figure 3.9). The cake will dry rapidly in a couple of seconds (allow 3-5 seconds). Assume that 5% moisture is contained in the cake (40 ml) and apply a wash ratio of 2.5. Therefore, wash with 2.5x40 = 100 ml acidic water at pH 2. Allow the cake to drain completely (allow 3-5 seconds). Remove the washed filter cake and place into a clean flask.

(e) Repulp the cake with fresh water (pH 6-7) to obtain a solid content of approximately 45% (add 895 ml water). Mix for 3 minutes.

(f) Simulate the cyclone stage by decanting 425 ml of water to obtain a slurry content of 60%. Measure the pH, which should be close to 3.

(g) Add 3 drops of concentrated caustic and mix thoroughly. Measure the pH after three minutes and continue mixing and/or add more caustic. A final pH of 6-7 must be obtained.

(h) Simulate the washing action of the wet gravity circuit by decanting all the water after the neutralisation step to obtain slurry with a solid content of 85-90%. Measure the volume of water decanted and replace with the same amount of fresh water. Mix thoroughly and decant all the water to conservatively simulate the primary belt filter.

(i) Dry both treated and untreated samples in an oven at 140^{o}C for 1h30min.

(j) This procedure was also repeated for a primary concentrate sample repulped with acidic water at pH 1.3 instead of pH 0.7 before filtration. The remainder of the procedure was kept exactly the same.

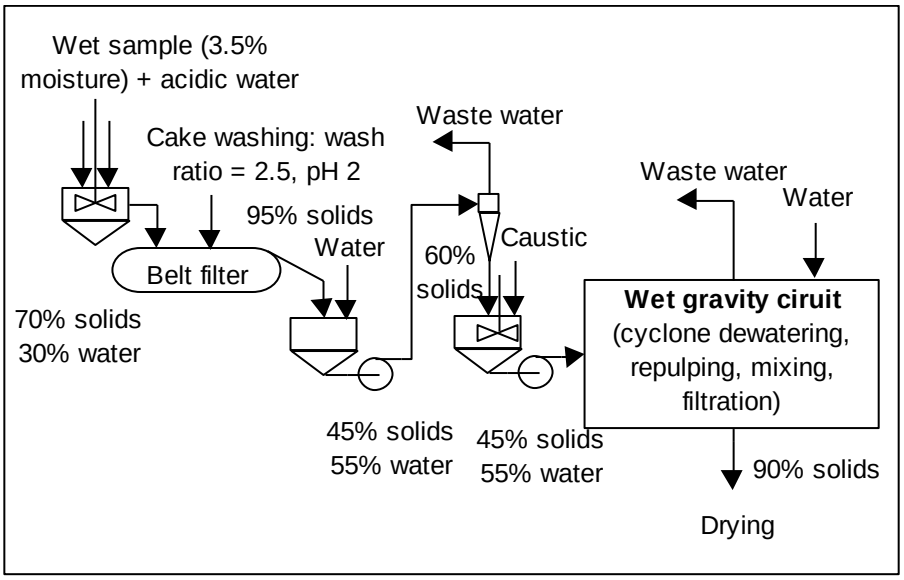

Figure 3.8: The filtration circuit for the removal of precipitated iron and other mineral surface contaminants, which was simulated in the laboratory. Filtration by means of the vacuum belt filter utilised in this circuit were simulated by using the laboratory vacuum funnel filter as shown in Figure 3.9. The cyclone stage was also simulated by manually decanting the water and the sump-pump stages were replaced by hand mixing.

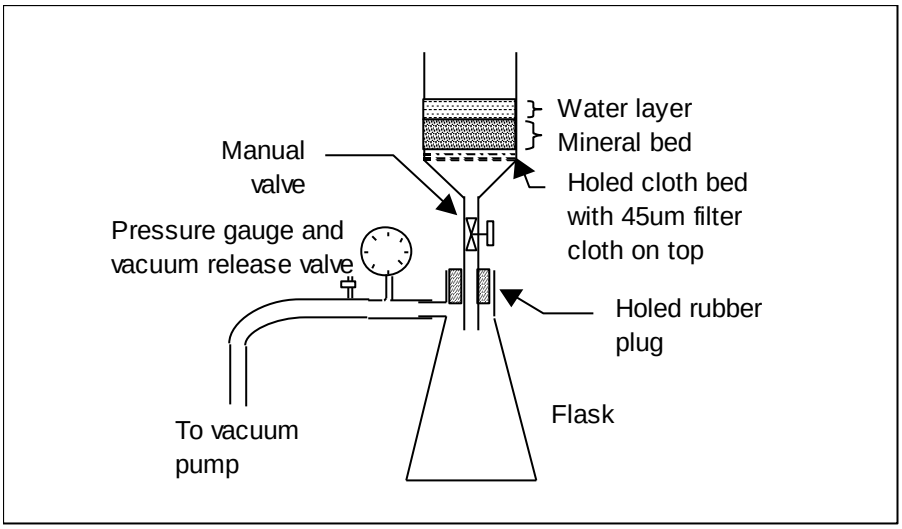

Figure 3.9: Experimental set-up of the filter equipment used during the experiments. Filtration tests were conducted at a vacuum of –50 to –70 kPa. This equipment is commonly used by industrial filter suppliers for the sizing and design of vacuum filters, such as the horizontal belt filters.

The procedure for the laboratory filtration experiments conducted with the filter equipment shown in Figure 3.9 is as follows:

(a) The thickness of the filter cake must be between 30 and 40mm to ensure optimum filter performance. Calculate the mass of solids required to ensure a 35mm cake thickness (assume a moisture content of 5-7%).

(b) Make-up slurry with a solid content of 70% using the mass of solids calculated in (a), which was 765g, and mix thoroughly. Use automatic mixer to keep particles in suspension.

(c) Set vacuum at –70 kPa.

(d) Close the manual valve shown in Figure 3.9.

(e) Quickly pour the slurry into the funnel. Ensure that the slurry is in suspension while pouring.

(f) Open manual valve rapidly and allow 3-5 seconds for the cake to dry and close the valve again. The moisture content of the cake should be between 5 and 7%.

(g) Steps (a) to (f) need to be repeated a few times until all the parameters are confirmed.

(h) If cake washing is required, the following steps must be taken:

- Keep the manual valve closed after it has been closed in step (f).
- Calculate the water content of the cake.
- Use a wash ratio of 2.5 to calculate the amount of wash water required (wash water = wash ratio x cake water content).
- Adjust the pH of wash water by adding concentrated sulphuric acid.
- Add the wash water to the cake. Care must be taken not to damage the cake, which could cause channelling of the water.
- Open the manual valve rapidly and allow to drain for 3 to 5 seconds; then closing the manual valve to stop the drainage.

(i) Analyse the cake and/or filtrate for iron.

3.1.5. PLANT TRIALS

HAL and wet gravity iron, and HAL pH and temperature balances were conducted in order to determine the distribution of iron and identify the type of iron complexes formed, respectively.

3.1.5.1. HAL iron, pH and temperature balances

Iron concentrations in the HAL circuit were determined at the different equipment by taking samples of approximately 100 ml. The samples were analysed for iron by using the procedure as described in Paragraph 3.1.1 – *Quantification of iron precipitation as a function of pH* and Equation 3.5. The pH values at the various points in the HAL circuit were determined by measuring the pH prior to acid addition (if applicable) of the 100 ml samples collected for iron analysis. The temperature profile of the circuit was determined by taking direct measurements at the relevant equipment. This information was required to theoretically determine the pH level at which precipitation of iron would occur and also to identify the most likely form(s) of iron complexes that would form in the HAL circuit.

3.1.5.2. Wet gravity iron concentrations and mass balances

The concentration of iron precipitates present in the process water and slurry of the wet gravity circuit was determined to establish if a relationship existed between the water quality of the process water (in terms of iron content) and the separation performance of the dry mill circuit. The iron balances and other experimental results were used to quantify how much of the precipitated iron attached to the mineral surfaces and the amount of precipitates that were fed to the dry mill circuit. Wet gravity iron and dry mill mineral mass balances were also recorded during periods when the caustic was temporarily stopped to confirm the impact of reduced volumes of precipitates on plant scale electrostatic separation. Iron concentrations in water samples were determined by the procedure described in Paragraph 3.1.1 – *Quantification of iron precipitation as a function of pH* and Equation 3.5. Approximately 100 ml per sample is required to allow for potential losses occurring during filtration (50 ml filtrate is required for iron titration). The following water samples were analysed for iron:

(a) Water of the primary spirals (collected at spiral).

(b) Water of the fines spirals (collected at spiral).

(c) HAL circuit process water (collected at the HAL water supply tank).

(d) Wet gravity process water (collected at dirty water tank).

(e) First primary concentrate transfer sump in the wet gravity circuit (collected at sump 407).

(f) Second primary concentrate transfer sump in the wet gravity circuit (collected at sump 420).

Slurry and concentrate samples were analysed to determine the concentration of dissolved, adsorbed and suspended iron complexes present. This information was used to set-up iron mass balances for the wet gravity circuit to quantify the amount of iron fed to the wet gravity circuit, which was distributed to the dry mill circuit as primary concentrate. The procedure is as follows:

(a) Collect approximately 1 litre each of primary and fine spiral feed (slurry), and 400 g of primary concentrate.

(b) Adjust the pH of the two slurry samples to 1.3 by adding a few drops of concentrated sulphuric acid. Record the volume of sulphuric acid added. Mix thoroughly.

(c) Adjust the pH of 100 ml water to 1.3 by adding a few drops of concentrated sulphuric acid to the water while mixing.

(d) Determine iron concentrations as explained in Paragraph 3.1.2.1 – *Determining concentrations of precipitates present on the mineral surfaces and sample liquid*.

(e) Refer to Figure 3.10 to determine the wet gravity iron mass balance.

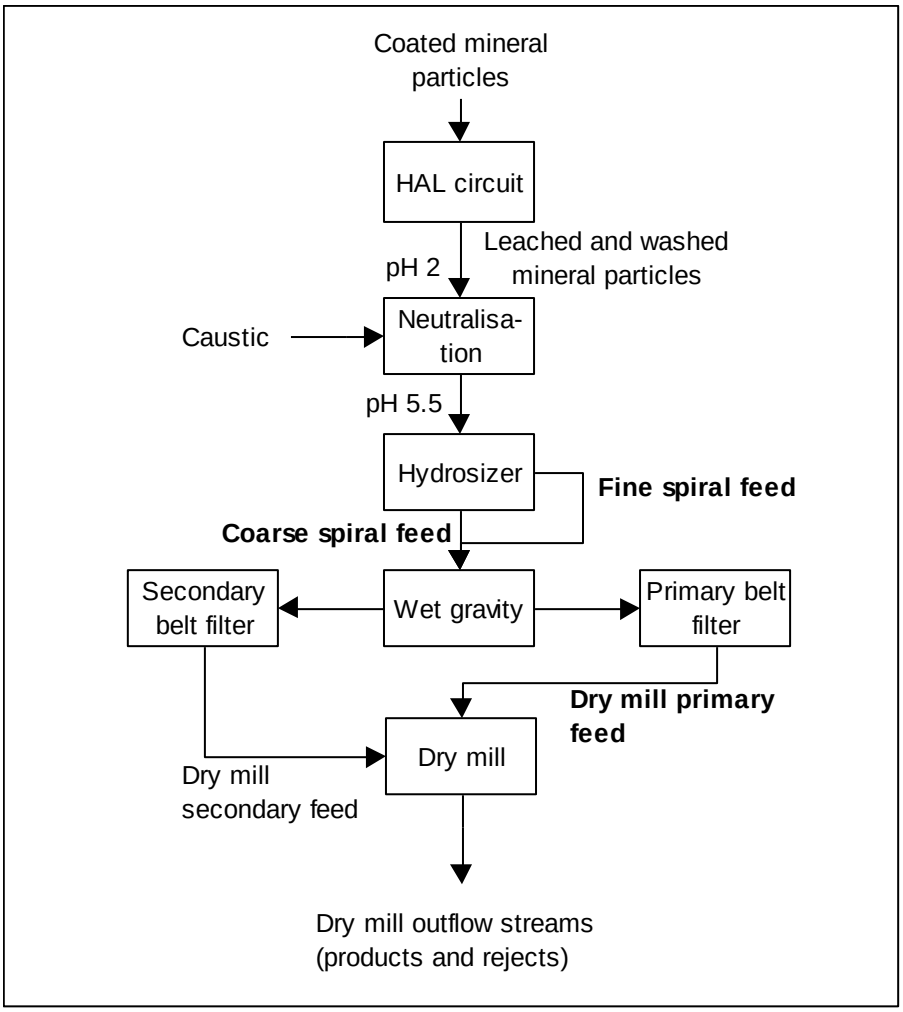

Figure 3.10: Block diagram showing the streams used in the iron balance of the wet gravity circuit to determine the amount of iron being distributed to the dry mill circuit as primary concentrate.

3.1.5.3. Temporarily stopping the addition of caustic in the HAL circuit

Caustic addition to the HAL attritioners was temporarily switched off during several plant trials. Iron concentrations in the wet gravity process water and the iron mass balances, as described in Paragraph 3.1.5.2 - *Wet gravity iron concentrations and mass balances*, were determined. The dry mill separation behaviour and mineral balances were simultaneously monitored. The outflow streams of the dry mill circuit, which were used to conduct the mineral balances, are shown in Figure 3.11. Stream mineral compositions were determined by mineralogical grain counting of daily composite samples (24 hours). Mass measurements were automatic readings obtained from the on-stream mass measurement scales via the PLC.

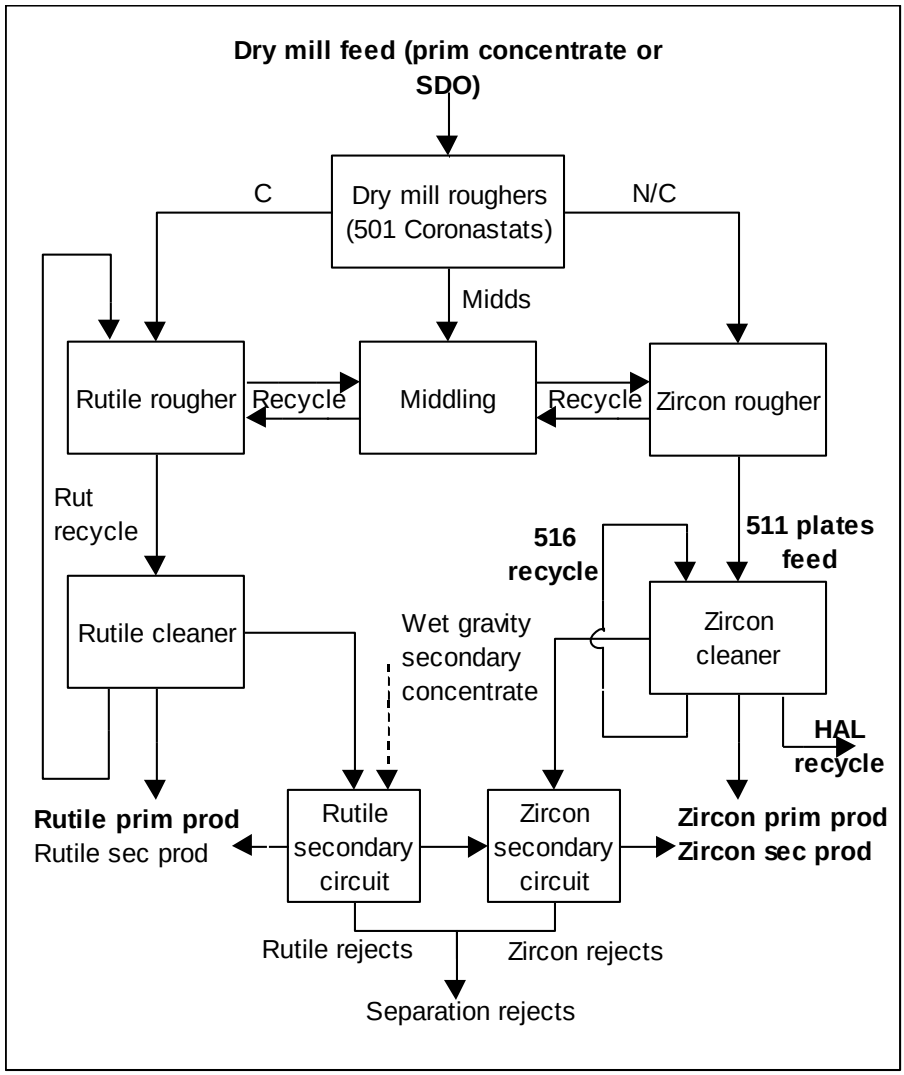

Figure 3.11: Simplified block diagram of the complex dry mill circuit at Namakwa Sands indicating the main recycling streams. Streams used in the mineral balance are indicated in bold.

3.2. ANALYTICAL METHODS

3.2.1. XRF AND AMDEL ANALYSES

Both the XRF and AMDEL exploit the interaction of radio-isotope and X-rays, which are important to chemically analyse minerals. They were therefore used for process control. The on-stream installed AMDEL provided quick (5-second intervals), but less accurate chemical analyses of a mineral stream. The final chemical grades of the mineral samples were confirmed with an XRF situated in the laboratory. The XRF had a relatively long turnaround time (30 – 60 minutes) and involved extensive sample preparation. It produced accurate results and was therefore used for final quality control. An XRF spectrometer uses primary radiation from an X-ray tube to excite secondary X-ray emission from a sample. The radiation emerging from the sample includes the characteristic X-ray peaks of major

and trace elements present in the sample. Dispersion of these secondary X-rays into a spectrum, usually by X-ray diffraction, allows these elements present to be identified in the sample. The height of each characteristic X-ray peak relates to the concentration of the corresponding element in the sample, allowing quantitative analysis of the sample for most elements in the concentration range of 1ppm to 100wt%.

3.2.2. SOLUTION CHEMISTRY

The total concentration of iron was determined by a standard method commonly used by laboratories. The method included oxidation of iron (II) to iron (III). Iron concentrations were determined via titration using dichromate (see method below). Full water analyses were conducted by the ISO accredited methods, by J.A. Santen of the water division laboratories of the SABS, Cape Town. The method for determining the iron concentration in a solution is as follows:

(a) Transfer 50 ml liquid sample (use pipette) into a conical flask.
(b) Add 7ml of concentrated hydrochloric acid and place on a pre-heated hot plate till the solution boils.
(c) Add a few drops of 5% stannous chloride to the hot solution until the yellow colour disappears.
(d) Allow the sample to cool down to room temperature and then add 5ml of 5% $HgCI_2$. Mix well and allow standing for 3 minutes.
(e) Add 15 ml of mixed acid and 5 drops of indicator to the solution.
(f) Place the solution on a magnetic stirrer and titrate against the standard $K_2Cr_2O_7$ solution.
(g) The end-point of the titration is detected with a permanent change in colour – from colourless to green to violet.
(h) Calculate the iron concentration by using Equation 3.20.

$$Fe\ (g/dm^3) = \frac{t \times 0{,}005 \times 1000}{V} \qquad \textbf{Equation 3.20}$$

3.2.3. MINERALOGICAL ANALYSIS

3.2.3.1. Representative sample splitting

Representative sampling splitting is important to ensure accurate and repeatable results. Great care must therefore be taken to ensure that splitting is done accurately, using the correct equipment.

(a) Dry samples (0% moisture)

Dry samples were divided into representative splits of equal mass and composition by means of a rotating splitter (supplied by Dickie & Stockler), dividing a dry sample into 8 splits that were almost identical.

(b) Wet samples (2-6% moisture)

The error associated with dividing wet samples into splits of equal mass and weight is much bigger than for dry sample splitting. A manual riffled sample splitter was used for this purpose.

3.2.3.2. Stereo microscope images

Stereomicroscope images of minerals assisted in the visual identifying of surface deposits and other mineralogical properties.

3.2.3.3. Grain counting

One of the quality control tools used at some mineral processing plants is microscopic determination of the mineralogical composition of samples from various wet or dry streams in the plant. This is usually performed using manual grain-counting techniques, where a trained operator identifies and counts the individual minerals on a glass slide via a stereomicroscope. A thin film of sugar water is applied evenly over a slide to ensure that a uniform monolayer of particles will stick to the slide. The stream composition is statistically calculated.

3.2.4. DETERMINING MOISTURE/WATER CONTENT OF SAMPLES

The moisture or water content of samples was simply determined by subtracting the dry mass from the wet mass. The method is as follows:

(a) Weigh the wet sample.

(b) Decant excess water without decanting any solids.

(c) Dry in an oven or on a stove long enough to ensure complete drying (the temperate of the sand can be used as guide line).

(d) Allow to cool down and weigh dry sample.

(e) Calculate the moisture content by using Equation 3.21.

$$\%\text{Moisture} = \frac{M - M_{Dry}}{M} \text{x}100 \qquad \textbf{Equation 3.21}$$

3.2.5. pH AND TEMPERATURE

An electronic pH meter (model MP220, supplied by Mettler Toledo) with an automatic temperature compensator was used for pH measurements. The meter was calibrated with three standards (pH 4, 7 and 9) before measurement. Temperature of solutions, mineral samples and surfaces (e.g. Coronastat roll) were taken with an infrared temperature gauge.

3.3. CHEMICALS AND MISCELLANEOUS ITEMS

The following chemicals were used in the experimental and analytical methods:

3.3.1. IRON TITRATIONS

(a) 5% stannous chloride solution: 5g stannous chloride dissolved in 5ml concentrated hydrochloric acid and diluted to 100ml with distilled water.

(b) 5% mercuric chloride solution: 5% of $HgCI_2$ dissolved in hot water to 100ml.

(c) Standard potassium dichromate solution (1ml of $K_2Cr_2O_7$= 0,005Fe): Dissolve 4.3899g of potassium dichromate dried at 110^oC for 1hour, in water and dilute to 1dm^3.

(d) Sodium diphenylamine sulphonate indicator solution: 0,2g of solid dissolved water and diluted to 100ml.

(e) 40% (m/v) sulphuric acid solution: 400g of concentrated sulphuric acid diluted with water up to 1dm^3 (reaction is exothermic; therefore, work in ice bath).

(f) Mixed acid solution: Make up a 1:1 Sulphuric acid solution (50$^{\%}$solution) and add 300ml from this solution to 150 ml concentrated phosphoric acid H_3PO_4 and dilute to 1dm^3 (work in ice bath due to exothermic reactions).

3.3.2. OTHER CHEMICALS: IRON PRECIPITATION AND CHEMICAL DESORPTION

(a) Concentrated sulphuric acid (98.08% H_2SO_4): supplied by MERCK KGaA, Germany.

(b) Concentrated caustic soda (also used in the plant).

(c) Distilled water: prepared by Namakwa Sands laboratory.

3.3.3. MISCELLANEOUS

(a) Whatman 185 mm diameter filter papers (No. 2): supplied by Whatman International Ltd, England.

(b) Electrical heat blower.

(c) Digital tachometer (model Dt-2235A).

(d) Glassware: Pyrex bowl, 50 ml burette, 50 ml pipette, measuring cylinder, glass rod, conical flasks.

(e) Magnetic stirrer.

(f) Wemco flotation cell (used for laboratory attritioning).

(g) Hot plate.

(h) Drying oven.

(i) Weighing balance (Metler PM 16-K).

3.4. NOMENCLATURE OF SYMBOLS USED

C_{F1} = Concentration (g/dm^3) of dissolved iron (II and III) in the filtrate after pH adjustment with sulphuric acid and filtration to remove suspended solids.

C_1 = Concentration (g/dm^3) of dissolved iron (II and III) after pH adjustment with sulphuric acid, but before filtration.

C_O = Concentration (g/dm^3) of dissolved and precipitated iron (II and III) in the original solution before pH adjustment with sulphuric acid.

C_{F2} = Concentration (g/dm^3) of dissolved iron (II and III) in the filtrate after pH adjustment with caustic and filtration to remove iron hydr(oxide) and other precipitates.

C_T = Total mass concentration (g/dm^3) of specie X in the sample with mass M.

C_{WL} = Mass concentration (g/dm^3) of specie X in the wash liquid (WL).

C_{SL} = Mass concentration (g/dm^3) of specie X in the sample liquid (SL).

C_L = Mass concentration (g/dm^3) of specie X in the liquid fraction removed for analysis.

M_{F1} = Mass (g) of dissolved iron (II and III) in the filtrate after pH adjustment with sulphuric acid and filtration.

M_1 = Mass (g) of dissolved iron (II and III) after pH adjustment with sulphuric acid, but before filtration.

M_O = Mass (g) of dissolved and precipitated iron (II and III) in the original solution before pH adjustment with sulphuric acid ($M_1 \approx M_O$).

M_{F2} = Mass (g) of dissolved iron (II and III) in the filtrate after pH adjustment with caustic and filtration.

$(M_{F2})_{corrected}$ = Mass (g) of dissolved iron (II and III) in the filtrate after pH adjustment with caustic and filtration. This mass takes into account the water retained by the hydrophilic filter cake.

M_P = Mass (g) of precipitated iron (II and/or III) hydr(oxides).

m_T = Total mass (g) of specie X, such as iron.

m_{WL} = Mass (g) of specie X in the wash liquid (WL).

m_{SL} = Mass (g) of specie X in the sample liquid (SL).

m_S = Mass (g) of specie X attached to mineral surfaces or present in the microscopic water layer surrounding mineral particles of the sample (S).

M = Total mass (g) of the sample including both solid and liquid phases.

$MD(NC)_{Fi}$ = Cumulative mineral distribution of a mineral specie to non-conductors at a specific fraction i (NC, M3, M2, M1 or C).

$MD(C)_{Fi}$ = Cumulative mineral distribution of a mineral specie to conductors at a specific fraction i.

M_{Dry} = Mass (g) of sample after drying and cooling.

V_{F1} = Volume (dm^3) of the filtrate after pH adjustment with sulphuric acid and filtration.

V_1 = Volume (dm^3) of solution after pH adjustment with sulphuric acid, but before filtration ($V_1 = V_O+V_A$).

V_A = Volume of concentrated sulphuric acid added to reduce pH to 1.3.

V_{F2} = Volume (dm^3) of the filtrate after pH adjustment with caustic and filtration.

V_T = Total volume (dm^3) of liquid, which is the sum of the wash liquid (WL) and sample liquid (SL).

V_{WL} = Volume (dm^3) of wash liquid (WL).

V_{SL} = Volume (dm^3) of sample liquid (SL).

%E = Efficiency of separation at a specific point on the performance graph.

ZD_{NC} = Zircon distribution to non-conductors.

RD_C = Rutile distribution to conductors.

RD_{NC} = Rutile distribution to non-conductors.

NC = Non-conductors

C = Conductors

CHAPTER 4

EXPERIMENTAL RESULTS

Objectives of Chapter 4:

- Explain the objectives of the individual experiments.
- Discuss the results obtained during the experimental testwork.

The results obtained for the experimental investigation are presented in this chapter. The main purpose of these experiments was to determine whether iron and other chemical species precipitate in the HAL circuit and attach to mineral surfaces, the impact of these attached species on mineral separation, and to determine a process solution that would ensure clean mineral surfaces.

Experiments used to quantify the impact on separation were repeated several times, but every time slightly differently in order to minimise the risks associated with investing capital in the implementation of a process solution.

4.1 TEMPERATURE AND pH OF THE HAL CIRCUIT

A temperature and pH survey was conducted on the HAL circuit to determine which were the most likely iron precipitate species to form as described in Chapter 2 - *Literature Review and Theoretical Considerations*. The temperature and pH profile of the HAL A circuit is summarised in Table 4.1. The HAL circuit consisted of two identical process circuits, referred to as sides A and B, which ran in parallel at 12 and 24 tph, respectively (refer to Figure 1.2). These streams were fed at different feed rates and residence times from the same feed bin, and therefore their physical and chemical properties could be considered as almost identical. Reactor discharge streams were processed in two parallel elementary wash circuits, consisting of a dewatering cyclone and classifier, before the slurry had been neutralised with caustic soda in attritioner banks. Process water obtained from the proceeding wet gravity and water contained in the HAL circuit slurry were fed to the HAL circuit via the HAL water tank. This water was used for the elementary mineral washing and slurry transfer.

The reactors discharged minerals (4-5% moisture content) at a temperature of approximately 85^{o}C. The temperature was cooled down by HAL process water in the quench sumps to about 40^{o}C. The pH was the lowest at this point and gradually increased to about 2-2.8 at the underflow of the upflow

classifiers before entering the attritioners where caustic was added to raise the pH to 5. The temperature of the slurry was increased by almost 10^{o}C due to attritioning. Process water from the HAL water tank entered the circuit at about 30^{o}C and at a pH of 4.5-5.

The experiments were conducted on a day when the ambient temperature was 35^{o}C and during stable operation of the HAL circuit. Therefore, the temperature and pH profile could be accepted as representative. Although not recorded, follow-up work confirmed the pH profile. Temperatures varied slightly by a couple of degrees as a result of lower ambient temperatures during the winter months.

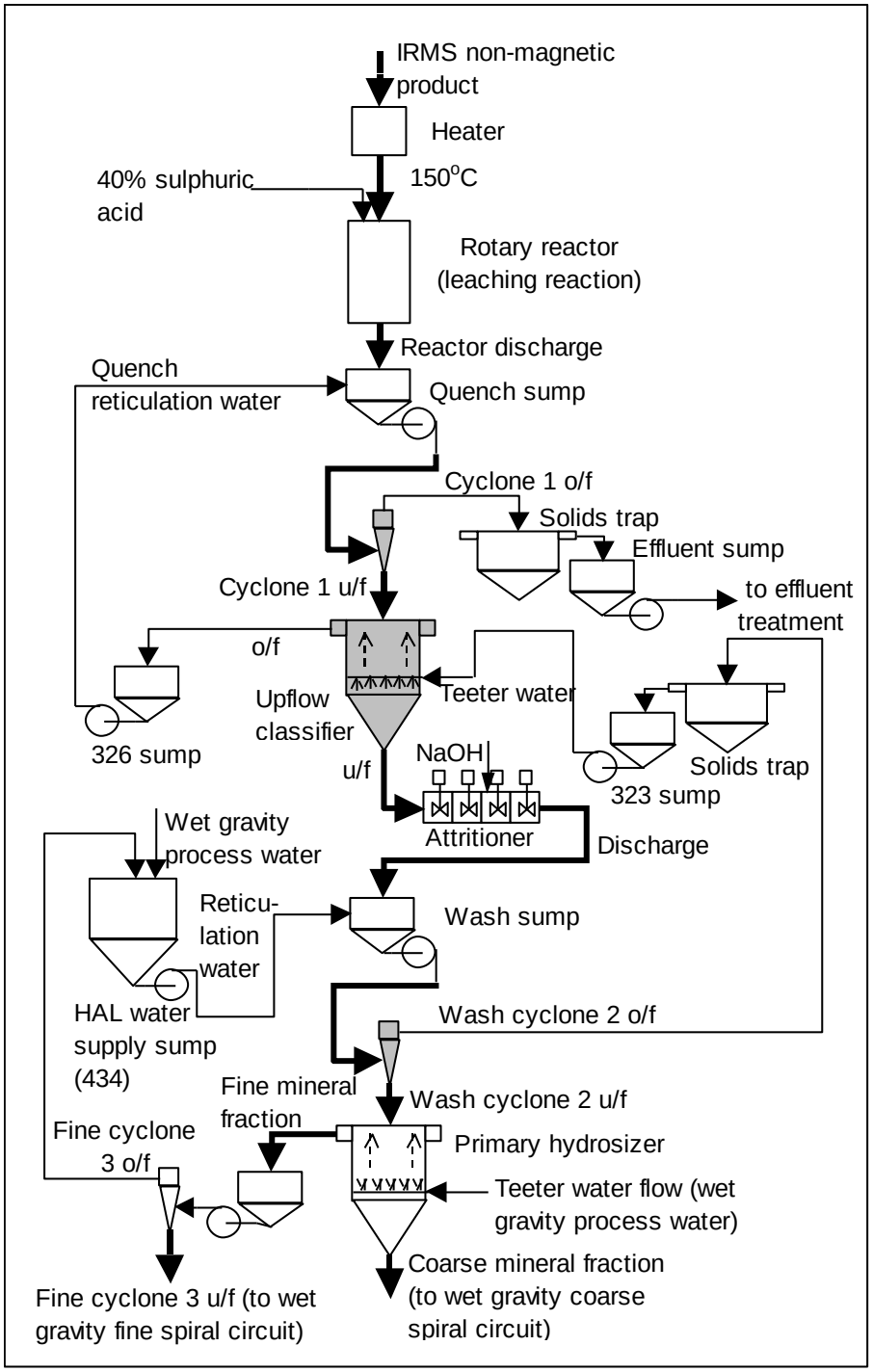

Figure 1.2: Process flow diagram of one of the parallel streams of the existing HAL circuit at Namakwa Sands. Thick lines indicate solid/slurry streams and normal lines indicate water streams. Mineral wash and dewatering equipment of the HAL circuit is indicated in bold.

It was noted during the course of the study that the pH profile changes were affected by certain conditions, which were:

- Decreasing washing efficiency primarily due to choked tuyers of the upflow classifiers. Spray water was introduced to the upflow classifiers through tuyers, which increased the velocity of the upflow stream of water required to wash the mineral particles. Any significant restriction to this flow would impact the washing efficiency.
- The washing efficiency was also affected by a decrease in cyclone efficiency mainly due to wear of the cyclone spigots, as well as a decrease in pump efficiency, also due to wear.
- An increase or decrease in the iron content associated with the mineral coatings resulting in fluctuating free acid concentrations.

It is clear from Table 4.1 that the temperature in the HAL circuit did not exceed 43^{o}C except at the discharge of the reactor, which was at 88^{o}C. The pH values started with 1.67 at the quench sump, where the dissolved iron was the highest, and ended up at 2.8 in the underflow of the upflow classifier before the pH was raised to a set point of 5 in the attritioners. It was interesting to note that the pH of the concentrated slurry stream of the underflow of the cyclone 2 was lower than the pH of its overflow; and although the pH had been raised to a set point of 5, the pH of the water in the HAL water tank was at a lower value of 4.08. It is important to mention at this point that the residence time of mineral transport in the A and B reactors and the proceeding washing stages were 45, 90 and 15 minutes, respectively. Mineral transport through the wet gravity circuit was about 15-20 minutes. Recycling of water in the HAL, and especially in the wet gravity circuit, was estimated to be approximately 4 hours.

Table 4.1: Temperature and pH profile of the HAL circuit (taken with an infrared temperature meter). The ambient air temperature was 35°C when the temperatures of the solutions were taken.

Stream	A side	
	pH	Temperature (°C)
Reactor discharge	-	88
Quench sump	1.67	40
Quench water sump (326)	1.88	33
Cyclone 1 underflow	1.51	36
Cyclone 1 overflow	1.61	37
Upflow classifier overflow	1.88	33
Upflow classifier underflow	2.83	34
Upflow classifier teeter water sump (323)	5.26	31
Attritioner discharge	Not measured	43
Wash sump	Not measured	30
Wash cyclone 2 underflow	4.03	33
Wash cyclone 2 overflow	5.26	33
Fine cyclone 1 underflow	Not measured	29
Fine cyclone 1 overflow	Not measured	30
HAL effluent	1.74	37
Primary hydrosizer overflow	Not measured	31
HAL water supply tank (434)	4.08	29

4.2 FE (III)/FE (II) RATIO

It was important to determine the iron (III)/iron (II) ratio and to establish if it fluctuated over time. A higher ratio would result in higher volumes of iron for precipitation. The determination of the total iron concentration by means of titration was a straightforward analytical technique and was found to be accurate when compared to more sophisticated techniques, such as ICP as used by the SABS. Quantification of Fe (II) and Fe (III) was more complicated and less accurate. Analyses were conducted by the SABS and CSIR.

The results were disappointing, and according to the SABS, not very reliable due to the potential ageing of the samples. . Experimental work conducted later in this study showed that this ratio could be determined relatively accurately by increasing the pH of the solution to a pH of approximately 5 in order to remove all of the ferric ions (Fe^{3+}) via filtration. Therefore, the iron analyses of the remaining solution (via titration) would reveal the concentration of ferrous ion. These analyses (see Paragraph 4.4 – *Iron precipitation curves*) indicated that concentration of ferric iron ranged from approximately 50% to close to 100% of the total iron concentration, which consequently resulted in fluctuating iron (III)/iron (II) ratios over time

4.3 PRECIPITATION OF SPECIES BY RAISING THE pH OF THE SOLUTION

A series of experiments were conducted to identify and quantify what specific species precipitated if the pH was increased to 5 and 7 to simulate the HAL neutralisation stage where caustic was added to increase the pH to 7. This set-point was later reduced to pH 5 to reduce the volume of precipitates formed. Iron precipitation curves were constructed to evaluate the change in iron concentration via an increase in pH. Mineral samples were rinsed with acidic water and the rinse water was analysed to determine if the precipitate species formed in the HAL neutralisation step was also present on the mineral surfaces, which would confirm the adsorption theory.

4.3.1. CHANGE IN CONCENTRATION OF CHEMICAL SPECIES PRESENT IN THE PROCESS WATER OF THE HAL CIRCUIT BY ADJUSTING THE pH

Table 4.2 provides a summary of concentrations of the major dissolved species present in the underflow of the upflow classifiers. The sample was filtered before being submitted for analysis. Caustic was added to a second sample to raise the pH to 5, thereby simulating the HAL caustic addition step, to identify the species that precipitates by increasing the pH. The sample was filtered to remove the resultant precipitates and the filtrate was submitted for analyses. The primary concentrate (dry mill feed sample) was rinsed with acidic water (pH 1.3 and liquid/solid ratio of 25 mass%) to remove precipitates attached to the surface and the analyses were corrected by accounting for the analyses of the acidic wash water. Aluminium, iron and sulphate concentrations decreased significantly by increasing the pH. Sodium, potassium and chloride increased with the addition of caustic. Note that the pH of both the before and after samples was lower and the pH of the primary concentrate was higher than the values measured before the samples had been submitted for analyses. These differences were ascribed to ageing due to a long turnaround time of the sample analyses.

Therefore, the results of experimental work conducted on the effluent stream (Table 4.3) were used to confirm the results of Table 4.2.

Table 4.2: Identifying the main HAL precipitation species by raising the pH with the addition of caustic soda. HAL attritioner feed samples was collected on the 20th May 2003.

Determinants	Unit of measure	Before caustic	After caustic	Prim conc [mg/kg dry sand]
PH at 25°C	-	0.70	3.1	1.3
Conductivity in at 25°C	mS/meter	8 460	3 700	-
Dissolved solids at 180°C		15 120	54 600	-
Turbidity in nephelometric units	-	54	1	-
Ca	Mg/l	590	524	13.43
Mg	Mg/l	29	27	0.932
Na	Mg/l	272	420	3.370
K	Mg/l	20	96	1.688
Cl	Mg/l	<5	57	5.0
SO_4	Mg/l	31 000	17 000	635.96
Total alkalinity as $CaCO_3$	Mg/l	<1	<1	-
Bicarbonate as $CaCO_3$	Mg/l	<1	<1	-
F	Mg/l	14	17	-
Sr	Mg/l	1	3	0.036
Ba	Mg/l	<0.05	0	0
Fe	Mg/l	111	0.51	1.241
Al	Mg/l	65	0.15	1.230

The results of Table 4.3 were obtained by raising the pH of the effluent water of the HAL circuit to 5.4 by the addition of limestone (particle size < 250µm, 97 mass% $CaCO_3$) followed by hydrated lime to increase the pH to 7, 8.5 and 10. The hydrated lime solution was prepared by mixing 90% CaO (unslaked lime) with water. Limestone was considered a cost-effective means of neutralising the effluent water. The results were found to be very useful and applicable for the purpose of this study. However, it is important that the reader do not confuse this precipitation process with the caustic soda precipitation process of the HAL circuit due to slightly different chemical reactions as discussed later in this paragraph. The composition of the effluent water was taken as the average of three samples assayed on 16, 18 and 19 December 2003. The composition over this period was very stable and the

abundant species in decreasing sequence were SO_4, total Fe (80% Fe (III)), Al, Ca and Mg. It was interesting to note that relatively high concentrations of Ti were measured. Although not analysed for all the species, the underflow of the upflow classifiers contained the same species as the effluent water of the HAL circuit, but at lower concentrations. It was expected that the same hydroxide compounds would have formed, compared to neutralisation with caustic soda, but neutralisation with limestone and lime would significantly reduce the sulphate concentration due to the formation of insoluble $CaSO_4$ compared to soluble $NaSO_4$ in the case of neutralisation with caustic soda.

It is clear from Table 4.3 that raising the pH of the effluent sample to a value of 7 resulted in a decrease in the concentrations of sulphate, iron (II), iron (III), aluminium, manganese, cadmium, chromium, nickel, titanium, uranium and thorium. Increase in concentrations of species, such as chloride, with the addition of limestone could be ascribed to the composition of the limestone and/or the water that was used for the test. It is important to mention that air was used to oxidise the Fe (II) to form Fe (III) during the addition of limestone and lime. From the results, and the fact that Fe (III) precipitates at relatively low pH values, one can see that almost 100% of the Fe (II) was oxidised after the first lime mixing stage (pH 7). The change in concentrations of the abundant species was observed as the pH was increased to 5.4, and it was noted that Fe (III) concentration decreased by 99.96% followed by a 99.9% reduction of aluminium. Ti was less abundant, but the concentration decreased by 99.97% when the pH was increased to 7. The relatively small amounts of radio-active species, namely uranium and thorium, also decreased significantly when the pH was increased to above 7.

Chemical desorption of mineral samples revealed that sulphates, iron and aluminium were present on the mineral surfaces. The acidic wash water analysed after rinsing of the primary concentrate contained relatively high concentrations of sulphate, calcium, chloride, sodium, potassium, iron, aluminium and magnesium (in order of decreasing magnitude). Sodium, potassium and chloride were expected to originate from the caustic soda and iron and aluminium formed as hydroxides during the neutralisation reaction. The chemistry of the mineral surfaces is discussed in more detail later in this section (see Table 4.2).

Table 4.3: Identifying the main HAL precipitation species by raising the pH with the addition of limestone followed by lime. The effluent stream of the HAL circuit was used for these analyses (the analyses of the effluent sample are the average of three samples collected over three days from 16 to 19 December 2003).

Determinants	Unit of measure	Effluent 16, 18-19 Dec'03	Limestone 16, 18-19 Dec'03	Lime 16, 18-19 Dec'03	Lime 16, 18-19 Dec'03	Lime 16, 18-19 Dec'03
pH at 25°C	-	1.2	5.4	7.0	8.5	10.0
Cl	mg/l	76	115	Not analysed	Not analysed	Not analysed
SO_4	mg/l	30 000	4 328	3 854	2 146	1 937
Ca	mg/l	489	515	478	46	1.3
Mg	mg/l	202	205	205	205	205
Fe (II)	mg/l	279	168	28	0	0
Fe (III)	mg/l	1 085	0.45	0.137	0.048	0.013
Fe(total)	Mg/l	1 364	168	28	0.048	0.013
Al	mg/l	745	0.9	4.12	0.04	0
Mn	mg/l	18	17	11	0.01	0
Ar	mg/l	0.090	0	0	0	0
Cd	mg/l	0.16	Not analysed	0.019	0.010	0.005
Cr	mg/l	23	Not analysed	0.16	0.11	0
Hg	mg/l	0.028	0	0	0	0
Ni	mg/l	1.5	0.15	0.16	0.085	0.042
Ti	mg/l	102	Not analysed	0.028	0.030	0.026
U	mg/l	0.8	0.2	Not analysed	Not analysed	<0.2
Th	mg/l	13	0.5	Not analysed	Not analysed	<0.2
Zr	mg/l	0.9	<1	Not analysed	Not analysed	<0.2

4.3.2. VISUAL OBSERVATIONS DURING PRECIPITATION EXPERIMENTS

Precipitation of species was visually observed when caustic was added to the process water of the HAL circuit. These recorded observations were useful, since they could be related to the process plant. Caustic was added to overflow and underflow samples of the upflow classifier A after removing suspended particles via filtration. These experiments were conducted in a relatively short period of time in May 2002 when the iron (III)/iron (II) ratio, as well as water composition, were constant.

Figure 4.1 shows photos of the filtered overflow sample of the upflow classifier A before and after caustic addition. A red-brown precipitate (iron hydroxide) formed at higher pH values (>2). It was important to observe the rapid rate at which these precipitates attached to the inside of the glass surface. Cleaning these surfaces was not effective when using fresh water at a neutral pH and it was found that rinsing with acidic water dissolved these precipitates effectively within a few seconds.

The visual observations of an iron precipitation experiment conducted with an upflow classifier overflow sample is summarised in Table 4.4. Analysis of this sample revealed that the majority of the iron was in the Fe (III) state and only trace amounts of Fe (II) were present. It was noted that iron started to precipitate at a very low pH of 1.2. Excessive precipitation occurred when the precipitate colour became brown, which occurred at a relatively low pH of 2.52. Almost 97% iron was precipitated at pH 4.28 where after the colour of the precipitate became reddish. At pH levels above 2.5, the precipitate became gel-like, which broke up into small 'particles' when vigorously mixed. These observations were confirmed by a series of tests.

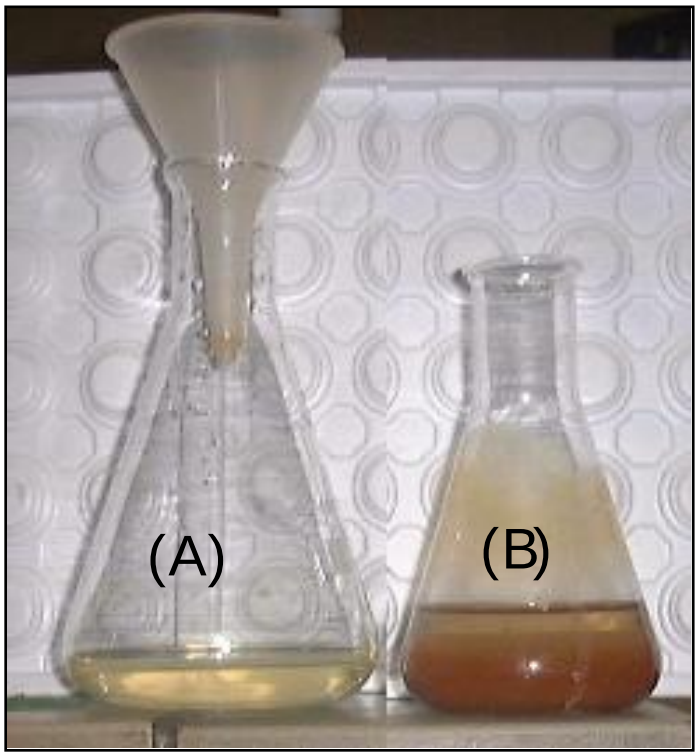

Figure 4.1: Photos showing an upflow classifier overflow sample before and after raising the pH by the addition of concentrated caustic. Suspended particles, such as clays, were removed by filtration prior to caustic addition.

Table 4.4: Observations noted during the precipitation experiment conducted in May 2002 when small drops of concentrated caustic were added to an overflow sample of the upflow classifier A (after filtration).

Sample	PH	Temp [^{0}C]	Fe precipitated [%]	Observation
1	0.89	18.4	0	Upflow classifier A overflow sample (after filtration; no precipitates were present. Solution was yellowish and transparent.
2	1.20	18.8	8.5	Very small amounts of white/yellowish precipitate formed, which dissolved easily when mixed.
3	1.48	19.6	19.1	Yellowish precipitate formed, which did not dissolve.
4	1.80	19.8	29.8	Very fine yellow precipitate 'particles' were visible.
5	2.52	20.1	67.2	Brown gel precipitate formed, which did not dissolve when mixed.
6	3.00	20.3	90.4	Large amounts of brown, gel precipitate formed. The solution was brown/yellow.
7	4.28	21.0	96.5	Brown gel precipitate reached maximum levels.
8	8.89	20.9	97.4	Excessive brown/red gel precipitate formed. Precipitate did not dissolve when mixed.
9	9.32	20.5	97.5	Excessive brown/red gel precipitate.
10	11.23	20.9	96.0	Excessive brown/red gel precipitate.
11	11.50	20.8	100.0	Excessive brown/red gel precipitate.

Concentrated sulphuric acid was added to a solution with iron-rich precipitate to visually determine the pH where all precipitates would be dissolved (see Table 4.5). The iron rich precipitate solution was prepared by adding concentrated caustic soda to the same original solution as used in the precipitation experiment of Table 4.4. It was observed that the brown precipitates, which formed at pH > 2.5, dissolved at pH 1.62, but that the solution was still brownish. The original greenish transparent colour returned at a pH of approximately 1.

Table 4.5: Summary of visual observations by incrementally adding concentrated sulphuric acid to an overflow sample of the upflow classifier A, rich in precipitated species, after the pH was increased to 9.26 with caustic. It is important to note that the same original solution was used as in the precipitation experiment of Table 4.5.

Sample	PH	Acid added [accumulated drops]	Observation
1	9.26	0	Brown precipitates – looked like muddy water.
2	8.5	1	Brown precipitates – looked like muddy water.
3	7.55	3	Brown precipitates – looked like muddy water.
4	6.36	5	Brown precipitates – looked like muddy water.
5	4.41	7	Brown precipitates – looked like muddy water.
6	3.73	9	Brown precipitates – looked like muddy water.
7	2.67	11	Brown precipitates – looked like muddy water.
8	2.18	13	Brown precipitates – looked like muddy water.
9	1.77	16	Brown precipitates – looked like muddy water.
10	1.62	19	Precipitate was broken down. Colour of the water was brown.
11	1.03	Not measured	No precipitate; solution was greenish as original solution.

Precipitation and the dissolution experiments were also conducted with the underflow of the upflow classifier A, which contained relatively low concentrations of dissolved iron. Observations are summarised in Table 4.6. Very small amounts of precipitates were noticed at pH 2.48, which changed to yellow and increased at pH 4. This precipitate became brown and broke down into fine suspended ‘particles’ at pH > 7.9. Sulphuric acid was added to dissolve the precipitate and it was noticed that the precipitate broke down into very small ‘particles’ at pH 2.4. More acid was added and all the precipitates were completely dissolved at pH 1.1, when the solution returned to its original light green colour.

Table 4.6: Summary of visual observations by incrementally adding concentrated sulphuric acid to an underflow sample of the upflow classifier A after the pH was increased with caustic.

Sample	pH	Caustic added [accumulated drops]	Acid added Yes/No?	Observation
1	1.61	0	No	No precipitate. Solution is transparent (light green).
2	2.48	1	No	Very small quantities of white/gel precipitate formed.
3	4.00	2	No	Yellow precipitate formed.
4	7.92	3	No	Precipitate broke down in small 'particles'.
5	11.19	4	No	Precipitate broke further down in small 'particles'.
6	2.4	0	Yes	Precipitate 'dissolved' into very fine 'particles'.
7	1.1	0	Yes	No precipitate. Solution returned to original light green colour.

These experimental observations were valuable, but the exact pH where the precipitates dissolved could not be determined with absolute confirmation. It is important to realise that the iron (III)/iron (II) ratio was very high during May 2002 when these experiments were conducted, and different observations would be expected at lower iron (III)/iron (II) ratios.

4.4. IRON PRECIPITATION CURVES

The iron precipitation curves were constructed in order to determine the pH at which precipitation started and to quantify the change in iron concentration with an increase in pH. This was very useful information especially for the design of a process solution to prevent the formation of these complexes. Iron precipitation was quantified by incrementally raising the pH of individual process water samples by adding small amounts of concentrated caustic soda. Suspended particles were removed by filtration prior to caustic addition, the precipitates were also removed by filtration, and the filtrate was analysed for total iron. The logarithm of the iron concentrations (mole/dm^3) and the % iron precipitated were plotted against the pH.

4.4.1. UPFLOW CLASSIFIER UNDERFLOW

Iron precipitation experiments conducted by using samples obtained from the underflow of the upflow classifiers were very important since this stream was fed to the attritioners where caustic was added to neutralise the slurry, consequently resulting in the precipitation of species. This information was critical for the design of a process solution, which would be used in identifying the optimum pH that would prevent the precipitation of iron.

Two experiments were conducted with samples from the underflow of the upflow classifiers. The results of the first experiment (and experiment C1 of the quench sump) were negatively affected by contamination of the chemicals and were consequently discarded. Newly prepared chemicals were used for all of the remaining precipitation experiments. The colour change (light green to purple) at the end points was dramatic and clearly visible.

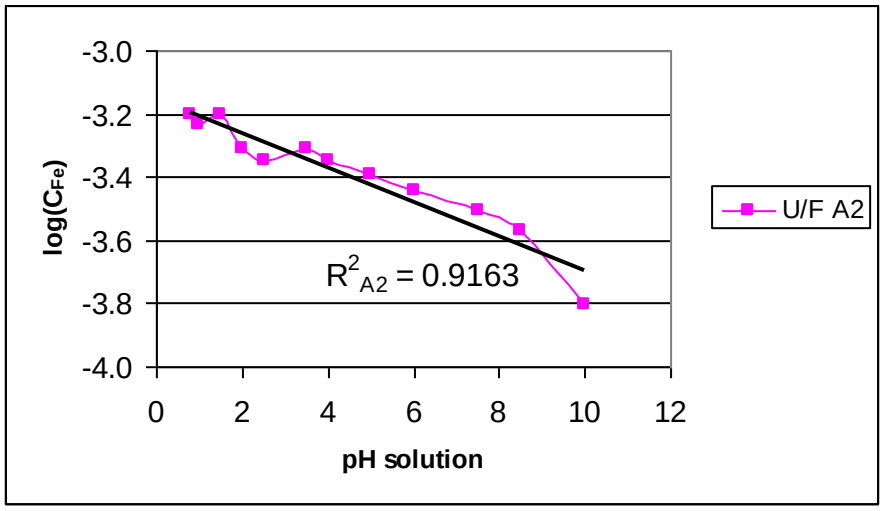

Figure 4.2: Precipitation of total iron by raising the pH of an upflow classifier underflow sample collected in the HAL circuit. The pH was increased by incrementally adding concentrated caustic to a filtered sample. The solution was mixed with an automatic stirrer. Run A2 was conducted on 29 April 2004.

It was found that the iron concentrations of the underflow streams of the upflow classifiers were relatively low (0.035 g/dm^3). Various other samples collected on different days were analysed and it was found that this concentration fluctuated between 0.027 and 0.23 g/dm^3, which was also confirmed by the analytical laboratories of SABS who obtained similar results (standard deviation of individual data points were 0.0016 g/dm^3). It was further observed that the iron concentration started to decrease

at pH slightly above 2. Fitting a linear regression line through the data points showed that the relationship between pH and iron concentration in the underflow of the upflow classifier was not truly linear due to the two oxidation states of iron.

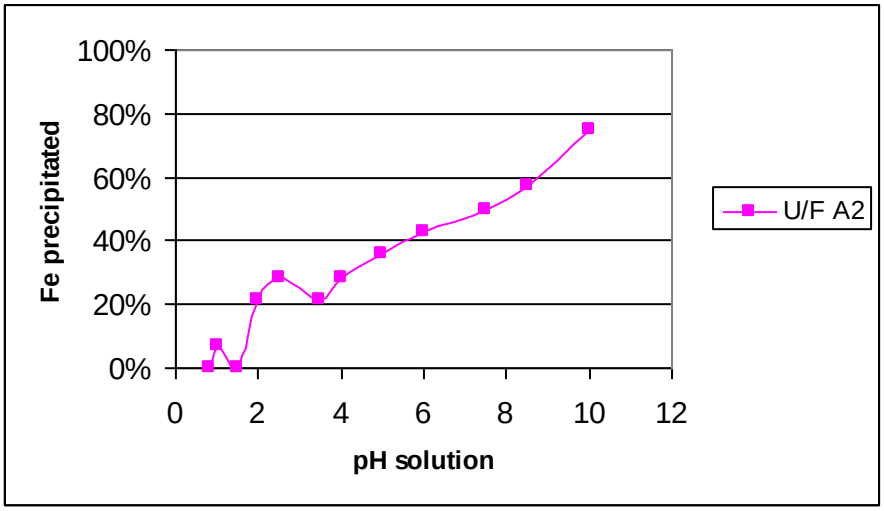

Figure 4.3: Precipitation of total iron of the individual underflow samples expressed as % of total iron present.

From the precipitation curve of experiment A2 (Figure 4.3), the second, third and fourth data points seemed too high, and incorrectly so when comparing this graph with the other precipitation curves. It important to note that approximately 38%, 50% and 78% of the total iron had precipitated at pH values of 5, 7 and 10, respectively.

4.4.2. UPFLOW CLASSIFIER OVERFLOW

The iron precipitation experiments were also repeated with samples obtained from the overflow of the upflow classifier and the quench sump, to determine the pH at which precipitation of iron occurred further up in the HAL process where high concentrations of iron occurred. This information was also used for the design of process solution, which would maximise the removal of dissolved iron prior to the addition of caustic. Iron precipitation experiments, using samples obtained from the overflow of the upflow classifier, were conducted two years apart. Sample B4 was collected and tested in April 2002, while experiments B1 to B3 were tested in April and May 2004. The results were significantly different (see Figure 4.4). Graphs B1 to B3 tend to be linear and graph B4 is definitely non-linear (combined polynomial and exponential). The final iron concentration in experiment B4 seemed to be incorrectly too high and could probably be ascribed to an analytical error. Although not shown,

experiment B4 was repeated within a period of a month with a fresh sample, which confirmed experiment B4. Standard deviations and average values of the data points of Graphs B1 to B3 are summarised in Table 4.7. The total iron (first data point) and the values after pH 3.5 at the lower iron concentrations deviated the most, but in general the repeatability of the data was acceptable for its intended application. Experiment B3 was conducted with a high degree of precision and the graph had the highest R^2-value, which was consequently used for the investigations.

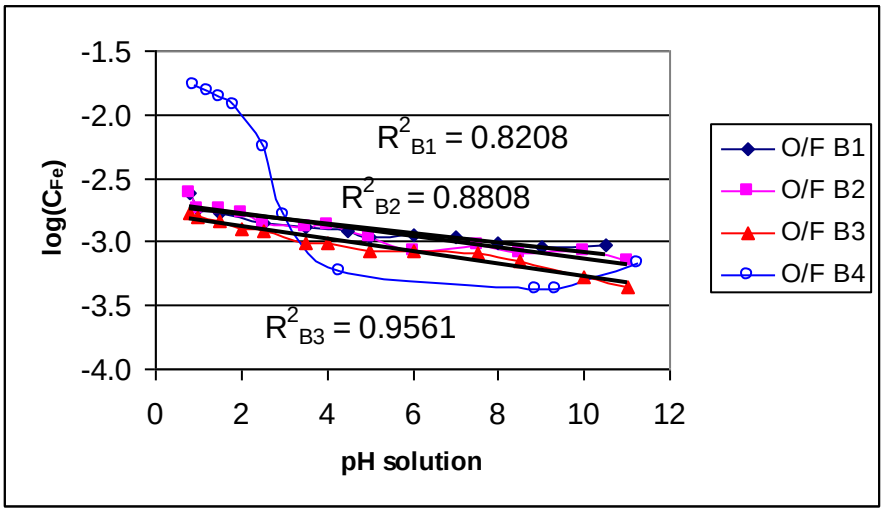

Figure 4.4: Precipitation of total iron by raising the pH of individual upflow classifier overflow samples collected in the HAL circuit. The pH was increased by incrementally adding concentrated caustic to a filtered sample. The solution was mixed with an automatic stirrer. The experiments of Run B1, B2 and B3 were conducted on 20 April, 29 April and 10 May 2004, respectively. Samples B1 – B3 were collected on the same day. Run B4 was performed in April 2002. Only samples from classifier A were used for these experiments.

From Graph O/F B3 of Figure 4.4, it is clear that the iron concentration decreased almost immediately when caustic was added. The concentration decreased linearly from 0.0925 g/dm^3 to 0.025 g/dm3 at the final pH of 11. The results of experiment B4, as shown by graph O/F B4, were completely different. The iron concentration was 0.94 g/dm^3 before caustic was added and it decreased at a very fast rate with an increase in pH. An iron concentration of 0.033 g/dm^3 was reached at a low pH of 4.28, where after it decreased very slowly until a minimum concentration of 0.024 g/dm^3 was reached at a pH of approximately 9.

Table 4.7: Average values and standard deviations of experiments B1, B2 and B3.

pH	Average	Standard deviation
0.8	0.1208	0.0245
1	0.0975	0.0087
1.5	0.0917	0.0088
2.5	0.0742	0.0058
3.5	0.0667	0.0101
5	0.0558	0.0072
6	0.0525	0.0087
10.5	0.0417	0.0146

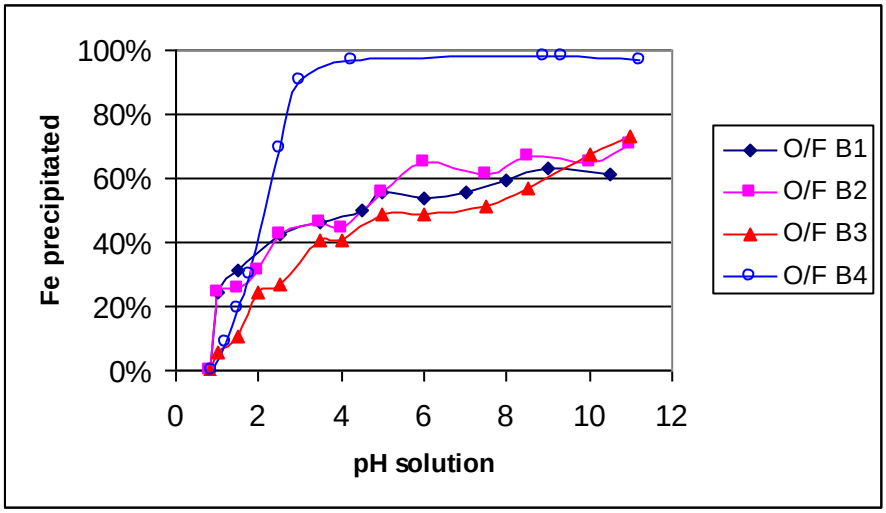

Figure 4.5: Precipitation of total iron of the individual overflow samples of classifier A expressed as % of total iron present.

Precipitation curves of the overflow of the upflow classifier are shown in Figure 4.5. From graph O/F B3, it is clear that precipitation started almost immediately when caustic was added, but only 11% precipitated at pH 1.5. At pH values exceeding 2, iron precipitation increased at a more significant rate (expressed as rate of precipitation per change in pH) and at pH 5 almost 50% of the iron had precipitated. The magnitude of precipitation decreased after pH 5 so that a total of 73% iron precipitated at pH 11. Iron precipitated at a steep gradient in experiment B4, to the extent that 90% had precipitated at a relatively low pH value of 3. Precipitation occurred at a relatively slow rate after pH 3 and the maximum precipitation of 97% had already occurred at a pH of 4.28. It was interesting to observe that the rate of precipitation was equivalent to that of experiment B3 at pH values below 1.5.

4.4.3. QUENCH SUMP

The result of experiment C1 was incorrect, as discussed in Paragraph 4.4.1 – *Upflow classifier underflow*, and was consequently discarded. The experiment was repeated twice. It is clear from Figure 4.6 that experiment C3 was once again conducted with a great degree of accuracy and precision, and a very good linear relationship was achieved (R^2-value of 0.9917). From the standard deviations and average values of experiment C2 and C3, as summarised in Table 4.8, it can be concluded that the repeatability of the two graphs was relatively poor, especially at pH exceeding values of 5 (at lower iron concentrations). Lower iron concentrations were more difficult to measure accurately.

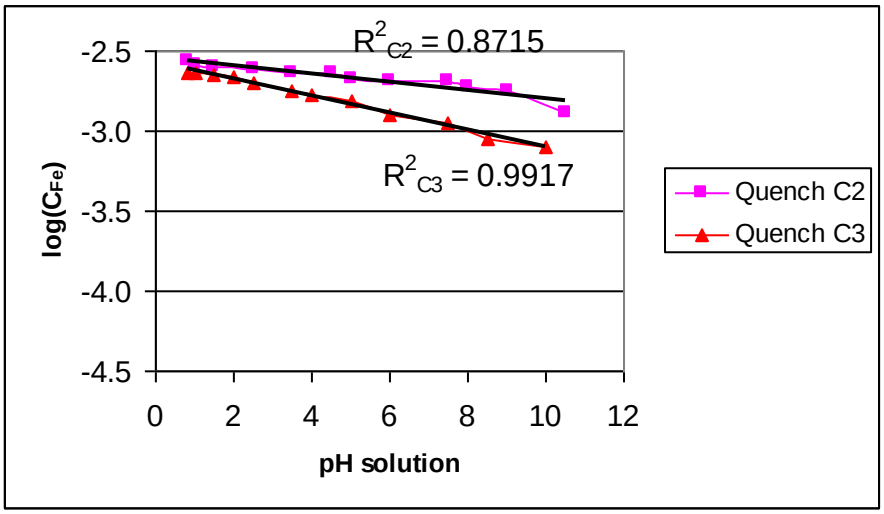

Figure 4.6: Precipitation of total iron by raising the pH of individual quench sump samples collected in the HAL circuit. The pH was increased by incrementally adding concentrated caustic to individual filtered samples. The solutions were mixed with an automatic stirrer. The experiments of Run C2 and C3 were conducted on 29 April and 10 May 2004, respectively. The samples were collected on the same day. Only samples from classifier A were used for the experiments.

It can be seen from graph C3 (Figure 4.6) that the total iron concentration decreased from 0.13 g/dm^3 to 0.045 g/dm^3 at pH 10. It is also clear that the iron concentration decreased almost immediately with an increase in pH.

Table 4.8: Average values and standard deviations of experiments C2 and C3.

pH	Average	Standard deviation
0.8	0.141	0.0159
1	0.135	0.0106
1.5	0.133	0.0106
2.5	0.123	0.0177
3.5	0.115	0.0212
5	0.101	0.0230
6	0.093	0.0327
7.5	0.089	0.0371
10.5	0.059	0.0194

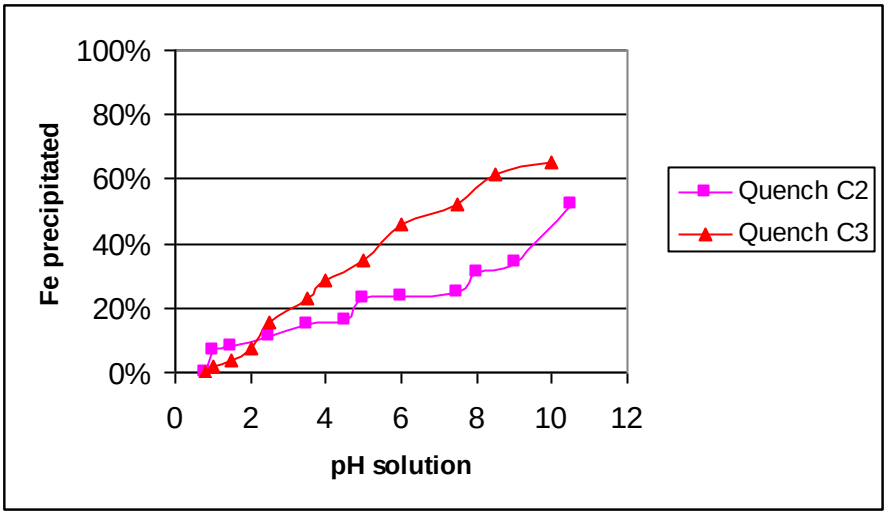

Figure 4.7: Precipitation of total iron of the individual samples of quench sump A expressed as % of total iron present.

Precipitation curves of experiment C2 and C3 are shown in Figure 4.7. It is clear from graph C3 that precipitation occurred at a relatively slow rate at pH values below 2, to the extent that only 4% and 8% iron precipitated at pH 1.5 and 2, respectively. A total of 50% iron precipitated at pH 7 and 65% precipitated at pH 10.

4.4.4. SUMMARY OF THE PRECIPITATION EXPERIMENTS CONDUCTED

All the selected graphs, as discussed in the previous paragraphs (A2, B3, B4 and C3), are compared in this section.

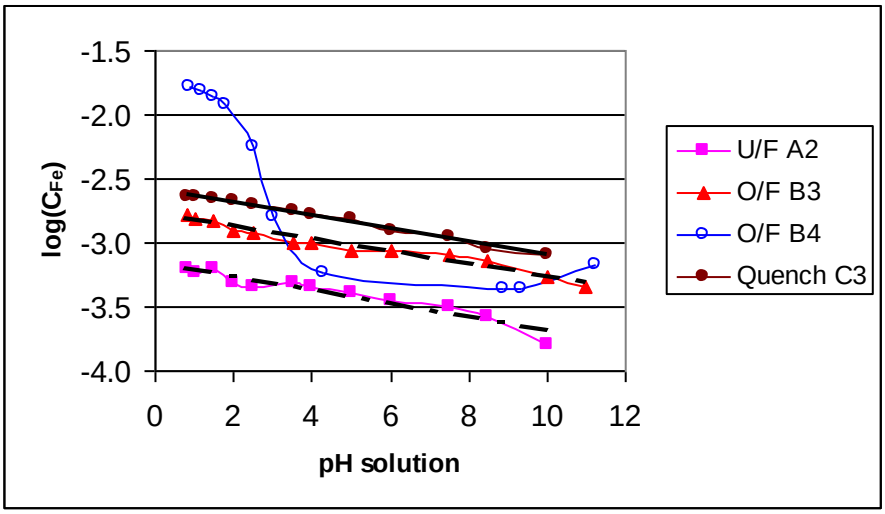

Figure 4.8: Summary of precipitation curves of samples of the underflow and overflow of upflow classifier A, and quench sump A of the HAL circuit. Only the curves with the best linear regressions (highest R^2 values) were selected.

It is clear from the linear curves shown in Figure 4.8 that the iron concentration increased from 0.0333 g/dm^3 to 0.0925 g/dm^3 to 0.139 g/dm^3 when moving counter-currently through the HAL circuit from the underflow of the upflow classifier to its overflow and to the quench sump. A more significant iron concentration difference occurred between the over and under flow of the upflow classifier than between the overflow of the upflow classifier and the quench sump. It is important to note that the underflow and overflow are separated by an upflow classifier, where the quench sump and the overflow of the upflow classifier are separated by a dewatering cyclone. It was interesting to note that the change in iron concentration versus pH was similar for all the selected experiments, as indicated by the gradients of the individual graphs. It was also observed that the final iron concentration after pH 10 decreased in the sequence of the quench, overflow and underflow of the upflow classifier.

Experiment B4 was conducted two years earlier (April 2002) and the results were completely different than that of experiment B3 as discussed earlier. The final iron concentration seemed to be similar to that of graph O/F B3. It was also clear that higher volumes of iron reacted with the caustic at lower pH values, which indicated a strong presence of ferric ion.

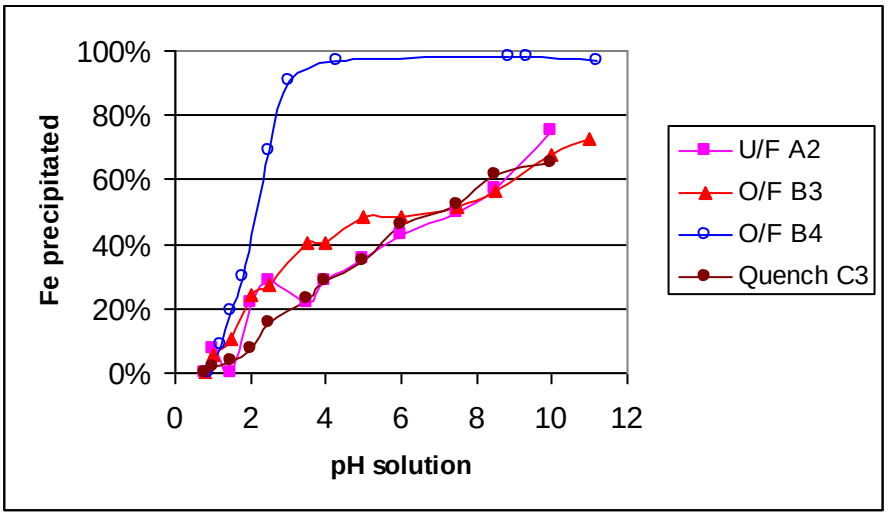

Figure 4.9: Figure 7 expressed as % precipitation of total iron.

Iron precipitation curves are summarised in Figure 4.9. Surprisingly, it was noted that almost all of the curves, except O/F B4, appeared to be almost identical. Approximately 50% of the total iron precipitated at pH 7 and a maximum of about 70% iron precipitated at pH 10, with the result that 30% iron still remained in solution. Graph O/F B4 clearly showed that precipitation occurred at a significantly faster rate and almost all the iron precipitated at a pH of above 4.

During the course of the iron precipitation experiments, it was noted that the iron concentrations fluctuated. Historical iron concentrations in the HAL circuit are summarised in Table 4.10. A definite decrease in concentration was noticed. The iron concentration in the quench sump, which was the first repulp stage after the reactors, decreased by more than 93% from 2.6 to 0.162 g/dm^3 from 23 April 2002 to 19 April 2004.

Table 4.9: Historical iron concentrations (g/dm^3) in the HAL circuit. Data entries follow the normal process flow sequence in the direction of mineral sand from the discharge of the reactors to the attritioner feed. Process paramaters such as mineral temperature fed to the reactors, acid additon rate and strength, and solid-liquid ratios were constant during the indicated period.

No	Sample	23-Apr-02	09-May-02	19-Apr-04
1	Quench A	2.6	5.32	0.162
2	Upflow classifier A cyclone o/f	1.88	3.21	Not analysed
3	Upflow classifier A o/f	0.94	1.26	0.139
4	Upflow classifier A u/f	0.23	0.18	0.033

4.5. IRON ADSORPTION TO MINERAL SURFACES

This section provides sufficient information that will prove the occurrence of iron adsorption to the mineral surfaces, which is confirmed by various experiments and mineralogical analyses. It also describes a mechanism for iron adsorption and quantifies the amount of iron distributed to the dry mill feed via iron balances conducted over the HAL and wet gravity circuits.

On 9 May 2002, high amounts of iron rich precipitates were visible in the wet gravity process water. Excessive quantities reported to the wet gravity secondary concentrate and were clearly visible on the secondary concentrate belt filter, as shown in the photo of Figure 4.10. This phenomenon gave birth to the first trial when caustic addition in the HAL circuit was temporary stopped to reduce the volume of precipitates formed. Results were very encouraging, which emphasised the importance of implementing a process solution to prevent iron precipitation and/or adsorption to mineral surfaces.

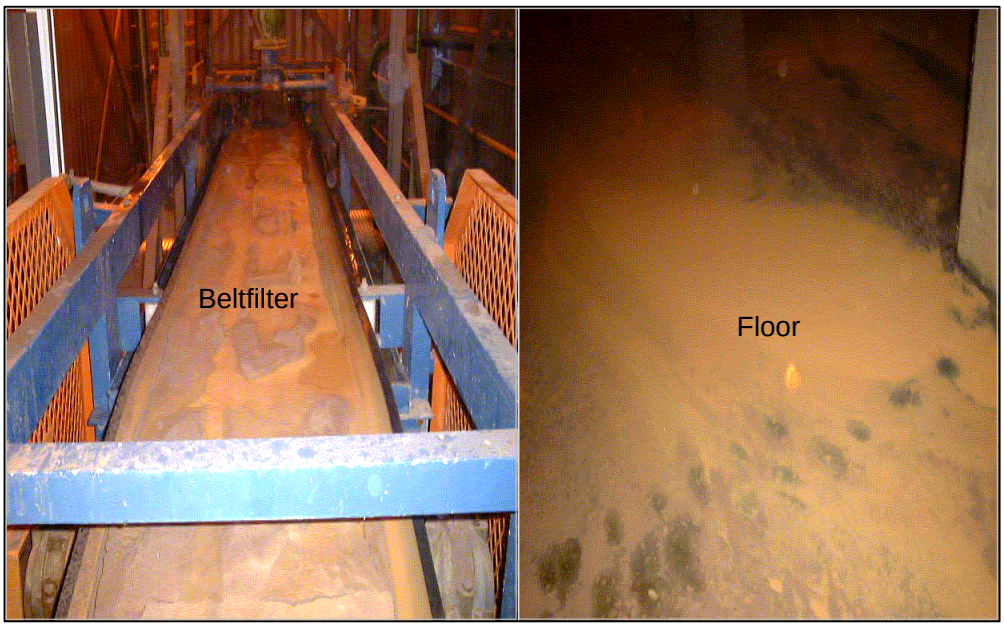

Figure 4.10: Iron rich precipitate (including slimes) visible on the secondary concentrate belt filter and floor of the wet gravity circuit.

4.5.1. ZETA POTENTIALS OF ZIRCON AND RUTILE MINERAL PARTICLES

Kosmulski et al. (2003) showed that iron hydr(oxide) has a positive zeta potential at pH values below 7.8 (see Table 2.4). Therefore, it was important to determine the zeta potential of zircon and rutile minerals in order to formulate the adsorption theory. Zeta potentials, as a function of pH, were determined for zircon and rutile product samples by H. Divey at the Department of Chemical Engineering, University of Cape Town. Concentrated sulphuric acid and sodium hydroxide were used to adjust the pH of a 10^{-3} M buffer solution (Na_2SO_4). Five readings were performed per pH value. The results are summarised in Table 4.10 and 4.11 and are considered to be representative due to the fact that the mineral samples were within chemical specification limits and were collected during normal and typical plant conditions. It is worth mentioning that the mineral samples were collected directly from the dry mill circuit and their surfaces were not cleaned prior to submitting the samples for analyses. Therefore, zeta potentials could have been affected by surface contaminants, such as iron hydroxides. However, the effect would have been negligible due to the almost negligible concentrations of these species relative to the concentration of the mineral grains. The University of Cape Town confirmed this to be correct. Zeta potential values were accurate and repeatable as indicated by the standard deviations. It was interesting to note that the standard deviations of zircon product samples were higher than rutile product samples for most of the pH values.

Table 4.10: Zeta potential (mV) of rutile mineral particles as a function of the pH of the solution.

pH	Reading	Reading	Reading	Reading	Reading	Average	Standard

	1	2	3	4	5		deviation
2.50	-14.0	-14.8	-15.9	-15.2	-15.5	-15.1	0.65
3.00	-16.5	-15.9	-16.6	-16.2	-15.8	-16.2	0.32
3.50	-16.5	-15.8	-17.1	-16.6	-16.8	-16.6	0.43
4.02	-17.5	-17.4	-17.3	-17.3	-17.4	-17.4	0.07
6.02	-19.5	-17.7	-17.4	-17.8	-17.3	-17.9	0.80
7.00	-39.1	-39.4	-38.7	-39.7	-38.5	-39.1	0.44
9.00	-49.3	-50.2	-47.6	-48.3	-46.0	-48.3	1.44

Table 4.11: Zeta potential (mV) of zircon mineral particles as a function of the pH of the solution.

pH	Reading 1	Reading 2	Reading 3	Reading 4	Reading 5	Average	Standard deviation
2.50	-17.8	-17.8	-17.1	-16.9	-17.6	-17.4	0.37
3.01	-20.8	-22.6	-19.8	-21.9	-20.6	-21.5	0.99
3.52	-26.1	-25.3	-25.9	-23.9	-23.9	-25.0	0.95
4.00	-24.3	-25.1	-26.1	-26.7	-26.6	-25.8	0.92
6.02	-25.3	-25.1	-24.8	-27.3	-25.9	-25.7	0.89
7.00	-45.5	-45.0	-44.1	-49.6	-42.3	-45.3	2.41
9.00	-50.3	-53.2	-51.8	-51.2	-48.8	-51.1	1.47

Experimental zeta potentials of zircon and rutile mineral particles were compared to those of hematite, goethite and goethite-hematite, as determined by Kosmulski et al. (2003). The graphs are shown in Figure 4.11. Although both negative, the zeta potential of rutile is slightly higher than that of zircon and both decrease sharply at pH 6 to 7. Kosmulski et al. (2003) determined the average of PZC value for Fe (III) hydroxides to be 7.99. It is observed from the graphs that hematite, goethite and goethite-hematite have zero zeta potentials at pH 7.3, 9.4 and 8.8, respectively. The zeta potentials were almost constant and opposite in sign for these iron species, including iron hydr(oxides), and mineral particles below pH 7. It was important to note that the pH of the process water after the HAL neutralisation step, which included the process water of the wet gravity circuit, was typically between 4.5 and 5. Zeta potential differences between the minerals and iron hydr(oxides) were maximised below pH 5.

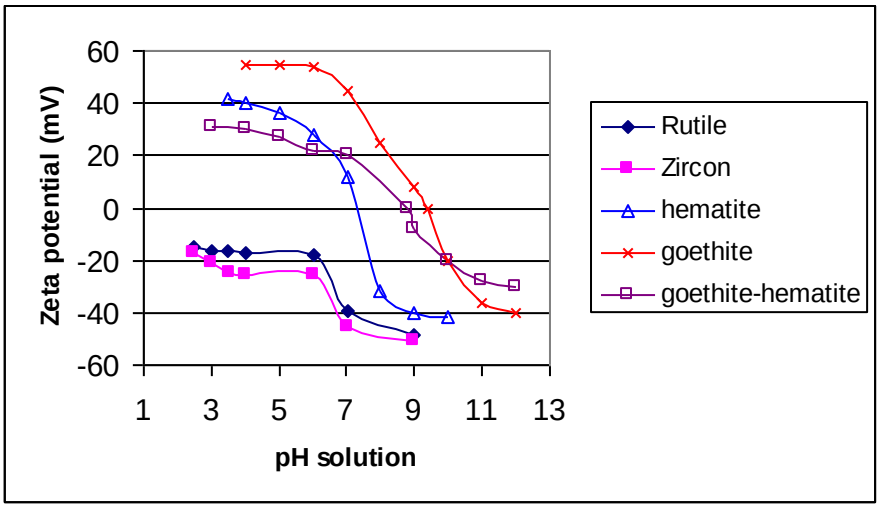

Figure 4.11: Zeta potential of rutile, zircon, hematite, goethite and goethite-hematite. The zeta potential of the last three species was obtained from literature. The zeta potential of rutile and zircon mineral particles was experimentally determined, the results of which are summarised in Tables 4.11 and 4.12:

4.5.2. IRON BALANCE OF THE HAL CIRCUIT

Iron balances were conducted in the HAL circuit to quantify the iron removal efficiency of the HAL wash circuit, which consisted of two cyclones and an upflow classifier. The second cyclone was placed after the caustic neutralisation stage.

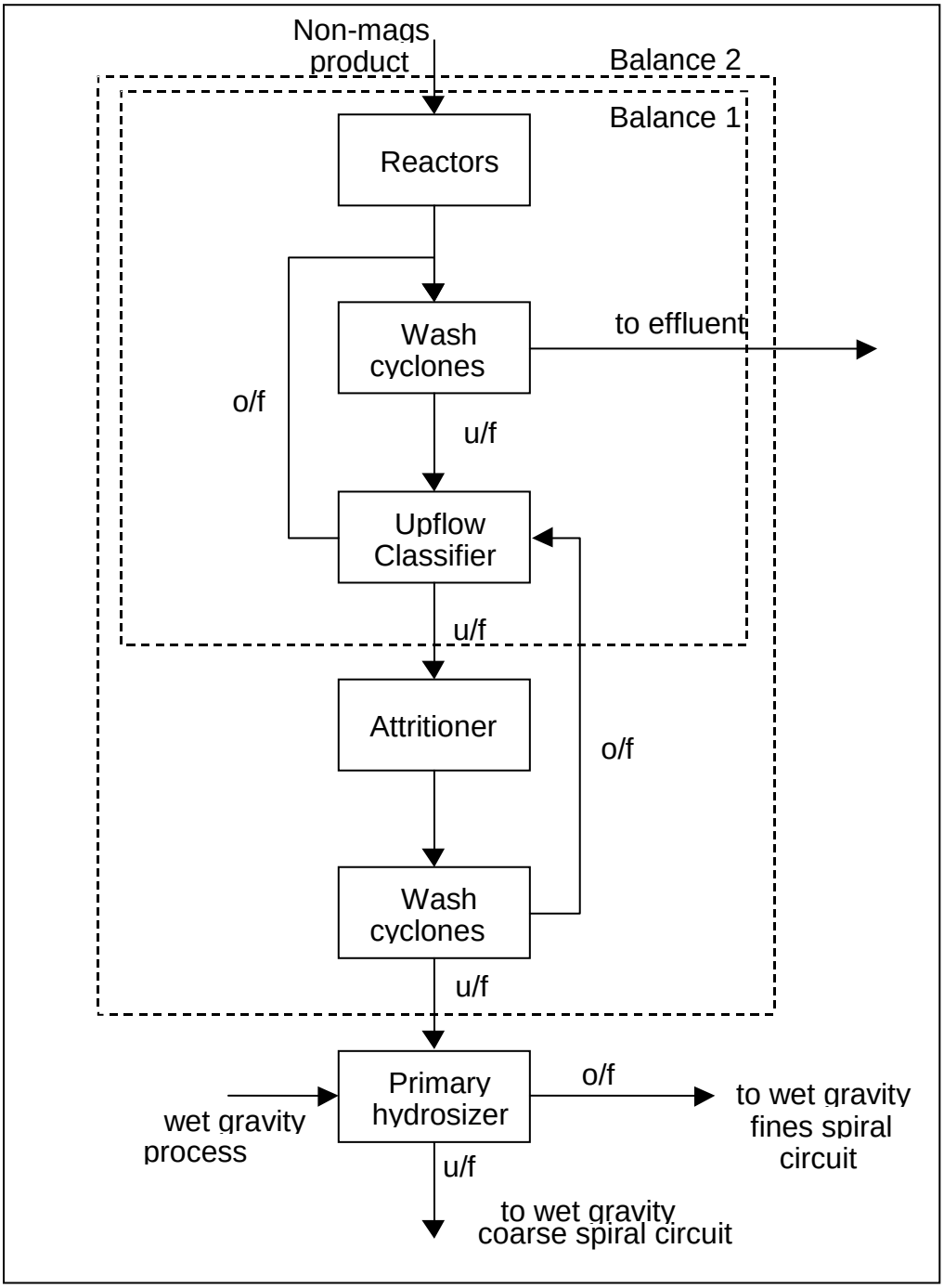

Figure 4.12: Simplified block diagram of the HAL circuit showing the main equipment (excluding sumps and pumps) and indicating battery limits of the mass balances by dotted lines.

Figure 4.12 is a simplified block diagram of the HAL circuit excluding sumps and pumps. Battery limits used to construct the individual mass balances are indicated by dotted lines. The balances were based on the fact that the amount of iron received from the wet gravity circuit was negligibly small compared to the iron concentrations of the HAL circuit, and were therefore not indicated in the block diagram. The underflow of wash cyclone 2 was fed to the wet gravity circuit.

Results of a dissolved iron balance (see 'Balance 1' of Figure 4.12), which were conducted during normal operation when the existing wash stages of the HAL circuit were operating normally, are summarised in Table 4.12. It is clear from the balance that 90.4 kg/hr leachable iron entered the HAL circuit by means of the reactor feed, and 3.7 kg/hr of this iron (4.1% of the leachable iron fed to the reactors) was fed to the attritioners. The pH was raised to 5, which would result in precipitation of Fe (III). The iron in the overflow of wash cyclone 2 was not included in this balance. However, the amount of iron (kg/hr) in the attritioners feed was not affected by this shortcoming.

Table 4.12: Typical iron balance in the HAL circuit during normal operation.

Stream	Flow rate (dry) [tph]	Water flow rate [m^3/hr]	Dissolved Fe concentration [kg/t]	Dissolved Fe concentration [kg/m^3]	Fe flow rate [kg/hr]
Reactor A	12	0.08	#2.66	-	31.9
Reactor B	22	1.3	#2.66	-	58.5
301 attritioner feed (68% solids)	12	5.6	-	0.31	1.7
302 attritioner feed (68% solids)	11	5.2	-	0.20	1.0
303 attritioner feed (68% solids)	11	5.2	-	0.20	1.0

The dissolved iron concentration in the reactor feed was calculated by leaching 1000 kg of reactor feed sample with 111 ml 40% sulphuric acid at 140^{o}C in an oven for 3 to 4 hours. The dried sample was mixed with 1000 ml water and attritioned for 30 minutes, and the water was filtrated and analysed for iron (standard iron titration). The iron concentration (2.66 g/dm^3) was converted to kg Fe/ton dry feed as follows: kg Fe/ton feed = [2.66kg/m^3]x[$10^{-3}m^3$]/[10^{-3}ton]. The dissolved Fe in the reactor feed was then simply calculated by multiplying this concentration by the reactor feed rate (dry).

The total iron distribution of the HAL circuit was determined more accurately by including the overflow stream of wash cyclone 2 in the balance (see 'Balance 2' of Figure 4.12) by measuring the iron concentration in the effluent. The iron in the underflow of the wash cyclone 2 was calculated by difference. The results are summarised in Table 4.13. A total of 99.5 kg/hr leachable iron entered the HAL circuit as reactor feed. Only 2.9 kg/hr was fed to the wet gravity circuit, which is equal to 2.9% of the leachable iron fed to the reactors. Thus, the iron removal efficiency of the HAL circuit was 100% - 2.9% = 97.1%. Accurate (less than 2.5% error) online mass measurements and flow rate data of the reactor feed and effluent were obtained from an impact weigher and automatic flow meter, respectively. It is important to note that the balance was based on the measurement of two streams, namely reactor feed and effluent, at a certain point in time. However, the data was found to be representative of the conditions at that point in time and to be accurate for qualitative discussions.

Table 4.13: Iron balance over the HAL circuit conducted during a period of good dry mill electrostatic separation. The balance was conducted on 26 July 2002.

Stream	Flow rate [tph]	Flow rate [m^3/h]	Fe concentration [kg/ton]	Fe concentration [kg/m^3]	Fe flow rate [kg/hr]
Reactor A	12	0.6	2.9	0	34.7
Reactor B	24	1.3	2.7	0	64.8
Effluent	0	[#]53	0	1.85	96.6
Wash cyclone u/f	36	19.4	0	0.05	[$]2.9

[$] Calculated by difference (reactor feed – effluent).

[#] The effluent contains 1.5 mass% solids. Therefore, the liquid flow rate is 52.2 m^3/hr

Iron concentrations in the HAL circuit were determined during a day when the dry mill electrostatic separation was classified as 'typical', characterised by normal zircon product output tons (23 April 2002), and during a day of poor electrostatic separation with low zircon output product tons (9 May 2002). Typical zircon product iron and production rates, during a normal production, day were <0.053% and 14.5-15 tph, respectively. The zircon product iron and output product tons on 9 May were >0.055% and 13 tph, respectively. Iron concentrations of the two days are summarised in Table 4.14. Samples from the HAL A side only were analysed since the B side, which runs in parallel with A, exhibits the same physical stream properties. HAL iron concentrations were much higher when comparing the poor production day (characterised by ineffective electrostatic separation and relatively high zircon product iron levels) with the normal production day. A sharp decrease in the iron concentration differences, as moving downstream in the circuit, was noticed. The iron concentration of the underflow of the upflow classifier was slightly lower on the poor electrostatic separation day. The reason for this was due to different solid-liquid ratios as a result of ineffective sampling at this point (practical constraints). Further analyses and repeated sampling revealed an increase in iron at this point that corresponded with an increase in iron at the quench sump and overflow of the upflow classifier.

Table 4.14: Total iron concentrations at different sample points in the HAL circuit. The samples were collected during poor electrostatic dry mill separation and consequently low output zircon and rutile product tons (09 May 2002) and during a day when the electrostatic separation was classified as 'normal' (23 April 2002).

Sample point	Description	23-April-2002 Normal Fe [g/dm^3]	09-May-2002 Poor Fe [g/dm^3]	Change [%]
1	Quench A	2.60	5.32	-104.6%
2	Upflow classifier A cyclone o/f	1.88	3.21	-70.7%
3	Upflow classifier A o/f	0.94	1.26	-34.0%
4	Upflow classifier u/f	0.23	0.18	21.7%

4.5.3. IRON BALANCE OF THE WET GRAVITY CIRCUIT

The objective of the iron mass balances was to determine the concentrations and distribution of total iron to the primary concentrate (dry mill feed) during different degrees of dry mill separation.

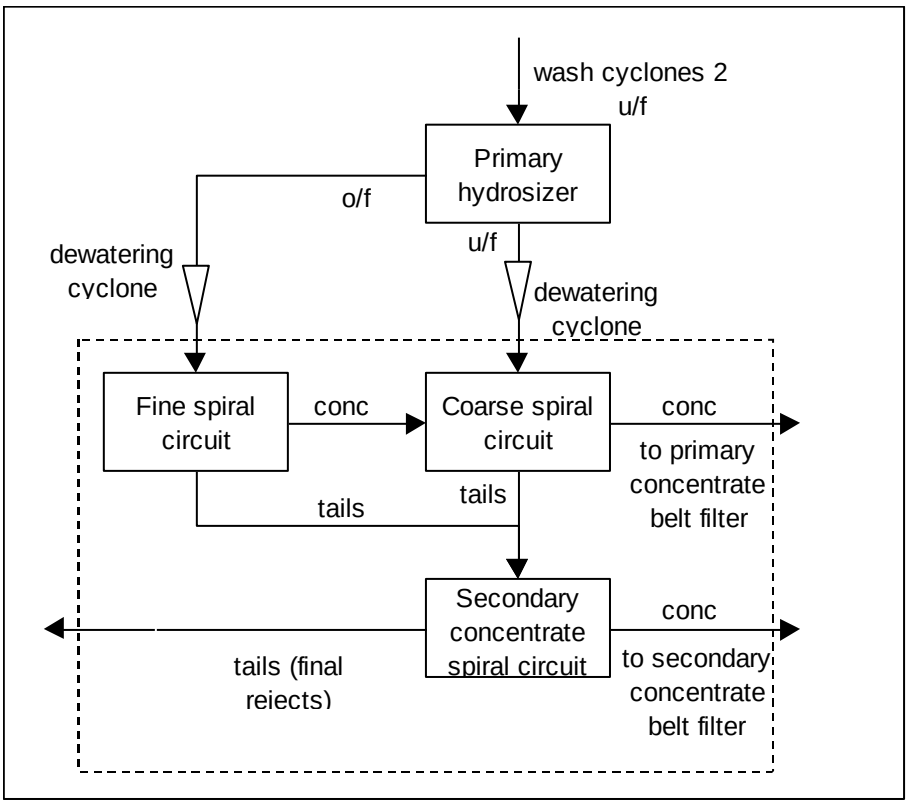

Figure 4.13: Simplified block diagram of the wet gravity spiral circuit showing the main processing sub-circuits (excluding sumps and pumps) with the dotted line indicating the battery limits used for the mass balance. The primary hydrosizer was considered as the first rougher stage of the wet gravity circuit. The water recycle streams were excluded in order to simplify the block diagram.

A simplified mineral process flow of the wet gravity circuit is given in Figure 4.13. Battery limits used to construct the mass balance are indicated by the dotted line. Iron fed to the wet gravity circuit was determined by analysing the underflow and overflow streams of the primary hydrosizer. Process water and slurry is flowing counter-currently through the wet gravity circuit and the process water is partially recycled in the wet gravity and HAL circuits. The mass flow rate of the underflow of the primary hydrosizer was determined by density and flow measurement by means of an online nuclear density metre and flow meter, respectively. The overflow was calculated by the difference of the HAL feed and underflow of the primary hydrosizer. Mass measurement was considered as relatively accurate.

The concentration of total iron in the feed to the coarse (or primary spiral) and fine spiral feed were determined by determining the mass% solids in the streams prior to reducing the pH to approximately 0.6 by adding small amounts of concentrated sulphuric acid. Adjustment of the pH was required to ensure that all precipitated iron was dissolved and that adsorbed iron was desorbed from mineral surfaces. Mixing was conducted at room temperature for a short period (5-10 minutes) to prevent potential leaching of any iron oxide coating still present on the mineral surfaces. Total precipitated and suspended iron in the primary concentrate were determined by mixing (5-10 minutes) 100 ml of acidic water (pH 0.6) with 400 g of concentrate collected from the discharge of the belt filter. The water was analysed for total iron.

Mass % iron was calculated as the fraction of iron per dry mineral mass. Iron distribution refers to % iron in wet gravity feed (sum of coarse and fine spiral feed) distributed to the primary concentrate, primary and fine spirals. The mineral mass balance in the wet gravity circuit was for all the mass balances. The degree of dry mill separation was categorised in terms of dry mill electrostatic separation performance, and consequently the production of prime zircon. The dry mill separation performance was categorised as follows:

(1) Poor (12 May 2003): Low output zircon product tons (average 13.8 tph) and the wet gravity process water was brownish due to the build-up of iron. Caustic addition was normal and switched on during this day.

(2) Good (14 May 2003): Caustic addition was temporarily switched off to reduce the occurrence of iron precipitation and re-attachment. Dry mill electrostatic separation improved significantly and zircon product tons exceeded 15.5 tph.

(3) Good (28 May 2003): Zircon product tons exceeded 15 tph. Caustic addition was switched on.

Results of the iron balance conducted during a time of poor electrostatic dry mill separation are summarised in Table 4.15. It can be seen from the results that 48.3% of the iron was distributed to the fine spiral feed, which comprised only 16.7% (6 tph) of the mineral fed to the wet gravity circuit. The primary spiral feed comprised 83.3% of the total mineral feed and 51.7% of the iron was distributed to these spirals, which are the main source of primary concentrate; 25.1% iron was distributed to the primary concentrate. The results showed that the primary concentrate, fine and primary spiral feed contained 0.0062%, 0.052% and 0.011% iron, respectively (expressed per mass of dry mineral).

Table 4.15: Iron distributed to the primary concentrate of the wet gravity circuit during poor electrostatic separation conditions in the dry mill circuit. The balance was conducted on 12 May 2003.

Stream	Dry flow rate [tph]	Sample (wet mass) [g]	Sample water [%]	Fe [g/dm^3]	Fe [mass%]	Fe [kg/hr]	Fe distribution [%]
Prim conc	26	206.8	4.9%	0.198	0.0062%	1.62	25.1%
Fine spiral feed	6	1929.8	89.7%	0.060	0.052%	3.12	48.3%
Prim spiral feed	30	1861.5	56.4%	0.086	0.011%	3.34	51.7%
Feed (prime+fine)	36	-	-	-	0.018%	6.46	100%

An iron balance was conducted during a trial when the caustic was temporarily switched off. Electrostatic separation improved significantly after about 4 hours, after the caustic was temporary switched off. Recycle loads in the dry mill circuit decreased and zircon product iron levels (XRF analysis) decreased from >0.055% to <0.052%. Mass balance results obtained on this good dry mill separation day are summarised in Table 4.16. It is important to compare the results of this balance with the balance of Table 4.15, which contains data of the period before the caustic was switched off. It can be noted from Table 4.16 that the iron distribution to primary concentrate was slightly lower and the distribution to the fine spirals was much higher. It is also important to note that the sum of the iron in the primary and fine spiral feed was slightly lower, but the iron in the primary concentrate was more than 35% lower during the trial when the caustic was switched off.

Table 4.16: Iron distributed to the primary concentrate of the wet gravity circuit conducted during a period of good dry mill electrostatic separation as a result of a pause in adding caustic to the HAL circuit. The balance was conducted on 14 May 2003

Stream	Dry flow rate [tph]	Sample (wet mass) [g]	Sample water [%]	Fe [g/dm^3]	Fe [mass%]	Fe [kg/hr]	Fe distribu-tion [%]
Prim conc	26	347.5	4.8%	0.129	0.0040%	1.04	21.8%
Fine spiral feed	6	2513.0	90.9%	0.062	0.062%	3.74	78.2%
Prim spiral feed	30	3032.3	56.3%	0.052	0.0067%	2.01	42.1%
Feed (prime+fine)	36	-	-	-	0.016%	5.75	100%

Another balance was conducted on a day (caustic on) when the dry mill electrostatic separation could be characterised as slightly above average. Zircon production was slightly lower compared to the trial when the caustic was temporarily switched off (refer to Table 4.16). Results of this balance are summarised in Table 4.18 and are compared to Table 4.16. It can be seen from the results that the iron concentration in the primary concentrate, as well as the distribution to the primary concentrate, was slightly higher compared to that of Table 4.16. Total iron, as the sum of the iron in the primary and fine spiral feed, was 20.3% lower compared to the no-caustic trial. It is important to note that the distribution to the primary spirals was 62.9% compared to the 37.1% distribution to the fine spirals. The mass% iron in the primary concentrate (0.0043%) was slightly higher compared to that of Table 4.16 (0.0040%), but much lower than the % iron shown in Table 4.16 (0.0062%).

Table 4.17: Iron distributed to the primary concentrate of the wet gravity circuit during good dry mill electrostatic separation conditions (with the caustic switched on). The balance was conducted on 28 May 2003

Stream	Dry flow rate [tph]	Sample (wet mass) [g]	Sample water [%]	Fe [g/dm^3]	Fe [mass%]	Fe [kg/hr]	Fe distribu-tion [%]
Prim conc	26	212.8	4.6%	0.140	0.0043%	1.12	24.5%
Fine spiral feed	6	1341.6	92.2%	0.024	0.028%	1.70	37.1%
Prim spiral feed	30	1745.0	60.0%	0.064	0.0096%	2.88	62.9%
Feed (prime+fine)	36	-	-	-	0.013%	4.58	100%

The balances summarised in Table 4.15, 4.16 and 4.17 provided very useful quantitive information in describing the adsorption of precipitated iron and its impact on the dry mill electrostatic separation performance related in terms of prime zircon production. However, the determination of the % iron in the feed to the primary and secondary spirals was less accurate mainly due to inaccurate sampling as a result of large volumes to be sampled in a relatively short period of time. This inaccurate sampling could have resulted in incorrect solid-liquid ratios and iron concentrations, which would affect the iron distribution results. It is also important to note that a large volume (55 m^3/hr out of approximately 80 m^3/hr) of the wet gravity process water is recycled through the primary hydrosizer as teeter water. Therefore, the samples of the feed to the primary and fine spirals included this internal recycling stream. Iron analysis of the primary concentrate was accurate mainly due to the consistency of this stream in terms of moisture and feed rate, and also due to the ease and efficiency of sampling of the discharge of the primary belt filter. Therefore, the % iron per dry mass of primary concentrate could be used as an effective method to quantify the attachment of iron to the mineral surfaces. It was found that the % iron in the primary concentrate correlated well with "good" and "bad" separation. "Good" separation was characterised by low iron concentratrions and the opposite was true for "bad" separation.

4.5.4. IRON BUILD-UP IN PROCESS WATER OF WET GRAVITY CIRCUIT

Wet gravity process water, at different sampling points, was analysed to determine if a correlation existed between dry mill electrostatic separation performance and the concentration of iron in the process water of the wet gravity circuit. A very strong and definite correlation was found, which is discussed in detail in the remainder of this section. Water samples were collected at the primary spirals, dirty water tank and HAL water supply tank. A few drops of sulphuric acid were added in order to decrease the pH to about 1.3 to dissolve iron precipitates prior to filtration. Iron precipitation experiments of section 4.4 revealed that the majority of the iron would dissolve at pH values below 1.5 and 2 for high and low concentrations of iron, respectively. Dry mill separation performance was qualitively and quantitively rated in terms of visual electrostatic separation performance and/or zircon output product tons, respectively. Results are summarised in Table 4.18 and the ratings versus iron concentrations are plotted in Figure 4.14. Descriptions of the ratings are provided in the heading of Table 4.18. It is important to highlight that caustic was switched off for 4 days out of 11.

It is noticed from Table 4.18 that the samples were randomly collected over approximately 2 months in 2002. The concentrations of the three different sample points were of the same magnitude. Dry mill

performance was quantified per iron concentration in the water of the first spiral stage, namely the primary spirals. This concentration was used mainly due to its constant water to solids ratio, which resulted in relatively stable iron concentrations. One shortcoming worth mentioning was related to the analyses of the primary spirals: the solids were separated from the liquid prior to adjusting the pH to 1.3, which could have resulted in lower iron concentrations due to the exclusion of the portion of iron already adsorbed to the mineral surfaces.

Namakwa Sands has often experienced electrostatic separation problems during poor weather conditions, which are often associated with a very low dew point (DP) and relative humidity (RH), absolute humidity less than 10 g moisture/kg air or a sudden change in one of these parameters. It was important to note that the electrostatic separation improved on 03-June-2003 when the caustic was switched off in the middle of poor weather conditions (low DP and RH). This was confirmed by various other trials, for example the one conducted on 10-June-2002 and a few other trials that are not recorded on this table.

Table 4.18: Quantification of accumulation of precipitated iron in the process water of the wet gravity circuit and qualitive analyses of the dry mill performance at the correspondent time. Dry mill electrostatic performance was rated in terms of visual separation performance and/or zircon output product tons (1 = poor electrostatic separation performance with zircon product tons < 14.5 tph, 2 = average electrostatic separation performance with zirc prod 14.5-15 tph, 3 = good dry mill performance and/or zirc prod tons > 15 tph).

Date	Prim Spirals g/dm^3]	Dirty water tank $[g/dm^3]$	HAL Water tank $[g/dm^3]$	Comments	Zircon production Rating
27-May-02	0.050	0.040	0.050	Dry mill stable, zir Fe >0.055%, zirc prod 15tph.	3
28-May-02	0.070	Not analysed	0.080	Dry mill unstable, zir Fe >0.050%, zirc prod 14.1 tph.	1
03-June-02	0.050	0.060	0.060	Stopped caustic 8 hrs before sample collection. BEFORE: dry mill unstable (zir Fe >0.055%, low DP and RH, zirc prod 13.5-14tph); AFTER: dry mill stable (zir Fe<0.050%, low DP and RH, zir prod 14.8-15 tph).	3
04-June-02	0.040	0.030	0.040	Caustic off: Dry mill stable, zirc prod 15 tph.	3
06-June-02	0.030	0.030	0.040	Caustic off & after start-up of total shut: dry mill is performing well (zirc prod 14 tph).	3
07-June-02	0.050	0.040	0.075	Dry mill stable, upflow class o/f pink (not soluble in HCl), zirc prod 15.5-16 tph, hum 10 g/kg.	3
10-June-02	0.050	0.050	0.065	Caustic off: dry mill stable, zirc prod >15 tph, hum <9 g/kg.	3
19-June-02	0.104	0.080	0.090	Dry mill unstable, zir Fe >0.055%, zir Ti problems, water brownish, zirc prod 13.5 tph, hum <10 g/kg. Caustic switched off & 4 hrs later: zir Fe 0.051%, zirc prod 15.5tph, dry mill recycle streams decreased)	1
31-July-02	0.045	0.035	0.020	Dry mill stable, zirc prod 15 tph.	3
01-Aug-02	0.065	0.035	0.030	Dry mill stable, zirc prod 14.5-15 tph	2
05-Aug-02	0.040	0.050	Not analysed	Dry mill stable, zirc prod 15-15.5 tph	3

Figure 4.14 summarises the iron concentration of the primary spiral as a function of the three different ratings. It is important to notice that the iron concentration for rating 3 (good dry mill performance) was less than 0.05 g/dm^3, more than 0.07 g/dm^3 for rating 1 (poor dry mill performance) and 0.065 g/dm^3 for rating 2. It is important to note that four out of the eight points at rating 3 were the same and are therefore not visible in the figure. The results were found to be reliable and a true reflection of the electrostatic separation performance of the dry mill circuit. Corrective action, such as a temporary pause in the HAL neutralisation step, or replacing the process water with fresh water, reduced the

concentration of iron in the process water to below 0.05 g/dm^3. This drastic action often resulted in an increase in production a couple of hours later.

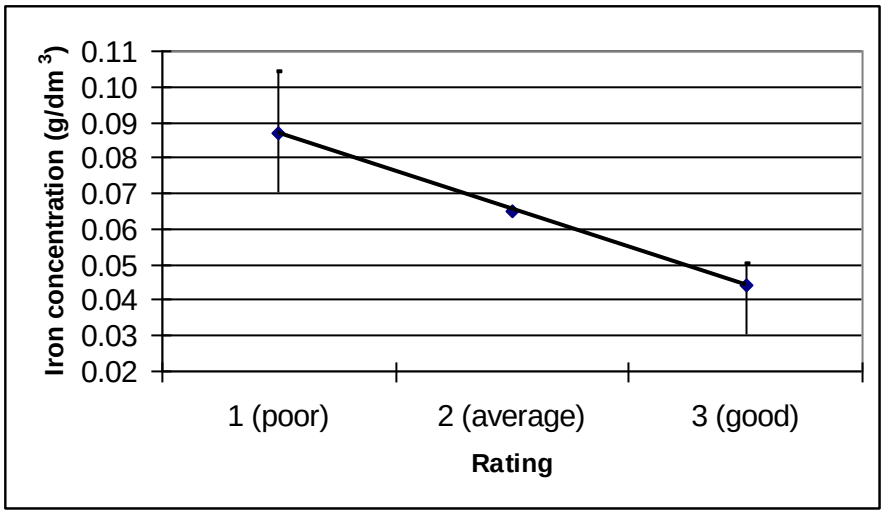

Figure 4.14: Dry mill electrostatic separation performance in terms of iron concentration of the water of the primary concentrate spirals. Dry mill electrostatic performance was rated in terms of visual separation performance and/or zircon output product tons (1= poor electrostatic separation performance with zircon product tons < 14.5 tph, 2 = average electrostatic separation performance with zirc prod 14.5-15 tph, 3 = good dry mill performance and/or zirc prod tons > 15 tph).

Daily composite IRMS feed samples were leached, attritioned and washed in the laboratory. Wet gravity process water samples were collected at the same time. The wash liquor of the processed IRMS feed and wet gravity process water samples were analysed for total iron with the objective of determining if a correlation existed between iron oxide associated with the ore body and iron build-up within the wet gravity circuit. Results are summarised in Table 4.19. Plotting a linear regression curve through the data points revealed that no correlation existed between the data points.

Table 4.19: Iron build-up in the wet gravity as a function of iron concentration present as mineral coating in the IRMS feed.

No	Date	IRMS feed [mass% Fe]	Prim Spirals [g/dm^3]	Dirty water tank [g/dm^3]	HAL water tank [g/dm^3]
1	12-Jul-02	0.32%	0.040	0.030	Not analysed
2	31-Jul-02	0.35%	0.045	0.035	0.020
3	01-Aug-02	0.45%	0.065	0.035	0.020
4	05-Aug-02	0.37%	0.040	0.050	Not analysed
5	06-Aug-02	0.30%	0.060	0.035	0.040
6	06-Sep02	0.42%	0.030	0.010	0.010

4.5.5. MINERALOGY OF MINERAL SURFACES

The purpose of the mineralogical analysis of mineral samples was to confirm the presence of chemical species on the surfaces of minerals during periods of ineffective electrostatic separation in the dry mill circuit. On 10 March 2003, both the AMDEL and XRF indicated high concentrations of iron (>0.06%) of the prime zircon product, resulting in an off-specification product. It was also noted that the off-specification samples did not meet the TiO_2 specification. Four samples, representing on-specification and off-specification zircon products, were submitted for mineralogical analysis. Results are summarised in Table 4.20. 'Other zircon' referred to metamict zircon and small amounts of stained zircon. 'Other minerals' referred to gangue garnet, quartz and trace amounts of other mineral particles. The results indicate that the zircon content was similar for all the samples, 'other' minerals were slightly more abundant in the on-specification samples, but the TiO_2 abundant minerals (rutile and leucoxene) were concentrated more significantly in the off-specification products. Metamict zircon was more or less consistently distributed in all samples.

Table 4.20: On and off-specification zircon product hourly samples collected on 10 and 11 March 2003. Off-specification products (21h00 and 02h00) are indicated in italics. Chemical analysis and stream composition were determined by XRF and grain counts, respectively.

Time	TiO_2 [%]	Fe_2O_3 [%]	Clear zrn [%]	Other zrn [%]	Tot zirc [%]	Rut [%]	Leuc [%]	Kyan [%]	Other [%]
12h00	0.053	0.054	95.18	4.64	99.82	0.02	0.01	0.09	0.07
18h00	0.091	0.055	94.01	5.72	99.73	0.10	0.01	0.08	0.08
21h00	*0.133*	*0.067*	*94.00*	*5.68*	*99.68*	*0.18*	*0.05*	*0.04*	*0.05*
02h00	*0.134*	*0.073*	*93.95*	*5.75*	*99.69*	*0.15*	*0.03*	*0.10*	*0.04*

The off-specification products were visually much darker with yellowish shades compared to the on-specification products. This was confirmed by stereomicroscopic images, which also showed that stained zircon was more frequent in the off-specification product samples. It was found that the high iron concentrations were connected to a yellowish mineral surface deposit as well as a prevalence of stained reddish (unleached) zircon grains as shown in Figure 4.15(a).

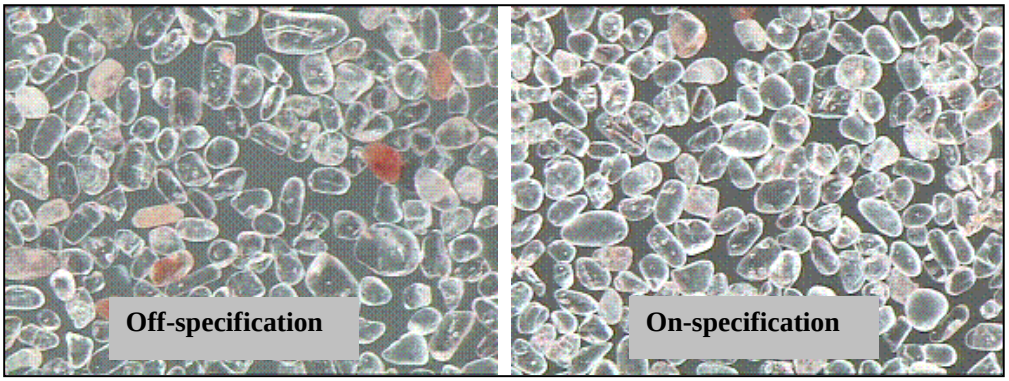

Figure 4.15(a): Stereomicroscopic images of on and off-specification zircon product samples collected on 10 March 2003 at 02h00 and 18h00, respectively.

4.5.6. ARTIFICIAL ADSORPTION OF PRECIPITATED SPECIES TO ZIRCON AND ACID WASH OF ZIRCON AND RUTILE PRODUCT SAMPLES

These tests were conducted in order to verify the adsorption theory and to quantify the amount of precipitates present on dry mill feed samples. Mineral samples were coated with precipitate prepared from the HAL process water. Dry mill samples were chemically washed. Chemical XRF analyses of the before and after samples were compared to determine which of the precipitates formed in the HAL circuit had adsorbed to the mineral particles. Therefore, if the species that were artificially 'forced' to adsorb to the mineral surfaces were present on the samples obtained from the plant, then it would confirm that these species actually do adsorb to the mineral surfaces under natural plant conditions. This theory would also be further confirmed if analyses of the rinse water contained the precipitate species formed in the HAL neutralisation stage.

Precipitation of species in the HAL circuit was simulated by raising the pH of a process water sample collected from the overflow of the upflow classifier A by adding concentrated caustic to raise the pH to above 7. Suspended clay particles were removed by filtration before caustic was added. The preparation work was performed at room temperature. Zircon and rutile product samples (1.5 kg each) were thoroughly mixed for approximately 15 minutes with the 'neutralised' mixture. The excess solution was decanted and the samples were dried in an oven for 3 - 4 hours and at 140^{o}C. Both samples were used for electrostatic separation tests and a split from the zircon product sample was submitted for XRF analysis of which the results are shown in Table 4.21.

It is clear from the table that adsorption of Fe_2O_3 was predominantly followed by Al_2O_3 and surprisingly TiO_2. Two important points must be emphasised, namely the likelihood of other precipitates forming at lower concentrations and their presence on the mineral surfaces were not included in the XRF analyses, and the volume of precipitate formation and adsorption to the mineral surfaces would be higher in the laboratory than at the plant. The XRF chemical analyses of the coated and uncoated samples, together with the laboratory electrostatic separation performance, provided important insight into the impact of adsorbed precipitate species.

Table 4.21: The pH of a 2-litre sample obtained from the overflow of the upflow classifier A was raised. The pH was increased from approximately 1.8 to 7 at room temperature. Approximately 1.5 kg zircon product was thoroughly mixed with the precipitate and the excess precipitate rich water was decanted. The sample was dried in an oven at approximately 140°C for 3 to 4 hours. Analyses of the normal (not coated) and coated samples were obtained with an XRF (powder analysis).

	Zircon product sample		
Species	Normal	Coated	Change
Al_2O_3	0.150	0.177	**+18.0%**
Fe_2O_3	0.050	0.061	**+22.0%**
TiO_2	0.117	0.134	**+14.5%**

The occurrences of HAL precipitate formation and its adsorption to mineral surfaces were determined by washing zircon and rutile product samples with acidic water solutions. All samples were initially washed with acidic water at pH 0.8, but the pH of the wash water was slightly increased to 1.3 during the course of the study. The reason for this was to reduce the potential of leaching unleached species and therefore it would only dissolve adsorbed iron and other precipitates. Iron precipitation experiments confirmed this to be correct in the case of low iron concentrations such as in the HAL attritioners. Rutile and zircon product samples of Table 4.22 and 4.23 were washed with acidic water at pH 0.8 and 1.3, respectively.

By comparing the unwashed zircon product samples of Table 4.22, it is clear that sample 2 was off-specification in terms of TiO_2 and slightly below the Fe_2O_3 specification. Sample 1 was within all the specification limits. Acid wash of both samples reduced the iron concentrations significantly to well below specification to almost similar levels. Aluminium concentrations were also reduced, but the reduction was relatively small. The impact of acid wash on TiO_2 concentration was negligible and the small differences could be ascribed to analytical errors. It is important to mention that the zircon samples were collected on a day when deterioration in electrostatic separation in the plant was visually observed, which was confirmed by lower zircon product recoveries.

Table 4.22: Two zircon product samples accumulated over a period of two hours were collected on 18 May 2004 when dry mill production of zircon and rutile were lower due to deterioration in electrostatic separation. Both samples were accurately split into two identical samples of which one split was intermittently rinsed with acidic water at pH 1.3 for 15 minutes. The samples were 'neutralised' by repeating washing and decantation with fresh water for 4 to 5 times. The acidic water was prepared by adding a few drops of sulphuric acid (98%) to the water. The chemical analyses of the mineral samples were obtained with a XRF (powder).

		Sample 1 (02h00)			Sample 2 (10h00)		
Species	Specifi-cation	Not washed	Washed	Change	Not washed	Washed	Change
Al_2O_3	< 0.30	0.191	0.176	-7.9%	0.214	0.206	-3.7%
Fe_2O_3	< 0.060	0.053	0.045	-15.1%	0.059	0.046	-22.0%
TiO_2	< 0.120	0.095	0.093	-2.1%	0.160	0.161	+0.63%

Analyses of washed and unwashed rutile product samples are shown in Table 4.23. Unwashed sample 2 was off-specification with respect to TiO_2. Both washed samples showed a reduction in Fe_2O_3, but less significantly than the zircon product samples of Table 4.22. Changes in concentration of TiO_2 and SiO_2 were insignificant and could be ascribed to analytical errors.

Table 4.23: Two rutile product samples, as sampled over a period of two hours, were collected on 5 and 14 April 2003. Both samples were accurately split in two identical samples of which one split was intermittently rinsed with acidic water at pH 0.8 for 5 minutes. Fresh water washing and decantation followed the acid rinse repeatedly until the pH of the water was approximately 6.5. The chemical analyses of the samples were obtained by XRF (fusions).

		Sample 1 (05-April-03)			Sample 2 (14-April-03)		
Species	Specifi-cation	Not washed	Washed	Change	Not washed	Washed	Change
Al_2O_3		0.500	0.603	+20.6%	0.397	0.437	+10.1%
Fe_2O_3	< 1.0%	0.589	0.559	-5.1%	0.609	0.551	-9.5%
TiO_2	> 94.0%	94.850	94.365	+0.5%	93.812	95.145	+1.4%
SiO_2	< 2.30%	2.244	2.258	-0.6%	2.149	2.144	-0.2%

Investigations up to this point have indicated that precipitation and consequent adsorption of iron (III) to mineral surfaces could be one of the main factors which have affected electrostatic separation in the dry mill circuit. Analyses were determined by the XRF and were therefore limited to Al_2O_3, Fe_2O_3, TiO_2 and SiO_2. It was important to verify if iron (III) complexes were the main contaminant affecting

electrostatic separation by determining the complete surface chemistry of the mineral samples by quantifying all the species that were present on the mineral surfaces. Chemical species deposited on mineral samples (by adsorption and other means) were removed by rinsing the samples for 10-15 minutes at room temperature with either fresh (pH 6.7) or acidic water (pH 1.6). Sulphuric acid was used to prepare the acidic solution. Background chemical assay readings were obtained by analysing the fresh and acidic water prior to washing. Approximately 9 kg dry mill feed (4% moisture) and HAL recycle (dry) mineral samples were rinsed with 2 250 ml water (25% of mass of sample). After washing, the water was submitted for chemical analyses and the obtained concentrations of chemical species (mg/l) were expressed in mg/kg sand by taking the mass of the mineral sample and volume of wash liquid into account. Background species introduced with the rinse water were subtracted by setting up a mass balance over the system and accounting for the moisture present in the dry mill feed samples.

Species present on the mineral surfaces of the HAL recycle were also expressed as % distribution of species present in the dry mill feed samples. The HAL recycle stream was chosen due to its observed behaviour, which often indicated a build-up of conductive mineral particles in the dry mill circuit. It was often observed that this particular stream, which recycled material from the dry mill back to the HAL circuit, increased in volume when a build-up of iron in the process water of the wet gravity circuit was noted or during periods when electrostatic separation was negatively affected. Therefore, mineral particles contaminated with species such as adsorbed iron would concentrate in the HAL recycle. The results showed that iron followed by aluminium were predominant in the HAL recycle. Results are summarised in Table 4.24.

Table 4.24: Surface chemistry of mineral particles obtained by rinsing mineral particles for 10-15 minutes with fresh and/or acidic water (pH 1.6) at room temperature. The wash water was analysed before and after rinsing. The surface chemistry was obtained by combining the chemical analyses with mass data to correctly account for dilution factors and chemical species introduced with the wash water.

Sample	Concentration of species, mainly precipitates, on the mineral surfaces [mg/kg sand]										
	Ca	Mg	Na	K	Cl	SO_4	Sr	Ba	Si	Fe	Al
Dry mill feed (wet) & fresh wash	8.13	0.79	2.210	0.586	6.2	36.28	0.070	0	2.41	0.142	0.134
Dry mill feed (wet) & acidic wash	13.4	0.93	3.370	1.688	5.0	636.0	0.036	0	3.43	1.241	1.230
Dry mill feed acidic vs fresh water variance	*65%*	*18%*	*53%*	*188%*	*-24%*	*1653 %*	*-49%*	*0%*	*42%*	*774%*	*818%*
HAL recycle (dry) & acidic wash	0	1.04	4.444	1.169	0	88.0	0.055	0.04	1.75	3.991	2.751
Distribution of species to HAL recycle	*0.0%*	*8.6%*	*10.1%*	*5.3%*	*0%*	*1.1%*	*11.8%*	-	*3.9%*	***24.7%***	***17.2 %***

A dry mill feed sample was split in two and rinsed with both fresh and acidic water. It could be observed from Table 4.24 that some species, such as Mg, Cl (and to some extent Si, Na and Ca) could be removed with fresh water rinsing. Species such as SO_4, Al, Fe, Sr and K could only effectively be removed with acidic washing. Na and Ca could be removed with both fresh and acidic water, but much more effectively with the latter (concentration increased by more than 50%). Si was removed relatively effectively with fresh water, but its concentration was increased by more than 40% when acidic water was used.

4.6. IMPACT OF ADSORBED SURFACE IRON ON ELECTROSTATIC SEPARATION AND THE QUALITY OF ZIRCON AND RUTILE PRODUCT

The purpose of these experiments was to quantify the impact of adsorbed precipitates on electrostatic separation. The first objective was to prove that the electrostatic separation efficiency of mineral particles was affected if they were artificially coated with a layer of HAL precipitates prepared in the laboratory. The impact of adsorbed precipitated iron was further determined by evaluating the dry mill performance during trials when neutralisation with caustic soda was temporarily paused, artificial cleaning of contaminated samples that were collected from the plant, and samples obtained before and after plant trials when the caustic was switched-off. Electrostatic separation performance of these samples was evaluated in the laboratory by means of a laboratory HTR (high tension roll) and Coronastat separators.

4.6.1. PLANT TRIALS: TEMPORARY PAUSE IN THE ADDITION OF CAUSTIC

These trials were conducted to quantify the impact of the precipitates adsorbed to the mineral surfaces on plant scale electrostatic separation in order to justify capital expenditure for the implementation of a process solution. Table 4.25 provides a qualitive summary of five plant trials when the caustic addition was temporarily switched off. It is important to note that poor electrostatic separation and low output zircon production occurred at trials 1, 2, 4 and 5 before the caustic was switched off. Zircon product iron concentrations were also relatively high and a significant decrease in the product iron and increase in zircon production occurred after the caustic was switched off. Low iron concentrations of both the zircon product and wet gravity process water were observed during trial 3 before the caustic was stopped. This trial was conducted directly after a combined HAL and wet gravity shutdown when the process water contained relatively small amounts of precipitated iron and other chemical species. This is important since it evaluated the impact of precipitated species at a time when the concentration and build-up of species in the process water was at a minimum level. Dry mill electrostatic separation was characterised effectively during this trial.

Table 4.25: Summary of trials when neutralisation of the product of the HAL circuit was temporarily paused by switching off the caustic for relatively short periods of time. These were repeated for 5 separate periods.

Trial	Caustic switched-off	Period [days]	Comment
1	09-May to 10-May-02	2	Excessive build-up of hydrous ferric oxide visible in wet gravity and sec conc belt filter. Low zirc and rut output prod tons (electrostatic separation problems). Zirc prod increased from 14 to >15 tph after caustic was switched-off (zirc prod Fe decreased from >0.055% to <0.045%).
2	03-June to 04-June-02	2	Strategic campaign from 28-May to 02-June-02. Fluctuating weather conditions and feed grade affected dry mill separation. Zirc prod increased from 13.5 to >15 tph after caustic was switched off (zirc prod Fe decreased from >0.055% to 0.050%). Improved electrostatic separation allowed dry mill grade to be adjusted, which caused rutile/leucoxene separation problems that resulted in lower rutile output tonnages.
3	06-June to 10-June-02	5	Caustic was terminated when Fe build-up was low after a total maintenance shut down. Rutile recoveries reduced due to wet gravity adjustments; reduced grade to increase zircon output tons. Zircon prod Fe < 0.050%.
4	19-June-02	2	Dry mill circuit very unstable due to electrostatic separation and grade related problems (high zirc prod Fe_2O_3 and TiO_2 levels). Switching off the caustic improved electrostatic separation and zirc prod tons improved from 13.5 to >15.5 tph (zirc prod Fe decreased from >0.056% to <0.050%). Rutile recoveries reduced due to wet gravity adjustments; reduced grade to increase zircon output tons.
5	14-May-03	1	Zirc and rut prod low due to electrostatic separation problems. Switching off the caustic increased zirc production from 13.8 to >15.5 tph and rut production from 2.0 to 2.8 tph.

The effect of switching off the caustic of the last trial is shown in Figure 4.15, which is a graphic presentation of real online tonnage data of the main streams in the dry mill circuit. The impact was quantified by comparing the average before and after data and the results are summarised in Table 4.26.

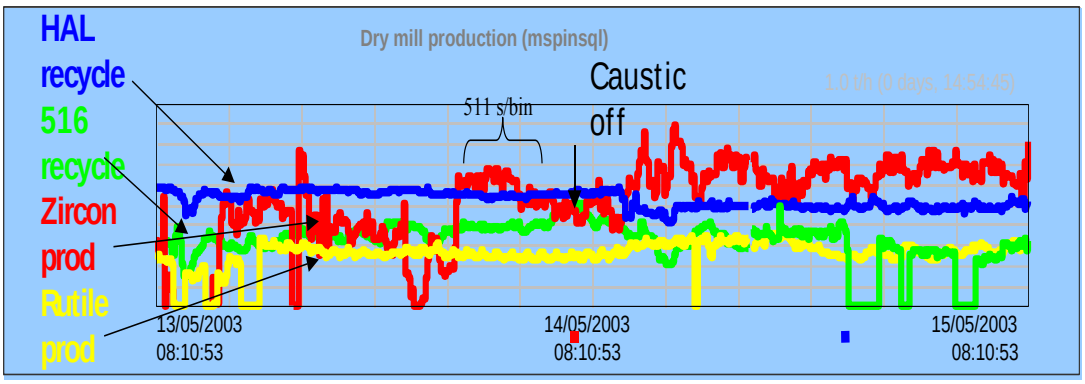

Figure 4.15: Online plant data showing the impact of switching off the caustic during Trial 5

Table 4.26 is a summary of the main mass streams of the dry mill circuit (as shown in Figure 4.15) before and after the caustic was switched off. It is important to note the changes in the mass balance a few hours after the caustic addition was stopped. The time delay was the result of the presence of inventory stock in the dry mill feed bin and the residence time of wet gravity circuit. The data shows significant reductions in the recycle streams (516 and HAL recycle) and significant increases in the 511 plate feed and product streams. The 511 plate feed was the feed to the final zircon cleaning circuit. Both the HAL recycle and 516 recycle streams removed conductive and magnetic material to produce an on-specification zircon product. High recycle loads were often an indication of a build-up of conductive mineral. Mineral recovery variances of both primary, secondary zircon (zirkwa) and rutile were 9.8%, 0.7% and 26.5%, respectively. The recovery of zircon to 511 plate feed increased by 4.4%.

Table 4.26: Summary of production data of Trial 5 when the caustic was temporarily switched-off on 14 May 2003.

Mineral stream	Before	After	[#]Variance in tonnage	[$]Difference in zircon and rutile dry mill recovery
	Tph	Tph	%	%
HAL recycle	2.8	2.5	-10.7	N.A.
516 recycle	8.8	5.9	-33.0	N.A.
511 plates feed	20.2	21.0	+4.0	+4.4
Zircon product	13.8	15.6	+13.0	+9.8
Zirkwa product	0.26	0.39	+50	+0.7
Rutile product	2.0	2.8	+40.0%	+26.5

[#]Variance = [(After-before)/Before]x100; [$]Difference = After-Before

Production data of Trial 4 is summarised in Table 4.27. This data was kept as back-up to prevent any potential loss of information due to potential PLC communication errors. Caustic addition was stopped at approximately 08h00. It is clear from the results that the zircon production was relatively low and XRF Fe_2O_3 concentrations were above 0.057% from 06h00 to 11h00. The zircon product was also off-specification in terms of TiO_2 (XRF analysis) at 08h00 and 10h00. The grade of zircon production, as well as TiO2 and Fe_2O_3, increased significantly from 12h00. Zircon product Al_2O_3 concentrations increased and dry mill feed grade deteriorated slightly during the night shift. These changes were related to wet gravity spiral adjustments during the day shift to increase the zircon recovery of this circuit. The increased recovery resulted in a reduction in the ZrO_2 content, but an

increase in the TiO_2 and Al_2O_3 content due to an increase in gangue minerals fed to the dry mill circuit. Tonnages decreased from 03h00 during the night shift due to a dry mill circuit stoppage as a result of equipment breakdown.

Table 4.27: Scanned production data of Trial 4 showing XRF analysis of the dry mill feed (SDO) and zircon product streams as well as tonnages of the zircon product stream.

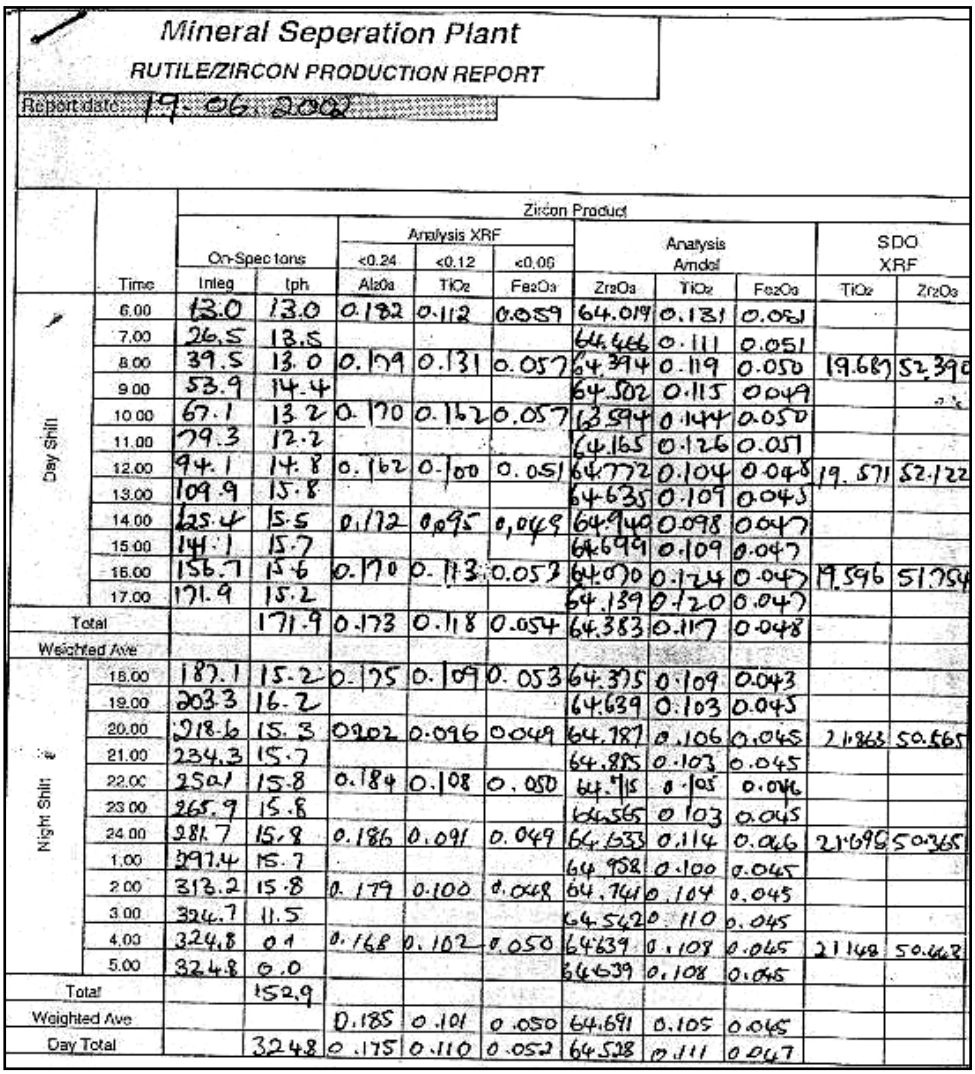

Mineral Seperation Plant

RUTILE/ZIRCON PRODUCTION REPORT

Report date: 19-06-2002

	Time	Zircon Product: On-Spec tons Integ	On-Spec tons tph	Analysis XRF <0.24 Al2O3	<0.12 TiO2	<0.06 Fe2O3	Analysis Amdel ZrO2	Amdel TiO2	Amdel Fe2O3	SDO XRF TiO2	SDO XRF ZrO3
Day Shift	6.00	13.0	13.0	0.182	0.112	0.059	64.019	0.131	0.061		
	7.00	26.5	13.5				64.466	0.111	0.051		
	8.00	39.5	13.0	0.109	0.131	0.057	64.394	0.119	0.050	19.689	52.396
	9.00	53.9	14.4				64.502	0.115	0049		
	10.00	67.1	13.2	0.170	0.162	0.057	63.594	0.144	0.050		
	11.00	79.3	12.2				64.165	0.126	0.051		
	12.00	94.1	14.8	0.162	0.100	0.051	64.772	0.104	0.048	19.571	52.122
	13.00	109.9	15.8				64.635	0.109	0.045		
	14.00	125.4	15.5	0.172	0.095	0.049	64.940	0.098	0.047		
	15.00	141.1	15.7				64.699	0.109	0.047		
	16.00	156.7	15.6	0.170	0.113	0.053	64.070	0.124	0.047	19.596	51.754
	17.00	171.9	15.2				64.139	0.120	0.047		
Total			171.9	0.173	0.118	0.054	64.383	0.117	0.048		
Weighted Ave											
Night Shift	18.00	187.1	15.2	0.175	0.109	0.053	64.375	0.109	0.043		
	19.00	203.3	16.2				64.639	0.103	0.045		
	20.00	218.6	15.3	0.202	0.096	0.049	64.787	0.106	0.045	21.863	50.565
	21.00	234.3	15.7				64.885	0.103	0.045		
	22.00	250.1	15.8	0.184	0.108	0.050	64.715	0.105	0.046		
	23.00	265.9	15.8				64.565	0.103	0.045		
	24.00	281.7	15.8	0.186	0.091	0.049	64.633	0.114	0.046	21.696	50.365
	1.00	297.4	15.7				64.958	0.100	0.045		
	2.00	313.2	15.8	0.179	0.100	0.048	64.741	0.104	0.045		
	3.00	324.7	11.5				64.542	0.110	0.045		
	4.00	324.8	0.1	0.168	0.102	0.050	64.639	0.108	0.045	21.148	50.648
	5.00	324.8	0.0				64.639	0.108	0.045		
Total			152.9								
Weighted Ave				0.185	0.101	0.050	64.691	0.105	0.045		
Day Total			324.8	0.175	0.110	0.052	64.528	0.111	0.047		

4.6.2. ELECTROSTATIC SEPARATION PERFORMANCE

The impact of iron hydr(oxide) on electrostatic separation performance was quantified in the laboratory by coating mineral samples with an iron precipitate rich solution, cleaning (chemically) the surfaces of plant samples and using samples collected before and during a plant trial when caustic was switched off.

4.6.2.1. Artificially coated mineral particles

Approximately 1.5 kg prime zircon and rutile product samples were thoroughly mixed with solutions rich in iron precipitate obtained from the secondary concentrate belt filter and overflow water of the upflow classifier A after increasing the pH to 5. The pH was increased to 5 instead of 7 to correspond with the HAL attritioner pH that was reduced from 7 to 5 during the course of the study.

Iron hydr(oxide) accumulated in the secondary concentrate of the wet gravity circuit due to the relatively low density of these oxides and the correspondent distribution of light particles in the wet gravity circuit. On the 9th of May 2002 high concentrations were visible as a yellow layer of approximately 1 mm thick on top of the belt filter cake. Electrostatic separation was severely affected on that day. A sample of the top layer was collected and mixed with fresh water. Entrapped mineral sand particles were allowed to settle and the solution, rich in iron precipitates, was decanted. This mixture was mixed for approximately 15 minutes with splits of zircon and rutile product samples (1.5 kg each). Excess liquid was decanted and the samples were dried in an oven at 140^{o}C for approximately 3 hours. The dried samples were labelled 'coated-1'. The uncoated samples were labelled 'uncoat-1'.

Overflow water of the upflow classifier A was filtered with a Millipore filter to remove suspended clay particles. Concentrated caustic soda was added at room temperature to raise the pH to 5. Yellowish iron precipitate formed visibly. Fresh zircon and rutile product samples were collected from the plant and split in two 1.5 kg samples each. One split of every product was labelled 'uncoated-2'. The other splits (1.5 kg each) were mixed for 15 minutes with 1.5 litres of the precipitate rich solution. Excess liquid was decanted and the samples were dried in an oven at 140^{o}C for approximately 3 hours. The samples were labelled 'coated-2'.

Electrostatic separation tests were important and would confirm that the precipitates obtained from the belt filter were indeed formed in the HAL circuit. This would only be true if the mineral particles behaved electrostatically the same as the particles artificially coated with precipitates prepared from the HAL process water. It would also confirm that precipitates fed from the HAL to the wet gravity circuit do end up in the final wet gravity concentrate streams. Individually coated and uncoated samples were heated to 85^{o}C and passed over a laboratory HTR equipped with 7 sample collecting trays with accurately controlled settings as indicated in Table 4.28. Spatial distribution performance curves were constructed by plotting the accumulative rutile against the accumulative zircon mass

distribution. The performance curves, Figures 4.16 and 4.17, were used to evaluate the electrostatic separation performance of coated and uncoated mineral particles in order to determine the impact of precipitated HAL species on the electrostatic separation of zircon and rutile mineral particles in the dry mill circuit.

Table 4.28: Experimental parameters used to obtain the performance curves of Figures 4.16 and 4.17. The experiments were conducted with a laboratory high-tension roll separator (HTR).

Performance curve	Description of coatings	Original sample	Mineral temperature [°C]	Roll temperature [°C]	Kilovolt setting [kV]	Roll speed [rpm]
Uncoated-1	No coating	Dry	85	52	31	240
Coated-1	Precipitate obtained from sec conc belt filter.	Dry	85	53	31	240
Uncoated-2	No coating	Dry	84	52	30	242
Coated-2	Filtered sample from the overflow of the upflow classifier at pH 5.	Dry	84	51	30	243

Electrostatic separation performance of the normal samples (uncoated) and the samples coated with the precipitate obtained from the secondary concentrate belt filter are shown in Figure 4.16. Optimum separation occurs when the zircon distribution to non-conductors is maximised and rutile distribution to non-conductors is minimised. At a zircon distribution of 70%, the coated sample had 26% rutile distributed to non-conductors compared to 14.8% of the uncoated sample. It is also important to compare the individual data points of the two graphs with respect to their distance from the intersection point of the x and y axis. The individual data points of the uncoated sample with respect to the coated sample were further away from 0 on the horizontal direction (zircon distribution), but closer to 0 on the vertical direction (rutile distribution).

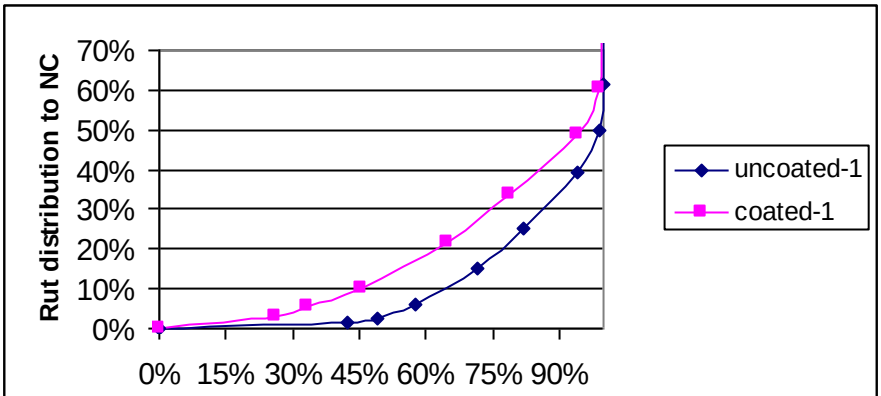

Figure 4.16: Electrostatic separation performance curves of uncoated and coated samples with an iron hydroxide precipitate and clay mixture obtained from the secondary concentrate belt filter on 9 May 2002. The curves were constructed by combining mass distribution data obtained by passing the samples over a laboratory HTR at standard settings.

The graphs of Figure 4.17 compare the impact on electrostatic separation of precipitate produced from the overflow water of the upflow classifier A from the HAL section. Suspended clay particles were removed by filtration before the pH was raised to 5. Zircon and rutile product samples of approximately 2 kg each were mixed with this precipitate rich solution and the excess solution was decanted prior to drying in an oven at 140^{o}C. The separation performances of the two samples were similar compared to the samples coated with precipitate obtained from the secondary concentrate belt filter (Figure 4.16). The individual data points were also spaced similarly along the x and y axis. At a zircon distribution of 70%, the coated sample had 15.8% rutile distributed to non-conductors compared to 8% of the uncoated sample.

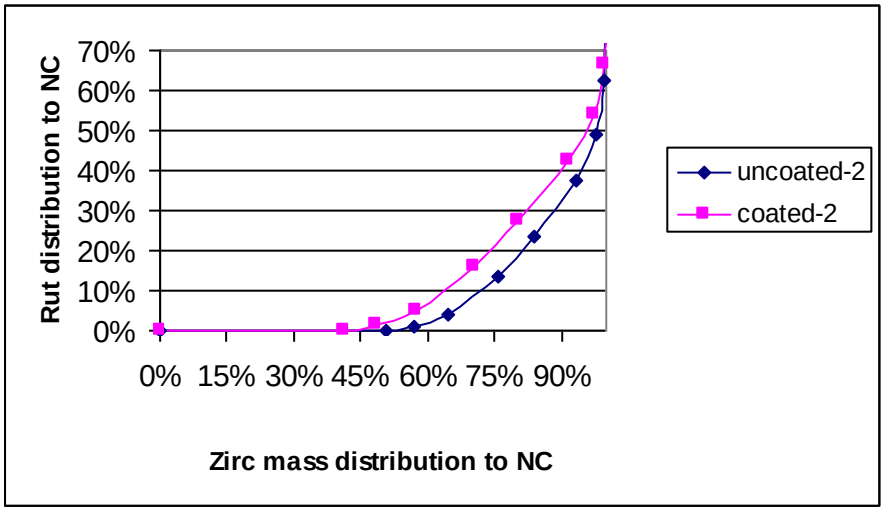

Figure 4.17: Electrostatic separation performance curves of uncoated samples and samples coated with an iron hydroxide rich precipitate. The precipitate was prepared by raising the pH to 5 of a pre-filtered upflow classifier overflow sample (overflow sample was collected in May 2002). The curves were constructed by combining zircon and rutile mass distribution data obtained by passing the samples over a laboratory HTR at standard settings.

The electrostatic separation efficiencies of the individual performance curves of Figures 4.16 and 4.17 are summarised in Table 4.29. Separation efficiency was expressed as the average of the zircon distribution to non-conductors and the rutile distribution to conductors. The calculation was simplified by calculating the rutile distribution to conductors as 100 minus the rutile distribution to non-conductors (therefore assuming no middling stream). It can be seen from the results that the separation efficiencies of uncoated-2 and coated-2 are higher than those of sample 1. The difference in separation efficiency was bigger for sample 1 than 2.

Table 4.29: Summary of separation efficiencies of the individual performance curves of Figures 4.16 and 4.17.

Performance curve	Mineral distribution to NC		Efficiency	% Difference (uncoated-coated)
	% Zirc	% Rut		
Uncoated-1	70.0%	14.8%	77.6%	0%
Coated-1	70.0%	26.0%	72.0%	5.6%
Uncoated-2	70.0%	8.0%	81.0%	0%
Coated-2	70.0%	15.8%	77.1%	3.9%

4.6.2.2. Actual plant samples: Laboratory electrostatic separation and process simulations of mineral wash circuits

The objectives of these tests were to quantify the impact of actually adsorbed surface species on electrostatic separation at the Mineral Separation Plant (MSP) of Namakwa Sands and to identify a suitable process for ensuring clean mineral surfaces. Separation efficiency results obtained from these graphs, together with recovery improvements obtained by the temporary pause in the addition of caustic, were used to financially justify capital expenditure for the implementation of this process solution.

Actual dry mill feed samples were collected during different periods and the electrostatic separation performance of the dry mill circuit was recorded during the time of sample collection. The majority of samples were collected from the discharge of the primary belt filter prior to the dryer. Only one sample (1a) was collected after the dryer. Collecting the samples before the dryer minimised the effect of the temperature on the mineral surface deposits such as iron hydroxides. Therefore, ageing of surface precipitates was minimised, which ensured more effective removal in the chemical washing process stages that were simulated in the laboratory. The electrostatic separation performance of the samples were determined by means of a laboratory coronastat separator using the parameters as summarised in Table 4.31. It was clear from the qualitative description of the dry mill performance (Table 4.30) that the dry mill feed quality could be grouped into three categories on the basis of electrostatic separation efficiency. The categories are: ‘difficult’ (12 and 13 May 2003), ‘good’ (14 May 2003), and ‘excellent’ (18 May 2003).

Table 4.30: Description of the dry mill performance at the time of sample collection.

Performance curve	Figure	Date of sample collection	Dry mill performance at time of sample collection
2a	4.18	13-May-03	Poor electrostatic separation and high recycle loads due to iron build-up. Average zirc and rutile production were 13.8 and 2 tph, respectively.
2b	4.18	14-May-03	Separations improved and recycle loads decreased significantly. Average zircon and rutile production were > 15.5 and >2.8 tph, respectively.
3a	4.19, 4.20	13-May-03	See 2b (same sample)
3b	4.19, 4.20	N.A.	N.A. (sample was treated with caustic in the laboratory).
1a	4.21	12-May-03	Poor electrostatic separation and low output zircon and rutile product tons due to iron build-up.
1b	4.21	N.A.	N.A. (sample was 'washed' in laboratory).
5a	4.22	13-May-03	See 2a (same sample)
5b	4.22	N.A.	N.A. (sample was 'washed' in laboratory).
6a	4.23	18-May-03	Excellent electrostatic separation and high output zircon product tons.. Low iron build-up.
6b	4.23	N.A.	N.A. (sample was 'washed' in laboratory).

Laboratory settings and process descriptions are summarised in Table 4.31. Samples which were taken straight from the plant without any surface cleaning are indicated as 'N.A'. It is important to mention that almost each set (e.g. 3a and 3b performance curves) of performance curves were conducted in a period of 1 hour associated with constant weather conditions (usually between 08h00 and 12h00 and between 14h00 and 17h00) to minimise the effect of atmospheric moisture on electrostatic separation. Only performance curves 2a and 2b were conducted on separate days. It was found that the repeatability of results could only be assured by keeping all the experimental parameters constant. It is clear from the table that experimental errors were minimised by ensuring that all machine settings and mineral temperatures were kept constant and equal.

Repeatability of the results were evaluated by combining the samples produced by the HTR separation and passing them over the HTR for a second time. If the variances of the individual mass fractions differed by more than 3%, the test was repeated until the errors were within acceptable limits. Samples were submitted for analyses only after acceptable repeatability had been achieved. This was important to certify absolute accuracy of the results by minimising potential experimental errors. This was

necessary to identify the optimum process, which was selected on the basis of relatively small improvements in electrostatic separability.

Table 4.31: Summary of experimental parameters used to construct the performance curves of Figures 4.18 – 4.22. All of the samples, except 1a and 1b, were wet dry mill feed samples (approximately 4% moisture) prior to laboratory processing and testing. The sample used for 1a and 1b was collected after the drier (secondary drier) of the dry mill circuit.

Performance curve	Description of process	Mineral temperature [^{o}C]	Roll temperature [^{o}C]	Kilovolt setting [kV]	Roll speed [rpm]
2a	N.A.	See 5a	See 5a	See 5a	See 5a
2b	Plant trial: caustic off	See 3a	See 3a	See 3a	See 3a
3a	Plant trial: caustic off	70	50	26.1	190
3b	Raise pH of sample to >6.5 by adding caustic	70	50	25.9	190
1a	N.A.	68	50	25.7	190
1b	Simplified CCD circuit (including attritioning)	67	47	25.8	191
5a	N.A.	68	51	26.1	190
5b	Filtration (pH 0.8)	68	52	26.0	190
6a	N.A.	67	51	26.3	190
6b	Filtration (pH 2)	68	52	26.0	190

(a) Caustic termination trial: Electrostatic separation performance of the before and after samples

Sample 2b was collected before the plant trial when the caustic was switched off. It is important to highlight that electrostatic separation in the dry mill was poor during the time of sample collection. Recycle streams were overloaded, which were the result of low electrostatic separation efficiency. Sample 2a was collected after the caustic was temporarily switched off. Dry mill electrostatic separation improved significantly, recycle streams were reduced to below normal loads, and zircon and rutile production increased 2 to 4 hours after the caustic was switched off. The sample was collected only after these changes were observed in the dry mill. The laboratory separation

performance tests were performed on two separate days. Atmospheric conditions were constant during these two days and the impact of the weather conditions was therefore assumed to be negligible.

Electrostatic performance curves of samples 2a and 2b are shown in Figure 4.18. It is clear from the performance curve that 2a (caustic off) outperformed 2b (caustic on). Note that the differences in separation were not that significant as for the artificially coated samples, mainly due to lower volumes of precipitate present on the mineral surfaces of plant samples. By comparing the relative distance from zero of the individual data points in the horizontal and vertical direction, a slightly different pattern was observed (in the vertical direction) compared to the samples artificially coated with precipitate obtained from the secondary concentrate belt filter and samples that were coated with precipitate prepared from the overflow water of the upflow classifier (see Figures 4.16 and 4.17, paragraph 4.6.2.1 – *Artificially coated mineral particles*). It was observed that the data points of 2b were spaced further than 2a from zero, not only in the horizontal but strangely also in the vertical direction.

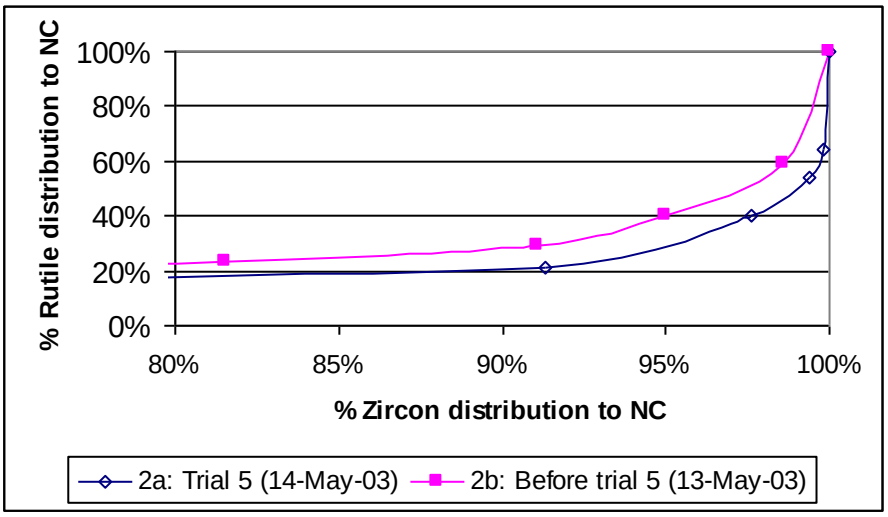

Figure 4.18: Laboratory electrostatic performance curves comparing the separation performance of two samples collected the day before and during trial 5 when the caustic was temporarily switched off on 14 May 2003. It is important to note that test work with the individual samples was conducted on two separate days.

(b) The effect of caustic on electrostatic separation of mineral particles after dissolved iron and other species have been reduced

The objective of this test was to determine the impact of caustic on electrostatic separation when dissolved species had been minimised prior to the neutralisation stage. This test was very important since it would identify what specific change (reduction in sodium hydroxide or reduction in the formation of precipitates) contributed to the improved electrostatic separation after the caustic was switched off. A dry mill feed sample (1.5 kg) was collected during a trial when the caustic was switched off (sample 3a) and mixed with 375 ml water. The pH of the water, after mixing, was 3.51. Six drops of concentrated caustic was added and the sample was mixed for a couple of minutes. The pH of the water, after mixing, was 6.86 and excess water was decanted prior to drying the sample in an oven at 140^{o}C for 3 hours. Mass fractions of 3a and 3b were found to be almost identical as shown in Figure 4.19.

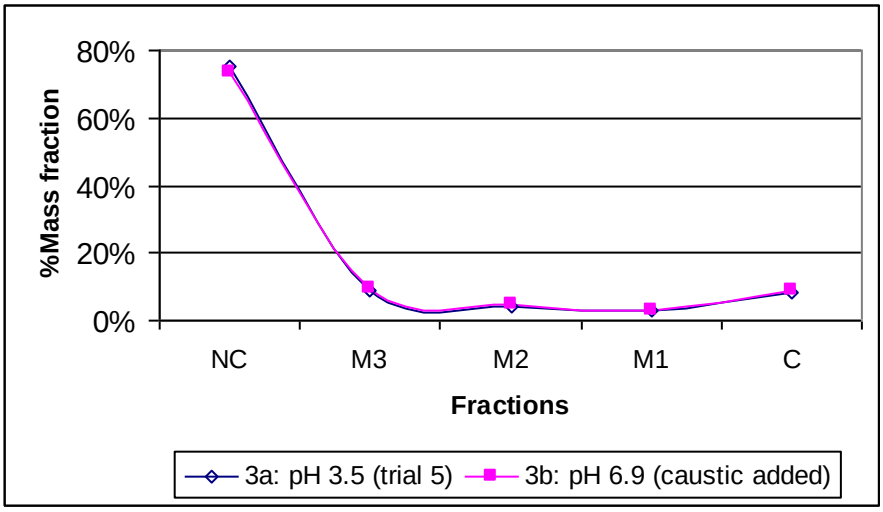

Figure 4.19: Mass splits comparing the separation performances of a sample collected from trial 5 before and after it had been neutralised with a few drops of concentrated caustic.

The performance curves were not exactly the same mainly due to one outlier at 90% zircon distribution (see Figure 4.20). This could possibly be attributed to grain count errors. All the other differences were within acceptable limits and the curves could be considered as identical.

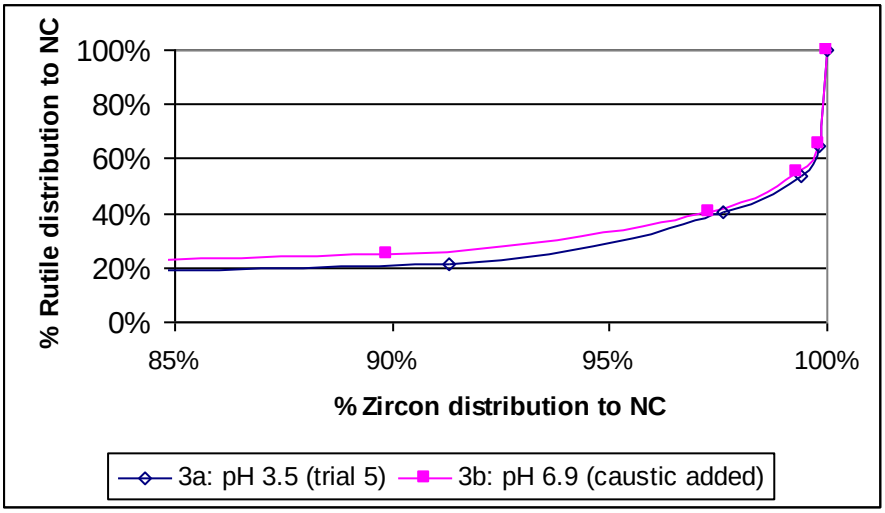

Figure 4.20: Laboratory electrostatic performance curves comparing the separation performance of a sample collected from trial 5 with one split neutralised with a few drops of concentrated caustic.

(c) Acid wash (pH 0.79) of dried dry mill feed samples – simplified CCD

A dried dry mill feed sample was collected from the dryer during a day when poor electrostatic separation was observed. The sample was processed through multiple stages to simulate a simplified counter-current-decantation circuit. The results of this test were discarded due to the accumulation of unforeseen experimental errors during the test. However, this test confirmed that precipitates attached and baked onto the mineral surfaces via the drying process were ineffectively removed by a chemical desorption process. Therefore, it emphasised the importance of cleaning mineral samples while the samples are still wet and the precipitates still fresh. This experiment highlighted the following:

(1) Ageing and/or change in properties of precipitates attached to the mineral surfaces occurred due to the drying process of the feed fed to the dry mill. It was clear from literature that iron hydroxide becomes chemically more stable with an increase in temperature (refer to Table 2.3 of Cigan et al., 1980). Iron hydroxide (and potentially other precipitates) would provide resistance to acidic washing after drying at relatively high temperatures.

(2) Attritioning generated relatively large amounts of slimes.

(d) Acid wash (pH 0.8) of wet dry mill feed samples – filtration simulation.

A wet dry mill feed sample (764 g) collected on 13 May 2003 (poor dry mill electrostatic separation) was split in two and the one split was repulped to 70% solids by mixing the damp sample with acidic water (pH 0.8) followed by vacuum filtration. Cake washing was applied using acidic water (pH 2) and a wash ratio of 2.5 (wash ratio = wash water/cake moisture). The washed filter cake was removed from the filter apparatus and repulped to 45% solids (typical solid content of the feed stream to a cyclone) followed by decantation to obtain 60% solids, thereby simulating a dewatering cyclone stage, which operates at a relatively low efficiency (80-85% solids can be achieved in the underflow of a dewatering cyclone that operate at a high efficiency). A few drops of concentrated caustic were added to raise the pH of the slurry to 6.7 (note that the pH is raised to 5 in the plant). The reader is referred to Chapter 3 – *Materials and methods* for the description and flow sheet of the wash circuit used for the preparation of the sample.

Natural mineral washing by the downstream wet gravity process and the final filtration step (primary belt filter) were simulated by decanting the excess water after the neutralisation step. Fresh water was added, which was decanted after mixing (simulating final pumping and filtration step of the wet gravity). Both washed and unwashed samples were dried in an oven at 140^{o}C for 1h30min. Performance curves of the washed and unwashed samples are shown in Figure 4.21.

All the data points, except the first point, of the washed samples were horizontally spaced further away from zero and vertically closer to zero. This was also observed for the artificially coated samples (refer to Paragraph 4.6.2.1 – *Artificially coated mineral particles*).

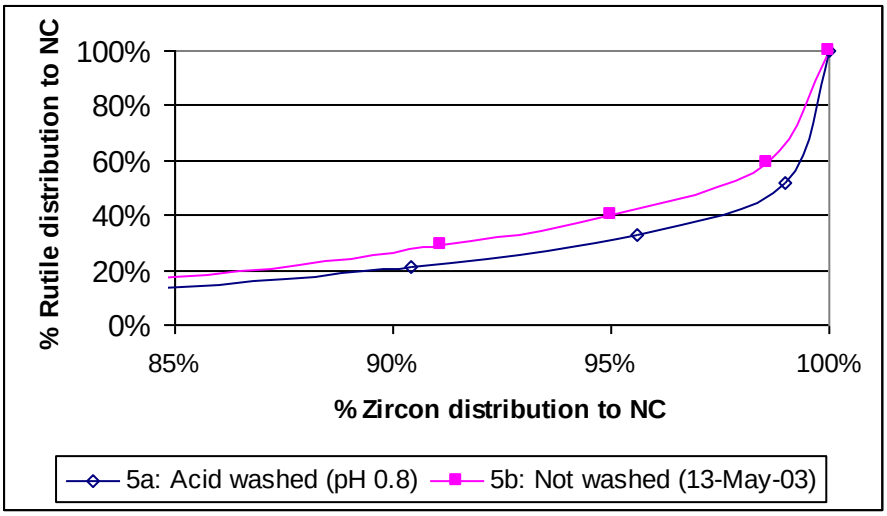

Figure 4.21: Laboratory electrostatic performance curves, comparing the separation performance of a sample collected directly before trial 5 and after one split, were repulped with acidic water (pH 0.8) before being vacuum filtered. Cake washing with acidic water (pH 2) and a wash ratio of 2.5 were applied followed by repulping with fresh water and decantation to remove excess water simulating a dewatering cyclone stage. Concentrated caustic was added after the final decantation step to increase the pH to 6.7. Both samples were dried in an oven at 140^{o}C prior to electrostatic separation.

(e) Acid wash (pH 1.3) of wet dry mill feed samples – filtration simulation

A wet dry mill feed sample was collected during a period of excellent dry mill electrostatic separation performance characterised by high output zircon product tons and low recycle loads. A split of the sample was washed by simulating the process flow circuit as described in the previous paragraph (d). The only differences were that the sample was repulped with acidic water at pH 1.32 prior to filtration, and the pH after neutralisation was slightly lower at 6.1. Both washed and unwashed samples were dried in an oven for 2 hours at 140^{o}C. It was encouraging to note from the performance curves that the washed sample outperformed the unwashed sample by far (see Figure 4.22). All the data points of the washed sample were vertically spaced closer to zero than the unwashed sample. Horizontally, the data points (except for the first point) were also spaced further away from zero. However, the horizontal spacing was not that much more significant than for the performance curves of Figure 4.21.

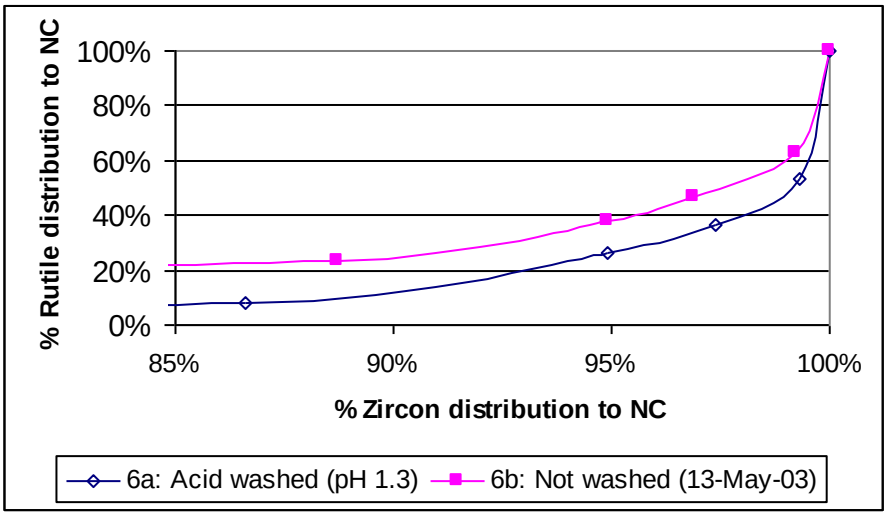

Figure 4.22: Laboratory electrostatic performance curves comparing the separation performance of a sample collected directly before trial 5, which was characterised by good dry mill performance. One split was repulped with acidic water (pH 0.1.3) before being vacuum filtered. Cake washing with acidic water (pH 2) and a wash ratio of 2.5 was applied followed by repulping with fresh water and decantation to remove excess water simulating a dewatering cyclone stage. Concentrated caustic was added after the final decantation step to increase the pH to 6.1. Both samples were dried in an oven at 140^{o}C prior to electrostatic separation.

(f) Separation efficiencies of test 2 to 5

Separation efficiencies were calculated as the average of the zircon distribution to non-conductors and rutile distribution to conductors. Rutile distribution to conductors was simply determined as 100 minus rutile distribution to non-conductors and therefore only assuming non-conductor and conductor split without middling fractions. The operating point was taken at 90% zircon distribution to non-conductors, which was the normal operating point of the plant scale coronastats in the 501 rougher duty. The results are summarised in Table 4.32.

Switching off the caustic (2b) resulted in a 1% improvement in separation efficiency. However, correspondent dry mill zircon recoveries increased from 3% to 9%. Raising the pH of a sample collected during the plant trial when the caustic was switched off had no impact on the separation efficiency. The filtration circuits caused separation efficiency differences of 3 and 7% for repulping with acidic water at pH 0.8 and 1.3, respectively. It is important to note that sample 6a was collected during a time of excellent dry mill electrostatic separation as a result of good feed. The reader is reminded that the relatively small efficiency improvements summarised in Table 4.32 were indeed repeatable, as discussed earlier in Paragraph 4.6.2.2 - *Actual plant samples: Laboratory electrostatic separation tests and process simulations of mineral wash circuits*. It is also important to remember

that these relatively small improvements in separability will accumulate over the multiple electrostatic stages of the dry mill circuit resulting in significant overall mineral recovery improvements.

Table 4.32: Summary of separation efficiencies of the individual performance curves of Figure 4.18 and Figures 4.20 to 4.22.

Performance curve	Process selection	At operating point			Efficiency improvement
		Zr distr	Rt distr	Efficiency	b-a
2a	N.A.	90%	28%	81.0%	-
2b	Plant trial: caustic off	90%	26%	82.0%	1%
3a	Plant trial: caustic off	90%	25%	82.5%	-
3b	Raise pH of sample to >6.5 by adding caustic	90%	25%	82.5%	0%
5a	N.A.	90%	28%	81.0%	-
5b	Filtration (pH 0.8)	90%	22%	84.0%	3%
6a	N.A.	90%	25%	82.5%	-
6b	Filtration (pH 2)	90%	11%	89.5%	7%

4.7. FILTRATION EXPERIMENTS

Laboratory filtration experiments were carried out to determine the optimum parameters that would ensure maximum iron removal. They were performed as one of the potential process solutions identified was a vacuum belt filter. The parameters evaluated were the slurry pH and density of the slurry fed to the filter, and the filter cake wash water. The results obtained from these tests were also found to be applicable (e.g. slurry pH) for the design of a counter-current-decantation circuit and were therefore included in this chapter. Slurry samples were collected from the underflow of the upflow classifiers of the HAL circuit. The results obtained from the filtration experiments are summarised in Tables 4.33, 4.34 and 4.35. The experiments were performed in three batches, namely 1a - 1c, 2a - 2d and 3a – 3f.

Table 4.33 summarises the properties of the feed, filter cake and filtrate prior to cake washing. Slurry densities (filter feed) of between 60 and 70 mass% were used, which are typical of the underflow of a dewatering cyclone. Concentrated sulphuric acid was added to reduce the pH of the slurry to between 0.6 and 1.9 (typical pH of underflow of upflow classifiers was about 2 at the time of sample

collection). The objective of lowering the pH was to determine the optimum pH required for dissolving the bulk of precipitated iron attached to the mineral surfaces and suspended in the slurry liquid.

Table 4.33: Summary of the properties of the feed of the individual laboratory filtration runs. All the experiments were conducted at the MSP applying a vacuum pressure of –30 kPa (meter pressure). The slurry samples were collected from the underflow of the upflow classifiers of the HAL circuit.

Run	Solids [%]	Acid added [ml]	Slurry pH	Filtrate 1 [ml]	Cake mass (wet) [g]	Cake moisture [%]
1a	76%	0	2	80	314.4	5.2%
1b	76%	0	2	85	376.1	7.2%
1c	65%	Not measured	1	124	259.0	4.7%
2a	68%	0.5	1.87	93	71.2	8.2%
2b	69%	1.5	1.60	95	56.2	5.7%
2c	69%	12.0	1.05	110	58.5	5.1%
2d	68%	80.0	0.68	175	51.6	5.8%
3a	65%	25	1.02	130	229	5.2%
3b	67%	18	1.02	110	217	4.6%
3c	63%	25	1.02	125	201	5.2%
3d	66%	90	0.67	182	212	5.9%
3e	63%	90	0.70	186	192	5.3%
3f	69%	105	0.74	193	231	4.4%

The results of the cake washing experiments are summarised in Table 4.34. Cake washing was applied to experiments 3b, 3c, 3e and 3f. A wash ratio (volume of wash liquid to volume of cake moisture) of approximately 3 was used. Acidic wash water at different pH levels, namely 0.5, 1.5 and 1.9, was used to determine the optimum pH for maximum iron removal.

Table 4.34: Summary of the cake washing results (vacuum pressure of –30 kPa meter pressure).

Run	Wash ratio [WL/CL]	Wash liquid [ml]	Wash liquid pH	Filtrate 2 [ml]	Filtr 1+ Filtr 2 [ml]
1a	NA	NA	NA	NA	80
1b	NA	NA	NA	NA	85
1c	NA	NA	NA	NA	124
2a	NA	NA	NA	NA	93
2b	NA	NA	NA	NA	95
2c	NA	NA	NA	NA	110
2d	NA	NA	NA	NA	175
3a	NA	NA	NA	NA	130
3b	3.2	30	1.9	33	143
3c	3.2	30	0.5	29	154
3d	NA	NA	NA	NA	182
3e	3.2	30	1.9	31	217
3f	3.8	30	1.5	26	219

Iron analyses of the filter cake are summarised in Table 4.35. The iron precipitation curves were used as guidelines for selecting the pH of both the slurry of filter feed and repulp of the filter cake. The filter cakes were repulped with acidic water at pH values of between 0.4 and 1.9 to dissolve and/or remove any iron retained in solution or precipitate form. This water (after repulping) was then analysed for iron and it was assumed that after repulping only negligible amounts of iron remained behind as mineral attachments. The filter cake of experiment 3f contained the lowest amount of retained iron.

Table 4.35: Summary of the amount of iron retained in the filter cake of the individual experiments.

Run	Cake mass [g]	Repulp water [ml]	Repulp pH	After mixing pH	Liq titrated [ml]	$Cr_2O_7^{2-}$ [ml]	Fe [g/dm^3]	Fe in cake [g]
1a	200	100	1.87	No reading	50	0.20	0.020	0.003
1b	200	100	0.86	No reading	50	0.55	0.055	0.010
1c	200	100	0.86	Not reading	50	1.30	0.031	0.004
2a	200	100	0.44	0.51	50	3.50	0.084	0.013
2b	200	100	0.44	0.62	50	4.70	0.112	0.016
2c	200	100	0.44	0.46	50	1.80	0.043	0.006
2d	200	100	0.44	0.41	50	1.40	0.033	0.005
3a	200	80	0.55	0.78	50	6.50	0.155	0.016
3b	200	80	0.55	0.74	49	5.70	0.139	0.014
3c	180	80	0.55	0.69	50	4.70	0.112	0.011
3d	180	80	0.55	0.82	50	5.60	0.134	0.015
3e	180	80	0.55	0.80	50	1.50	0.036	0.003
3f	180	80	0.55	0.71	50	0.80	0.019	0.002

Table 4.36 contains the iron analyses of the filtrate and total iron in the feed (sum of iron retained in the filter cake and the iron in the filtrate). The iron removal efficiencies of the individual experiments are also shown, which are plotted in Figure 4.24.

Table 4.36: Summary of the amount of iron in the filtrate and the iron removal efficiency determined for the individual experiments

Run	Liq titrated [ml]	$Cr_2O_7^{2-}$ [ml]	Fe [g/dm^3]	Fe in filtrate [g]	$Fe_{cake}+Fe_{filtrate}$ [g]	Fe removal efficiency [%]
1a	50	0.20	0.020	0.002	0.005	34.9%
1b	50	0.15	0.015	0.001	0.011	44.9%
1c	50	6.80	0.162	0.020	0.024	82.7%
2a	50	1.00	0.024	0.002	0.015	14.4%
2b	50	3.50	0.084	0.008	0.024	33.2%
2c	50	5.20	0.124	0.014	0.020	69.1%
2d	50	4.50	0.108	0.019	0.024	80.0%
3a	50	9.40	0.225	0.029	0.046	64.1%
3b	50	8.00	0.191	0.027	0.041	66.8%
3c	50	7.20	0.172	0.026	0.038	70.0%
3d	50	6.90	0.165	0.030	0.045	67.3%
3e	50	5.80	0.139	0.030	0.034	89.7%
3f	50	6.40	0.153	0.033	0.036	93.8%

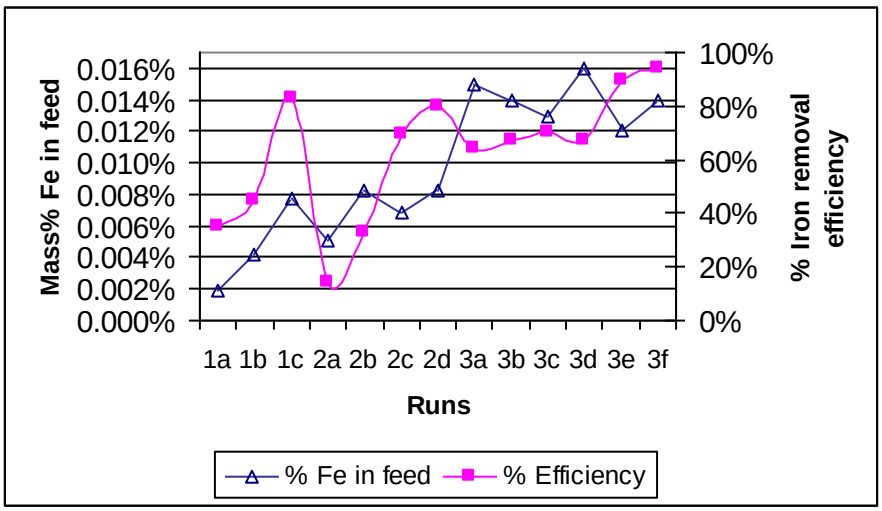

Figure 4.23: Iron removal efficiencies compared to the amount of iron in the slurry feed expressed as %.

The graphs of Figure 4.23 was used to identify the optimum conditions that would ensure maximum iron removal during filtration, and also for the design of a counter current decantation circuit (CCD). The most important function of this graph was to assist with the determination of the optimum pH

required for dissolution of precipitated iron attached to the mineral surfaces and also to understand the physical nature of the attached iron.

It was clear from the graph of the % iron in the feed that the experiments could be divided in two distinct groups, namely group A (experiments 1a-c and 2a-d) characterised by relatively low amounts of iron in the feed, and group B (experiments 3a – f) characterised by relatively high amounts of iron in the feed. It is important to remember that the feed material was collected at the same time and therefore the individual samples should contain equal amounts of iron. It was also interesting to observe the fluctuating iron removal efficiencies of group A compared to more stable efficiencies of group B. All the efficiencies of group B were above 64%, with the highest for experiments 3e and 3f at 89.7% and 93.8%, respectively. No cake washing was applied in the experiments for group A. The experiments for group B were more repeatable and the results seem to more trustworthy than those of group A. The experiments of group B will now be discussed in more detail.

The pH of the feed slurry of experiments 3a-c and 3d-f were 1.02 and approximately 0.7, respectively. The final filter cakes of all the experiments were repulped with acidic water at pH 0.55 to determine the amount of iron retained and the iron removal efficiency of the experiment. No cake washing was applied in experiments 3a and 3d, and the filter cakes of experiments 3b and 3e were washed with acidic water at pH 1.9. The filter cake of experiment 3c was washed with acidic water at pH 0.5, which did not improve the iron removal efficiency compared to the experiments where wash water at a higher pH was used. Experiment 3f, with the highest iron removal efficiency, was washed with wash water at a slightly lower pH of 1.5. Therefore, the highest iron removal efficiency was achieved with the feed slurry at a pH of 0.7 and applying cake washing (wash ratio of 3.8) with the pH of the wash liquid at 1.5. Relatively large volumes of sulphuric acid would be required to reduce the pH to 0.7 and both the capital and maintenance cost of a potential process solution operating at these low pH values would be expensive. It is important to recall that the highest separation efficiency was achieved when a dry mill feed sample was repulped at pH 1.3-1.5, filtered and the filter cake washed with acidic water at pH 2. Therefore, it appeared to be economically wise to implement a process solution at slightly higher operating pH values.

CHAPTER 5

DISCUSSION OF RESULTS

Objectives of Chapter 5:

- Discuss the main results obtained during the experimental testwork.
- Highlight the significant findings of this study.
- Compare results with those available in literature.
- Briefly discuss the results of a process solution implemented as a result of this study.

This chapter provides sound scientific explanations extracted from the experimental results presented in Chapter 4 – *Experimental results* for the impact of the HAL circuit on production of zircon and rutile and their final product grades. An overview of the chemistry of the HAL circuit is provided and the major species of concern are highlighted. A scientific explanation for the precipitation and re-attachment of iron to the surfaces of zircon and rutile mineral particles is derived, and the impact of this re-attached iron on electrostatic separation is discussed. Finally a process solution, which has been implemented as a direct result of this study, is briefly discussed.

Literature has provided abundant information on the chemistry and formation of iron precipitates. The chemistry of the HAL process water was unique in the sense that it contained a range of chemical species at different concentrations, which resulted in different experimental iron precipitation curves. Very little information was found in literature on the impact of surface contaminants on electrostatic separation mainly due to the secrecy of the mineral sand industry. Collins and Farmer (2003) showed that the electrostatic separation of zircon and rutile mineral particles could be improved by applying ultrasonic attritioning to remove the natural iron rich coatings (hematite). Removal of iron rich coatings to enhance electrostatic separation was known and was the main function of the HAL reactors and attritioners. Namakwa Sands, and seemingly other mineral sand operations, was oblivious to the formation of iron hydr(oxides) in the HAL circuit and their attachment to mineral particles to alter the electrostatic properties of the particles. This significantly affected electrostatic separation in the dry mill circuit. It was a surprise not to find any literature on this topic.

5.1 HAL CHEMISTRY

Chemical analyses of the HAL process water revealed that the abundant dissolved species, in sequence of decreasing magnitude, were SO_4, Fe, Al, Ca, Mg and Ti (Table 4.3). All of the species, except SO_4, were constituents of the natural surface coatings of the mineral particles. Sulphate was introduced in the process with sulphuric acid. Titanium was believed to originate predominantly from the titanium rich rutile and titanium mineral particles present in the natural mineral coatings. Almost negligibly low concentrations of these species were present in the fresh water fed via the canal system from the Clanwilliam dam. Other species, in sequence of decreasing magnitude, were present in smaller to trace amounts. These species were Cl, Cr, Mn, Th, Ni, Zr, U, Cd, Ar and Hg. The water contained radio-active U and Th species originating from the mineral monazite, which dissolves in sulphuric acid.

Iron was the most significant specie, not only due to its abundance, but also due to its complex forming characteristics. It was present in both the ferrous form and also predominantly in the ferric oxide form. The iron (III)/iron (II) ratio varied and the iron (III) concentration varied from anywhere between 50% and almost 100% of the total iron concentration. This was an important finding because analyses conducted in 1994 and during the start of the study showed that ferric oxide is by far the abundant species and that only trace amounts of ferrous oxide were present in the mineral coating. It could be concluded that the iron (III)/iron (II) ratio was a function of the ore body and certain parts in the ore body had higher concentrations of ferric oxide. The total iron concentration varied as well and also seemed to change within the ore body. It was also a function of the efficiency of attritioning at the mine, which was the first attempt to reduce the volume of the coating to minimise the acid usage of the HAL reactors. Factors such as attritioner downtime resulted in an increase in the total iron concentration.

Further analyses were focussed on the underflow of the upflow classifiers (Table 4.2) due to the reaction of these species with sodium hydroxide, which were introduced at the attritioning stage that followed the upflow classifiers. Comparing the analyses with that of the effluent, it is clear that the concentrations of iron, aluminium, magnesium and potentially titanium were significantly reduced by the cyclone and upflow classifier process stages. Species present in low concentrations, as identified in the effluent water, were not included in the analyses. The abundant dissolved species (> 100 mg/litre), in sequence of decreasing magnitude, were SO_4, Ca, Na and total Fe. The sulphate concentration was high due to the addition of a few drops of concentrated sulphuric acid (98%) to adjust the pH from 2 to 0.7. This pH adjustment was implemented to ensure that precipitated species suspended in the process water were dissolved prior to filtration. The concentration of sodium was

relatively high due to the addition of caustic in the attritioners, which were partially fed back to the upflow classifiers via process stages.

Hayes (1993) showed that ferrous ion started to precipitate at higher pH values than ferric ion and that the slope of iron concentration versus pH was also different. Therefore solutions containing different iron (III)/iron (II) ratios will have different precipitation graphs with different slopes. It was important to find that the iron precipitation versus pH plots and the slopes of the logarithm of the iron concentrations versus pH were almost identical for all the different samples taken in the HAL circuit (Figure 4.8). This proved that iron (II) oxidation to form Fe (III) was almost negligible in the HAL circuit (taking into account that these samples were collected in the same period and thus a constant iron (III)/iron (II) ratio). This was confirmed by Cigan et al. (1980) who showed that ferrous ion would be oxidised very slowly to ferric ion in an acidic medium.

5.2 PRECIPITATION OF COMPLEXES IN THE HAL CIRCUIT

This study was mainly focussed on ferric hydr(oxide) due to the relatively low pH required for its formation and its significant impact on the separation process, which will be discussed thoroughly in the coming sections. Preventing the formation of iron hydr(oxide) would therefore prevent the formation of most of the other precipitate species due to the fact that they start precipitating at higher pH values compared to the relatively low pH required for iron (III) precipitation.

Raising the pH from 2 to 5 (by the addition of caustic soda) of the slurry being fed to the attritioners in the HAL circuit resulted in the precipitation of sulphates, iron (III) and aluminium (in sequence of decreasing volumes). Of the original sulphate, iron (III) and aluminium concentrations, a total of 45.2%, 99.5% and 99.8% precipitated, respectively. Iron and aluminium precipitated as hydroxides and sulphates, and other anions formed complexes with iron hydroxide. This was confirmed by Cigan et al. (1980) who explained that when a solution containing predominantly iron (III)-sulphate species is heated or neutralised, the sulphato complexes themselves undergo hydrolysis to form mixed sulphato-hydroxyl iron (III) species. Small amounts of sulphates precipitated as $CaSO_4$. Iron (III) hydroxide particles (which were sometimes visible in the wet gravity process water, belt filter and floor areas (see Figure 4.10), and gypsum crystal growth on the wet gravity process equipment) provided visual confirmation for the precipitation of calcium and iron. More than 99% of the Fe (III) precipitated at a pH of 4. Trace elements also precipitated at these elevated pH levels.

5.3 PHYSICAL CONDITIONS RESULTING IN THE PRECIPITATION OF IRON

The parameters, which were affecting the precipitation of iron were pH, iron concentration, iron (III)/iron (II) ratio, the temperature of the solution, residence time of the dissolved iron in the solution and loss in efficiency of the HAL process equipment.

Iron (III) started to precipitate at a pH of 1 - 1.2 in the quench sumps (<0.095 mol/dm^3 total dissolved Fe with about 50% ferric oxide) and overflow of the upflow classifiers (<0.023 mol/dm^3 total dissolved Fe with about 50% ferric oxide), and at a pH of 1.5 - 1.8 in the underflow of the upflow classifiers (<$4.12x10^{-3}$ mol/dm^3 total dissolved Fe with about 50-100% ferric oxide). These different pH values, where iron started to precipitate, were directly the result of the iron (III) concentration, which decreased while moving downstream through the HAL circuit. The iron (III)/iron (II) ratio was important since a higher ratio would result in more iron (III) precipitating.

It was important to find that the experimental results contradicted the work of Dutrizac and Monhemius (1986), which investigated the precipitation of iron in 0.5M $Fe_2(SO4)_3$ solutions. They concluded that iron (III) started to precipitate at a pH of between 2 and 3. This difference could probably be ascribed to the presence of a range of other chemical species present in the process water of the HAL circuit, where litterature used more pure solutions. The experimental results of this study compared well with the theoretical precipitation curve constructed by Hayes, 1993 (refer to Figure 2.3), which also showed a linear relationship between the logarithm of the iron concentration and the pH of the solution, and that iron precipitation commenced at similar pH values. Hayes showed that Fe (II) would theoretically start to precipitate at pH 6. It was interesting to note a very gradual and almost negligible change in gradient at pH 8 (see overflow and underflow precipitation curves of Figure 4.8). Thus, it appeared that the precipitation of iron (II) started to increase at pH > 8. This was confirmed by Welham et al. (2000) and Cigan et al. (1980) who showed that ferrous ion would precipitate at pH 7–8 at a Fe (II) concentration of 0.0226 – $4.12x10^{-3}$ mol/dm^3 (Figure 2.5).

Small amounts of iron (III) would also precipitate as iron sulphates and jarosites in the reactors, which were fed at a mineral temperature of 150^oC. However, it could also be possible that the iron in the HAL circuit actually precipitated as jarosite and iron sulphates at the low pH values of less than 3, as indicated by Figure 2.1 (Dutrizac and Monhemius, 1986), and not as $Fe(OH)_3$. Iron hydroxide would predominantly form at the attritioners where caustic was added to increase the pH to 5.

From the iron concentrations, temperature and pH profile of the HAL circuit, as well as individual studies of Dutrizac and Monhemius (1986), Cigan et al. (1980), Hayes (1993) and Welham et al. (2000), it could be concluded that the iron precipitates were predominantly iron hydroxides, which would partially be converted to goethite in the dryers of the dry mill circuit (temperature of minerals are increased to 65 – 74^{o}C). Negligible amounts of iron (III) would also precipitate as iron sulphates and jarosites in the HAL reactors. Small amounts of goethite could also be expected in the process water of the wet gravity circuit mainly due to the long recycling time of the process water. The experimental results of this paragraph resulted in the following two important temporary and permanent process changes:

(1) Plant trials: Plant trials were conducted by temporarily switching off of the caustic, which resulted in the pH being reduced from 7 to 2. This reduced the volume of precipitate that formed and the downstream impact of this could be evaluated. The impact was significant (will be discussed later) and resulted in a process change to be implemented.
(2) pH set-point adjustment: The pH set-point was consequently reduced from 7 to 5 thereby reducing the amount of precipitates formed. The impact of this was almost negligible mainly due to the fact that Fe (III) precipitation would only be reduced at pH less than 4. However, this change reduced the precipitation of other species, and reduced the caustic usage, and was therefore sustained.

5.4 PHYSICAL PROPERTIES OF NATURAL MINERAL SURFACE COATING COMPARED TO IRON HYDROXIDE PRECIPITATE FORMED IN THE HAL

The mineral particles mined at Namakwa Sands are coated with a natural surface coating rich in iron (hematite), aluminium, calcium and magnesium. This coating is hard and can only be effectively removed by a combination of a chemical hot acid leaching (HAL) and attritioning. Ineffective removal of this coating would result in residual iron on mineral particles, resulting in the final zircon product not meeting the required specifications determined by the customers. The coating is both magnetic and conductive, resulting in non-magnetic and non-conductive particles (e.g. zircon) behaving magnetically and conductively. Therefore, ineffective removal of this coating will result in a loss in production of zircon in the magnetic and electrostatic circuits of Namakwa Sands.

Iron hydroxide precipitates formed in the HAL neutralisation stage have different physical properties to the iron present in the natural mineral coatings prior to leaching. Iron hydroxide is also conductive, but it is non-magnetic. It only becomes magnetic when heated at temperatures above 800-1000^{o}C (Weiser, 1939), which was not the case at Namakwa Sands. This precipitate adsorbs anions, such as

sulphates and chlorides, in the acidic mediums of the HAL and wet gravity process water. Kosmulski et al. (2003) confirmed that iron hydr(oxides) contribute substantially to the adsorption of toxic elements even when the mass fraction of iron hydr(oxides) is relatively low. They also confirmed that the affinity of iron hydr(oxides) to anions and cations is pH dependent. It has a positive zeta potential below a pH of 7.99 causing it to adsorb to surfaces with an opposite zeta potential. Weiser (1939) revealed that iron hydroxide is hydrophilic, which was confirmed by one of the first iron precipitation experiments where the precipitate was left open on a scale exposed to the atmosphere. The mass increased rapidly and continuously due to an increase in atmospheric moisture absorbed.

Experimental testwork showed that iron hydroxide precipitates formed large colloidal particles suspended in the solution precipitates, which were relatively stable. It also formed more rapidly than the rate at which it dissolved when acid was added. The pH had to be reduced lower than the original values where the iron originally started to precipitate (refer to Table 4.5 and 4.6). Therefore, dissolution of iron precipitates was less effective compared to its formation. This tremendous surface development and very low solubility was confirmed by Weiser (1939).

5.5 ADSORPTION MECHANISM OF PRECIPITATES

During the early phases of the study, it was questioned whether precipitates formed in the HAL circuit adsorbed to the mineral surfaces, and if they remained attached through the many pumping, spiral and cyclone stages of the wet gravity circuit to be eventually fed to the dry mill circuit. The answer to this question was determined by artificially coating mineral particles in the laboratory with precipitate prepared from a sample of the overflow of the HAL upflow classifier and from a precipitate and slime mixture obtained from the top layer of the secondary concentrate belt filter. The coated samples were passed over a laboratory electrostatic separator and the separation behaviour of the individual minerals was compared with uncoated samples (see Figure 4.16 and 4.17). Zircon and rutile minerals of the two samples reacted similarly. This could only be true if the nature, and thus chemical composition, of the coatings was the same, which implies that the precipitate adsorbed to mineral particles in the HAL circuit and that it remained attached. This was confirmed by chemically cleaning mineral particles from a number of dry mill feed samples with acidic water to remove any precipitates which were potentially attached (chemical desorption). Electrostatic separation performances of unclean versus clean samples (see Figures 4.21 and 4.22) were compared and, surprisingly, the unclean zircon and rutile particles behaved exactly the same as those artificially coated, which could only be true if the coatings and their chemical compositions were the same as the artificial ones. This confirmed that

precipitates formed in the HAL circuit did attach to mineral particles and remains attached to mineral particles in spite of the many shear forces.

XRF analyses of a normal and artificially coated zircon product samples showed a 22.0%, 18.0% and 14.5% increase in the concentrations of Fe_2O_3, Al_2O_3 and TiO_2, respectively (Table 4.21). These species were also found on the surfaces of on-specification and off-specification zircon product samples collected from the dry mill circuit during normal operation (Table 4.22), which proved the presence of precipitate species on mineral surfaces and revealed their impact on the grade of the final zircon and rutile products.

The acidic wash water analysed after rinsing of the primary concentrate contained relatively high concentrations of sulphate, calcium, chloride, sodium, potassium, iron, aluminium and magnesium (Table 4.2), which further confirmed the occurrence of adsorption of species.

$Fe(OH)_3$ obtains a positive charge in acidic mediums and will adsorb negatively charged ions, such as sulphate and chloride, which would explain its association with iron, and therefore also partially explains its presence on the mineral surfaces. However, its abundance, and the presence of the other species (anions), required further investigation.

The adsorption of species to the surfaces of zircon and rutile mineral particles could be explained in terms of their zeta potentials. Both zircon and rutile have negative zeta potentials over the full pH range. Iron (III) hydr(oxides) have positive zeta potentials below pH 7.99 (refer to Paragraph 4.5.1 – *Zeta potential of zircon and rutile mineral particles*). Therefore, $Fe(OH)_3$ will adsorb to the mineral surfaces at pH below 7. It is important to remember that the pH of the process water in the HAL (after caustic addition) and wet gravity circuits, was typically between 4.5 and 5, which would result in the mineral particles adsorbing to iron hydroxides and other species due to opposite charges. This adsorption mechanism was confirmed to be accurate by a study conducted by Bandini et al. (2001) that showed that Fe_2O_3 (hematite) adsorbed to the surfaces of quartz and galena (PbS) particles due to opposite zeta potentials (see Figure 2.7). They confirmed an increased rate of adsorption as the pH was reduced from 10 to 4 due to a consequent increase in the zeta potential of hematite.

Precipitates will attach more readily to zircon than rutile due to its lower zeta potential and its surface will therefore contain higher concentrations of adsorbed species. Although not investigated, other

chemical species with an opposite surface charge will also adsorb to the mineral surfaces. XRF analyses of zircon product samples, after rinsing the samples with acidic water (pH 1.3), showed significant reductions in the concentrations of Fe_2O_3 (15-22 mass%). Concentrations of Al_2O_3 were less significantly reduced up to 8% and TiO_2 concentrations were also slightly reduced in some instances (refer to Table 4.20, 4.21 and 4.22). Rinsing of rutile product samples with acidic water also reduced the Fe_2O_3 concentrations (5-10 mass%), but less significantly than for zircon particles. The increase in Al_2O_3 increased was unexpected and the reason could not be established (refer to Table 4.23). These, together with other repeated results, confirmed that zircon particles were more selective than rutile particles and would therefore adsorb species more abundantly than rutile.

5.6 ADSORPTION OF IRON PRECIPITATES FED TO THE WET GRAVITY CIRCUIT

Iron analyses of the wet gravity process water showed an increase in the concentration of iron over time (Table 4.18) due to the recycling of water in the wet gravity circuit in order to minimise the consumption of fresh water. Iron was fed to the wet gravity circuit from the HAL circuit via a cyclone that discharged into the primary hydrosizer, which was the first gravity separation stage of the wet gravity circuit (Figure 4.12). This cyclone dewatered slurry of the repulping stage, located directly after the attritioners, where the pH was raised. It consequently contained relatively small amounts of iron (III) hydroxide and dissolved ferrous ion. These precipitates act as nucleus, which not only adsorb other species but are adsorbed to the surfaces of mineral particles, as discussed previously. It is important to emphasise the ratio of fresh versus HAL process water. Approximately 28 m^3/hr of process water from the HAL circuit (after neutralisation) entered the wet gravity circuit and contained 2.9 kg/hr of iron at the time of the balance (see Table 4.13). The wet gravity circuit consumed 50 m^3/hr fresh water. Thus the HAL process water comprised a significant 56% of the amount of fresh water used. Therefore, it would be expected that iron precipitates and other species would accumulate at a fast rate. Iron concentrations reached critical levels within 4 days after start-up with fresh water.

Iron balances in the wet gravity circuit showed that approximately 25% of the iron present in the feed to the primary and fine spirals of the wet gravity circuit attached to the mineral particles of the primary concentrate, which was the main stream to the dry mill circuit (Table 4.15 and 4.17). The consequence of this was an increase in mineral surface attachments as iron hydroxide (and other precipitates) were accumulating in the process water of the wet gravity circuit, resulting in a gradual decrease in dry mill zircon and rutile recoveries over time. Visual observations of the dry mill electrostatic performance and actual production rates indicated that poor electrostatic separation occurred when the iron build-up reached a critical value of higher than 0.07 g/dm^3. Good electrostatic

separation occurred at iron concentrations below 0.05 g/dm^3 (see Figure 4.14). It was found that these limits were repeatable at Fe (III)/Fe (II) ratios of approximately 2:1. The critical value decreased to 0.05 g/dm^3 if Fe (III) was predominantly present in the HAL process water. This was due to an increase in the formation of iron (III) hydroxide and a consequent decrease in dissolved Fe (II). The colour of the wet gravity water became yellowish/brownish as the iron concentration reached high to critical limits. The accumulation of the iron in the wet gravity circuit was a function of the operational instability of the HAL circuit, loss in efficiency of the upflow classifiers, increase in the Fe (III)/Fe (II) ratio, increase in the concentration of iron in the HAL circuit (due to an increase in hematite in the natural surface coating as a function of the ore body), and increase in the water recycling periods due to extended running periods of the wet gravity circuit.

A temporary pause in the addition of caustic to the attritioners resulted in a decrease in the amount of iron in the primary spiral feed and primary concentrate. The sum of the iron in the feed to the primary and fine spirals remained relatively constant. Therefore, it could be concluded that the dissolved iron was diluted in the process water of the wet gravity circuit, which would still result in precipitation and attachment to mineral surfaces. However, the amount of iron attachment was significantly less, but not completely eliminated (Table 4.16). This was only a temporary solution to reduce the amount of iron precipitates and the trials could not be extended due to the corrosive effect of the low pH.

5.7 IMPACT OF ATTACHED PRECIPITATES ON ELECTROSTATIC SEPARATION AND GRADE OF FINAL ZIRCON AND RUTILE PRODUCTS

HAL precipitates affected the separation performance of both zircon and rutile mineral particles. Electrostatic separation tests showed that contaminated zircon particles behaved conductively, and contaminated rutile particles behaved slightly less conductively than clean particles in an electrostatic separator (Figure 4.16, 4.17, 4.18, 4.22 and 4.23). The net effect was the accumulation of predominantly zircon, and to a lesser extent rutile particles, in the middling fraction of an electrostatic separator (e.g. HTR and Coronastat). This resulted in an increase in the recycling loads in the electrostatic dry mill circuit and a consequent loss in production of mainly zircon product. These increased recycling loads resulted in an increase in spillage generated due to the formation of bottlenecks. It is important to emphasise that precipitates attached to mineral surfaces affected the electrostatic separation performance of all of the electrostatic machines in the dry mill circuit. Therefore, an almost negligible deterioration in electrostatic separation performance, accumulated over the many stages of the dry mill circuit, resulted in a significant decrease in the recovery of mainly zircon and secondly of rutile product.

A further very important discovery was made when analysing the surface chemistry of mineral particles of one of the main dry mill recycle streams (*HAL recycle*), which increased in volume during periods of poor electrostatic dry mill separation. This stream contained more than 94% zircon particles and was found to be a very important and true visual indicator of the surface condition of mineral particles within the dry mill zircon circuit. Its main function was to remove conductive zircon and small amounts of rutile minerals from the final zircon product stream. It recycled the minerals back to the HAL reactors. Analyses of the surface revealed that iron and aluminium precipitates were most abundantly distributed to the minerals of the HAL recycle. A total of 24.7 mass% adsorbed iron present in the dry mill feed was distributed to the HAL recycle, which explained the conductive behaviour of this stream. It was also interesting to note that aluminium distribution to the HAL recycle was the second highest at 17.2% (refer to Table 4.24). This could explain the conductive behaviour of coated zircon (due to the iron component) and non-conductive behaviour of coated rutile particles (due to the aluminium component). Reducing the amount of precipitates formed in the HAL circuit (e.g. stopping of caustic addition) reduced the volume of this stream by more than 10% (see Table 4.26). The process solution implemented at the end of this study reduced the volume by more than 20% (see Paragraph 5.9 –*Implementation of a process solution*).

Iron hydroxide precipitates attached to the mineral surfaces are hydrophilic and adsorbed atmospheric moisture, which caused the contaminated mineral particles to be more sensitive to weather changes. This caused severe circuit instabilities and a consequent loss in production of both zircon and rutile particles. This was magnified especially during weather transition periods when there was a sudden change in the dew point or relative humidity. Howe and Poe (1970) and Prinsloo (1998) discussed the effect of humidity adsorption from the atmosphere to the mineral particle surfaces, which they confirm had a negative impact on electrostatic separation.

Plant trials that were performed by temporarily switching off the caustic, reduced the amount of precipitates formed. The impact on electrostatic separation in the dry mill circuit was significant and a 3 to 7% improvement in prime zircon recovery was achieved. An improvement in rutile recovery was also notable, but the impact was less significant mainly due to the remaining difficulty in separating rutile and leucoxene effectively. It was also important to observe that the effect of weather conditions were less significant than during normal operation when the caustic was switched on. Recycling loads in the dry mill circuit decreased significantly by 10 - 30%.

Precipitates formed in the HAL circuit mainly increased the Fe_2O_3 (+15 to 22%), and to a smaller degree the Al_2O_3 (+4 to 8%), and in some cases the TiO_2 (+2%) concentrations of the final zircon product as well. Rutile product grades were less sensitive to precipitates, which caused an increase in mainly the Fe_2O_3 concentration (+5 to 9%).

It was disappointing to find that literature did not provide any significant scientific evidence of the impact of adsorbed iron hydroxides and other precipitates on the electrostatic separation process. Collins and Farmer (2003) removed natural mineral surface coatings, predominantly hematite, with ultrasonic attritioning, which improved electrostatic separation. However, this was known by Namakwa Sands hence the function of the HAL circuit to remove these natural coatings as described by Collins and Farmer. It is also important to emphasise that the physical properties of hematite, present in the natural mineral surface coating of heavy minerals in their natural environment, are different to those of iron hydr(oxide) and other precipitates formed in the HAL neutralisation stage. Dance and Morrison (1991) confirmed that changes in the surface conditions could produce highly variable mineral conductivity and thus electrostatic separation. These changes include absorbed physical or chemical coatings. This was the first encouraging clue from literature, but unfortunately the author did not specify the chemical species nor quantify their impact on electrostatic separation, consequently producing zircon and rutile minerals.

It could be concluded that the experiments discussed in this chapter have added significant value to the understanding of the impact of iron hydroxide (and other chemical species) on the production of zircon and rutile in the mineral sand industry. They have not only emphasised, but it also quantified, the importance of clean mineral surfaces. It was important to realise that the concentration of dissolved and consequently precipitate species at the attritioners was not only relatively low, but it also had a significant impact on the production of mainly zircon product.

5.8 FILTRATION EXPERIMENTS

Experimental results of the filtration experiments were important since they established the following:

- Chemical cleaning of dry mill feed samples by means of acid wash and solid-liquid separation would improve the electrostatic separation efficiency by 3-7% if washed with acidic water at optimum conditions.

It is important to emphasise that only a 1% improvement in separation efficiency was achieved when the caustic was temporarily switched off (see Table 4.32). However, this 1% improvement in separation efficiency accumulated over the many electrostatic stages of the dry mill circuit, which resulted in a 1-4% improvement in recovery of prime zircon. Therefore, a 3-7% improvement in separation efficiency (as a result of effective mineral washing) would result in far more than 1-4% improvement in recovery of prime zircon (zircon recovery improvements of more than 10% were also recorded – see Table 4.26). It is also important to highlight that the 7% separation efficiency was achieved by means of a dry mill feed sample collected during a period of relatively low concentrations of iron in the process water of the wet gravity circuit and during excellent dry mill performance in terms of zircon recovery. Higher improvements could therefore be expected if a sample was cleaned when higher concentrations of iron were present in the process water, which was normally the case.

- The economical conditions used to achieve optimum mineral washing, and consequently maximum improvement in separation efficiency, was to reduce the pH of the slurry to 1.3, effective solid-liquid separation, and applying cake washing with acidic water at pH 1.5.

  Iterative simulations were consequently set-up and used to determine the optimum process solution, which would maximise the removal of iron and consequently ensure optimum mineral recoveries. It was found that a counter-current-decantation circuit would achieve equivalent to even higher iron removal efficiencies. This circuit will be discussed later in this section.

- Implementation of a process solution that would maximise the removal of dissolved iron, thereby significantly improving the electrostatic separation efficiency in the dry mill circuit and consequently the recovery of mainly prime zircon and to a lower extend rutile product.

5.9 IMPLEMENTATION OF A PROCESS SOLUTION

The objective of the process solution was to separate the mineral particles from the process water (rich in dissolved iron and other species) at a low pH to minimise the formation of precipitates. A counter current decantation circuit (CCD) was selected due to its low water requirement, relatively low capital cost compared to that of filtration circuits, and excellent slimes removal efficiency. Woollacott and Eric (1994) confirmed that a very high removal efficiency of contaminants could be achieved with

such a circuit if the optimum number of stages is selected. The number of stages and optimum placement of equipment within the CCD were determined with iterative simulations, as mentioned previously. The selected CCD circuit consisted of a hydrosizer (classifier), three dewatering cyclone stages, a solid trap, four pumps, and a mixer for final neutralisation with caustic soda after the dissolved iron was removed (see Figures 5.1 and 5.2). A hydrosizer was selected due to its excellent ability to remove slimes (< 45 µm particles), high removal efficiency of iron and other dissolved species, as well as its robustness. The existing HAL wash circuit was incorporated in the iterative simulations of the new circuit.

It was experimentally determined, by means of the iron precipitation and filtration experiments, that the *economical* pH required to ensure that the iron remains in solution was 1.3 – 1.5 for relatively high iron concentrations (quench sumps and overflow of upflow classifiers), pH 2-2.5 for relatively low iron concentrations (underflow of upflow the classifiers), and pH 3-3.5 for very low iron concentrations (hydrosizer of CCD circuit). It is important to emhasise that the *economica*l pH is slightly higher than the *optimum* pH. At the optimum pH the formation of iron hydroxide is totally prevented, but it is not economically prefered due to the requirement of acid to reduce the pH. Running at a slightly higher pH would not require sulphuric acid to adjust the pH. Negligible small amounts of iron would precipitate at this pH, which was experimentally confirmed to have a negligible impact on the electrostatic separation process.

The IRR of the project, at a capital estimate of R5m (2003 money terms), was 49% and its net present values (NPV) at discount rates of 0% and 15% were R34.986m and R9.195m, respectively. The project was justified on the basis of a 1% improvement in prime zircon, 0.4% decrease in zirkwa and zero improvement in rutile recovery. Rutile recovery was assumed to remain constant due to the remaining inefficient separation of rutile and leucoxene. Leucoxene was the main contaminant of the rutile product and it could only be removed by exploiting the density differences of rutile and leucoxene minerals. Secondary zircon (zirkwa) recovery would be reduced by 0.4% due to a shift in zircon particles to prime zircon. The caustic usage was expected to decrease by a minimum of 50%. The inputs and results of the financial model is summarised in Table 5.1.

Table 5.1: Inputs of the financial model used to economically justify the mineral wash project

Input	Value
Capital cost (R)	5 000 000
Capital cost depreciation	40% (1st year) and 20% (2nd, 3rd and 4th year)
Operational cost (R/month)	20 000
Increase in mineral product recoveries	Prime zircon (+1.0%), zirkwa (-0.4%), rutile (0%)
Company tax rate	30%
Product selling prices	390 USD/ton (prime zircon), 290 USD/ton (zirkwa)
Rand/dollar exchange rate	7:1
Spoornet transport cost (R/ton)	72.73
Zircon distribution cost (material handling) (R/ton)	162.85
Zirkwa distribution cost (material handling) (R/ton)	243.94
IRR	49%
Payback period(months)	24
NPV	R34.986m (0% discount rate), R9.195m (15% discount rate)

The new circuit was commissioned in September 2004 and the results exceeded all expectations. The most encouraging results were an iron removal efficiency of more than 99.97% (design efficiency was 99.98%), a significant 3-7% improvement in prime zircon recovery (zirkwa recovery remained constant), 90% reduction in caustic usage and a reduction in dry mill dust levels to significantly below the OEL (Occupational Exposure Limit). The fresh water usage and the volume of effluent water discharged remained unchanged. Dry mill plant data indicated that the rutile recovery also improved. However, the exact recovery improvements were difficult to quantify.

Sulphuric acid usage could be reduced by 5-10% due to preventing the formation and adsorption of iron hydroxide that caused iron excursions of the final zircon product. This acid reduction would further reduce the cost of further effluent neutralisation due to a reduction in the acid concentration of the effluent stream. Therefore, the economics of this project was very encouraging and the financial parameters used to justify the project were exceeded.

It was important to compare the iron removal efficiency obtained by the simulation (99.98%) with the theoretical efficiency of 99.99% calculated by the equation derived by Woollacott and Eric (1994). The equation was specifically derived for counter current circuits and assumed a constant solid/water (R) ratio for the underflow and overflow streams of the individual dewatering equipment. It also assumed a constant feed density to all of these separators. All of these parameters could be changed

in the simulation and different efficiencies for different dewatering equipment could also be used. The parameters used to derive this number were 6 washing stages (including 2 from the HAL circuit), 40 mass% mineral sand in the individual feed streams of the dewatering equipment, 80 mass% solids in the underflow streams of the dewatering equipment and without any solid particles in their overflow streams. Comparing the actual iron removal efficiency of 99.97% with the calculated (99.99%) and simulated (99.98%) ones, it was clear that the simulation was slightly more accurate than the derived equation. However, the equation proved to be valid and could be used for the selection of the correct number of stages. The simulation was more complex to set-up, but it provided valuable information, such as stream densities and volumetric flows, which could not be calculated by the equation. This information was directly used for the sizing of equipment, pumps and pipes.

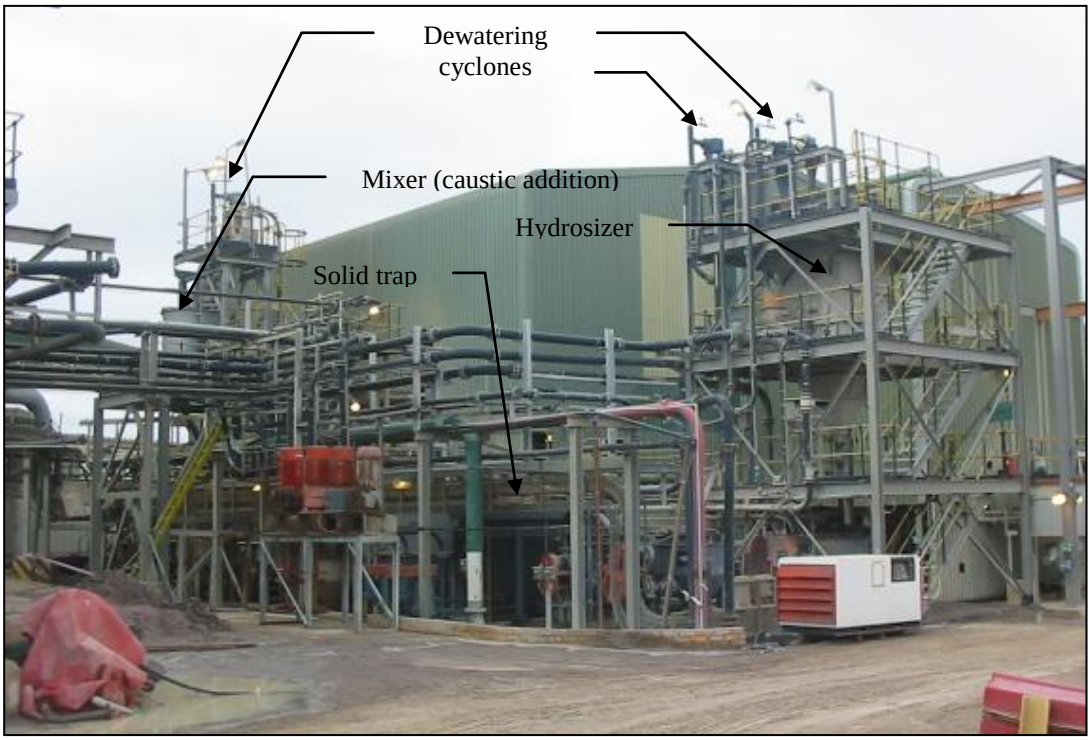

Figure 5.1: The newly constructed mineral wash circuit at the MSP

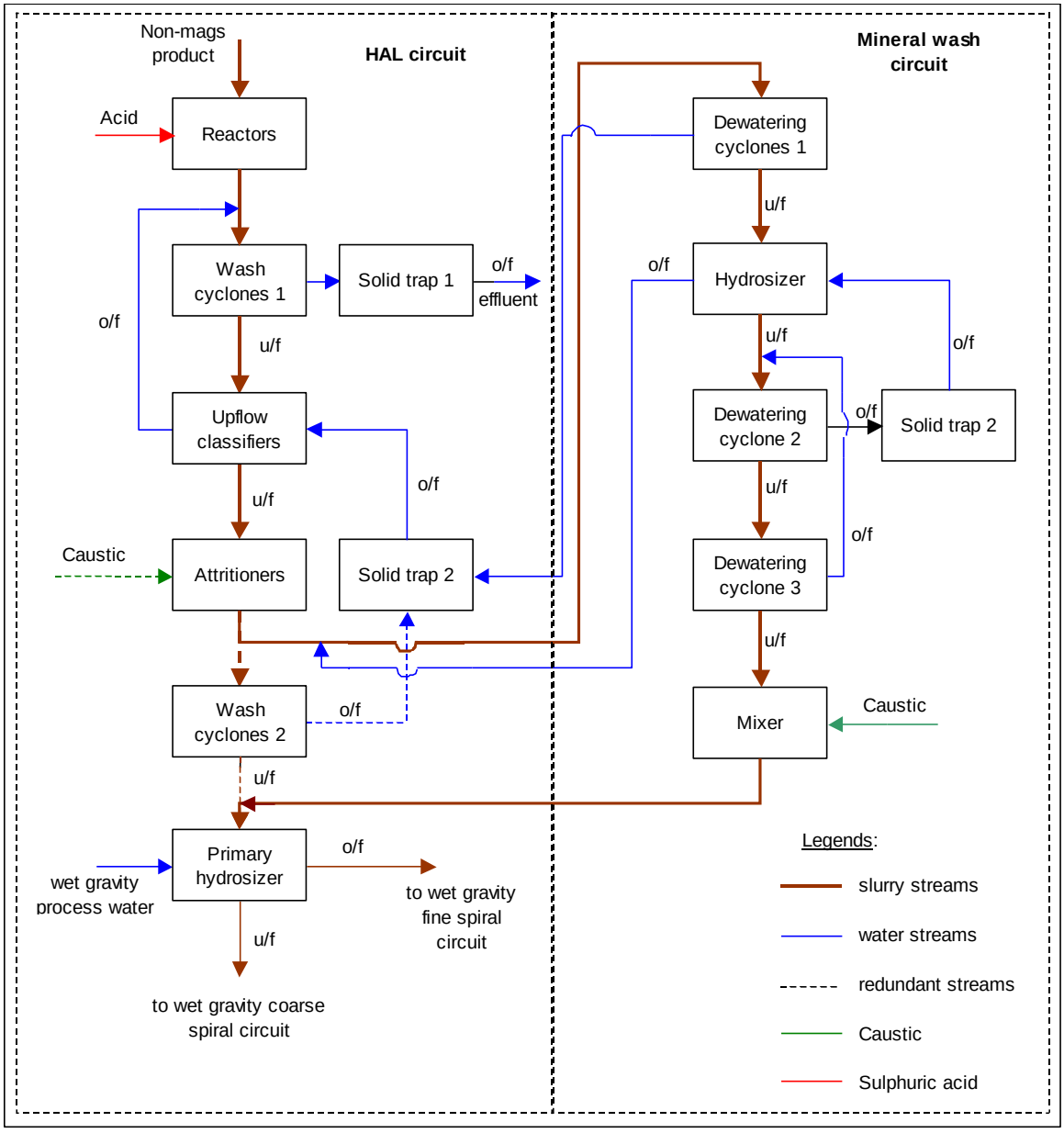

Figure 5.2: A simplified process flow sheet of the mineral wash circuit showing only the main process equipment and interface with the HAL circuit.

5.10 CLARIFYING OPERATIONAL OBSERVATIONS

The study also clarified the following previously unexplained observations identified by the operationing personnel:

(a) Poor pH control versus zircon and rutile production

Poor control of the addition of caustic to the attritioners resulted in the pH of the slurry increasing to between 7 and 8. This resulted in an increase in the formation of iron hydroxide and other precipitates. Secondly, it also increased the pH of the upflow classifiers resulting in precipitation of large amounts of iron. The impact on production was dramatic due to the attachment of iron and other precipitates.

(b) Loss in efficiency of the upflow classifiers versus zircon and rutile production

The efficiency of the upflow classifiers often decreased due to blockages in the teeter water tuyers, which restricted the iron removal efficiency of these units. This resulted in an increased volume of dissolved iron being discharged to the attritioners, which consequently increased the formation of iron precipitates attaching to the mineral surfaces affecting their electrostatic separation performance.

(c) Colour of the wet gravity process water versus zircon and rutile production

It was reported that poor electrostatic separation occurred when the colour of the wet gravity process water became yellow-brownish. Iron analyses of the wet gravity process water showed that high levels of iron hydroxide suspended in the process water was the main cause for this colour change. Iron hydroxide formed in the HAL attritioners were fed to the wet gravity circuit via a dewatering cyclone. It accumulated over time due to the recycling of water in this circuit. Electrostatic separation, and consequently the production of zircon and rutile products, was severely negatively affected when the iron concentration reached a limit of 0.07 g/dm^3 (refer to Figure 4.14). The water appeared yellow-brownish at this concentration.

(d) Poor AMDEL versus XRF correlation

The AMDEL was used as a quick but less accurate online measurement to control the grade of zircon and rutile final products. Process adjustments were made based on the readings (1 every minute) of the AMDEL and final grades were confirmed on an hourly basis by means of an XRF. AMDEL and XRF correlations were affected by high concentrations of precipitates on the mineral surfaces, which affected the surface condition of the mineral particles. AMDEL readings are based

on the surface and XRF readings are based on the bulk properties of a mineral sample. Consequently, contaminated mineral surfaces resulted in incorrect AMDEL readings that caused a deviation from the XRF.

5.11 IMPORTANT ANALYTICAL METHODS DEVELOPED

Useful analytical methods were developed and implemented at Namakwa Sands as a result of this study. These methods proved to be important tools for effective process control. The methods were:

(a) Chemical desorption: Analysing the rinse water after rinsing mineral particles with diluted sulphuric acid (pH 1.3) or fresh water (pH 6-7) were found to be relatively easy and cost-effective in determining the concentration of precipitates on other unwanted species on the mineral surfaces. Acidic washing removed precipitates (e.g. iron and aluminium hydroxide) and fresh water washing removed deposited salts (e.g. sodium).

(b) Separability tests: Comparing the separability of a dry mill feed sample with a standard sample (clean sample after acidic wash) identified any electrostatic separation differences. A laboratory Coronastat at standard settings and constant weather conditions were used to separate the samples. These separability tests were found to be very useful and accurate in establishing if a decrease in zircon recovery was caused by incorrect machine settings in the dry mill circuit or due to a reduction in mineral separability.

(c) Repeatability of electrostatic separation tests: Repeatability of electrostatic tests was achieved by repeating separation tests until the mass splits were almost identical. Stream analyses were only conducted after repeatability was achieved.

(d) Iron build-up in the wet gravity circuit: Water samples at different points in the wet gravity circuit were analysed for total iron. The process water of the wet gravity circuit had to be flushed (replaced by fresh water) if the analyses of the primary spirals reached a critical value of 0.07 g/dm^3.

(e) Monitoring blockage of tuyers of the upflow classifiers: Blockage of tuyers affected the efficiency of the upflow classifiers. Implementation of frequent pH monitoring was found to be effective in detecting blockages, which were followed by a decrease in the pH from a normal range of 1.8-2 to <1.8. This reduced the unnecessary downtime to inspect tuyers.

(f) Iron (III)/iron (II) ratio: This ratio was important since a high ratio would result in the formation of increased volumes of iron hydroxide and consequent loss in production. Iron

(III) could be removed by filtering after increasing the pH of the HAL process water (e.g. overflow of upflow classifiers) to about 5. The remaining iron would be predominantly ferrous oxide.

(g) Zeta potential of mineral particles: This method was developed by the University of Cape Town and could be exploited to other minerals (not only zircon and rutile particles), such as slime particles and quartz. Zeta potentials were found to be very useful in determining adsorption mechanisms.

(h) Quantification of slimes concentrations: Slimes (< 45 um) were quantified by rinsing samples with fresh water and decanting the slimes suspended in the water after a few seconds, allowing the heavy mineral particles to settle. This was repeated until the rinsing water was clear and free of slimes. The amount of slimes was quantified by means of mass difference. This simplistic method was found to be accurate, repeatable and quick, and was therefore also implemented at the magnetic circuit of the MSP and at the process circuits of the mine site.

CHAPTER 6

CONCLUSIONS AND RECOMMENDATIONS

This study revealed the significant impact of the HAL circuit on the production of zircon and rutile products at the MSP. Previous optimisation work initiated by Namakwa Sands on the HAL circuit focused mainly on improving the leaching efficiency of the reactors in order to reduce the acid usage. Very little attention was focused on the remainder of the circuit, which was thought to be robust and its downstream effect was wrongly assumed to be negligible. This study provided scientific proof for the precipitation of iron and other metal species in the HAL circuit, and the attachment of these species to the surfaces of mineral particles at the Mineral Separation Plant of Namakwa Sands. The impact of these precipitates was quantified, and it was shown that they had a significantly negative impact on the electrostatic separation of zircon and rutile particles, and consequently on the production of mainly zircon product. The study also clarified a few previously unexplained operational phenomena. Literature contained abundant information on the formation of iron complexes, also providing sufficient information in order to derive an adsorption theory, which explained why iron hydr(oxides) attached to the surfaces of zircon and rutile particles. However, literature did not provide any significant insight in regard to the physical properties of the precipitates, their impact on the grade of final zircon product, and the separation of zircon and rutile particles. Other mineral sand operations could not be approached due to the secrecy of the mineral sand industry and other similar legal agreements. The most significant outcome of this study was the design, construction and successful implementation of a counter current decantation circuit, which was constructed at a capital cost of approximately R5m (2004 money terms). This circuit was referred to as the mineral wash circuit and exceeded all design criteria. Based on the results obtained in this study, a few conclusions could be made which are discussed in the following paragraph.

6.1 CONCLUSIONS

The main objectives of the study were met in the following ways:

(a) Importance of HAL circuit

The HAL circuit fulfilled an important roll not only in terms of the removal of the natural surface coating covering the mineral particles, but also in the removal of the dissolved precipitates prior to

neutralisation of the slurry. Inefficiencies in either of the two functions would result in zircon, and to a lesser degree, rutile product grade fluctuations as well as ineffective separation of zircon and rutile particles in the downstream dry mill circuit.

(b) HAL chemistry

The most abundant species dissolved in the HAL process water were SO_4, Fe, Al, Ca, Mg and Ti. Iron was present as both ferrous and ferric ions with the latter being more abundant and varying in concentrations from 50-100%. This ratio seemed to be a function of the ore body with certain spots being very rich in ferric ion. Oxidisation of ferrous to ferric ion was negligible in the HAL circuit due to the high acidic conditions. The process water was radioactive due to small amounts of U and Th originating mainly from dissolved monazite minerals. The concentration of dissolved iron was reduced by 90-94% by the HAL circuit prior to caustic addition and SO_4, Ca, Na, and consequently Fe was the abundant species at this point in the process.

(c) Precipitation of complexes in the HAL circuit and the physical conditions causing precipitation of iron

Neutralising the slurry in the attritioners resulted in the partial precipitation of sulphates and the complete precipitation of iron (III) and aluminium in sequence of decreasing volumes. Iron (III) precipitation was mainly a function of the pH and iron concentration of the solution. A loss in efficiency of the dewatering and washing equipment, such as upflow classifiers, resulted in increased volumes of iron precipitates. Precipitation started at a pH of 1 - 1.2 in the quench sumps and overflow of the upflow classifiers, and at pH of 1.5 - 1.8 in the underflow of the upflow classifiers. It was important to realise that preventing iron precipitation would also prevent most of the other species precipitating due to the low pH at which it started to precipitate. More than 99% of the Fe (III) precipitated at a pH of 4. Therefore, iron species remaining in solution at a pH of more than 5 were in the ferrous form. Precipitation of ferrous ion increased in volumes at pH > 8. Iron precipitates were predominantly iron hydroxides, which would partially be converted to goethite in the dryers of the dry mill circuit. The iron hydroxide precipitates adsorbed anions, such as SO_4, due to the relatively low pH of the process water after neutralisation.

(d) Physical properties of natural mineral surface coating compared to iron hydroxide precipitate

The natural coating covering the mineral particles present in the ore body contained large concentrations of hematite (Fe_2O_3), aluminium and silica. The hematite component caused the coated particles to be conductive and magnetic.

The physical properties of this coating changed once it was dissolved and precipitated. Zircon mineral particles coated with iron hydroxide and other precipitates were conductive, but still non-magnetic. Rutile mineral particles became slightly less conductive probably due to the Al $(OH)_3$ component. Iron hydroxide is hydrophilic and it rapidly adsorbed atmospheric moisture.

(e) Adsorption mechanism of precipitates

Iron hydroxide attached to the surfaces of zircon and rutile particles due to opposite zeta potentials. Zircon and rutile had a negative zeta potential and iron hydroxide positive. The relatively low pH of the process water after caustic neutralisation was the ideal condition for adsorption to the mineral surfaces. Zeta potentials of zircon were more negative than rutile resulting in these particles being more selective, which will consequently adsorp higher volumes of iron.

(f) Impact of attached precipitates on electrostatic separation and grade of final zircon and rutile products

Coated mineral particles behaved slightly to moderately conductive and coated rutile particles behaved slightly more non-conductive in an electrostatic separator. This caused an increase of mainly zircon particles in the middling fractions of the electrostatic separators, which resulted in the volume of recycle loads increasing significantly. The net effect was a decrease in the separation efficiency and consequently 3-7% lower zircon recoveries. Rutile recoveries were also negatively affected. The hydrophilic nature of iron hydroxide caused the electrostatic separation of coated mineral particles to be very sensitive to fluctuations in the atmospheric moisture, which resulted in a significant loss in production of both zircon and rutile products. Precipitates attached to the surfaces of the minerals affected mainly the grade of the zircon product causing an increase in the Fe_2O_3, Al_2O_3 and sometimes TiO_2 concentrations.

(g) Clarifying operational observations

The study also revealed that a few previously unexplained phenomena were directly caused by either the precipitation of iron hydroxide and other species or their attachment to the mineral surfaces. The phenomena were:

1. The effect of poor pH control on the production of zircon and rutile in the HAL circuit.
2. Loss in efficiency of the upflow classifiers affected zircon and rutile production negatively.
3. The colour of the wet gravity process water was a function of the concentration of iron hydroxide. A brownish colour indicated high concentration of iron hydroxide, which had a severe negative impact on the electrostatic separation of zircon and rutile and consequently its production.
4. AMDEL versus XRF correlation was affected by iron hydroxide and other precipitates attached to the mineral surfaces of the mineral particles of the dry mill feed.

(h) Implementation of a process solution

The design, construction and successful implementation of a counter current decantation circuit were the direct outcome of this study and reduced the dissolved iron concentration by more than 99.97% prior to caustic addition. The impact of this circuit was significant and all design parameters and expectations were exceeded.

(i) Other important outcomes of this study

1. Important analytical methods were developed and implemented, which helped to control the process effectively.

2. The rate of acid addition to the HAL reactor could be reduced due to the elimination of zircon product iron excursions caused by the precipitation and adsorption of iron. This had significant positive environmental and financial implications for Namakwa Sands. Reduction of the slime concentrations due to counter current washing also improved the health conditions inside the dry mill building.

3. Literature did not provide any information regarding the effect of iron hydroxide and other precipitates formed in the HAL circuit. This information could not be found in literature and this study could significantly benefit the mineral sand industry.

4. The impact of fluctuating atmospheric humidity, which significantly impacted the production of zircon and rutile, was reduced as a direct result of the counter current mineral wash circuit.

6.2 RECOMMENDATIONS

The following recommendations could be made as a result of this study and for a continuation study:

(a) Decreasing the pH set-point from 7 to 5

Decreasing the pH set point from 7 to 5 would reduce the volume of precipitate formed and also the amount of caustic used. This would lengthen the build-up period of iron in the process water of the wet gravity circuit. This set-point change was implemented during the early phase of the study the attritioners were still used as neutralising stage.

(b) Moving the caustic neutralisation stage

Caustic was added to the attritioners before the final dewatering cyclone. Moving the caustic addition point after the dewatering cyclone (neutralising the underflow of the cyclone) would reduce the concentration of acid and dissolved species by more than 70%. This would result in a saving in caustic and reduce the amount of iron hydroxide and other precipitates formed, which would improve the recovery of zircon and rutile in the dry mill. A caustic mixer was installed about two months prior to the commissioning of the mineral wash circuit and it was fed via the underflow of the dewatering cyclone. Caustic usage was reduced by more than 70% and zircon and rutile recovery improved slightly.

(c) Construction of mineral wash circuit

The most significant outcome of this study was the design, construction and commissioning of a counter current decantation circuit. It was labelled the ‘mineral wash circuit’ due to its inherent purpose to clean mineral particles. The project was successfully implemented and the formation of

precipitates was almost completely eliminated due to the fact that more than 99.97% iron was removed prior to caustic addition.

(d) Raise the pH set point after mineral washing

The mineral wash circuit removed all of the dissolved electrolytes including alkaline species, such as calcium and sodium, and the net effect was a weakening in the buffer capacity of the process water of the wet gravity circuit and a consequent reduction in pH. The pH decreased from 4.5 - 5 to 4, which caused corrosion of steel pipes in the wet gravity circuit. Experimental work showed that the impact of caustic on electrostatic separation were negligible after dissolved species had been removed. Therefore, it is suggested that the pH set point in the mixture be increased so that the pH of the wet gravity process water at the 'dirty water tank' be increased to 4.5-5.

(e) Install online conductivity meter to measure washing efficiency of the new circuit

Conductivity (µS/cm) of water samples was found to be a good indication of the amount of electrolytes in the samples and therefore could be used as an indication of the washing efficiency of the mineral wash circuit to identify any process deviations. Tests should be conducted to determine if the feed to the mixer (prior to caustic addition) or the discharge of the mixer (after caustic addition) must be monitored. Readings should be monitored online via the SCADA system. The process equipment and water balance of the mineral wash circuit must be set up in such a way as to minimise the conductivity readings, which would ensure maximum removal of dissolved iron and other species. Conductivity readings of the samples measured at the discharge and feed of the mixer were typically between 150 and 250 µS/cm.

(f) Install online conductivity meter prior to belt filter to monitor water quality of the wet gravity circuit

Monitoring of the conductivity of the process water in the wet gravity circuit will be useful to monitor the build-up of electrolytes, which could impact electrostatic separation in the dry mill circuit. Therefore, it is recommended that an online conductivity meter installed prior to the belt filter. This would also ensure effective re-use of treated effluent water, which will be implemented in the near future.

(g) Implement final washing stage prior to primary and secondary belt filters

Implementation of washing stages prior to the two belt filters (mainly the primary belt filter) will remove the remaining trace amounts of electrolytes and slime particles, which will ensure optimum clean mineral surfaces and should almost eliminate the dust concentrations in the dry mill circuit. These washing stages could be designed to remove fine particles as the main objective (+45-75 µm). Removal of fine particles might further improve dry mill zircon and rutile recoveries. Washing prior to the belt filters would ensure maximum re-use of treated process water.

(h) Implement washing stage to remove slimes from the magnetic ilmenite feed stream

The mineral wash circuit was very successful in the removal of slimes. Slimes and dust levels in the magnetic ilmenite circuit at the MSP were excessive due to insufficient desliming at the secondary concentration plant (SCP). These slimes caused a decrease in efficiency of the HTR separators. Therefore, it is highly recommended that the implementation of a wash circuit at the SCP be investigated.

(i) Implement an independent HAL spillage removal system

Spillage generated due to HAL circuit instabilities could only be removed by manual labour. A washing system existed to introduce this spillage back into the HAL process, but this option caused major circuit instabilities mainly due to fluctuating mass balances and stream densities. This resulted in poor washing efficiency of the mineral wash circuit and poor dry mill feed grade. Therefore, it is recommended that the existing spillage wash system be incorporated in an independent spillage removal system. This system will eliminate any circuit instabilities and will create a stockpile of spillage, which could be treated separately.

(j) Monitor mineral particle surfaces on a continuous basis

Mineral surfaces must be analysed continuously to monitor the concentration of chemical species. This could also be used to monitor the efficiency of the mineral wash circuit.

(k) Determine the adsorption mechanism of slime particles

The possibility of adsorption of slimes particles to mineral surfaces was not included in this study. However, it is a possibility that an adsorption mechanism exists and it should be investigated due to its potentially negative impact on the production of zircon, rutile and ilmenite. It was also expected that different types of slimes particles would have different adsorption mechanisms. Measuring of the zeta potential of slime particles must be conducted as a starting point.

REFERENCES

Bandini P., Prestidge C.A. and Ralston J., 2001. Colloidal iron oxide slime coatings and galena particle flotation. *Minerals Engineering*, Vol. 14, No. 5, pp. 487-497.

Baxter G.P. and Hoover C.R., 1912. J. Am Chem. Soc. 34, p.1657.

Bhatti T.M., Bigham J.M., Carlson L. and Tuovinen O.H., 1993. Mineral products of pyrrhotite oxidation by thiobacillus ferrooxidans. *Applied & Environmental Microbiology,* No. 59, pp. 1984-1990.

Bigham J.M., Schwertmann U., Traina S.J., Winland R.L. and Wolf M., 1996. Schwertmannite and the chemical modeling of iron in acid sulphate waters. *Geochimica et Cosmochimica Acta.* No. 60, pp. 2111-2121.

Cigan J.M., Mackey T.S. and O' Keefe T.J., 1980. Lead-Zinc-Tin. *TMS-AIME world symposium on metallurgy and environmental control.* The Metallurgical Society of AIME, pp. 97-117, 532-559.

Collins A.F. and Farmer A.D., 2003. The application of power ultrasound to the surface cleaning of heavy mineral sands. *Heavy Minerals Conference*, Cape Town, pp.39-42.

Cornell R.M. and Scwertmann U., 1994. The iron oxides, VCH, Weinheim.

Dance A.D. and R.D. Morrison, 1991. Quantifying a black art: The electrostatic separation of mineral sands. *Minerals Engineering*. UK: Pergamon Press, Vol. 5, No. 7, pp. 751-765.

Dutrizac J.E., 1983. Jarosite-type compounds and their application in the metallurgical industry. *Hydrometallurgy – Research, development and plant practice*. The Metallurgical Society of AIME, pp. 531-551.

Dutrizac J.E. and Monhemius A.J., 1986. Mineralogical overview of iron control in hydrometallurgical processing. *Iron control in hydrometallurgy*. Chichester: Ellis Horwood Limited, pp. 19-46.

Ernstsson M. and Larsson A., 1999. A multi-analytical approach to characterize acidic adsorption sites on quartz powder. *Colloids and Surfaces,* pp. 215-230.

Fornsiero D., Fengsheng L. and Ralston J., 1994. Oxidation of galena: II, electrokinetic study. *J. Colloid Interface Sci.*, 164, pp. 333-342.

Fuerstenau, D.W., Gaudin, A.M. and Miaw, H.L., 1958. The influence of alumina slimes on galena flotation. *Amer. Inst. Min. Eng. Trans.* 211, pp. 792-795.

Gaboriaud F. and Ehrhardt J., 2002. Effects of different crystal faces on the surface charge of colloidal goethite (α-FeOOH) particles: An experimental and modeling study. *Geochimica et Cosmochimica Acta*. USA: Elserivier Science Vol. 67, No. 5, pp. 967-983.

Gaudin, A.M., Faurstenau, d.W. and Miaw, H.L., 1960. Slime coating in galena flotation. *Trans. Can. Inst. Min. Metall.*, 56, pp. 960-963.

Hayes P.C., 1993. Aqueous solution processing. *Process Principles in Minerals and Materials Productions*. Brisbane: Hayes Publishing Company, pp.227-317.

Howe T.M. and Pope M.I., 1970. The effect of conditioning agents on the surface conductivity of powders, in relation to electrostatic separation. *Congrès International de la préparation de minerals,* pp. 59-66.

Hunter R.J., 1981. Zeta potential in colloid science: principles and applications. London: Academic Press.

Kosmulski M., Maczka E., Lartych E. and Rosenholm J.B., 2003. Synthesis and characterization of goethite and goethite-hematite composite: experimental study and literature survey. *Advances in colloid and interface science*, 103, pp.57-76.

Lawver J.E. and Wright I.L., 1969. A cell for measuring the electrical conductivities of granular materials. *Transactions of the Society of Mining Engineers*, AIME, vol. 244, pp. 78-81.

Learmont, M.E. and Iwasaki, I., 1984. Effect of grinding media on galena flotation. *Miner. Metall. Process.*, 1, pp. 136-143.

Parsonage, P.G., 1985. Effects of slime and colloidal particles on the flotation of galena. *Dev. Miner. Process.*, 6, pp. 111-139.

Petrucci R.H. and Harwood W.S., 1997. General Chemistry: Principles and modern applications. New Jersey: Prentice Hall, 7th addition, p. 975-976.

Prestidge, C.A., Skinner, W.M., Ralston J. and Smart R.St.C., 1995. The interaction of iron (III) species with galena surfaces. *Colloids Surfaces,* 103, pp. 325-339.

Prinsloo A, 1998. Invloed van veranderlikes op rutile/zircon skeiding (Namakwa Sands). *Test work report.*

Schwertmann U., Bigham J.M. and Murad E., 1995. The 1st occurrence of scwertmannite in a natural stream environment. *European Journal of Mineralogy.* No. 7, pp. 547-552.

Schwertmann U. and Cornell R.M., 1991. Iron oxides in the laboratory, VCH, Weinheim.

Sousa Neto V.O., Silva C.C., Almeida A.F.L., Figueiró S.D., Góes J.C., de Paiva J.A.C., Magalhães and Sombra A.S.B., 2001. Study of the electrical conductivity and piezoelectricity in iron doped collagen films. *Solid State Science*, pp. 43-51.

Svarovsky L., 1985. Solid-Liquid separation Processes and Technology. In: *Handbook of Powder Technology*, Vol. 5, Williams J.C. and Allen T. (eds.); Amsterdam: Elsevier.

Tuovinen O.H., Bhatti T.M., Bigham J.M., Hallberg K.B., Garcia O. and Lindstrom E.B., 1994. Oxidative dissolution of arsenopyrite by mesophilic and moderately thermophilic acidophiles. *Applied & Environmental Microbiology.* No. 60, pp. 3268-3274.

Veglió F., Passariello B., Barbaro M., Plescia P. and Marabini A.M., 1998. Drum leaching tests in iron removal from quartz using oxalic and sulphuric acids. *International Journal of Mineral Processing,* 54, pp. 183-200.

Weiser H.B., 1939. Inorganic colloid chemistry. New York: Wiley, Vol 2, p. 588-591.

Weiser H.B. and Milligan W.O., 1939. Inorganic colloid chemistry. *Chem,* Rev. 25, p.1.

Welham N.J., Malatt K.A. and Vukcevic S., 2000. The Stability of iron phases presently used for disposal from metallurgical systems – a review. *Minerals Engineering*, Vol. 13, No. 8-9, pp. 911-931.

Woollacott L.C. and Eric R.H., 1994. Mineral and Metal Extraction – An overview. The South African Institute of Mining and Metallurgy: Johannesburg.